Knowledge-aided Sensor Data Processing for Maritime Situational Awareness

DISSERTATION

zur
Erlangung des Doktorgrades (Dr. rer. nat.)
der
Mathematisch-Naturwissenschaftlichen Fakultät
der
Rheinischen Friedrich-Wilhelms-Universität Bonn

vorgelegt von

Giulia Battistello
aus
Rom, Italien

Bonn, November 2020

Angefertigt mit Genehmigung der Mathematisch-Naturwissenschaftlichen Fakultät
der Rheinischen Friedrich-Wilhelms-Universität Bonn

1. Gutachter: Prof. Dr. Wolfgang Koch
2. Gutachter: Prof. Dr. Peter Martini

Tag der Promotion: 23.04.2021
Erscheinungsjahr: 2021

Abstract

The research work focuses on the development of innovative sensor data processing techniques for traffic surveillance, which aim at improving the performance yielded by state-of-the-art tracking solutions when a dynamically evolving target scenario is sensed by heterogeneous, geographically distributed sensors. Specifically, the maritime environment is considered, since the lack or deficiencies of customized techniques is currently in the spotlight due to the rising of events such as illegal migration, sea piracy, and accidents in new highly-trafficked sea routes. Maritime surveillance applications rely on multiple sensors, which might be located on the coast, on board patrolling or commercial vessels, or air/space-based platforms. This plethora of information sources urges for ad hoc data processing techniques. However, such techniques suffer from intrinsic problems due to the characteristics of the vessel traffic or to the space/time constraints of the observations.

Specifically, the PhD work aims at facing the following - often recorded - phenomena that hinder target tracking and identification performance: (i) lack and/or intermittence of sensor measurements due to occlusions or limited sensor coverage; (ii) spoofed or erroneous position messages from ships and (iii) false alarms originated by the sensors due to the presence of clutter (e.g. echoes from land and wind parks). These phenomena, experienced by active and passive coastal radars and collaborative systems such as Automatic Identifications Systems or Long Range Identification and Tracking system, lead to discontinuous, inaccurate and false vessel tracks in the maritime traffic picture.

The fundamental concept proposed by the PhD work is the exploitation of external information in the target tracking stage. This is specifically valid in the maritime context, which is rich in contextual (e.g., coastline, location of ports, sea lanes, corridors and interdicted areas, oil spills, clutter conditions) and target-related informa-

tion (e.g., target behavioral models, declared and preferred routes). These factors constrain the evolution of the target in the observed scenario, hence they can be exploited when attempting at reconstructing the target track from the available, scarce and inaccurate measurements. The crucial question is how and at what step of the target tracking processing chain this external information should be used in order to maximize the payoff.

Constrained filtering has been investigated in the past in general terms. However, application-oriented mathematical models are required for including the context information (our "knowledge") as constraint in the non-linear estimation problem. Specifically, Bayesian non-linear filtering strategies are considered within the research work and different mathematical models (i.e., the Navigation Field and the Sea Lane concepts) are formulated. This leads to the conceptualization and development of innovative Knowledge-based tracking filters, which are demonstrated to improve track performance metrics, such as continuity, accuracy and false track rate. Exhaustive performance assessment is carried out over simulated maritime traffic scenarios.

Finally, within the PhD research, the introduced techniques are tested in the frame of operational applications, such as (i) active radar surveillance in coastal areas, (ii) collaborative vessel traffic monitoring in high seas and coastal areas, and (iii) passive radar surveillance in coastal areas. The availability of sensor data allows tuning the developed models to the operational (realistic) maritime scenarios, and providing a clear insight into Knowledge-based data processing techniques for area surveillance.

Keywords **- Knowledge base, context information, target tracking, constrained Bayesian filtering, data association, Extended Kalman filter, particle filter, Kullback-Leibler divergence, maritime situational awareness, navigational field assisted target tracking, sea lane assisted target tracking, knowledge-based MHT, vessel route prediction, vessel monitoring, AIS, coastal radar, passive radar.**

Acknowledgments

I would like to thank all the people who supported me during these years and made this work possible.

My deep gratitude goes to my supervisors, Prof. Dr. Peter Martini, head of Fraunhofer FKIE, and Prof. Dr. Wolfgang Koch, head of the Sensor Data and Information Fusion department at Fraunhofer FKIE, for the possibility they gave me to start my doctorate in the department and for the continuous encouragement.

A special thanks goes indeed to my direct responsible, Dr. Martin Ulmke, head of the Distributed Sensor Systems group, for his contribution in defining the path of my research, for his guidance through each stage of the process and for the fruitful discussions, either technical or motivational. Thank you Martin to push me during this long journey, for your revision and comments.

I would like to thank my colleague Dr. Martina Broetje, for the inspiring work she made in the target tracking field and the friendly collaboration of these years, which has been fundamental for this work. Thanks to all colleagues of the SDF department to share this experience.

Last but not the least, I would like to thank my husband Massimo for his encouragement and unconditional support throughout writing this thesis and my life.

Contents

1 Introduction **1**

1.1 Motivations and Objectives 6
1.2 Work Structure 11

2 Fundamentals of Maritime Situational Awareness **13**

2.1 Maritime Surveillance Sensors and Related Technical Requirements . . 17
2.1.1 Active Radar 17
2.1.2 Automatic Identification System 22
2.1.3 Satellite Automatic Identification System 25
2.1.4 Long Range Identification and Tracking 27
2.1.5 Space Earth Observation Sensors: Satellite-Synthetic Aperture Radar 28
2.1.6 Passive Radar 30
2.2 Maritime Knowledge Base Description 32
2.3 Summary 37

3 Fundamentals of Multi-Sensor Data Processing **39**

3.1 Bayesian Target Tracking 39
3.1.1 System Equations 40
3.1.2 State Estimation Problem 41
3.1.3 Linear Gaussian Systems 43
3.1.4 Non-linear Systems 45
3.1.5 Data Association Problem 49
3.2 Measures of Performance 53
3.2.1 Root Mean Squared Errors 54
3.2.2 Kullback-Leibler Divergence 55
3.3 Summary 56

4 Context Exploitation for Target Tracking **57**

4.1 Constrained Bayesian Filtering 58
4.1.1 Inclusion of Constraints in the Prediction Step 60

4.1.2 Inclusion of Constraints in the Update Step 61
4.2 State-of-the-art Constrained Algorithms 61
4.2.1 Rejection Sampling 62
4.2.2 Pseudo Measurements 63
4.2.3 Roadmap Assisted Target Tracking 63
4.2.4 Blind zone Assisted Target Tracking 69
4.3 Summary 72

5 Innovative Solutions for Maritime Situational Awareness Context-based Target Tracking 75
5.1 Navigation Field Assisted Target Tracking 76
5.1.1 Context Modelling 76
5.1.2 Filter Implementation: Model I - Force as Acceleration 78
5.1.3 Filter Implementation: Model II - Force as Angular Acceleration 81
5.2 Sea Lane Assisted Target Tracking 82
5.2.1 Target and Context Modelling 83
5.2.2 Filter Implementation: Context driven Target Model Switching 84
5.3 Knowledge-based Multiple Hypotheses Tracker 87
5.3.1 Context Modelling 88
5.3.2 Filter Implementation 88
5.4 Summary 91

6 Application-Experimentation I: Active Radar Surveillance in Coastal Areas 93
6.1 Navigation Field Based Vessel Monitoring 93
6.1.1 Test Scenarios and Simulation Rationale 94
6.1.2 Simulation Results 97
6.2 Sea Lane Based Vessel Monitoring 106
6.2.1 Test Scenarios and Simulation Rationale 106
6.2.2 Simulation Results over Scenario I 109
6.2.3 Simulation Results over Scenario II 117
6.3 Summary 120

7 Application-Experimentation II: Collaborative Vessel Traffic Monitoring In High Seas and Coastal Areas 121
7.1 Vessel Route Prediction 122
7.1.1 Route Prediction Module Architecture 123

7.1.2 Route Prediction Module Algorithms 127
7.1.3 Test Scenarios and Simulation Rationale 128
7.1.4 Results on Real Data Sets 130
7.2 Summary 134

8 Application-Experimentation III: Passive Radar Surveillance in Coastal Areas **135**
8.1 Vessel Monitoring in the Baltic Sea 136
8.1.1 Experimental System Set Up 136
8.1.2 Test Scenario and Simulation Rationale 139
8.1.3 Results on Real Data Set 143
8.2 Vessel Monitoring in the Canadian Arctic 150
8.2.1 Passive Radar Measurements and Tracks Simulator 151
8.2.2 Test Scenario and Simulation Rationale 161
8.3 Summary 173

9 Conclusions **175**

List of Figures **177**

List of Tables **183**

List of Acronyms **185**

List of Own Publications **187**

Bibliography **191**

CHAPTER I

Introduction

"Remote Sensing is gathering information about an object without touching it", [FRH86].

Most human activities rely on the way the world around is sensed by him, and on the way he is able to reason on the information collected through his senses. Since ages, people have extended their senses through the use of devices and adapted their reasoning to the newly collected data. A straightforward example is a person looking at an object through a lens, and inferring the characteristics of the object despite the "enhanced" vision of it.

Sensors are nowadays well established tools of our daily life. However, sensor data are by nature incomplete, inaccurate, and affected by errors due to the sensing process itself. The human brain is able to cope with these deficiencies in a very effective way (as an example, the role of the human analyst is still actual in many applications), if it is not overwhelmed by the amount of data, the duration of the observation, or the operative conditions. In such cases the use of automatic processing techniques (or "reasoning" techniques) is attempted. Are they able to mimic the capability of human brain against imperfect senses?

A wide scientific literature is available on data processing techniques devoted to the estimation of unknowns from error-prone sensor measurements. Statistical estimators are well established in guidance and navigation applications, as well as in surveillance devices, for which the presence, position and kinematics of the moving object(s) represent often the unknown.

As far as surveillance applications are concerned, a wide class of data processing

algorithms are commonly referred to as **tracking techniques**, whose fundamentals have been laid down by Kalman et al. [Kal60, KB61]. They rely on the statistical characterization of the sensing "problem": both target evolution and the measurement process are modeled as stochastic processes. Originally, the tracking algorithms were based on linear models, i.e. the target and the measurement processes are described by linear relationships among the variables. Then, they have been quickly extended to non-linear models in order to approximate real observation conditions in a closer way [Sor85]. The typical sources for non-linearity are the measurement process (e.g., a sensor that estimates the relative angle of arrival of the detected signal and attempts at reconstructing the Cartesian coordinates of the emitting object) as well as the target cinematic model (e.g., an object accelerating along its trajectory). The final goal of these algorithms is generally to make the collected measurements usable (in a friendly and confident way) by the User, or, in other words, to improve the quality of the "sensing service".

Another important milestone in the research on data processing techniques consists of the application of the tracking techniques to heterogeneous measurement sets, such as for example the ones provided by two different sensors or by geographically distributed sensors. The basic problem in multi-sensor systems is *"to integrate a sequence of observations from a number of different sensors into a single best-estimate of the state of the environment"*, [DW88]. In this framework, the estimation techniques are often referred to as **data fusion**. At the end the processing of multi-sensor data is *"a process dealing with the association, correlation, and combination of data and information from single and multiple sources to achieve refined position and identity estimates, and complete timely assessments of situations and threats, and their significance. The process is characterized by continuous refinements of its estimates and assessments, and the evaluation of the need for additional sources, or modification of the process itself, to achieve improved results"*, [Why87]. Hall and Llinas [HL97] provided the following well-known definition of data fusion: *"data fusion techniques combine data from multiple sensors and related information from associated databases to achieve improved accuracy and more specific inferences than could be achieved by the use of a single sensor alone"*. A detailed overview of state-of-the-art techniques is reported in [BP99] from the point of view of tracking, and in [HM04] from the point of view of data fusion.

Focusing on surveillance sensors, it is possible to group the applied algorithms into classes or blocks of an overall data processing architecture. Most **surveillance applications** in this field yield indeed similarities and commonalities. For instance, they often require a detection stage to extract the information of interest (i.e. detections,

hits or plots) from the wide set of raw data. This step is commonly followed by a filtering/tracking stage, which attempts at refining the measurement and reduce the effect of erroneous measurement on the overall result. The filtered data (i.e. track) is built up in order to have enough accuracy and confidence to support the "right" decision by the User. A similar task is also assigned to the fusion stage that combines heterogeneous bits of information. This can work on sensor data or generic information sources, such as human reports, databases or social media. All these steps - from the collected raw data to the final results provided to the User - can work in real time or in near real time according to the application.

Radar, cameras, communication interceptors as well as GNSS-based devices benefit from such processing architectures. Taking into consideration the well-known Joint Directors of Laboratories (JDL) model for Sensor Data Fusion [Why87], it is possible to define five levels of data processing:

- Level 0 - Preprocessing: it consists of the basic information extraction process at the signal and pixel levels. This level reduces the amount of data and maintains useful information for the high-level processes;
- Level 1 - Object refinement: This already includes spatio-temporal alignment, association, correlation, clustering or grouping techniques, state estimation, removal of false positives, identity fusion, and the combining of features that were extracted from images. Generally speaking, classification, identification and object tracking belong to this stage.
- Level 2 - Situation assessment: This aims at establishing relationships (i.e., proximity, communication) between the objects and identifying patterns in order to perform higher level inference.
- Level 3 - Impact assessment: this level evaluates the impact of the detected activities through future projection. Goal is to identify possible risks, vulnerabilities, and operational opportunities.
- Level 4 - Process refinement: this level provides resource and sensor management.

The above-described levels correspond to logical functions that might be present in the processing scheme for the addressed sensor data. The specific algorithm will depend on the nature of the collected data and/or information itself, and will be described in this work on case by case basis.

However, it is worth underlining another general feature of the processing scheme, i.e.,

the difference between centralized and decentralized data fusion. A centralized architecture means that the fusion node resides in the central processor that receives the information from all sources in terms of raw measurements. This scheme is theoretically optimal if data can be correctly aligned in time and space. The main drawback is usually the large amount of data to be transferred. Therefore, distributed architectures are quite common. In this case, a network of nodes collaborate, each with its own processing capabilities: measurements from each source node are processed independently through data association techniques (Level 0 and 1) before the information is sent to the fusion node. Of course, other hybrid schemes do exist and can be derived from these two.

The selection of the data processing scheme depends on the considered application. In this work, among others, the following **Use Case** is addressed. An extended maritime area or multiple maritime sectors are monitored by the User for security or safety purposes. Task of the User is to detect, recognize and follow each vessel passing by, and eventually detect anomalies in their behavior (e.g., entering prohibited zones, deviating from the expected route, etc.). This also includes small rapid vessels. To this aim, a set of active and passive sensors are deployed over the territory, including coastal radars and networks of transponders (e.g., the Automatic Identification System, AIS). A distributed fusion architecture is considered: each sensor is equipped with its own tracking algorithm and delivers plots and tracks to the central data processing node. The fusion engine is responsible for compiling the fused picture of the maritime traffic and deliver it to the automatic reasoning engine. This latter will mimic the human reasoning in identifying the anomalies and detecting risks. This might be fully automatic or supervised by the Operator, and usually results into the generation of alarms in real time or off-line reports. This Use Case is depicted in Figure 1.1.

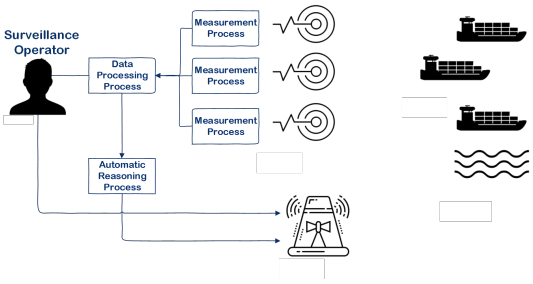

Figure 1.1: Example use case addressed in this PhD work.

As described above, the main task of the considered data processing scheme is to compile the common operational picture (COP) of the maritime traffic for the automatic reasoning tool or for the operator in charge of the monitoring service. The **operative goal** is to increase the situational awareness in the area. The compiled picture should include the position and kinematics of all vessels in the area of interest (that could be a port area, the entire national coastal waters, or high sea Exclusive Economic Zone), and the identification or classification of each vessel. This latter information is based on typical vessel attributes that are collected or measured by the sensor and made available to the fusion engine (as recipient of the track messages). Exemplary attributes are ship's IMO (International Maritime Organization) identification number, ship class or size, port of destination, estimated time of arrival, etc. These features are also prone to errors (human or due to the statistical process) which need to be considered during the association step or when compared to a vessel database. The final picture will be "common", i.e., the information coming from different sensors should be fused before presentation to the User, and should support operations. This usually turns into a requirement on the latency between the acquisition of measurements and the time it is available for the User.

The **performance** of tracking techniques has been characterized and assessed in several forms in literature (e.g. [RD00]). This work addresses the application requirements: this means that in order to fulfill the task of increasing the maritime situation awareness and support the User in his decision tasks, the outputs of the fusion engine have to yield specific performance values. The analyzed processing techniques will be then "successful" if they achieve these Use Case dependent values. These requirements are detailed in Section 2, and dictate the performance metrics of the techniques. The key metrics are the following:

- **Track continuity**, which quantifies the capability of the tracking algorithm to maintain the track "confirmed" even in presence of measurements with large errors, absence of updates, or target dense environment with measurement-track association errors. The commonly observed effect in these cases is the segmentation of the track into multiple non-connected tracks with different identifiers - as if originated by different targets. This leads to misinterpretation of the tactical picture.

- **False Track Rate**, which quantifies the rate of formation of false tracks being originated by false alarms of from unassociated measurements. This phenomenon could be due to a target-dense environment and the resulting overlapping of measurements, or by clutter effects that introduce false detection hits.

Another cause could be a spoofing signal, which turns into a fake target or fake location of a real vessel within the monitored area.

- **Track accuracy**. This corresponds straightforwardly to the (average) difference between the real position of the target and the estimated one. This depends on the sensor measurement accuracy as well as to the update rate, the target kinematics, and the algorithm itself.

The relation of these parameters to the likelihood of using the results contained in the COP is straightforward, as showed by the following examples. The continuity of the track allows correctly assessing the behavior of a given vessel, which might be then labelled as dangerous, illegal or in danger. The accuracy of the track allows generating alarms (e.g., for the Coast Guard and rescue centers) if the vessel approaches too closely dangerous areas, such as the coast. A high rate of false alarms might lead to useless interventions of the Coast Guard or even neglecting actions requested by true vessels, since deeply submerged by the false alarms.

It might be also possible to define the performance in terms of Data Fusion techniques. In this case, we might refer to the **False Association rate**, which quantifies the error rate during the association of measurements to existing tracks or between two tracks. However, the resulting effect - at COP level - will be again encoded by the above-defined performance metrics at track level. For this reason, we will refer to the former exclusively.

1.1 Motivations and Objectives

The introduction demonstrates the wide use of data processing techniques for surveillance applications, which fostered over the last 80 years a significant amount of research work. However, state-of-the-art techniques still yield performance deficiencies mainly due to the complex operative conditions, which might depart from the theoretical models. They unavoidably fail in considering all the constraints of the "real world", since these constraints are hard to describe in quantitative terms. An overall assessment of maritime surveillance awareness (MSA) data processing performance in real conditions does not exist. Sensors are generally defined with maximum performance values, which are achieved in benign conditions, but their characterization in real conditions is protected by the intellectual property rights of the manufacturer. Moreover, the details of the algorithms are not generally known. End Users, as well, tend not to disclose the performance of their surveillance networks due to the strategic relevance of this data. A quantitative assessment of the problem is therefore hardly possible.

However, the same questions on the achieved performance are raised in case of accidents at sea. For example, the absence of real-time alarms in the COP in case of approaching vessels in the proximity of the coast might be unexpected, especially because observations relied on the coastal surveillance network capabilities.

One significant example is given by the Costa Concordia case. Costa Concordia was a cruise ship built in 2004 by the Fincantieri's Sestri Ponente yards in Italy and operated from 2005 until 2012 by the Costa Crociere subsidiary of Carnival Corporation. On 13 January 2012 in calm seas and overcast weather, after departing Civitavecchia (the port for Rome, Italy), on a 7-night cruise, at 21:45 local time, Costa Concordia hit a rock off Isola del Giglio, on the western coast of Italy about 100km (62 NM) northwest of Rome. A 53 m long gash was made in the port-side hull, along 3 compartments of the engine room (deck 0); resulting in power losses, leading to a loss of propulsion and loss of electrical systems, which crippled the ship. Taking on water, the vessel tipped over the port side. Twenty-four minutes later, strong winds pushed the vessel back to Giglio Island, where she grounded 500 m north of the village of Giglio Porto, resting on her starboard side in shallow waters, with most of her starboard side underwater (en.wikipedia.org/wiki/Costa_Concordia, latest access on 23rd August 2019). In this case it seems that no alarm was generated by the coastal surveillance systems for the ship transiting in dangerous areas.

Figure 1.2: The sinking cruise ship Costa Concordia on January 13th, 2012 (www.corriere.it/gallery/cronache/01-2012/costa-concordia/3/tragedia-giglio-gigante-costa-inclinato_4ea8800c-3e92-11e1-8b52-5f77182bc574.shtml, latest access on 23rd August 2019)

The unavailability of sensor data (or good enough sensor data) in conjunction with other accidents is also hardly justifiable. On April 12th, 2015, the radar sensor located on the southern dam of the port of Ravenna in Italy was broken since a few months. The merchant vessels Lady Aziza and Gokbel collided on December 28th a mile off the port of Ravenna. Experts said that even with a fully operational radar, the track accuracy would have not been enough to avoid the accident.

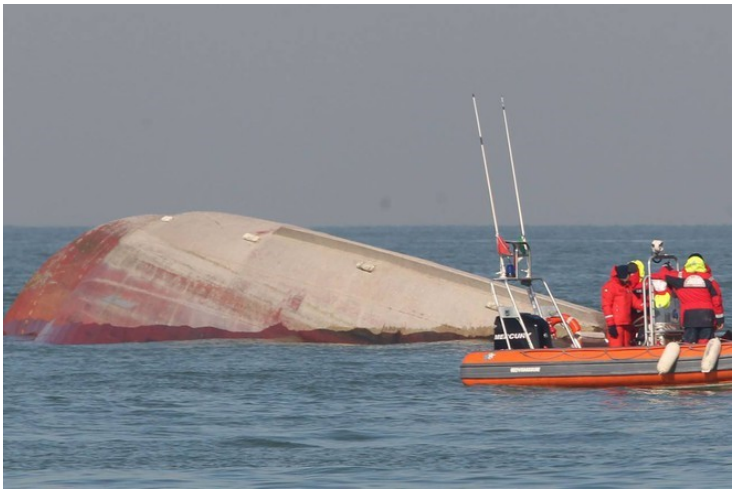

Figure 1.3: Result of the collision between the Lady Aziza and Gokbel merchant vessel on December 28th, 2015 (www.ilrestodelcarlino.it/ravenna/cronaca/naufragio-gokbel-marinaio-morto-identificato-1.1456429, latest access on 23rd August 2019).

A sequence of collisions between military ships and merchant ships has generated the question if GPS- or AIS-spoofing techniques are already in use. The generation of a false AIS track (or equivalently the lack of an AIS track in the operational picture) is expected to reduce the early warning capabilities of other vessels for collision avoidance. This means that the reliability of the cooperative systems, such as the AIS, needs to be high or needs to be supported by non-cooperative sensing. The complementarity of the data sources should be used not only as back-up but also to prevent the mystification of the picture.

In the three mentioned accidents, a common aspect can be found: a priori information was available, but it was not used for different reasons. The presence of hazardous routes, the unavailability of a sensor, or the likely presence of fake targets in the

Figure 1.4: Collision of US military ships due to AIS spoofing (Jim Richards' twit on 20th August, 2017).

COP are a priori information that the human brain is able to process. Would it be possible then to integrate this kind of information into the automatic tracking and fusion algorithms?

This research work aims at supporting this analysis and tackles - from a theoretical and experimental perspective - the introduction of a **Knowledge Base** (KB) into data processing algorithms for the MSA. Knowledge is a generic term that refers to any relevant information to infer on the sensor data. In the maritime surveillance applications, typical knowledge is related to the geographical information about the coastline, ports, corridors, bathymetry, vessels databases, etc., whose detailed description is provided in Section 2. Nowadays, this knowledge is not part of the automatic processing scheme, even though a few attempts have been made to introduce constraints in the filtering techniques. At Level 0 of the JDL Model, it is not rare that the detection algorithms use some sort of knowledge to filter out false alarms. At Level 1, the identification step is mostly based on external databases, which can be considered as a sort of knowledge. This is particularly true whenever identification is based on attributes (e.g., operative modes) and not only on single-shot emission parameters (e.g., frequency).

In this work, the Knowledge Base is exploited at Level 1 of the JDL Data Fusion architecture, i.e., within tracking and association algorithms. Alternative approaches with the introduction of the KB at higher levels are of course possible, but probably

harder to assess.

The inclusion of the Knowledge Base elements in the statistical estimation problem (i.e., single-target tracker) is likely to result in the following benefits:

- Improve the *track continuity* and *track accuracy* in presence of intermittent sensor data (i.e. measurements);
- Improve the *false track rate* in presence of false sensor data and when operating in cluttered areas.

Considering the mathematical formulation of the well-known detection and tracking schemes, the Knowledge Base could be exploited in any step of the detection and/or tracking algorithm, such as state prediction and update, including the data association, and to track initialization.

Independently from how the Knowledge might be exploited, the research activity plan is structured as follows:

1. Review of the maritime sensors and the available Knowledge Base (e.g. the context information on the environment in which the target evolves and its related information);
2. Review of the state-of-the-art techniques for Knowledge Base Bayesian filtering;
3. Formulation of mathematical models for the maritime Knowledge Base. The models will be functional to the KB inclusion in data processing techniques and will be based on concise description of the modeled elements. These descriptors will encode the impact over the static/dynamic target system in terms of affected parameters, constraints or exercised forces;
4. Design and development of data simulators for the addressed scenarios, which will extend the conventional target dynamics simulations in order to include the features addressed in the KB models.
5. Design of innovative filtering techniques in the framework of the target tracking tasks (i.e. prediction/association/update), which exploit the identified KB elements;
6. Definition of suitable measures of performance in order to assess the improvement

Generally speaking, the Knowledge will be mapped over an N-dimensional domain, which originates from the standard 2D spatial domain in which the targets evolve.

The spatial domain will contain the local distribution of the effects of each modeled "knowledge" element. Similarly, target feature domains (e.g., kinematics or target shape) will be formed in order to encode the effect that each modeled element has on that specific attribute. Data processing will be then conducted conventionally over the 2D domain, or over the N-dimensional domain.

In order to demonstrate how the use of the KB brings improvement to specific aspects, real maritime surveillance applications that rely on different sensors will be considered:

- Active Radar Surveillance in Coastal Areas;
- Collaborative Vessel Traffic Monitoring In High Seas and Coastal Areas;
- Passive Radar Surveillance in Coastal Areas.

1.2 Work Structure

The work in this Thesis is structured as follows.

Chapter 2 reviews the requirements dictated by the maritime domain to guarantee a certain level of Maritime Domain Awareness (MDA). Then it provides an overview of the sensors available for the maritime surveillance, including both in-situ and space based sensors, with a special focus on active and passive radar technologies since they represent the basis for consolidated vessel monitoring techniques such as Vessel Traffic System (e.g. active coastal radars) and innovative solutions for surveillance at sea (the passive radars). Finally, this Chapter summarizes the Knowledge Based elements that could be taken into account in the design phase of innovative vessel tracking algorithms.

Chapter 3 recalls the fundamental of the data processing technique used in this thesis. Specifically, the Bayesian target tracking methodology is addressed, with a special focus on the various tracking filters (linear and non-linear) and data association strategies used in this research work. Also the measures of performance usually adopted to evaluate the vessel tracking algorithm results are presented in the Chapter. Specifically, the evaluation instruments to compare different knowledge-based filtering techniques and to evaluate the tracking results with respect to the non KB applications are provided.

Chapter 4 introduces the concept of constrained Bayesian filtering, whose theoretical formulation represents the basis for the context based target tracking techniques developed in this research work. Specifically, it is shown how hard constraints can

be included both in the prediction step and the update step of the Bayesian recursion, bringing to the same result form the Bayesian perspective. Some state-of-the-art algorithms are also recalled in the Chapter. They include two basic examples of general purpose algorithms that exploit the context in the prediction and in the update steps, respectively. Moreover, other KB algorithms tailored for ground vehicles target tracking applications are also reported.

Chapter 5 presents the knowledge based tracking filters designed for maritime surveillance applications. These filters incorporate different KB elements, being some of them a priori known, like the geographic information about coastline and ports, and other online estimated and/or received during the data processing task itself, such as the identification number of the vessel or the destination port, usually contained in messages provided by cooperative maritime information data sources (e.g. Terrestrial and Satellite AIS, LRIT, etc.). The mathematical model of the knowledge is derived and the filters modified properly to handle its inclusion. As already mentioned, the knowledge can affect the prediction or the update step in the filter, or can also have an impact on the target detection task. Examples of these possibilities are provided in the Chapter.

Chapter 6, **Chapter 7** and **Chapter 8** are devoted to the presentation of maritime surveillance applications in which the derived KB filters have been used to track the vessels. Such applications are related to real exemplary scenarios in which the targets evolve and deal with different kinds of sensor. Specifically, the problem of tracking vessels in coastal areas in presence of intermittent sensor measurements from active radars is addressed in the Chapter 6. Chapter 7 deals with the traffic monitoring in coastal areas and high seas in presence of discontinuous data from collaborative data sources (i.e. AIS). Finally, Chapter 8 addresses the same problem but dealing with a monitoring system based on the passive radar technology. For all the applications, it is demonstrated how the exploitation of KB filters allows the vessels monitoring task also when gaps of measurements are experienced, improving the tracks continuity and the quality of the overall maritime picture. Moreover, the use of the context information in the tracking filters leads to the reduction of the false tracks rate in the area. Finally, for the vessel monitoring in remote areas application (which is presented in Chapter 8), it is shown how the knowledge of geographical information about the coastline and the possibility to resort to passive radar vessel detections instead of satellite based sensors measurements, bring to a continuous maritime picture.

Chapter 9 contains the conclusions of this work. The major achievements and results are here summarized and the possible extensions for future work are finally presented.

CHAPTER II

Fundamentals of Maritime Situational Awareness

According to the NATO definition [NAT08], the Maritime Situational Awareness is defined as *"the understanding of military and non-military events, activities and circumstances within and associated with the maritime environment that are relevant for current and future NATO operations and exercises where the Maritime Environment (ME) is the oceans, seas, bays, estuaries, waterways, coastal regions and ports"*. The International Maritime Organization (IMO) is using a similar concept; IMO defines Maritime Domain Awareness (MDA) as *"the effective understanding of anything associated with the maritime domain that could impact the security, safety, economy, or environment of the sea"*, [Off07]. In the latter definition, the maritime domain includes all areas and things of, on, under, relating to, adjacent to, or bordering on a sea, ocean, or other navigable waterway, including all maritime-related activities, infrastructure, people, cargo, and vessels and other conveyances.

No matter of the definition used, MSA results from intelligence capabilities, policies and operational relationships used to integrate all available data, information and intelligence in order to identify, locate, and track potential threats to maritime interests. MSA provides accurate, relevant and collaborated maritime threat information to operational and law enforcement entities, supporting a variety of tactical, operational, and strategic requirements. MSA results from persistent monitoring of maritime activities in such a way that trends can be identified and anomalies detected. It is a layered picture of the current state and trends that includes information pertaining to MSA pillars (vessels, cargo, people and infrastructure) and related economic and environmental issues. The most important step to achieve Maritime Security is the improvement of collaboration for enhanced Maritime Situational Awareness, both be-

tween nations and organizations, but also between various agencies within the same nation or organization. Without a comprehensive and mutually shared understanding of what is occurring in the maritime environment, vital opportunities to detect and mitigate threats at global scale or critical vulnerabilities at the earliest opportunity may be lost.

Although collaboration and information sharing are complicated, everyone is in agreement that it is required for effective MSA. Success in MSA hinges on the ability to work together and on the ability to use sensor resources in an intelligent way, both by getting the most possible out of sensors used today and by finding new sensors capable of contributing to greater situational awareness.

One of the main and widespread service supporting the maritime situational awareness is the **Vessel Traffic Service** (VTS) [oMAtNI16], which is designed with the objective to (i) aid the mariner in the safe and efficient use of navigable waterways (**Safety of Navigation**), (ii) afford unhindered access to pursue commercial and leisure activities (**Unhindered Access**), and (iii) contribute to keeping the seas and adjacent environment free from pollution (**Clean Seas and Waterways**). Vessel traffic services are provided by VTS Operators within a designed area, which could be restricted to a port or harbour (i.e. Port-VTS) or extended to the coastal environment (i.e. Coastal-VTS). A Port-VTS is mainly concerned with vessel traffic to and from a port or harbour or harbours, while a Coastal-VTS is mainly related to vessel traffic passing through the area. A VTS could also be a combination of both types, [(IM97]. An example of a VTS Operative Center is hereafter reported.

Figure 2.1: VTS operative center (picture taken from coastalsafety.com/vessel-traffic-services-vts/).

Whatever the case, different functions, internal and external, have to be performed to implement the service. The internal functions concern all the activities to enable a VTS to operate. Data collection, data evaluation and decision-making tasks belong to this group. The external functions are executed with the purpose of influencing the vessel traffic characteristics. They relate to the primary traffic management functions of rule-making, allocation of space, routine control of vessels and manoeuvres to avoid collisions, as well as to other management functions (i.e. enforcement, remedial and ancillary activities).

By the way, the most important functions of a VTS are those related to, contributing to and thereby enhancing the activities listed in the first column of the Table 2.1. Specifically, Table 2.1 shows how these activities are linked to the three VTS objectives listed before.

Table 2.1: Relationship between VTS functions and VTS objectives.

	VTS Objective		
Activities	**Safety of Navigation**	**Unhindered Access**	**Clean Seas and Waterways**
Safety of Life at Sea	X	-	-
Safety of Navigation	X	X	X
Search and Rescue	X	-	-
Efficiency of Vessel Traffic Movement	X	X	X
Protection of the Marine Environment	-	-	X
Supporting Maritime Security	X	X	-
Supporting Law Enforcement	X	X	X
Protection of Adjacent Communities and Infrastructure	-	-	X

Based on the VTS objectives, three types of vessel traffic services are provided to the maritime Users: the Information Service (IS), the Traffic Organization Service (TOS) and the Navigational Assistance Service (NAS), [oMAtNI12]. The IS involves maintaining a traffic image and allows interaction with traffic and response to developing traffic situations. It provides essential and timely information to assist the

on board decision-making process. The TOS prevents the development of dangerous maritime traffic situations and provides for the safe and efficient movement of vessel traffic within the declared VTS area. It concerns the operational management of traffic and the planning of vessel movements and is particularly relevant in times of high traffic density or when vessel movements may affect the traffic flow. Finally, the NAS provides essential and timely navigational information to assist in the on board navigational decision-making process and to monitor its effects. It may also involve the provision of navigational advice and/or instruction.

In order to provide the services, a **VTS System** (i.e. hardware, software and their behaviour as a coherent entity, excluding personnel and procedures) has to be set up. A VTS system is a complex system which typically comprises one or more of the following elements:

- Radio Communication;
- Sensors (e.g. Radar, Automatic Identification System, Environmental Monitoring, Electro Optical Systems, Radio Direction Finder, Long Range Sensors);
- Data Processing;
- VTS Human/Machine Interface;
- Decision Support;
- External Information Exchange.

To this aim, the VTS Authority defines (in accordance with the IALA Recommendation V-119 [oMAtNI09]) the operational requirements and the associated validation requirements that should be applicable to all parts of the VTS system. They should delineate the VTS areas and sub-areas or sectors in which one ore more VTS Services (IS, TOS, NAS) have to be provided, together with the types and sizes of vessels which are required or expected to participate in the VTS. The requirements should also address the navigational hazards and traffic patterns and the human factors including health and safety issues. The tasks to be performed by System users, the operational procedures and the cooperation with external stakeholders are important frameworks to the requirement definition process. Finally, the business continuity, availability, reliability and disaster recovery and all the legal related issues have to be taken into account. Availability and reliability figures for the overall system should be defined by the VTS authority based on the risk assessment results, from which individual equipment reliability may be derived. The availability is defined in IMO Resolution A.915 (220 Ref.40) as: *"The percentage of time that an aid, or system of*

aids, is performing a required function under stated conditions. The non-availability can be caused by scheduled and/or unscheduled interruptions". Availability = (service time - out of service time) / service time.

Once the operational requirement are defined, they may be grouped in different classes in order to facilitate the derivation of the technical requirements (e.g. the functional requirements) at system level. The definition of the technical requirements as well as the determination of a provisional system concept may follow an iterative process. The derived technical requirements are also grouped in different classes, for example:

1. The VTS centre, sites, sensors and processing;
2. Recording and replay including the post situational analysis;
3. Redundancy and Resilience.

Specifically, this work will address the requirements related to the first item of the above list, i.e. the VTS sensors and the sensor data processing, with a special focus on the target tracking capability. Thus, some sensors used in a VTS system (e.g. active radar and the Automatic Identification System) are described in the following section and some related technical requirement are presented. Other sensors supporting the MDA but not included in a VTS system are also described.

2.1 Maritime Surveillance Sensors and Related Technical Requirements

2.1.1 Active Radar

Active radars (AR) widely support maritime surveillance applications and the Vessel Traffic Service (VTS). Specifically, they support the following operational functions of the maritime service: (i) Path, time and track prediction, (ii) Evaluation of the Closest Point of Approach (CPA) and the Time to Closest Point of Approach (TCPA), (iii) Anchor Watch, (iv) Vessel Vector determination, (v) Course, Speed and Identity evaluation, and (vi) alerting collisions.

These radars are non-coherent sensors in S- (2.0-4.0 GHz), X- (8.0-12.0 GHz), and recently K-band (18.0-27.0 GHz), as reported in [Bri04]. Their performance requirements are highly influenced by target and scenario characteristics, e.g., ship size, traffic density, sea state and atmospheric clutter conditions. Generally, X-band systems provide a high resolution performance, whereas S-band radars are less affected by rain and fog.

Figure 2.2: VTS radar tower in Hamburg (Germany) (picture taken from the web, www.lightphotos.net/photos/index.php).

As the **detection and measurement capability** is concerned, theses radars should be able to detect and track all types of surface objects defined by the VTS authority in normal weather conditions. As already mentioned, such capabilities depend on the characteristics of the radar and the target. Table 2.2 illustrates typical target parameters, including reflection characteristics, and identifies the detection capabilities required for differing types of targets.

The standard **detection range**, dictated by IALA guidelines, goes from few nautical miles (e.g. 3NM) for rubber boats up to tens of miles (e.g. 25NM) for cargoes and cruise ships, depending on the antenna elevation and on the sea state. The **acquisition rate** is variable depending on the antenna rotation speed, typically varying from $10rpm$ for long range to $25rpm$ for short and medium range applications. As the radar resolution capabilities are concerned, the **angular resolution**, which depends on the antenna dimensions, varies from 0.6° and 1.2° for the X-band radar, and from 1.8° and 4° for the S-band. The **range resolution** (which is tens of meter) is poor and usually limits VTS radars identification capabilities. Powerful radars, which fully exploit coherent processing in order to achieve better performance (i.e. larger coverage in range, higher spatial resolution and better target identification), are deployed by military corps to monitor strategic coastline locations.

Table 2.2: Target reflection characteristics.

Target Type		**Design Requirements**		
		Radar Cross Section		**Height of Target**
		S-Band	**X-Band**	
1	Aids to Navigation etc. -without radar reflector. Small open boats, fiberglass, wood or rubber with outboard motor and at least 4 meters long, small speedboats, small fishing vessels, small sailing boats and the like.	–	$1m^2$	$1m$ ASL
2	Inshore fishing vessels, sailing boats, speedboats and the like.	–	$3m^2$	$2m$ ASL
3	Aids to Navigation with radar reflector.	$4m^2$	$10m^2$	$3m$ ASL
4	Small metal ships, fishing vessels, patrol vessels and the like.	$40m^2$	$100m^2$	$5m$ ASL
5	Coasters and the like.	$400m^2$	$1000m^2$	$8m$ ASL
6	Large coasters, bulk carriers, cargo ships and the like.	$4000m^2$	$10000m^2$	$12m$ ASL
7	Container carriers, tankers etc.	$40000m^2$	$100000m^2$	$18m$ ASL

An important issue is represented by the requirement posed by the VTS authority with respect to the **plot extraction** and **tracking**. Plot extraction, i.e. the process of detecting and determining the target characteristics such as kinematics and intensity by analyzing the radar signal, should be automatic (see IALA Guideline [oMAtNI07a]) and should provide a minimum of plots per rotation which vary according to the basic, standard or advanced recommendation level. The implementation of clutter and noise reduction techniques (i.e. white noise suppression, interference rejection and sea and rain clutter processing adaptation to varying propagation conditions) help in keeping the number of the extracted plots in line with the performance requirements. The extracted plots are considered potential targets and they could be associated with the previously established tracks or they could initiate new tracks, i.e. tentative tracks. Then, if the plots from the consecutive radar scans are associated to those tentative track, they become confirmed tracks, otherwise they are discarded. The process of track initiation, confirmation and maintenance goes under certain conditions of Probability of Detection (P_D) and Probability of False Alarm (P_{FA}). Table 2.3 reports the most important radar track performance parameters, together with the minimum P_D value for the track initiation. For track maintenance a lower minimum P_D can apply and a $P_{FA} \leq 0.01$ should be considered. Finally, a confirmed track is terminated if one of the following conditions apply: (i) it moves outside a user defined maximum range or into a user defined non-tracking area, (ii) track's quality falls below a predefined threshold, or (iii) the track cannot be updated with new plots over a certain length of time.

The radar system should also manage the presence of **false tracks**, which may appear as result of disturbances (e.g. noise, clutter and ghost echoes). In this case the requirement on the maximum number of allowed false track depends on the application. They should be totally avoided in safety areas and kept under a low threshold for surveillance and traffic monitoring applications.

Moreover, in proximity of occlusion areas, the radar system could not be able to track the targets. The **track loss** occurs when the $P_D < 1$ in combinations of target manoeuvres. Usually the VTS operator should correct manually this problem and this should be done only once per hour in the areas subject to the requirements of Table 2.3.

Also the **track swap** and **merging** phenomena (i.e. swapping track identity or merge tracks of different targets when they move close together) could occur and usually manually corrected by the operator.

Table 2.3: Radar tracking performance parameters.

Plot Extraction and Tracking Performance for each individual radar in a system				
		Recommendation Level		
Parameter		**Basic**	**Standard**	**Advanced**
Number of plots per antenna rotation		≥ 1000	≥ 2500	≥ 5000
Number of confirmed tracks		≥ 100	≥ 200	≥ 300
Minimum Radar P_D for track initiation		0.9	0.8	0.7
Time for confirmation of tentative track		≤ 1 minutes		
Time from track confirmation to achievement of specified accuracy		≤ 2 minutes		
Time from data loss to automatic track termination		≥ 1 minutes		
Speed of tracked objects		≤ 50 knots		≤ 70 knots
Turn rate of tracked objects		$\leq 10°$/second		$\leq 20°$/second
Accuracy in track position	Range	$\leq$ 0.75 % of range covered by the individual radar or 10m + selected pulse length, whichever is the greater		$\leq$ 0.5 % of range covered or 5m + pulse length
Accuracy in track position	Bearing	$\leq 1°$ in X-band; $\leq 2°$ in S-band		$\leq 0.5°$ in X-band; $\leq 1°$ in S-band
Accuracy of track data	Speed	≤ 2 knots	≤ 1 knot	≤ 1 knot
Accuracy of track data	Course	$\leq 5°$	$\leq 2°$	$\leq 2°$

Finally, the track data are delivered together with radar image data and eventually clutter data as output of the VTS radar service.

2.1.2 Automatic Identification System

The Automatic Identification System (AIS) is a shipboard broadcast system that acts like a transponder, operating in the Very High Frequency (VHF) maritime band. It is a mandatory navigation safety communication system under the provisions of the International Convention for the Safety of Life at Sea (SOLAS), [Org80], which requires ships of 300 gross tonnage and upwards engaged on international voyages, cargo ships of 500 gross tonnage and upwards not engaged on international voyages, and all passenger ships to be fitted with transponders that broadcast the position of the ship and the identification number of the ship. Smaller vessels may voluntarily carry Class B AIS transponders, which transmit less information than Class A transponders but still including position, vessel type and identification, speed and heading. Approximately, 70000 ships worldwide are equipped with Class A AIS. In April 2009 the EU passed legislation[1] requiring all EU fishing vessels over $15m$ length to be Class A AIS equipped by mid-2014, and the US is also moving to expand the range of vessels required to carry AIS. Not only ships but also Aids to Navigation (AtoNs) are equipped with AIS. The structure of the AIS is depicted in Figure 2.3.

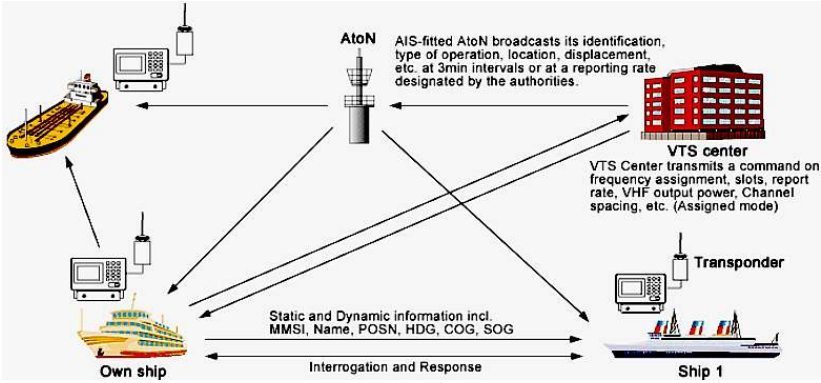

Figure 2.3: Automatic Identification System (AIS) (picture taken from the web, www.bluebird-electric.net).

[1] Directive 2009/17/EC of the European Parliament and of the Council of 23 April 2009, amending Directive 2002/59/EC establishing a Community vessel traffic monitoring and information system.

AIS data are not encrypted, hence publicly available with relatively simple AIS receiving equipment. Protocols for data interpretation can be found in the relevant Directives or through the Internet. AIS equipped ships broadcast many information, including position (to GPS accuracy), time, navigational information (heading, course over ground, speed over ground, rate of turn, etc.) and ship identity (MMSI number, call-sign, name, type of ship, etc.). This information can be received by other ships, aircraft, satellite or terrestrial base stations, and displayed on electronic chart data. Originally intended to help avoid ship collisions, AIS has a far higher reporting rate than other systems like VMS, from once every 6 minutes down to every 2 seconds. However, its range is currently limited to 20-100NM. The frequency of AIS transmissions increases with speed as reported in Table 2.4, [IR14].

Table 2.4: AIS message frequency transmission.

Ship Speed	**Transmission Rate**
Ship at anchor	3 minutes
Ship with speed 0-14 knots	12 seconds
Ship with speed 0-14 knots and changing course	4 seconds
Ship with speed 14-23 knots	6 seconds
Ship with speed 14-23 knots and changing course	2 seconds
Ship with speed $>$ 23 knots	3 seconds
Ship with speed $>$ 23 knots and changing course	2 seconds

It is required, that every ship fitted with AIS shall maintain AIS in operation at all times except where international agreements, rules or standards provide for the protection of navigational information. The AIS standard calls up to 26 different types of AIS messages, summarized in Table 2.5.

In the VTS framework, the AIS service is intended to enhance safety of life at sea, the safety and efficiency of navigation and the protection of the marine environment. The service should provide timely, relevant and accurate information to users to support the decision-making processes of a VTS. This information foresees vessel data (i.e. vessel position reports and movement information) and the status on AIS equipment and management functions for the control of the AIS network. The quality of the transmitted information to the mariners in a crucial point for the AIS, as well as other aids to navigation and tools, pilotage systems and navigation management systems. The reliability of information transmitted and received via AIS is one major lack of the system. The validity of AIS data received from ships is dependent on the proper installation of AIS, correctly interfaced and functioning ship's equipment, and correct

manual input of static and voyage-related data. Detailed studies into ship courses related to AIS data performed in the area of the Baltic showed that destination, estimated time of arrival (ETA) and also draught data are often faulty (up to an amount of 40%). These spotlight results were proved by another case study end of February 2004 in major European ports. Nearly 50% of the observed targets had navigational status errors (p.54 of IMO Model Course).

Table 2.5: AIS message types.

Message Categories	**Fields**	**Reporting Intervals**
Position reports (types 1,2,3,4,18,19)	Ship ID (MMSI) GPS Position Course over Ground Speed over Ground Rate of Turn	2 seconds at full speed (>23knots) 6 seconds at speed of 14-23knots 10 seconds < 14knots 3 minutes at anchor
Static/Voyage reports (types 5,24)	Ship ID (MMSI) Name IMO Call Sign Length Destination ETA	6 minutes or when data amended
AToNs (type 21)	Ship ID (MMSI) Type GPS Position AtoN status	3 minutes
Search and Rescue Aircraft (type 9)	Ship ID (MMSI) Name GPS Position Speed Altitude	10 seconds
Safety (types 12,13,14)	various	as required
Binaries (types 6,7,8,25.26)	various	as required

2.1.3 Satellite Automatic Identification System

Operating in the VHF range, the AIS transponders on board ships are very effective cooperative data sources for monitoring coastal and territorial waters from shore-based base stations (within a 35-50NM horizontal range). Through the installation of ad hoc AIS receivers on board a network of Low Earth Orbit (LEO) satellites, the Satellite AIS (S-AIS) has extended the coverage of the AIS system over the global seas, and it is now a powerful, standardized and proven technology for vessel traffic monitoring. The satellite receivers are fully compatible with existing AIS transponders, not needing any additional changes to existing ground-based equipment, see [ORB]. In general terms, the infrastructure of the companies providing S-AIS services consists of earth-orbiting satellites, associated ground stations and data processing systems (e.g. Figure 2.4).

Figure 2.4: exactEarth infrastructure for the operation of satellite-based AIS for vessel monitoring (picture taken from the web, www.exactearth.com/technology).

Thus, the AIS services applications on vessel monitoring, security, environment and Search & Rescue are extended to a global framework through the use of satellites, [exa15a]. As consequence, the navigation service provided by the S-AIS is dictated to the satellites' revisit frequency (e.g. position of satellites and locations of the ground stations to downlink the information). This was one of the S-AIS major limitation: the S-AIS reports were made available to the operators with a half hour-delay on average. Nowadays, with the recent expansion of some satellite constellations (Figure 2.5), a real-time global maritime vessel detector and tracker is a reality.

Figure 2.5: Real time satellite global coverage (picture taken from the web, www.exactearth.com/technology).

The companies exactEarth Ltd. (one of the major provider of S-AIS services) and Harris Corporation have recently delivered the exactView^{TM} product, [exa15b], which is able to combine the simultaneous global satellite coverage and the instantaneous downlinking of AIS information, providing a real time global ship tracking in 1 minute (Figure 2.6). This responds to the ever-growing demand for an immediate MDA and it brings an enormous contribution in enhancing the safety of life at sea and the efficiency of navigation.

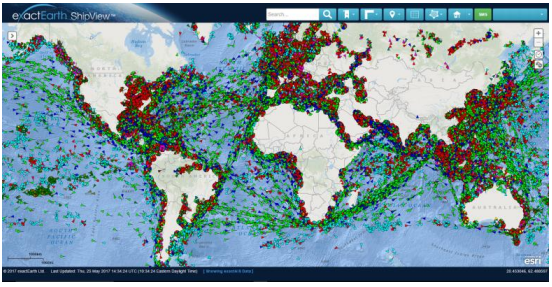

Figure 2.6: exactEarth-RT (Real Time) global vessel detection and tracking (picture taken from the web, www.exactearth.com/technology).

2.1.4 Long Range Identification and Tracking

The Long Range Identification and Tracking (LRIT) system is designed to collect and disseminate vessel information on identity and position received from the International Maritime Organization (IMO) member States ships that are subject to SOLAS Convention [Org80]. Ships on international voyages including cargo ships of 300 gross tonnage and upwards, passenger ships, and mobile offshore drilling units have to be equipped with the system. The LRIT concept is based on satellite communications, enabling the coverage extension if compared to coastal monitoring systems. The overall LRIT system is depicted in Figure 2.7.

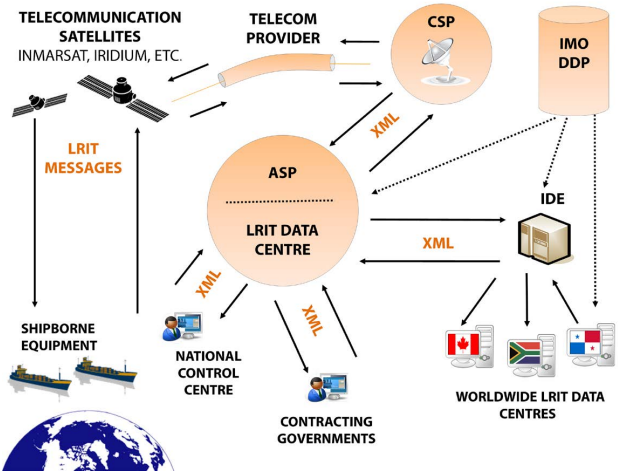

Figure 2.7: LRIT system components.

The LRIT shipborne equipment transmits position information to the Communication Service Provider (CSP), which provides the communication infrastructure and services to ensure the end-to-end secure transfer of the LRIT message between the ship and the Application Service Provider (ASP). The ASP provides a communication protocol interface and add information to the LRIT message between the CSP and the LRIT Data Centre. Here the information is collected and then forwarded to the Users in according to the LRIT Data Distribution Plan (LRIT DDP), which defines rules and access rights (i.e. which users can receive what LRIT information). Finally, the International LRIT Data Exchange (IDE) routes the information between Data Centres according to the DDP, [Age15].

Requirements for LRIT equipment are specified in [(IM08]. An LRIT message is transmitted from the ship via its shipborne equipment which includes the identity of the ship, the ship's GNSS position (based on the WGS 84 format), date and time associated with the GNSS position. Further ship identifiers (e.g., the IMO identification number, the MMSI number, the ship name), other timestamps, and the LRIT Data Centre identifier are added by the application service provider as the data travels through the LRIT system network. The system specifies that Flag States should ensure as a minimum that four position messages per ship per day (every 6 hours) are sent, stored, and are made available for others countries entitled to access LRIT information.

Differently from the other self-reporting system (i.e. the AIS system), the ship data are not broadcasted, but collected by the appointed authorities, therefore allowing a higher security of information exchanged. As already mentioned, the LRIT default ship reporting rate is every six hours (but end users are allowed to request on-demand the current vessel position), while the AIS reports are delivered at a rate that is appropriate to the speed of the vessel. This difference is mainly related to the aim of both systems: AIS is meant to be used to avoid ship collisions while LRIT is used to monitor certain ships of interest to the state. As presented in [Lap14], LRIT data could present anomalies related to the ship's identification information (e.g. wrong IMO number, fake MMSI, fields left blank). These errors could derive from an incorrect process of adding information to the LRIT message by the ADS. Also the timestamps could presents deviation from what described in the specification [(IM08].

2.1.5 Space Earth Observation Sensors: Satellite-Synthetic Aperture Radar

In recent decades there was a major increase in the amount of satellites launched with the purpose of gathering information on the earth surface. The number of sensors that are currently available and the technological advances achieved, make it possible to gather more and accurate information, almost in real-time. The collected information from these sensors is of great value to a variety of activities in the scientific community and to the private sector. The European Union's Earth Observation Programme Copernicus ([Cop]) for example, offers information services based on in situ (non-space) and satellite Earth Observation data for six different applications, including security aspects in the maritime surveillance. The Copernicus Maritime Surveillance (CMS) Service, implemented by the European Maritime Safety Agency (EMSA), has again the main objective to guarantee the safety of navigation, to support to fisheries control, to combat marine pollution and law enforcement at sea (Figure 2.8). Copernicus is served by a set of dedicated satellites (the Sentinel families [Cop]), which

are developed for the specific needs of the programme, and contributing missions (existing commercial and public satellites).

Figure 2.8: Copernicus Maritime Surveillance (CMS) Service Tasks (picture taken from [Age18]).

Several LEO platforms (e.g. TerraSAR-X, Radarsat-2, COSMO-SkyMed, etc.) are indeed equipped with Synthetic Aperture Radar (SAR) sensors that continuously collect data over sea regions. Generically speaking, SAR is a coherent active microwave remote sensing technique able to provide bi-dimensional reflectivity images of large areas (some tens of kilometers) with fine resolutions (at the order of meters). Each pixel within the image gives a complex reflectivity value that can be related with the geometrical and physical structure of the imaged scatterers. Two dimensions define the image, namely: the azimuth dimension fixed by the path of the sensor and the range dimension fixed by antenna pointing. Images of the sea surface are formed in near real time (NRT) and delivered to ground stations mostly in Europe, Canada and

US. Then, service providers offer services related to (i) Ship Detection, Identification and Classification, (ii) Oil Spill Detection and (iii) Ice Monitoring. Such services can also support the identification of anomalous behaviours, such as AIS data spoofing or the presence of ships in forbidden areas. An example of SAR images from TerraSAR-X and Radarsat-2 in reported in Figure 2.9(a) and Figure 2.9(b), respectively. The detections are indicated with cyan and red dots. While the red points represent for sure ships (detections have been validated by meas of other sensors, e.g. AIS), the blue ones can be either vessels or false detections/alarms.

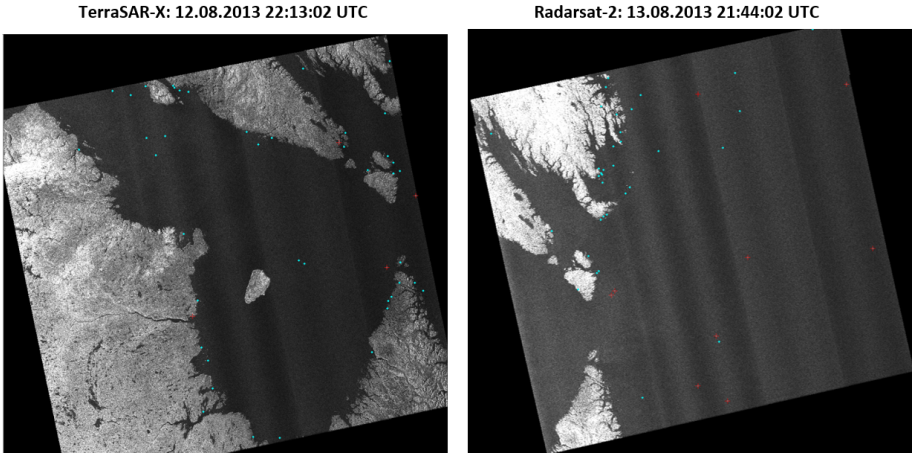

Figure 2.9: SAR Images from TerraSAR-X (a) and Radarsat-2 (b).

Typical features of SAR products are: (i) spatial resolution ranging from 1 m to 100 m; (ii) swath widths from 10 km to 500 km; (iii) multi-satellite revisit rate for the same site that varies from one to three days depending on the observed area. The main limitations in Earth Observation data exploitation reside in (i) long revisit times offered by satellites with respect to vessel traffic monitoring requirements, (ii) product delivery time hindered by supervised processing strategies, and (iii) difficult trade-off between False Alarm Rate (FAR) and the probability of detection.

2.1.6 Passive Radar

Passive radar technologies have gained relevance in recent years, since they finally transited from the role of scientific demonstrators to commercial products for air and maritime surveillance. Such devices work by nature as bistatic radars (i.e., systems

with separate location of transmitter and receiver) and do not "pollute" the electromagnetic spectrum, since they do not emit any signal. They exploit indeed signals that are already present in the Area of Interest (AoI), which are usually referred to as "illuminators of opportunity". Examples are Radio/TV signals [HMR05,How99], digital radio and television (DAB, DVB) signals [SC05], GSM signals [TSL+05], wireless local area network (WiFi) signals [GWB08], and satellite broadcast [GBB+02]. Few studies proposed WiMAX-based passive radar for MSA purposes [WLH09,CWGS10]. They addressed passive radars as promising for maritime surveillance applications: the simulations demonstrated specific scenarios where WiMAX radar may be used as a low cost surveillance device for detecting both small and large marine vessels in port areas and open waters. The combination of such sensors with conventional active radars could potentially expand the coverage of coastal systems while introducing significant cost savings.

Despite the absence of own transmitted waveforms, they are capable of detecting moving targets by Passive Coherent Location techniques (PCL, [GB05]). A PCL system comprises a receiving unit that extracts from the electromagnetic environment both the reference signal (direct path from the illuminator of opportunity) and the surveillance signal, the latter being a reflection from the moving target. Then, it generally compares the reference and surveillance signal by correlation and calculates the bistatic range difference or Time Difference of Arrival (TDoA) and the Doppler frequency. A series of these measurements allows estimating the position and the velocity of the target. Even though the waveform is not optimal for the specific surveillance application, the achieved results are valid at operational level, and such systems demonstrated to effectively complement active systems in areas that cannot be polluted by additional transmissions. One of the drawback of PCL systems is related to the bistatic geometry of the system: the passive range-only position estimation is ambiguous, since it appears as an iso-range 2D ellipse. If a second dislocated transmitter is available, the intersection of the two ellipses can reduce the ambiguity down to two positions. The ambiguity can be also reduced to two positions if an additional estimate of the direction of arrival (DoA) measurement is taken into account. The first position represents the true target and the second one acts like a "ghost" that can only be discarded if advanced tracking techniques are applied ([Bro12]). This leads to favoring the use of networks of PCL sensors (receivers) that collaborate in the detection and tracking tasks. This raises the complexity of the data processing techniques to support such an amount of heterogeneous data. Due to the complexity of the sensor geometry and the related processing scheme, the PCL application is very likely to suffer from phenomena such as false positives, ghost tracks, lack or inter-

mittence of data. To this aim, the contribution coming from an external Knowledge might represent the key for wider deployment of this technology.

Figure 2.10: Fraunhofer FKIE experimental passive radar system based on GSM signals.

2.2 Maritime Knowledge Base Description

The main target in maritime surveillance is to enable the automatic monitoring, analysis and understanding of activities at sea, i.e. the MSA. As previously mentioned, ancillary information or higher level of abstraction are to be used in order to combine information "bits" with common origin but different in nature, time and/or space. In this perspective the availability of an accurate Base of Knowledge might have a significant role.

As defined in [GR08] a knowledge based system uses a priori information to improve the performance of deterministic and adaptive systems. Although the exact form of this a priori knowledge is problem- dependent, a Knowledge based system consists of a knowledge base containing information specific to a problem domain and an inference engine that employs reasoning to yield decisions. The first applications of Knowledge-base to adaptive radar techniques have been pioneered in 2002 by the Defence Advanced Research Projects Agency (DARPA) in US, in the frame of the

Knowledge aided Sensor Signal Processing and Expert Reasoning (KASSPER) program, which focused on Ground Moving Target Indication (GMTI) and Synthetic Aperture Radar (SAR) algorithms for military applications. A series of lectures have been devoted to KB-radar signal and data processing by NATO RTO in 2003-2006 to promote cooperation on this topic. Several publications resulted from this research effort of several scientists in the world. An interesting application of Knowledge-base in tracking systems has been formulated and experimented by the Authors in [GR08]. Specifically, they resort to a wide Knowledge Base consisting of:

- Geographical maps;
- Meteo maps;
- Road maps;
- Clutter maps;
- Target characteristics, such as maximum speed.

This knowledge was injected - as a set of rules - into the measurement, association and identification steps of the processing scheme.

If we focus on maritime domain, it is quite straightforward to define the boundaries of the problem. Looking at the synthetic data extracted by EU Scientists in the frame of the Blue Hub project (bluehub.jrc.ec.europa.eu, Figure 2.11), it is evident, how the maritime traffic itself follows some unwritten rules.

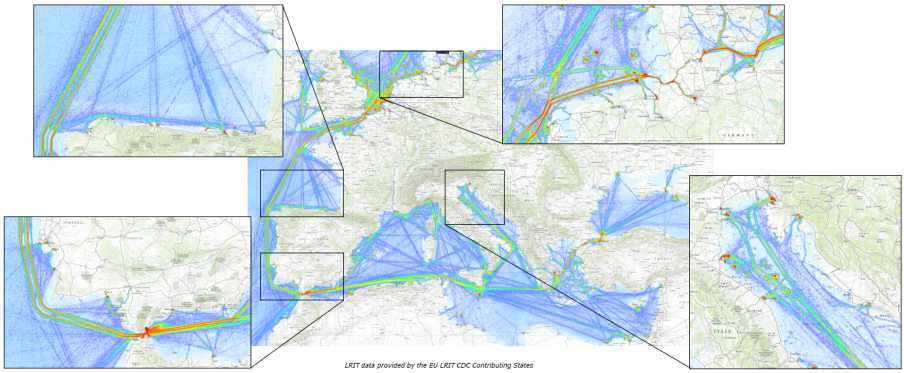

Figure 2.11: European Commission Blue Hub - Transform data into knowledge, [ea14].

Several “un-sensed” elements have or are expected to have influence on the evolution of the maritime traffic; these represent sources of a priori information that can be used in target inference. A priori information is to be intended as any knowledge on the observed scenario, which is collected before the measurement and estimation process; it can be either statically (once before the observation period) or dynamically (before each traffic picture update) collected. Very well known example of a priori information is the geographic map of roads, along which moving targets are expected to move. This knowledge is effectively used in GMTI applications, [UK06]. As the maritime scenario is concerned, numerous elements potentially contribute to the Base of Knowledge building up. Following the considerations reported by the Authors in [VSB+08], Table 2.6 and Table 2.7 summarize key sources of a priori information. Estimation of different degrees of inference might exploit different bases of knowledge. The identification of the best composition of the base for a given estimation process is beyond the scope of this work.

Table 2.6: A priori information for maritime domain (part I).

A priori Information	**Information Source**	**Time Availability**	**Refresh Rate**	**Influence on the Traffic**
Port	GIS-based information is commonly available off-the-shelf	Fixed	Pre-loaded before fusion	Origin / Destination of main traffic routes
Coastline	GIS-based information is commonly available off-the-shelf	Fixed	Pre-loaded before fusion	Routes parallel to the coast, influence on target kinematics
Highways and Corridors, Interdicted Areas	Info maintained by Maritime Authorities	Updated every season or according to special events (e.g. oil spill, storm, accident)	Pre-loaded before fusion	Constraints on target route
Declared and preferred routes	Info contained in AIS message or provided by shipping companies	Updated every journey for a given ship	Captured from AIS messages or pre-loaded from external sources	Constraints on target route
Target dimensions	Info contained in AIS messages, estimated by active sensors and contained in vessel database	Fixed	Captured from radar measurements, messages or retrieved by database after identification	Influence on target kinematics and behaviour
Traffic separation schemes	Info maintained by Maritime Authorities	Updated every season or according to special events (e.g. oil spill, storm, accident)	Pre-loaded before fusion	Constraints on target route
Kinematic behavioral rules	Info maintained by Maritime Authorities	Updated according to local procedures, rules and special events	Pre-loaded before fusion	Constraints on target behaviour

Table 2.7: A priori information for maritime domain (part II).

A priori Information	**Information Source**	**Time Availability**	**Refresh Rate**	**Influence on the Traffic**
Aid to Navigation	GIS-based information and Nautical Charts are commonly available off-the-shelf	Fixed	Pre-loaded before fusion	Constraints on main traffic routes
Oil spills	Provided in near real time by Authorities and Service Providers	For each detected event	Pre-loaded before fusion, and updated regularly	Constraints on traffic route and target behaviour
Clutter conditions	Provided in near real time by Authorities and Service Providers	For each anomalous event or routinely	Pre-loaded before fusion, and updated regularly	Constraints on traffic route and target behaviour
Target Behavioral Models	No source available, models can be extracted from navigation procedures	Fixed, depending on geographic location	Pre-loaded before fusion (self-cognitive systems might help)	Constraints on target intent
Maritime Target Database	No source available	Typical radar and Earth Observation signatures to be collected	Queries during target identification process	Constraints on target behaviour and intent

2.3 Summary

This chapter introduced the main operational requirements for the addressed surveillance applications and illustrates the key sensors contributing to the data sets. In addition, elements of the knowledge base are presented, which are likely to contribute to the innovative techniques discussed in this work.

CHAPTER III

Fundamentals of Multi-Sensor Data Processing

This Section recalls the fundamentals of the multi-sensor data processing with a special focus on the Bayesian estimation framework, which allows determining recursively the hidden states of a dynamical system on the basis of the observation data (i.e. system measurements). How to integrate a sequence of observations from different data sources into a single best-estimate of the state of the environment represents the basic problem in multi-sensor systems [DW88].

3.1 Bayesian Target Tracking

The estimation process attempts to calculate the statistics of the *state* (i.e. condition of the system as a function of time) of a static or dynamically evolving system based on noisy *measurements* provided by a single or multiple sensors in an optimal manner, i.e., by maximizing a reasonable optimality criterion. Figure 3.1 gives an overview of the relevant components of the general estimation problem.

The **system** is affected by disturbances, i.e. the *system noise* or *process noise*, and possibly by some kind of *control input*. The system state is observed by a **sensor** which is influenced by measurement errors. A **state estimator** processes the noisy sensor measurements and utilizes the knowledge about the system state evolution as well as an adequately chosen sensor output model to obtain an estimate of the system state.

In the following, the basic principle of estimation in the context of *discrete-time linear systems* is presented and briefly explained. Based on the Bayesian formalism,

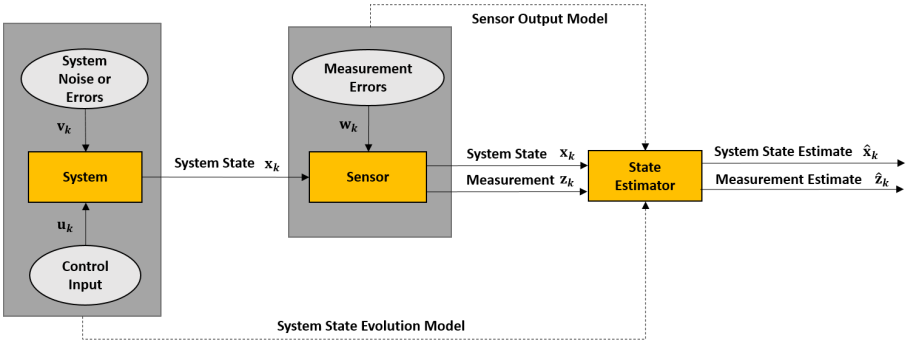

Figure 3.1: Components of the general estimation problem.

the system state described in Section 3.1.1 is sequentially calculated through a two-step estimation scheme, as discussed in Section 3.1.2. A linear state space model can be derived from the state equations, which leads to the Kalman filter type update equations, as shown in Section 3.1.3, The more general non-linear case is discussed in Section 3.1.4. Finally, the problem of data association, which deals with the assignment of the sensor measurement to the target state is addressed in Section 3.1.5.

3.1.1 System Equations

The general state space representation of a discrete-time system evolving from time step t_k to t_{k+1} can be written as [BSLK01, Koc14]

$$\mathbf{x}_{k+1} = \mathbf{f}_k(\mathbf{x}_k) + \mathbf{v}_k \quad , \tag{3.1}$$

where $\mathbf{f}_k$ is a possibly non-linear function of the target state vector $\mathbf{x}_k$, and $\mathbf{v_k}$ is the input disturbance or process noise. The target state and the process noise vectors have dimensions of n_x and n_v, respectively. For simplicity, it is assumed that there is no known input/control $\mathbf{u}_k$ affecting the system. The Equation (3.1) assumes that the system state at time step t_{k+1} depends on the state at time step t_k. If a non-linear relationship between sensor measurements $\mathbf{z}_k$ and system state and an additive stochastic disturbance affecting the measurements are assumed, then the sensor output can generally be written as [BSLK01, Koc14]

$$\mathbf{z}_k = \mathbf{h}_k(\mathbf{x}_k) + \mathbf{w}_k \quad , \tag{3.2}$$

where $\mathbf{h}_k$ is a non-linear function of the target state vector $\mathbf{x}_k$, and $\mathbf{w}_k$ is the measurement noise vector with dimension n_z. The random process and measurement noises in the Equations (3.1) and (3.2) introduce non-deterministic components into the system state equations. Thus, in order to handle the stochastic behavior adequately, it is necessary to formulate the estimation problem within a probabilistic framework.

3.1.2 State Estimation Problem

The general objective of the stochastic problem is to infer the system state $\mathbf{x}_k$ from the available information of noisy sensor measurements $\mathcal{Z}^k = \{Z_1, Z_2, ..., Z_k\}$, with $Z_k = \{\mathbf{z}_k^m\}_{m=1}^{m_k}$ the sensor data at each time step t_k consisting of m_k measurement vectors $\mathbf{z}_k^m$. If we consider $\mathbf{x}_k$, $\mathbf{v}_k$, $\mathbf{z}_k$ and $\mathbf{w}_k$ as random variables, from a Bayesian point of view this estimation problem is solved by the recursive evaluation of the probability density function (pdf) $p(\mathbf{x}_k|\mathcal{Z}^k)$. Such recursion comprises two main steps, the **prediction** and the **update** of the state vector descriptors. Finally a **retrodiction** step allows the refinement of the estimated states and the probability densities functions.

Let us assume that at time step t_{k-1} the *posterior pdf* $p(\mathbf{x}_{k-1}|\mathcal{Z}^{k-1})$ is available. The *prior pdf* $p(\mathbf{x}_k|\mathcal{Z}^{k-1})$, i.e. the prediction density function of $\mathbf{x}_k$, is given by the *Chapman-Kolmogorov* equation:

$$p(\mathbf{x}_k|\mathcal{Z}^{k-1}) = \int p(\mathbf{x}_k|\mathbf{x}_{k-1})\, p(\mathbf{x}_{k-1}|\mathcal{Z}^{k-1})\, d\mathbf{x}_{k-1} \quad , \tag{3.3}$$

where $p(\mathbf{x}_k|\mathbf{x}_{k-1})$ is the the *transitional pdf*, which describes the evolution of the system on the basis of the evolution model in Equation (3.1). Here, the Markov property ([BSLK01, Lof90a]) is assumed for the stochastic process, i.e., the state $\mathbf{x}_k$ at t_k only depends on the state at the previous time step t_{k-1} and all system states $\mathbf{x}_l$ with $l < (k-1)$ are irrelevant for the calculation of $p(\mathbf{x}_k|\mathcal{Z}^{k-1})$.

Once the measurements Z_k at t_k are available, the prior pdf is updated with the new information as a consequence of Bayes rule, ([Koc10]):

$$p(\mathbf{x}_k|\mathcal{Z}^k) = \frac{p(Z_k|\mathbf{x}_k)\, p(\mathbf{x}_k|\mathcal{Z}^{k-1})}{\int p(Z_k|\xi_k)\, p(\xi_k|\mathcal{Z}^{k-1}) d\xi_k} \quad . \tag{3.4}$$

The conditional pdf $p(Z_k|\mathbf{x}_k)$ is the *likelihood function*. It contains the sensor output model in Equation (3.2) and reflects all possibilities to interpret the given sensor output. The denominator in Equation (3.4) serves as normalization factor. The

conditional pdf $p(\mathbf{x}_k|\mathcal{Z}^k)$ is the *posterior density* as it is obtained after computing the normalized product of likelihood and prior density.

Finally, the evaluation of the past pdf $p(\mathbf{x}_l|\mathcal{Z}^k)$, which allows making statements about the past system state $\mathbf{x}_l$ at $t_l < t_k$, is made by combining the object evolution model $p(\mathbf{x}_{l+1}|\mathbf{x}_l)$ with the previous filtering $p(\mathbf{x}_l|\mathcal{Z}^l)$ and prediction $p(\mathbf{x}_{l+1}|\mathcal{Z}^l)$ densities according to:

$$p(\mathbf{x}_l|\mathcal{Z}^k) = \int \frac{p(\mathbf{x}_{l+1}|\mathbf{x}_l)\; p(\mathbf{x}_l|\mathcal{Z}^l)}{p(\mathbf{x}_{l+1}|\mathcal{Z}^l)} p(\mathbf{x}_{l+1}|\mathcal{Z}^k) d\mathbf{x}_{l+1} \quad , \tag{3.5}$$

where the term $p(\mathbf{x}_{l+1}|\mathcal{Z}^k)$ represents the previous retrodiction.

Once the posterior pdf in Equation (3.4) is available, different criteria can be defined to obtain the optimal estimate of the system state. For example, the *minimum mean square error* (MMSE) and the *maximum a posteriori* (MAP) estimators are commonly used. The MMSE estimate is defined as the value of $\mathbf{x}_k$ which minimizes the *mean square error* (MSE) [BSLK01], i.e.,

$$\hat{\mathbf{x}}^{MMSE}(\mathcal{Z}^k) = \arg\min_{\hat{\mathbf{x}}} E\left[(\hat{\mathbf{x}} - \mathbf{x}_k)^\top (\hat{\mathbf{x}} - \mathbf{x}_k) \,\middle|\, \mathcal{Z}^k\right] \quad . \tag{3.6}$$

On the other hand, the MAP criterion searches the argument that maximizes the posterior density $p(\mathbf{x}_k|\mathcal{Z}^k)$:

$$\hat{\mathbf{x}}^{MAP}(\mathcal{Z}^k) = \arg\max_{\mathbf{x}_k} p(\mathbf{x}_k|\mathcal{Z}^k) \quad . \tag{3.7}$$

A close analysis of the Equations (3.3) and (3.4) reveals the fundamental structure of a Bayesian tracking filter: based on the knowledge of the posterior density at the previous time step t_{k-1} and the transitional density, the prior pdf in Equation (3.3) can be computed. After that, the posterior density for the current time step reported in Equation (3.4) is calculated as the normalized product of the the prior density and the likelihood function, which is determined by the current sensor data and the sensor model. Thus, a Bayesian tracking filter results in a sequential update scheme for the recursive calculation of the conditional target state pdf[1] $p(\mathbf{x}_k|\mathcal{Z}^k)$, consisting of a prediction step and a subsequent filter update step at each iteration:

[1] It will be shown later that the Bayesian update scheme is not restricted to the propagation of conditional target state pdf's.

$$p(\mathbf{x}_{k-1}|\mathcal{Z}^{k-1}) \xrightarrow[\text{Motion Model}]{\textbf{Prediction}} p(\mathbf{x}_k|\mathcal{Z}^{k-1}) \xrightarrow[\substack{\text{Sensor Model}\\ \text{New Sensor Data}}]{\textbf{Filter Update}} p(\mathbf{x}_k|\mathcal{Z}^{k}) \quad . \tag{3.8}$$

3.1.3 Linear Gaussian Systems

3.1.3.1 Kalman Filter

Under the restrictive assumptions of linear system equations and Gaussian noises (i.e. process and measurement disturbances), the optimal solution for the recursive scheme in Equations (3.3) and (3.4) is available in closed form and given by the **Kalman Filter** (KF, [BSLK01, Koc14, Lof90a, Lof90b]). Under these assumptions, the Gaussian structure of the recursively calculated target state pdf $p(\mathbf{x}_k|\mathcal{Z}^k)$ is conserved at each time step. The system equations in Equations (3.1) and (3.2) become:

$$\mathbf{x}_{k+1} = \mathbf{F}_k\mathbf{x}_k + \mathbf{v}_k \tag{3.9}$$

$$\mathbf{z}_k = \mathbf{H}_k\mathbf{x}_k + \mathbf{w}_k \quad , \tag{3.10}$$

where $\mathbf{F}_k$ and $\mathbf{H}_k$ are the evolution and the measurement matrices of dimension $(n_x \times n_x)$ and $(n_z \times n_x)$, respectively. The random sequences $\mathbf{v}_k$ and $\mathbf{w}_k$ are zero-mean white Gaussian with covariances $\mathbf{Q}_k$ and $\mathbf{R}_k$, i.e. $\mathbf{v}_k \propto \mathcal{N}(\mathbf{v}_k; 0, \mathbf{Q}_k)$ and $\mathbf{w}_k \propto \mathcal{N}(\mathbf{w}_k; 0, \mathbf{R}_k)$.

A Gaussian distribution exhibits the particular feature that it is fully determined by its first two moments, i.e., its mean and the associated variance (or covariance in the context of multivariate random variables). Therefore, the recursive update scheme of the Kalman filter consists of update equations for the estimated mean target state and the associated estimated covariance. In the following, the recursive Kalman filter prediction-update equations are reported.

The **prediction step**, which can be illustrated by

$$p(\mathbf{x}_{k-1}|\mathcal{Z}^{k-1}) \xrightarrow[\mathbf{F}_{k-1},\,\mathbf{Q}_{k-1}]{\text{Motion Model}} p(\mathbf{x}_k|\mathcal{Z}^{k-1}) \quad , \tag{3.11}$$

$$\mathcal{N}(\mathbf{x}_{k-1}; \mathbf{x}_{k-1|k-1}, \mathbf{P}_{k-1|k-1}) \xrightarrow[\mathbf{F}_{k-1},\,\mathbf{Q}_{k-1}]{\text{Motion Model}} \mathcal{N}(\mathbf{x}_k; \mathbf{x}_{k|k-1}, \mathbf{P}_{k|k-1}) \quad , \tag{3.12}$$

utilizes the target dynamics model to compute a first estimate of the target state $\mathbf{x}_{k|k-1}$ and its covariance $\mathbf{P}_{k|k-1}$, given the posterior pdf $p(\mathbf{x}_{k-1}|\mathcal{Z}^{k-1})$ at time t_{k-1}. Due to the linearity of the target motion model and the white Gaussian process noise with covariance $\mathbf{Q}_{k-1}$, the motion model is introduced into the algorithm by the normal density $\mathcal{N}(\mathbf{x}_k; \mathbf{F}_{k-1}\,\mathbf{x}_{k-1}, \mathbf{Q}_{k-1})$. The Equation (3.3) can be written as

$$p(\mathbf{x}_k|\mathcal{Z}^{k-1}) = \int \underbrace{\mathcal{N}(\mathbf{x}_k; \mathbf{F}_{k-1}\,\mathbf{x}_{k-1}, \mathbf{Q}_{k-1})}_{\text{Motion model}} \underbrace{\mathcal{N}(\mathbf{x}_{k-1}; \mathbf{x}_{k-1|k-1}, \mathbf{P}_{k-1|k-1})}_{\text{Posterior pdf at } t_{k-1}} d\mathbf{x}_{k-1} \quad . \tag{3.13}$$

The integrand can be transformed into a product of two Gaussians in which one pdf does no longer depend on the integration variable $\mathbf{x}_{k-1}$ by making use of the identity [Koc06a, Koc14]

$$\mathcal{N}(\mathbf{a}; \mathbf{b}, \mathbf{A})\; \mathcal{N}(\mathbf{c}; \mathbf{B}\,\mathbf{a}, \mathbf{C}) = \mathcal{N}(\mathbf{c}; \mathbf{B}\,\mathbf{b}, \mathbf{D})\; \mathcal{N}(\mathbf{a}; \mathbf{b} + \mathbf{E}\,\mathbf{d}, \mathbf{A} - \mathbf{E}\mathbf{D}\mathbf{E}^\top) \quad , \tag{3.14}$$

with $\mathbf{d} = \mathbf{c} - \mathbf{B}\mathbf{b}$, $\mathbf{D} = \mathbf{B}\mathbf{A}\mathbf{B}^\top + \mathbf{C}$ and $\mathbf{E} = \mathbf{A}\mathbf{B}^\top\mathbf{D}^{-1}$. This yields the following Kalman filter prediction equations for the mean and covariance of the prior density $p(\mathbf{x}_k|\mathcal{Z}^{k-1})$:

$$\mathbf{x}_{k|k-1} = \mathbf{F}_{k-1}\,\mathbf{x}_{k-1|k-1} \quad , \tag{3.15}$$

$$\mathbf{P}_{k|k-1} = \mathbf{F}_{k-1}\,\mathbf{P}_{k-1|k-1}\,\mathbf{F}_{k-1}^\top + \mathbf{Q}_{k-1} \quad . \tag{3.16}$$

As the **filter update step** is concerned

$$\mathcal{N}(\mathbf{x}_k; \mathbf{x}_{k|k-1}, \mathbf{P}_{k|k-1}) \xrightarrow[\mathbf{H}_k\,,\,\mathbf{R}_k\,,\,\mathbf{z}_k]{\text{Sensor Model}\atop\text{New Sensor Data}} \mathcal{N}(\mathbf{x}_k; \mathbf{x}_{k|k}, \mathbf{P}_{k|k}) \quad , \tag{3.17}$$

the Kalman filter equations are obtained as follows: as the measurement equation (3.10) is a linear function of the target state, it is reasonable to write the likelihood pdf as $p(\mathbf{z}_k|\mathbf{x}_k) = \mathcal{N}(\mathbf{z}_k; \mathbf{H}_k\,\mathbf{x}_k, \mathbf{R}_k)$. Then, the Bayes theorem in Equation (3.4) is given by

$$p(\mathbf{x}_k|\mathcal{Z}^k) = \frac{\mathcal{N}(\mathbf{z}_k; \mathbf{H}_k\,\mathbf{x}_k, \mathbf{R}_k)\;\mathcal{N}(\mathbf{x}_k; \mathbf{x}_{k|k-1}, \mathbf{P}_{k|k-1})}{\int \underbrace{\mathcal{N}(\mathbf{z}_k; \mathbf{H}_k\,\xi_k, \mathbf{R}_k)}_{\text{likelihood function}}\;\underbrace{\mathcal{N}(\xi_k; \mathbf{x}_{k|k-1}, \mathbf{P}_{k|k-1})}_{\text{prior density}}\,d\xi_k} \quad . \tag{3.18}$$

The integrand in the denominator can be again transformed into a product of two Gaussians in which one pdf no longer depends on the integration variable ξ_k by exploiting the formula in Equation (3.14). In addition, also the Gaussian product in the numerator can be rewritten based on the Equation (3.14). This leads to the following Kalman filter update equations for the mean and covariance of the posterior density $p(\mathbf{x}_k|\mathcal{Z}^k)$:

$$\mathbf{x}_{k|k} = \mathbf{x}_{k|k-1} + \mathbf{K}_k(\mathbf{z}_k - \mathbf{H}_k\,\mathbf{x}_{k|k-1}) \quad , \tag{3.19}$$

$$\mathbf{P}_{k|k} = \mathbf{P}_{k|k-1} - \mathbf{K}_k\,\mathbf{S}_k\,\mathbf{K}_k^\top \quad , \tag{3.20}$$

$$\mathbf{S}_k = \mathbf{H}_k\,\mathbf{P}_{k|k-1}\,\mathbf{H}_k^\top + \mathbf{R}_k \quad , \tag{3.21}$$

$$\mathbf{K}_k = \mathbf{P}_{k|k-1}\,\mathbf{H}_k^\top\,\mathbf{S}_k^{-1} \quad , \tag{3.22}$$

where $\mathbf{S}_k$ is the covariance matrix of the innovation and $\mathbf{K}_k$ is the Kalman filter gain matrix. Due to its mathematical structure, the Kalman gain introduces a high degree of adaptivity into the filter equations: depending on the possibly time-varying motion and measurement model error covariances, the gain matrix $\mathbf{K}_k$ determines how much information of the currently processed sensor data needs to be added to the predicted state estimate to deliver an optimal estimation result. The update equations of the Kalman filter (Equation (3.19) to Equation (3.22)) have a predictor-corrector structure, because the first estimate of the target state at time step t_k, which is based on the target motion model and the input from t_{k-1}, is corrected or improved by the current sensor measurements, yielding the optimal estimate of the target state at time step t_k.

3.1.4 Non-linear Systems

The problem of estimating the target state on the basis of the sensor measurements might become highly non-linear. Non-linearity comes from several sources. For example, the target range, range rate and bearing measurements from a conventional radar system undergo the non-linear coordinate transformation to the Cartesian state space. Also the target dynamics could be non-linear especially when the target is subject to significant angular speed and acceleration (e.g. turning maneuver). Similar estimation problems are often handled by decomposing the maneuver into phases

([RAG04,KBSPK00]), hence switching among different target dynamic models. Nevertheless, for some phases the assumption of linear system equations and Gaussian noise do not hold, and the optimal Bayes solution to the filtering problem needs to be approximated. The **Extended Kalman Filter (EKF)** falls into the local linearization class of approximate solutions. So, when non-linear and non-Gaussian conditions hold, the EKF offers an approximation of the posterior pdf in Equation (3.4). Other approaches are based on the **Unscented Transformation (UT)** ([JU97,JU04]), grid-based numerical integration, and sequential Monte Carlo estimation ([Tan96,DFG01,RAG04]). The closeness to the optimum depends on the tracking conditions. For instance, the EKF approximation presented in [BU11] diverges from the optimal solution in highly non-linear/non-Gaussian conditions. Conversely, the **Particle Filter (PF)** allows solving optimally the Bayesian filtering problem - independently from the severity of the non-linearity - if a large number of particles is considered. Particles are indeed a numerical approximation of the probability density function of the target state, which is sought in the Bayes approach. Specifically, the EKF, the Unscented Kalman Filter (UKF) and the PF non-linear filtering techniques are briefly recalled in the following, since they are used in the tracking algorithms developed in this research work.

3.1.4.1 Extended Kalman Filter

The extended Kalman filter is based on the first-order local approximation of the functions $\mathbf{f}(.)$ and $\mathbf{h}(.)$ in the state and measurement Equations (3.1) and (3.2). The mean value and the covariance matrix of the pdfs in Equations (3.3) and (3.4) result:

$$\mathbf{x}_{k|k-1} = \mathbf{f}_{k-1}(\mathbf{x}_{k-1|k-1}) \quad , \tag{3.23}$$

$$\mathbf{P}_{k|k-1} = \mathbf{F}_{k-1}\mathbf{P}_{k-1|k-1}\mathbf{F}_{k-1}^{T} + \mathbf{Q}_{k-1} \quad , \tag{3.24}$$

and

$$\mathbf{x}_{k|k} = \mathbf{x}_{k|k-1} + \mathbf{K}_k[\mathbf{z}_k - \mathbf{h}_k(\mathbf{x}_{k|k-1})] \quad , \tag{3.25}$$

$$\mathbf{P}_{k|k} = \mathbf{P}_{k|k-1} - \mathbf{K}_k\mathbf{S}_k\mathbf{K}_k^{T} \quad , \tag{3.26}$$

where

$$\mathbf{S}_k = \mathbf{H}_k \mathbf{P}_{k|k-1} \mathbf{H}_k^T + \mathbf{R}_k \quad , \tag{3.27}$$

$$\mathbf{K}_k = \mathbf{P}_{k|k-1} \mathbf{H}_k^T \mathbf{S}_k^{-1} \quad . \tag{3.28}$$

Matrices $\mathbf{F}_{k-1}$ and $\mathbf{H}_k$ result from the linearization of functions $\mathbf{f}_{k-1}$ and $\mathbf{h}_k$: they coincide with the Jacobian of the two equations [DFG01], evaluated at the latest estimate of the state $\mathbf{x}_{k-1|k-1}$ and $\mathbf{x}_{k|k-1}$, respectively.

3.1.4.2 Unscented Kalman Filter

The unscented Kalman filter basic idea is to exploit the unscented transformation to approximate the posterior pdf $p(\mathbf{x}_k|\mathcal{Z}^k)$ by a Gaussian density represented by a set of deterministically chosen points, instead of linearizing the functions $\mathbf{f}(.)$ and $\mathbf{h}(.)$ that describe the state evolution and the measurement equation, respectively.

Let us consider the non-linear filter problem described in the Equations (3.1) and (3.2). Under the assumption of a Gaussian distribution for the posterior pdf, i.e. $p(\mathbf{x}_{k-1}|\mathcal{Z}^{k-1}) = \mathcal{N}(\mathbf{x}_{k-1}; \mathbf{x}_{k-1|k-1}, \mathbf{P}_{k-1|k-1})$, a set of N sample points χ_{k-1}^i and their weights W_{k-1}^i with $i = 0, ..., N-1$ are taken to represent this density.

The prediction step is performed as follows:

$$\mathbf{x}_{k|k-1} = \sum_{i=0}^{N-1} W_{k-1}^i \mathbf{f}_{k-1}(\chi_{k-1}^i) \quad , \tag{3.29}$$

$$\mathbf{P}_{k|k-1} = \sum_{i=0}^{N-1} W_{k-1}^i \left[\mathbf{f}_{k-1}(\chi_{k-1}^i) - \mathbf{x}_{k|k-1}\right] \left[\mathbf{f}_{k-1}(\chi_{k-1}^i) - \mathbf{x}_{k|k-1}\right]^T \quad , \tag{3.30}$$

where the predicted density, i.e. $p(\mathbf{x}_k|\mathcal{Z}^{k-1}) \propto \mathcal{N}(\mathbf{x}_k; \mathbf{x}_{k|k-1}, \mathbf{P}_{k|k-1})$, is represented by a set of N sample points $\chi_{k|k-1}^i = \mathbf{f}_{k-1}(\chi_{k-1}^i)$. Then, the predicted measurement is given by

$$\mathbf{z}_{k|k-1} = \sum_{i=0}^{N-1} W_{k-1}^i \mathbf{h}_k(\chi_{k|k-1}^i) \quad . \tag{3.31}$$

The update step is:

$$\mathbf{x}_{k|k} = \mathbf{x}_{k|k} + \mathbf{K}_k(\mathbf{z}_k - \mathbf{z}_{k|k-1}) \quad , \tag{3.32}$$

$$\mathbf{P}_{k|k} = \mathbf{P}_{k|k-1} - \mathbf{K}_k\mathbf{S}_k\mathbf{K}_k^T \quad , \tag{3.33}$$

where

$$\mathbf{K}_k = \mathbf{P}_{xz}\mathbf{S}_k^{-1} \quad , \tag{3.34}$$

$$\mathbf{S}_k = \mathbf{R}_k + \mathbf{P}_{zz} \quad , \tag{3.35}$$

$$\mathbf{P}_{xz} = \sum_{i=0}^{N-1} W_{k-1}^i \left[\chi_{k|k-1}^i - \mathbf{x}_{k|k-1}\right] \left[\mathbf{h}_k(\chi_{k|k-1}^i) - \mathbf{z}_{k|k-1}\right]^T \quad , \tag{3.36}$$

$$\mathbf{P}_{zz} = \sum_{i=0}^{N-1} W_{k-1}^i \left[\mathbf{h}_k(\chi_{k|k-1}^i) - \mathbf{z}_{k|k-1}\right] \left[\mathbf{h}_k(\chi_{k|k-1}^i) - \mathbf{z}_{k|k-1}\right]^T \quad . \tag{3.37}$$

It has to be stressed that the explicit evaluation of the Jacobian is not necessary for this algorithm, as conversely expected in the EKF formulation. As the selection of the sample points χ_{k-1}^i and their weights is concerned, different choices are possible but not addressed in this Section. For their evaluation, is it possible to refer to the works in [JU04, oSTTAB08].

3.1.4.3 Particle Filter

Particle Filters are Sequential Monte Carlo (SMC) techniques, which use a discrete representation of probability density functions. The pdf $p(\mathbf{x}_k|\mathcal{Z}^k)$ in Equation (3.4) is approximated by a weighted sum over N_p *particles*, $\{\mathbf{x}_k^i, \pi_k^i\}_{i=1}^{N_p}$, as:

$$p(\mathbf{x}_k|\mathcal{Z}^k) \approx \sum_{i=1}^{N_p} \pi_k^i \delta(\mathbf{x}_k - \mathbf{x}_k^i) \quad , \tag{3.38}$$

where $\mathbf{x}_k^i$ is the state vector and π_k^i the weight of the $i-th$ particle. Hence, the aim in the particle filter setting is to recursively determine the particles' states and the weights. There are different possibilities to build a particle filter, whose basic steps are often the same. The steps can be summarized as follows ([RAG04]):

- **Prediction**: it draws the $\mathbf{x}_k^i$ particle from the proposal distribution, i.e. the transitional prior pdf $\mathbf{x}_k^i \sim p(\mathbf{x}_k^i|\mathbf{x}_{k-1}^i)$ through the adopted process model;

- **Update**: it evaluates the corresponding weight π_k^i from the likelihood function, $\tilde{\pi}_k^i = \pi_{k-1}^i p(Z_k|\mathbf{x}_k^i)$;
- **Normalization**: it normalizes the weights of the N_p particles, $\pi_k^i = \tilde{\pi}_k^i / \sum_{i=1}^{N_p} \tilde{\pi}_k^i$;
- **Resampling**: it performs resampling.

The resampling step is introduced to solve the problem of the filter degeneration: with time, only few particles will have non-zero weights resulting in a poor approximation of the posterior density $p(\mathbf{x}_k|\mathcal{Z}^k)$. To solve this issue, the resampling discards the particles with low importance weights and multiplies the samples with high importance weights. Depending on the algorithm, this step is performed at each iteration, like in the in the Sequential Importance Resampling (SIR) particle filter algorithm ([DFG01]), or according to certain criterion (e.g. when the effective sample size $N_{eff} = 1/\sum_{i=1}^{N_p}(\pi_k^i)^2$ falls below some threshold N_{thr}).

As there are, in principle, no restrictions on the functional form of the transitional pdf nor on the likelihood function, it is easy to include even strongly non-linear constraints in a particle filter. Typical implementations are the *rejection sampling* and the *pseudo measurement* approaches, discussed in Sections 4.2.1 and 4.2.2, respectively. In spite of the usually simple implementation, the efficiency of the particle filter strongly depends on the actual system equations and constraints, in particular on the overlap of the prior pdf with the likelihood function [DFG01].

3.1.5 Data Association Problem

In real world applications, the assumption of dealing with unique sensor measurement is often not valid. Sensor measurements are generally incomplete, imprecise, ambiguous and uncertain due to different factors, such as thermal noise or the presence of clutter (i.e. unwanted response from objects which are not of interest). In order to deal with these factors within the Bayesian target state estimation process, the detection probability P_D and the spatial false measurement density ρ_F have to be taken into account.

If the sensor is characterized by a $P_D < 1$ and $\rho_f > 0$ the likelihood function $p(Z_k|\mathbf{x}_k)$ in Equation (3.4) has to be generalized in order to comprise all the possible sensor data interpretations. Due to $P_D < 1$, the target might be detected or missed and because of $\rho_F > 0$ also several false alarms are potentially included in the current data set $Z_k = \{\mathbf{z}_k^j\}_{j=1}^{m_k}$, where m_k denotes the number of measurements at time t_k. Under the assumption that only one detection per target is possible and that the P_D is independent from target state, the expression of the *generalized likelihood function* is given by [BP99, BSLK01]:

$$
\begin{aligned}
p(Z_k, m_k|\mathbf{x}_k) &= \Lambda \left[(1 - P_D) + \frac{P_D}{\rho_F} \sum_{j=1}^{m_k} p(\mathbf{z}_k^j|\mathbf{x}_k) \right] \\
&= \Lambda \left[(1 - P_D) + \frac{P_D}{\rho_F} \sum_{j=1}^{m_k} \mathcal{N}(\mathbf{z}_k^j; \mathbf{H}_k\mathbf{x}_k, \mathbf{R}_k^j) \right],
\end{aligned}
\tag{3.39}
$$

where Λ is independent from $\mathbf{x}_k$ and given by $\Lambda = \rho_F^{m_k}/(m_k!)\ e^{-\rho_F|\mathrm{FoV}|}$, with FoV as the field of view of the sensor. Based on this likelihood function, a Bayesian tracking filter is able to handle the sensor outputs in such real scenarios. The first addend, $(1 - P_D)$, describes the missed detection hypothesis whereas the sum of pdfs denotes the m_k hypotheses that the detection with index j is the correct target measurement and all others are false alarms.

The presence of false measurements and/or missed target detections could affect the overall target tracking algorithm, especially when the incoming measurements have to be assigned to the already existent targets (i.e. data association problem). Many data association techniques are presented in literature, which can be mostly differentiate between *hard* and *soft* techniques, depending on the measurement/target association type ([BP99]). In this Section, a brief overview of the Multiple Hypotheses Tracker (MHT, [BP99, Bla04, Koc06a]) is provided, which enumerates different hypotheses for data associations and provides the best scoring hypothesis or the merged results of all of them as tracking result.

3.1.5.1 Multiple Hypotheses Tracker

Given the iterative structure of the Bayesian tracking filter in Section 3.1.2, the combination in the update step of the m_k sensor measurements with the generalized likelihood in the Equation (3.39) generates $(m_k + 1)$ hypotheses for a single Gaussian prior density and for each time instant t_k. If all of them are kept, they will exponentially grow with the consecutive iterations. In order to manage this effect, methods for hypotheses reduction are considered, like gating, pruning and merging, which allow maintaining only the relevant hypotheses at each time step. The Multiple Hypotheses Tracker takes into account the above mentioned techniques. The key idea is to describe the posterior pdf $p(\mathbf{x}_k|\mathcal{Z}^k)$ by a Gaussian mixture. This is done by generating a hypotheses tree starting by an appropriate initialization. A new measurement brings a new hypothesis, which represents the probability that the measurement belongs to the target.

To obtain the posterior density at t_k, let us consider the posterior pdf at t_{k-1} as a Gaussian mixture of n_{k-1} individual track hypotheses:

$$p(\mathbf{x}_{k-1}|\mathcal{Z}^{k-1}) = \sum_{i=1}^{n_{k-1}} w_{k-1}^{i} \mathcal{N}(\mathbf{x}_{k-1}; \mathbf{x}_{k-1|k-1}^{i}, \mathbf{P}_{k-1|k-1}^{i}) \quad , \tag{3.40}$$

where the individual weights w_{k-1}^{i} have to fulfill the condition $\sum_{i=1}^{n_{k-1}} w_{k-1}^{i} = 1$. The hypotheses in Equation (3.40) are then predicted and updated according to the new measurements.

As the prediction step is concerned, the prior density $p(\mathbf{x}_k|\mathcal{Z}^{k-1})$ is evaluated assuming the target moving according to a linear motion model characterized by white Gaussian noise:

$$p(\mathbf{x}_k|\mathcal{Z}^{k-1}) = \sum_{i=1}^{n_{k-1}} w_{k-1}^{i} \mathcal{N}(\mathbf{x}_k; \mathbf{x}_{k|k-1}^{i}, \mathbf{P}_{k|k-1}^{i}) \quad , \tag{3.41}$$

where the state estimates $\mathbf{x}_{k|k-1}^{i}$ and the covariances $\mathbf{P}_{k|k-1}^{i}$ of each hypothesis are obtained by the Kalman filter prediction Equations. Then each predicted hypothesis i is evaluated with each incoming measurement using the bayesian formalism (i.e. update step). By combining the prior in Equation (3.41) with the generalized likelihood in Equation (3.39) and by resorting to the product formula in (3.14), the posterior pdf at the time t_k is again given as a weighted sum of Gaussian:

$$p(\mathbf{x}_k|\mathcal{Z}^{k}) = \sum_{i=1}^{n_{k-1}} \sum_{j=0}^{m_k} w_{k}^{ij} \mathcal{N}(\mathbf{x}_k; \mathbf{x}_{k|k}^{ij}, \mathbf{P}_{k|k}^{ij}) \quad , \tag{3.42}$$

where m_k is the number of the incoming measurements and $j = 0$ denotes the missing detection case. Specifically, the weight factor w_k^{ij} is given by:

$$w_k^{ij} = \frac{\hat{w}_k^{ij}}{\sum_{i=1}^{n_{k-1}} \sum_{j=0}^{m_k} \hat{w}_k^{ij}} \quad , \tag{3.43}$$

where

$$\hat{w}_k^{ij} = \begin{cases} w_{k-1}^{i} \frac{P_D}{\rho_F} \mathcal{N}(\mathbf{z}_k^{j}; \mathbf{H}_k \mathbf{x}_{k|k-1}^{i}, \mathbf{S}_k^{ij}) & \text{if} \quad j > 0 \quad \text{(detection)}, \\ w_{k-1}^{i}(1 - P_D) & \text{if} \quad j = 0 \quad \text{(missdetection)}. \end{cases} \tag{3.44}$$

The state vector and the covariance matrix estimates in Equation (3.43) can be evaluated via Kalman filtering. In this case, for $j > 0$ we have:

$$\mathbf{x}_{k|k}^{ij} = \mathbf{x}_{k|k-1}^{i} + \mathbf{K}_k^{ij}(\mathbf{z}_k^j - \mathbf{H}_k\,\mathbf{x}_{k|k-1}^{i}) \quad , \tag{3.45}$$

$$\mathbf{P}_{k|k}^{ij} = \mathbf{P}_{k|k-1}^{i} - \mathbf{K}_k^{ij}\,\mathbf{S}_k^{ij}\,(\mathbf{K}_k^{ij})^{\top} \quad , \tag{3.46}$$

$$\mathbf{S}_k^{ij} = \mathbf{H}_k\,\mathbf{P}_{k|k-1}^{i}\,\mathbf{H}_k^{\top} + \mathbf{R}_k^j \quad , \tag{3.47}$$

$$\mathbf{K}_k^{ij} = \mathbf{P}_{k|k-1}^{i}\,\mathbf{H}_k^{\top}\,(\mathbf{S}_k^{ij})^{-1} \quad . \tag{3.48}$$

Since the prediction-update recursion is performed for each possible hypothesis - measurement combination, the number of the hypotheses increases from scan to scan by factor $(m_k + 1)$.

As already mentioned, to contrast the exponential growth of the number of hypotheses, specific hypotheses reduction techniques can be applied to make the MHT algorithm real-time capable. Specifically, we deal with:

- **Gating**: only the measurements, the predicted covariances and the measurements error covariances that fit in a specific area (gate) are evaluated;
- **Pruning**: all the hypotheses with weight smaller than an appropriate threshold are deleted;
- **Merging**: the hypotheses with very similar state vectors and covariances are merged into one hypothesis.

An example of the evolution in time of an MHT hypotheses tree is reported in Figure 3.2 without and with application of the mixture reduction methods listed above. Specifically, one or two detections are registered during the time interval $[t_k, t_{k+3}]$. The root of the tree is the original hypothesis. The first expansion of the hypothesis tree is done by using all the possible assignments of the first measurement. Empty circles take into account the false detections.

Summarizing, the above described MHT algorithm is a single target tracker, whose implementation steps include: (i) the initiation of a tentative track from a selected measurement and the formation over time of the correspondent hypotheses tree; (ii) prediction of the tree according to the target motion model; (iii) update of the tree with the new measurements and eventually false detections; (iv) implementation of hypotheses reduction techniques and (v) track evaluation. In addition, the steps related to the track management issues (i.e. track initialization, confirmation and

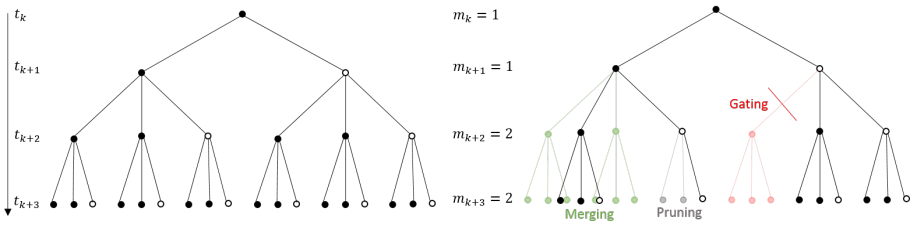

Figure 3.2: Evolution of exemplary MHT hypothesis tree.

deletion) foresee the evaluation of the *sequential likelihood ratio (LR) test*, introduced in [vK02]. The LR function is sequentially calculated on the basis of the hypotheses weights, yielding to track scores for each track. The comparison of the scores with thresholds related to decision errors (e.g. probabilities of accepting measurements in presence of measurement sequence containing measurements and false detections or only false detections) allows taking decisions about the track. The detailed description of the MHT algorithm adopted in this thesis and the track management aspects are provided in [Bro12].

3.2 Measures of Performance

The evaluation of tracking algorithms performance depends on the complexity of the scenario in which the system evolves. It can be straightforward for scenarios with a few widely spaced targets and no false signals, or extremely complex for environments with multiple and closely-spaced targets. In the first case, a system track is updated with measurements from the same target and as performance evaluation is concerned, the track state estimate can be easily compared with the true state of its target, which represents the only source of measurements for that track. Alternatively, the track state estimate can be compared to the only true target state that is near to it in state space. On the other hand, for complex scenarios the evaluation of tracking performance results complicated due to possible ambiguities in measurement-to-track association, misassociation and missed targets.

The tracking filters presented in this work have been designed and developed for a single-target environment (i.e. under the assumption that targets are well separated in space, thus avoiding problem in associating incoming detections to already established tracks). Specifically, two Measures of Performance (MoP) are hereafter reported, both used to compare tracking filters in Monte Carlo simulations. The measures of

performance are computed for each track assigned to a target, for each time stamp of the simulation and for each Monte Carlo run. Then the average of each MoP for a target is computed over all Monte Carlo runs and it is repeated for each target and each time stamp.

3.2.1 Root Mean Squared Errors

The Root Mean Squared errors are the most common metrics used to evaluate the performance of a filter. They are mostly used to determine the accuracy of a track, i.e. how the track assigned to a target deviates to the truth state of the target itself. In the following the expressions for these errors in position, velocity, speed and course are given. Given N Monte Carlo runs, for the 2D position vector $\mathbf{x} = [x, y]$ with observed errors $\tilde{x}_i$ and $\tilde{y}_i$, the RMS position error is given by:

$$\mathrm{RMS}(\tilde{\mathbf{x}}) = \sqrt{\frac{1}{N}\sum_{i=1}^{N}\left(\tilde{x}_i^2 + \tilde{y}_i^2\right)} \quad . \tag{3.49}$$

Correspondingly, for the velocity vector $\dot{\mathbf{x}} = [\dot{x}, \dot{y}]$ the RMS velocity error is given by:

$$\mathrm{RMS}(\tilde{\dot{\mathbf{x}}}) = \sqrt{\frac{1}{N}\sum_{i=1}^{N}\left(\tilde{\dot{x}}_i^{\,2} + \tilde{\dot{y}}_i^{\,2}\right)} \quad . \tag{3.50}$$

The RMS speed error is given by:

$$\mathrm{RMS}(\tilde{s}) = \sqrt{\frac{1}{N}\sum_{i=1}^{N}\tilde{s}_i^2} \quad , \tag{3.51}$$

where $\tilde{s}_i = s_i - \hat{s}_i$ is the observed error of the speed $s_i = \sqrt{\dot{x}_i^2 + \dot{y}_i^2}$ and $\hat{s}_i$ its estimation.

Similarly, the RMS course error is evaluated as:

$$\mathrm{RMS}(\tilde{\theta}) = \sqrt{\frac{1}{N}\sum_{i=1}^{N}\tilde{\theta}_i^2} \quad , \tag{3.52}$$

where $\tilde{\theta}_i = \theta_i - \hat{\theta}_i$ is the observed error of the course $\theta_i = \tan^{-1}\left[\frac{\dot{x}_i}{\dot{y}_i}\right]$ (measured from the y axis, i.e. North, clockwise) and $\hat{\theta}_i$ its estimation.

3.2.2 Kullback-Leibler Divergence

The comparison between tracking filters by using metrics based on point estimators (e.g. the root mean squared errors) leads to proper results when performed under Gaussian assumptions and linear target dynamics. However, if the problem is such that the second order moment can be sufficiently well approximated by a Gaussian density, but not the higher order moments, then another measure is needed ([HKGN06]). The Kullback-Leibler Divergence (KLD) is taken as reference for comparing the empirical distributions of EKF and PF, for example.

Given two *continuous* densities on $\mathbf{R}^d$, p and q, the KLD $D_{KL}(p,q)$ is defined as:

$$D_{KL}(p,q) = \mathbf{E}_p\left[log\ \frac{p}{q}\right] = \int p(x) log\ \frac{p(x)}{q(x)}\, dx, \tag{3.53}$$

D_{KL} is non-negative, not symmetric in p and q, zero if the distributions exactly match and potentially equal infinity. As reported in [CGPB11] and [WKV09], under the hypothesis of i.i.d samples from p and q, an asymptotic unbiased and mean square consistent estimator of the expression in (3.53) can be defined.

Let $\{X_1, ..., X_n\}$ and $\{Y_1, ..., Y_m\}$ be i.i.d. drawn samples from the distributions p and q, respectively. The estimator of $\hat{D}_{KL}(p,q)$ is given by:

$$\hat{D}_{KL}(p,q) = \frac{d}{n}\sum_{i=1}^{n} log\ \frac{\nu_{k_i}(i)}{\rho_{l_i}(i)} + \frac{1}{n}\sum_{i=1}^{n}\left[\psi(l_i) - \psi(k_i)\right] + log\ \frac{m}{n-1}, \tag{3.54}$$

where $\nu_{k_i}(i)$ is the Euclidean distance between X_i and its k_i-nearest neighbour in $\{Y_i\}$, $\rho_{l_i}(i)$ is the Euclidean distance between X_i and its l_i-nearest neighbour in $\{X_j\}_{j\neq i}$, and ψ is the Digamma function, i.e. the logarithmic derivative of the Gamma function.

In order to compare the EKF (continuous) and PF (discrete) distributions, is it possible to proceed as follows:

- A reference distribution ($\mathrm{PF_{Ref}}$) is generated using a PF with a high number of samples ($\mathrm{N_{pRef}}$);
- A PF with $\mathrm{N_{pPF}}$ particles, such that $\mathrm{N_{pPF}} << \mathrm{N_{pRef}}$, is considered and the KLD between PF and $\mathrm{PF_{Ref}}$ distributions is calculated, $\hat{D}_{KL}(\mathrm{PF}, \mathrm{PF_{Ref}})$;
- The EKF distribution is sampled for comparison. To limit the effect of this approximation a high number of samples $\mathrm{N_{pEKF}} = \mathrm{N_{pRef}}$ has to be chosen for computing the $\hat{D}_{KL}(\mathrm{EKF}, \mathrm{PF_{Ref}})$;

- Finally $\hat{D}_{KL}(\mathrm{PF}, \mathrm{PF}_{\mathrm{Ref}})$ and $\hat{D}_{KL}(\mathrm{EKF}, \mathrm{PF}_{\mathrm{Ref}})$ are compared in terms of mean value.

The above described procedure will be adopted to compare the different tracking filters developed in this PhD work.

3.3 Summary

The Chapter introduced the fundamental concepts of Bayesian target tracking. Specifically, linear and non-linear tracking filters (e.g. KF, EKF, UKF and PF) were recalled as references for the development of the tracking filters addressed by this PhD work. As data association techniques are concerned, the MHT algorithm was presented in the form described in [Bro12]. Data association problem is not directly addressed in the tracking filters developed in this Thesis, but the MHT is used to show the tracking results for the maritime surveillance application presented in Chapter 8. Finally, the RMS errors and the KLD were presented as measures of performance adopted to evaluate the vessel tracking algorithm results.

CHAPTER IV

Context Exploitation for Target Tracking

The Bayesian recursion, illustrated in Section 3.1, allows incorporating different kinds of external factors, such as equality and inequality constraints, which can be modeled as linear or non-linear functions of the target state vector. Context information for target tracking can be indeed considered as a constraining factor, since it affects the possible evolution of some of the positional/kinematic components of the state vector either bounding them or limiting a given non-linear combination of them. Such constraining effect generally varies over time (i.e., at each time instant in the considered discrete-time system model), and depends from the state vector itself. This is due for example to the spatial (geographic) layout of the context in the area where the target evolves. In addition, the context-driven constraint might be fulfilled by the system in all cases (i.e., hard constraint), such as for instance the boundary between land and sea for a ground moving target, or mostly (i.e., soft constraint), such as the adherence to a traffic separation scheme.

In literature several algorithms are reported, which take into account constraints in the estimation process, depending on the addressed application and the nature of the constraint itself. A quite exhaustive overview is reported by Simon in [Sim10]. In this survey, a preliminary distinction between the available techniques for linear and non-linear dynamic systems and linear and non-linear constraints is provided.

Specifically, when the system evolution is described by *linear* equations, techniques like estimate projection [SC02], gain projection [GH07], probability density function truncation [SS10] and interior point likelihood maximization [BBP09] can be adopted for incorporating *hard inequality and linear* constraints. Other techniques, like model reduction [WDW92], perfect measurements [WCC02] and system projection [KB07]

are used for dealing with equality constraints. In case of linear systems, the Kalman filter (Section 3.1.3) represents the solution for the recursive constrained state estimation. If the constraints result as *non-linear*, a linearization step is required before adopting the above mentioned techniques in the Kalman filter. If the constraints maintain their non-linearities, solutions like the extended Kalman filter (EKF), unscented Kalman filter (UKF) and particle filter (PF) - see Section 3.1.4 - are considered for the target estimation process. Others methods to include the inequality constraints are discussed in literature: among them we mention the second order expansion of non-linear constraints [YB08] and the Moving Horizon Estimation (MHE, [RRL01]).

As *non-linear* systems are concerned, EKF, UKF, MHE and PF-based algorithms combined with various techniques to handle constraints have been proposed in the literature. The MHE approaches result attractive but require excessive computational effort, [RRM03]. Techniques based on sequential Monte Carlo (SMC) methods are prone to the inclusion of additional information since they present no restriction on the type of models (e.g. target dynamics, noise distributions, etc.). Considering different motion models or filter parameters allows as well using KF extensions as constrained tracking filters.

Generally speaking an underlying aspect when comparing constrained Bayesian filters is the *entry point* of the constraint in the recursive formulation of Bayes. As recalled in the Section 3.1, each estimation iteration is split into *prediction* and *update* steps, which lead to the calculation of the posterior density of the state vector $p(\mathbf{x}_k|\mathcal{Z}^k)$ through the evaluation of the prior pdf $p(\mathbf{x}_k|\mathcal{Z}^{k-1})$ and the likelihood function $p(Z_k|\mathbf{x}_k)$. The prior pdf is then calculated on the basis of the posterior pdf $p(\mathbf{x}_{k-1}|\mathcal{Z}^{k-1})$ at the previous time instant and the transitional probability $p(\mathbf{x}_k|\mathbf{x}_{k-1})$. The algorithms derived within the general Bayes formulation generally constrain either the prior pdf (or better the transitional density) or the likelihood function. The mathematical modification of the unconstrained pdf into the constrained pdf then varies from filter to filter, largely depending on the application sought for the estimator.

The general formulation of the constrained Bayesian filtering is reported in the following, where the equivalence between the introduction of the constraint in the prediction step and in the update step from a Bayes point of view is demonstrated.

4.1 Constrained Bayesian Filtering

In this Section the Bayesian recursion for the inclusion of constraints in the tracking process is presented. Let us consider the most generic case, i.e., the context informa-

tion is available at the time instant t_k in terms of *non-linear inequality* constraint on the target state $\mathbf{x}_k$:

$$\mathbf{a}_k \leq \mathbf{C}_k(\mathbf{x}_k) \leq \mathbf{b}_k \quad , \tag{4.1}$$

where $\mathbf{C}_k : \mathbb{R}^{n_x} \rightarrow \mathbb{R}^{n_c}$. The constraint as defined in Equation (4.1) can be exactly satisfied (*hard* constraint) or it can present uncertainties. This could be due to the uncertainty of the boundaries, i.e. the vectors $\mathbf{a}_k$ and $\mathbf{b}_k$, or to the uncertainty of the constraint $\mathbf{C}_k$, which is allowed to exceed the boundaries with a certain probability (*soft* constraint). In the following we focus on the perfect knowledge of *hard* constraints and the constraints space. The analysis of the soft constraint case is out of the scope of this Paragraph.

Given these considerations, let C_k be the set of states satisfying the Equation (4.1) and C^k the sequence of C_k up to the time k:

$$C_k = \{\mathbf{x}_k : \mathbf{x}_k \in \mathbb{R}^{n_x}, \mathbf{a}_k \leq \mathbf{C}_k(\mathbf{x}_k) \leq \mathbf{b}_k\} \tag{4.2}$$

$$C^k = \{C_0, C_1, ..., C_k\} \quad . \tag{4.3}$$

The inclusion of the sequence of constraints in (4.3) in the Bayesian formalism requires the evaluation of the *constrained posterior pdf* $p(\mathbf{x}_k|\mathcal{Z}^k, C^k)$, where the conditioning is with respect to C^k, too.

The two-step recursion (prediction and update) for the evaluation of the constrained posterior pdf is modified in accordance to the new conditioning. The expression in Equation (3.8) becomes:

$$p(\mathbf{x}_{k-1}|\mathcal{Z}^{k-1}, C^{k-1}) \xrightarrow[\text{Motion Model}]{\textbf{Constrained Prediction}} p(\mathbf{x}_k|\mathcal{Z}^{k-1}, C^k) \xrightarrow[\substack{\text{Sensor Model}\\ \text{New Sensor Data } \mathbf{z}_k}]{\textbf{Filter Update}} p(\mathbf{x}_k|\mathcal{Z}^k, C^k). \tag{4.4}$$

$$p(\mathbf{x}_{k-1}|\mathcal{Z}^{k-1}, C^{k-1}) \xrightarrow[\text{Motion Model}]{\textbf{Prediction}} p(\mathbf{x}_k|\mathcal{Z}^{k-1}, C^{k-1}) \xrightarrow[\substack{\text{Sensor Model}\\ \text{New Sensor Data } \mathbf{z}_k}]{\textbf{Constrained Filter Update}} p(\mathbf{x}_k|\mathcal{Z}^k, C^k). \tag{4.5}$$

Specifically, the information about the constraint can be either exploited in the prediction or in the update step ([PPB+12]), as stated in the Equations (4.4) and (4.5) respectively, leading to the same result from the Bayesian point of view as demonstrated in the following.

4.1.1 Inclusion of Constraints in the Prediction Step

In this case the *prior pdf* is defined as follows:

$$\begin{aligned}
p(\mathbf{x}_k|\mathcal{Z}^{k-1}, C^k) &= \int p(\mathbf{x}_k, \mathbf{x}_{k-1}|\mathcal{Z}^{k-1}, C_k, C^{k-1}) d\mathbf{x}_{k-1} \\
&= \int \frac{p(\mathbf{x}_k, \mathbf{x}_{k-1}, \mathcal{Z}^{k-1}, C_k, C^{k-1})}{p(\mathcal{Z}^{k-1}, C_k, C^{k-1})} d\mathbf{x}_{k-1} \\
&= \int \frac{p(\mathbf{x}_k|\mathbf{x}_{k-1}, \mathcal{Z}^{k-1}, C_k, C^{k-1}) p(\mathbf{x}_{k-1}, \mathcal{Z}^{k-1}, C_k, C^{k-1})}{p(\mathcal{Z}^{k-1}, C_k, C^{k-1})} d\mathbf{x}_{k-1} \\
&= \int \frac{p(\mathbf{x}_k|\mathbf{x}_{k-1}, \mathcal{Z}^{k-1}, C_k, C^{k-1}) p(\mathbf{x}_{k-1}|\mathcal{Z}^{k-1}, C_k, C^{k-1}) p(\mathcal{Z}^{k-1}, C_k, C^{k-1})}{p(\mathcal{Z}^{k-1}, C_k, C^{k-1})} d\mathbf{x}_{k-1} \\
&= \int p(\mathbf{x}_k|\mathbf{x}_{k-1}, \mathcal{Z}^{k-1}, C_k, C^{k-1}) p(\mathbf{x}_{k-1}|\mathcal{Z}^{k-1}, C_k, C^{k-1}) d\mathbf{x}_{k-1} \\
&= \int p(\mathbf{x}_k|\mathbf{x}_{k-1}, C_k) p(\mathbf{x}_{k-1}|\mathcal{Z}^{k-1}, C^{k-1}) d\mathbf{x}_{k-1} \quad .
\end{aligned} \tag{4.6}$$

The current state $\mathbf{x}_k$ in the transitional density $p(\mathbf{x}_k|\mathbf{x}_{k-1}, C_k)$ is conditioned to the current set of constraints C_k and not to the previous constraint history.

The *posterior pdf* definition is given by:

$$\begin{aligned}
p(\mathbf{x}_k|\mathcal{Z}^k, C^k) &= \frac{p(\mathbf{x}_k, \mathbf{z}_k, \mathcal{Z}^{k-1}, C^k)}{p(\mathbf{z}_k, \mathcal{Z}^{k-1}, C^k)} \\
&= \frac{p(\mathbf{z}_k|\mathbf{x}_k, \mathcal{Z}^{k-1}, C^k) p(\mathbf{x}_k, \mathcal{Z}^{k-1}, C^k)}{p(\mathbf{z}_k, \mathcal{Z}^{k-1}, C^k)} \\
&= \frac{p(\mathbf{z}_k|\mathbf{x}_k, \mathcal{Z}^{k-1}, C^k) p(\mathbf{x}_k|\mathcal{Z}^{k-1}, C^k) p(\mathcal{Z}^{k-1}, C^k)}{p(\mathbf{z}_k|\mathcal{Z}^{k-1}, C^k) p(\mathcal{Z}^{k-1}, C^k)} \\
&= \frac{p(\mathbf{z}_k|\mathbf{x}_k) p(\mathbf{x}_k|\mathcal{Z}^{k-1}, C^k)}{p(\mathbf{z}_k|\mathcal{Z}^{k-1}, C^k)} \quad .
\end{aligned} \tag{4.7}$$

The inclusion of constraints in the prediction step requires the evaluation of the *constrained transitional density* $p(\mathbf{x}_k|\mathbf{x}_{k-1}, C_k)$ in the Equation (4.6).

4.1.2 Inclusion of Constraints in the Update Step

The *prior pdf* is defined as follows:

$$\begin{aligned} p(\mathbf{x}_k|\mathcal{Z}^{k-1}, C^{k-1}) &= \int p(\mathbf{x}_k, \mathbf{x}_{k-1}|\mathcal{Z}^{k-1}, C^{k-1}) d\mathbf{x}_{k-1} \\ &= \int p(\mathbf{x}_k|\mathbf{x}_{k-1}, \mathcal{Z}^{k-1}, C^{k-1}) p(\mathbf{x}_{k-1}|\mathcal{Z}^{k-1}, C^{k-1}) d\mathbf{x}_{k-1} \\ &= \int p(\mathbf{x}_k|\mathbf{x}_{k-1}) p(\mathbf{x}_{k-1}|\mathcal{Z}^{k-1}, C^{k-1}) d\mathbf{x}_{k-1} \quad . \end{aligned} \tag{4.8}$$

The *posterior pdf* definition is given by:

$$\begin{aligned} p(\mathbf{x}_k|\mathcal{Z}^k, C^k) &= \frac{p(\mathbf{x}_k, \mathbf{z}_k, \mathcal{Z}^{k-1}, C_k, C^{k-1})}{p(\mathbf{z}_k, \mathcal{Z}^{k-1}, C_k, C^{k-1})} \\ &= \frac{p(\mathbf{z}_k|\mathbf{x}_k, \mathcal{Z}^{k-1}, C^k) p(\mathbf{x}_k, \mathcal{Z}^{k-1}, C^k)}{p(\mathbf{z}_k, \mathcal{Z}^{k-1}, C^k)} \\ &= \frac{p(\mathbf{z}_k|\mathbf{x}_k) p(C_k|\mathbf{x}_k) p(\mathbf{x}_k|\mathcal{Z}^{k-1}, C^{k-1})}{p(\mathbf{z}_k|\mathcal{Z}^{k-1}, C^k) p(C_k|C^{k-1})} \quad . \end{aligned} \tag{4.9}$$

In this case, the existence of constraints brings to the definition of the *constrained likelihood function* $p(C_k|\mathbf{x}_k)$ in the Equation (4.9).

By comparing the equations (4.7) and (4.9) it is easy to demonstrate that they coincide from the Bayesian point of view if the following equivalence holds:

$$p(\mathbf{x}_k|\mathcal{Z}^{k-1}, C^k) = \frac{p(C_k|\mathbf{x}_k) p(\mathbf{x}_k|\mathcal{Z}^{k-1}, C^{k-1})}{p(C_k|C^{k-1})} \quad . \tag{4.10}$$

The inclusion of equality constraints in the Bayesian recursion can be handled similarly.

4.2 State-of-the-art Constrained Algorithms

This section presents some state-of-the-art algorithms for recursive target state estimation exploiting the context information. The constrained tracking filters have been derived on the basis of the Bayesian recursion presented in Section 4.1, where the context has been properly modeled in order to be included in the formalism depending on the application. It has to be stressed that some algorithms include the context information in the prediction phase of the tracking process, others are characterized by a constrained target state update. Specifically, two general methods for

constraint exploitation in target tracking are recalled, the *rejection sampling* and the *pseudo measurement* approach, both used for several target tracking applications. Finally, other two algorithms for tracking ground targets (e.g. vehicles) are reported: the *roadmap assisted target tracking* and the *blind zone assisted target tracking*. The latter two algorithms have been developed to support the ground situation awareness of highly dynamic scenarios with many ground moving targets. This application requires computer aided extraction and maintenance of target tracks in the surveillance area. Although the use of airborne ground moving target indication (GMTI) radar promises high radar coverage of the surveillance region (regardless of daytime or weather conditions), several issues make automatic target tracking difficult, e.g., the clutter notch of the sensor, terrain obscuration, missed detections, false alarms or data assignment ambiguities in the case of closely spaced targets. Specifically, the two presented algorithms exploit different types of constraints: (i) constraints on the motion of road targets and (ii) constraints on the target state and sensor-target geometry implied by the (negative) outcome of a GMTI sensor measurement.

4.2.1 Rejection Sampling

The **rejection sampling** method imposes the constraints on the prior pdf, specifically on the transitional density in the Equation (4.6), which is modified as follows (see [PPB+12]):

$$p(\mathbf{x}_k|\mathbf{x}_{k-1}, C_k) \propto \begin{cases} p(\mathbf{x}_k|\mathbf{x}_{k-1}) & \text{if } \mathbf{x}_k \in C_k, \\ \alpha p(\mathbf{x}_k|\mathbf{x}_{k-1}) & \text{otherwise.} \end{cases} \tag{4.11}$$

The constrained pdf is the original $p(\mathbf{x}_k|\mathbf{x}_{k-1})$ restricted to C_k. The parameter α is generally chosen in the interval $[0, 1[$. For the *hard* constraints case, such value is set to $\alpha = 0$.

This approach can be straightforward applied to a particle filter tackling the nonlinear estimation problem: only the particles that satisfy the constraints are accepted, the others are rejected. The solution is extremely simple, but is computationally expensive. In particular, the time required to perform rejection-sampling, i.e., to generate a given number of particles is not known a priori. The smaller the fraction of the state space that fulfills the constraint, the more inefficient the rejection sampling approach becomes. For *equality* constraints this method cannot be applied at all, since the probability that a randomly drawn particle fulfills the constraint vanishes.

4.2.2 Pseudo Measurements

The **pseudo measurements** approach deals with constraining the instantaneous measurement. Specifically, the constraint is considered as an additional measurement. This impacts the posterior pdf and requires the evaluation of the constraint based likelihood function $p(C_k|\mathbf{x}_k)$ in (4.9):

$$p(C_k|\mathbf{x}_k) = \begin{cases} 1-\alpha & \text{if } \mathbf{x}_k \in C_k, \\ \alpha & \text{otherwise,} \end{cases} \tag{4.12}$$

where $\alpha \in [0, 1[$, which is multiplied to the measurement-induced likelihood function. Specifically, we have $\alpha = 0$ to deal with the *hard* constraint case.

In a particle filter application (see [PPB+12]) $p(C_k|\mathbf{x}_k)$ affects the weight of particles or even reduces them to zero if the (hard) constraint is not fulfilled. While in the rejection sampling approach (Section 4.2.1) the computation time is a priori unknown, in the pseudo measurement approach, there can be a large number of particles with small or vanishing weight leading to an inefficient filter, too. Like in the rejection sampling approach, the filter becomes more and more inefficient the smaller the constraint state space is. For this reason, in the limit of *equality* constraints, both variants cannot be applied.

4.2.3 Roadmap Assisted Target Tracking

The use of roadmaps to enhance the tracking performance is a typical example of *map matching*, a frequently applied approach, e.g., for navigation systems. Information about roadmaps can be exploited in different steps of the tracking filter (see for example [AGOR02, AS03, KKU06, Str08, ZKL08, OSG09]), e.g. by projecting the measurements or the state vectors to the road. In a road network or in the case of winding roads, however, the projections of the state vector estimate and the covariance onto the road are ambiguous. A different approach consists in modelling the target dynamics in the road coordinates. In the simplest case, this leads to a description of the target state in reduced dimensions, using the mileage and speed as target state parameters. As real roads are not strictly one-dimensional, their width, i.e. the motion transversal to the road direction, has to be modeled too. In [Koc06b, UK06] an approach that models the target motion in road coordinates and performs the data processing in Cartesian coordinates is presented and here recalled. The nonlinear mapping between the two coordinate systems is done using a *Gaussian mixture* approach.

4.2.3.1 Context Modelling

A road can mathematically be described by a continuous 3-D curve $\mathcal{R}^*$ in Cartesian coordinates and is parametrized by the corresponding arc length l with $\mathcal{R}^* : l \mapsto \mathcal{R}^*(l)$ can be approximated by a polygonal curve $\mathcal{R}$ consisting of n_r piecewise linear segments. The $n_r + 1$ nodes of this polygonal curve are given by the 3-D node vectors

$$\mathbf{r}_s = \mathcal{R}^*(l_s), \quad s = 1, \ldots, n_r + 1 \tag{4.13}$$

and for each road segment a normalized tangential vectors

$$\mathbf{t}_s = \frac{\mathbf{r}_{s+1} - \mathbf{r}_s}{|\mathbf{r}_{s+1} - \mathbf{r}_s|}, \quad s = 1, \ldots, n_r \tag{4.14}$$

can be derived. With the segment length $\lambda_s = l_{s+1} - l_s$ and the indicator function defined by

$$\chi_s(l) = \begin{cases} 1 & \text{for } \; l \in [l_s, l_{s+1}) \\ 0 & \text{otherwise} \end{cases} \qquad s = 1, \ldots, n_r \tag{4.15}$$

the polygonal curve $\mathcal{R}$ is then given by

$$\mathcal{R} : l \in [l_1, l_{n_r+1}) \mapsto \mathcal{R}(l) = \sum_{s=1}^{n_r} \left[\mathbf{r}_s + (l - l_s)\mathbf{t}_s\right] \chi_s(l) \tag{4.16}$$

with $\mathcal{R}^*(l_s) = \mathcal{R}(l_s) = \mathbf{r}_s$ and $s = 1, \ldots, n_r + 1$. Thus, each segment s of the polygonal road $\mathcal{R}$ is determined by the node vector $\mathbf{r}_s$, the arc length λ_s, and the normalized tangential vector $\mathbf{t}_s$. In addition, both the width and the accuracy of the road are described by a covariance matrix $\mathbf{R}_s^r$ which also accounts for the discretization error introduced by $\lambda_s - |\mathbf{r}_{s+1} - \mathbf{r}_s|$, i.e., the difference between the length of a segment and the actual distance traveled along this segment. Such a description makes sense when an estimate of the target position transversal to the road direction is not required, i.e., in particular when the measurement uncertainty is significantly larger than the width of the road or lane.

4.2.3.2 Filter Implementation: Tracking with Road Networks

Road network data generally contains several road sections, each consisting of a certain number of linear segments connected at specific nodes. This yields a complex structure exhibiting crossings and junctions. The basic idea of a tracking scheme utilizing complex roadmap data is, first of all, to introduce a local road for each target which consists of only a limited number of segments. Depending on the specific motion of a target along the road network, this local road then needs to be continuously adapted: as the target approaches the head of the road, new segments are added, and segments with vanishing probability at the tail of the road are pruned. In addition, the orientation of the local road is reversed if a target moves backwards along the associated road segments.

The trajectory of a realistic road target will include junctions and crossings. In such a case, the arising ambiguity can easily be resolved over time by utilizing a multiple model [BSL95] approach with respect to the generated local roads. The possible paths of the moving object at the junction or crossing lead to different road hypotheses h with $h = 1, ..., N_h$, where each has a different continuation of the previous local road after the junction. An example for this is shown in Figure 4.1. If a target approaches a junction or crossing, a road hypothesis for every possible continuation after the junction is generated. In the subsequent time steps, the probability of a particular road hypothesis, conditioned on the accumulated measurement sequence, is then calculated at the end of the filter update based on the computed component weights. In that way, the tracking algorithm is able to handle the arising ambiguity due to the different possible trajectories of the target. This ambiguity is then resolved over time as the target passes the junction or crossing and moves further away. The obtained target measurements then facilitate the discrimination among the different road hypotheses.

Following the approaches in [Koc06b, UK06], the state vector of a road target at time step t_k is described in the road coordinate system, i.e., by its arc length l_k along the road and by the associated speed $\dot{l}_k$ as $\mathbf{x}_k^r = [l_k, \dot{l}_k]^\top$. In the following, a single iterative loop of the road tracking scheme is summarized. First of all, it is assumed that the target state pdf in continuous road coordinates at time step t_{k-1} is available and given by the expression

$$p(\mathbf{x}_{k-1}^r|\mathcal{Z}^{k-1}) = \sum_{h=1}^{N_h} P_{k-1}(h|\mathcal{Z}^{k-1})\; p(\mathbf{x}_{k-1}^r|h, \mathcal{Z}^{k-1}) \quad . \tag{4.17}$$

When the pdf for each road hypothesis h is determined by a single Gaussian, the pdf

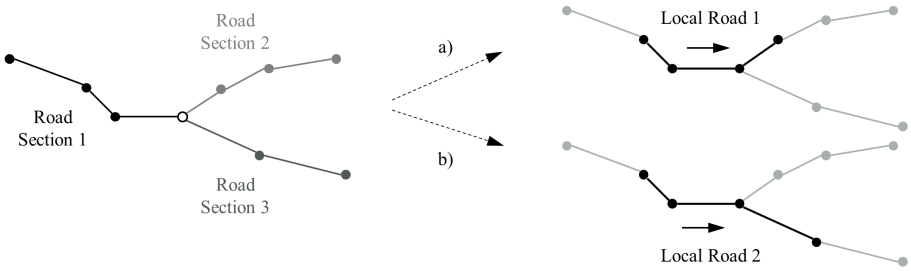

Figure 4.1: Left: Exemplary road network consisting of three road sections. Right: Local roads generated for a target which moves from left to right and approaches the junction.

take the form of a Gaussian mixture. Applying the Chapman-Kolmogorov equation (3.5), the predicted pdf, too, is given by a Gaussian mixture in continuous road coordinates.

This prior then has to be transformed into the ground coordinate system, so that the sensor data can be processed, i.e.,

$$\underbrace{p(\mathbf{x}_k^r|\mathcal{Z}^{k-1})}_{\text{in road coordinates}} \xrightarrow[\text{roadmap error}]{\text{roadmap}} \underbrace{p(\mathbf{x}_k^g|\mathcal{Z}^{k-1})}_{\text{in ground coordinates}} \quad . \tag{4.18}$$

By utilizing the linear segmentation of the constructed local road for each road hypothesis h with $n_r(h)$ segments (as discussed in the previous section), the prior density in ground coordinates is computed as ([UK06]):

$$p(\mathbf{x}_k^g|\mathcal{Z}^{k-1}) = \sum_{h=1}^{N_h} P_{k-1}(h|\mathcal{Z}^{k-1}) \left[\sum_{s=1}^{n_r(h)} P_k^h(s|\mathcal{Z}^{k-1})\, p(\mathbf{x}_k^g|s, \mathcal{Z}^{k-1}) \right] \quad . \tag{4.19}$$

The expression $P_k^h(s|\mathcal{Z}^{k-1})$ denotes the probability that the target moves on segment s of local road h, based on the accumulated sensor data $\mathcal{Z}^{k-1}$.

The segment dependent pdf in ground coordinates in (4.19) is calculated from the pdf in road coordinates as:

$$p(\mathbf{x}_k^g|s, \mathcal{Z}^{k-1}) = \int p(\mathbf{x}_k^g|\mathbf{x}_k^r, s)\; p(\mathbf{x}_k^r|s, \mathcal{Z}^{k-1})\; d\mathbf{x}_k^r \quad . \tag{4.20}$$

Assuming Gaussian error on the road segments of the map, the transition density (4.20) is Gaussian, too, and the integration provides a pdf in ground coordinates, constrained to the segment s:

$$p(\mathbf{x}_k^g|s,\mathcal{Z}^{k-1}) = \mathcal{N}(\mathbf{x}_k^g; \mathbf{x}_{k|k-1}^g(s), \mathbf{P}_{k|k-1}^g(s)) \tag{4.21}$$

and the segment dependent pdf (4.20), then, can be calculated as a Gaussian distribution. Explicit formulas for the arguments in (4.19) are given in [UK06].

In this approach, the pdf in road coordinates is unconstrained, but it is mapped by (4.18) to a pdf in ground coordinates that is constrained by the road geometry. As the mapping is based on Gaussian distributions, the constraints are, exactly speaking, only statistical and, therefore, soft.

In the filter update step, each component on the r.h.s. of (4.19) is updated with m measurements. After the generation of all hypotheses, each segment-dependent density $p(\mathbf{x}_k^g|m,s,\mathcal{Z}^k)$ is individually transformed back from Cartesian to road coordinates by a simple projection onto the corresponding road segment:

$$\underbrace{p(\mathbf{x}_k^g|m,s,\mathcal{Z}^k)}_{\text{in ground coordinates}} \xrightarrow{\text{roadmap}} \underbrace{p(\mathbf{x}_k^r|m,s,\mathcal{Z}^k)}_{\text{in road coordinates}} \quad . \tag{4.22}$$

The pdf in continuous road coordinates for every road hypothesis h yields, for each of the generated hypotheses, a Gaussian mixture of segment-dependent probability densities with mean and covariance as given in [UK06]. For simplicity, this is then approximated by second-order moment-matching [BSLK01], resulting in a single density

$$p(\mathbf{x}_k^r|h,m,\mathcal{Z}^k) \approx w_k^m(h)\,\mathcal{N}(\mathbf{x}_k^r; \mathbf{x}_{k|k}^{r,m}(h), \mathbf{P}_{k|k}^{r,m}(h)) \quad , \tag{4.23}$$

with the component weights $w_k^m(h) = \sum_{s=1}^{n_r(h)} P_k^h(s|\mathcal{Z}^{k-1})\, w_k^m(s)$. The posterior density of the target state in continuous road coordinates can finally be written as

$$p(\mathbf{x}_k^r|\mathcal{Z}^k) = \sum_{h=1}^{N_h} P_k(h|\mathcal{Z}^k)\, p(\mathbf{x}_k^r|h,\mathcal{Z}^k) \quad , \tag{4.24}$$

with the posterior for each road hypothesis h determined by

$$p(\mathbf{x}_k^r|h,\mathcal{Z}^k) = \sum_{m=0}^{m_k} w_k^m(h)\ \mathcal{N}(\mathbf{x}_k^r; \mathbf{x}_{k|k}^{r,m}(h), \mathbf{P}_{k|k}^{r,m}(h)) \quad . \tag{4.25}$$

As the new updated pdf in road coordinates (4.24) has the same structure as the one at time t_{k-1}, (4.17), this closes one iteration of the tracking filter, depicted in Figure 4.2:

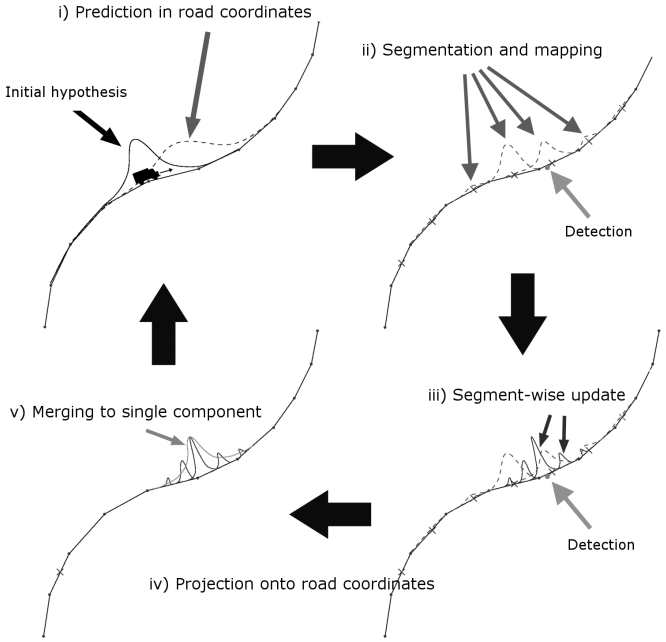

Figure 4.2: Scheme of one iteration of the roadmap assisted tracking filter: i) prediction in continuous road coordinates, ii) segmentation into road segments and mapping to Cartesian coordinates, iii) data processing in Cartesian coordinates, iv) projection onto road coordinates, v) merging (moment matching) to a single component [LSE16].

4.2.3.3 Particle Filter Approach

Alternatively to the Gaussian mixture approach described above, particle filter techniques can be applied (see e.g, [AGOR02, AS03, UK06, OSG09]). Here the particle

states are given by two-dimensional vectors, describing position (mileage) and speed along the road. The low dimensionality of the state vectors has the advantage to enhance the efficiency of particle filter sampling. A corresponding *sampling importance resampling* (SIR) particle filter is described and evaluated in [UK06]. The non-linear mapping to ground coordinates can be done exactly within the errors of the underlying roadmap. In this mapping, a noise term, proportional to the road segment width, is added which shifts the particle position across the road direction. The noise terms describes both the road width and the road mapping error. The particle positions in Cartesian coordinates are used to calculate the likelihood function and, hence, the updated particle weights. The SIR particle filter has been used as a benchmark for the above described Gaussian mixture approach and it has been shown that, for realistic scenarios and system parameters, the performance of the latter almost always is optimal [UK06].

4.2.4 Blind zone Assisted Target Tracking

For the tracking of ground moving targets, measurements of airborne *ground moving target indication* (GMTI) radar [Sko08] are well-suited due to its favorable wide-area illumination, all-weather, day and night availability as well as real-time capabilities. In general, moving objects are detected based on the Doppler shift in the reflected signal, induced by the radial motion of the targets. However, a large amount of the back-scattered radiation originates from the ground, but due to the motion of the sensor platform, these clutter measurements are also colored in Doppler, i.e., exhibit a nonzero Doppler shift. Therefore, a sophisticated clutter suppression technique has to be applied first in order to cancel out the general clutter background, before true detections from moving objects can be obtained and passed along to the tracking unit. The state-of-the-art technique for this clutter cancellation is *space-time adaptive processing* (STAP) [Gue03, Kle06], which performs an optimal two-dimensional suppression of the clutter distribution.

A major challenge for a tracking algorithm using detections from airborne GMTI radar arises from the fact that reflections from moving targets can be suppressed by the STAP clutter filter. This is mostly the case if the radial speed of the target is below the *minimum detectable velocity* (MDV) threshold which indicates the width of the clutter distribution in the Doppler domain. Such *low-Doppler targets* may arise due to an unfavorable target-sensor geometry, slow targets, or due to a stopping manoeuvre. These targets will not be detected by the sensor, yielding possibly long sequences of missed detections. This blind spot of the GMTI sensor is called *Doppler blind zone* and its width is given by MDV.

If a target is masked by the Doppler blind zone, this introduces a constraint which confines the target motion to a certain region. In [KK01,Koc06b,Koc07], the Doppler blind zone information is accounted for in a Bayesian tracking filter by utilizing a state-dependent detection probability, which takes low values whenever an object's range-rate is inside the suppressed Doppler interval. The impact of this blind zone on the detection probability is modeled by an inverse Gaussian, yielding a soft blind zone constraint. In the following, this technique is discussed.

4.2.4.1 Context Modelling

The distance from the blind zone center depends on the target state $\mathbf{x}_k$ and sensor position $\mathbf{r}_k^S$ and is defined by the *Doppler notch function*, $n_D(\mathbf{x}_k, \mathbf{r}_k^S) = \dot{r}_k - \dot{r}_k^c$, i.e., the difference in range-rate between target and surrounding main lobe clutter. Using standard transformation rules, this expression is given in Cartesian coordinates by

$$n_D(\mathbf{x}_k, \mathbf{r}_k^S) = \frac{\mathbf{r}_k - \mathbf{r}_k^S}{||\mathbf{r}_k - \mathbf{r}_k^S||}\dot{\mathbf{r}}_k \tag{4.26}$$

and is thus equal to the target velocity projected onto the line-of-sight vector between sensor and target. Another important quantity is the already mentioned width of the blind zone given by the MDV. In general, the MDV is not a constant sensor parameter for a given scenario setup [MKK14] but depends on a possible spacial separation between transmit and receive unit of the radar (bistatic setup), the array antenna configuration and the look angle of the receive antenna towards the target. But in the following, the MDV will be assumed constant which holds for the monostatic sideways-looking case.

An appropriate modelling of the detection probability impacted by the Doppler blind zone has to account for the following implications:

1. The detection probability P_D has to depend on the state vector of the target, i.e., $P_D = P_D(\mathbf{x}_k)$.
2. P_D has to be small or even vanish if $|n_D(\mathbf{x}_k, \mathbf{r}_k^S)| < \text{MDV}$.
3. For $|n_D(\mathbf{x}_k, \mathbf{r}_k^S)| \gg \text{MDV}$, i.e., far away from the blind zone, P_D has to depend solely on the directivity pattern of the antenna and the distance between sensor and target.

To meet the above condition while preserving the Gaussian framework of (extended) Kalman filtering, the following functional form of the the detection probability P_D has been proposed [KK01]:

$$P_d(\mathbf{x}_k, \mathbf{r}_k^S) = p_d(r_k, \varphi_k, \theta_k) \left[1 - e^{-\log 2 \left(\frac{n_D(\mathbf{x}_k, \mathbf{r}_k^S)}{\mathrm{MDV}} \right)^2} \right] \quad , \tag{4.27}$$

where $p_d(r_k, \varphi_k, \theta_k)$ accounts for the receive directivity pattern which depends on the Rx azimuth angle towards the target and the target range. The particular form of the detection probability is chosen to approximately resemble the influence of the STAP clutter suppression. If the Doppler notch function equals the current width of the blind zone, then $P_d = p_d(\varphi_k, \theta_k, r_k)/2$. Hence, target detections become more and more unlikely as the target moves deeper into the blind zone region and vanish at the blind zone center where the target's range-rate matches the range-rate of the main lobe clutter.

4.2.4.2 Filter Implementation: Inclusion of Doppler Blind Zones

The knowledge on the Doppler blind zone is incorporated into the Bayesian tracking filter by expanding (4.26) in first order around the predicted target state and, then, substituting the target state dependent detection probability (4.27) into the likelihood function (see [KK01]).

This yields a fictitious measurement $\tilde{z}_f$ and fictitious observation matrix $\tilde{\mathbf{H}}_f$:

$$\tilde{z}_f = n_D(\mathbf{x}_{k|k-1}, \mathbf{r}_k^S) + \tilde{\mathbf{H}}_f \mathbf{x}_{k|k-1} \tag{4.28}$$

$$\tilde{\mathbf{H}}_f = -\frac{\partial}{\partial \mathbf{x}_k} n_D(\mathbf{x}_k, \mathbf{r}_k^S)\Big|_{\mathbf{x}_k = \mathbf{x}_{k|k-1}} \quad . \tag{4.29}$$

In that way, the exponential in (4.27) can be rewritten as a Gaussian which linearly depends on the target state vector $\mathbf{x}_k$, yielding

$$P_d(\mathbf{x}_k, \mathbf{r}_k^S) = p_d(r_k, \varphi_k, \theta_k) \left[1 - c_D \, \mathcal{N}(\tilde{z}_f; \tilde{\mathbf{H}}_f \mathbf{x}_k, v_D) \right] \quad , \tag{4.30}$$

where $c_D = \mathrm{MDV}/\sqrt{\log(2)/\pi}$ is a normalization factor and $v_D = \mathrm{MDV}^2/(2 \log 2)$ is the variance of the fictitious measurement $\tilde{z}_f$ in the range-rate domain.

The implications of this detection probability, representing a refined GMTI sensor model, can easily be illustrated by calculating the likelihood function which is now a function of the measurement and the constraint:

$$p(C_k, \mathbf{z}_k|\mathbf{x}_k) = \left(1 - P_d(\mathbf{x}_k, \mathbf{r}_k^S)\right) + \frac{P_d(\mathbf{x}_k, \mathbf{r}_k^S)}{\rho_f} \mathcal{N}(\mathbf{z}_k; \mathbf{H}_k \mathbf{x}_k, \mathbf{R}_k) \quad , \tag{4.31}$$

similar as in (3.39), but with a state dependent detection probability.

With the standard expression for P_d, this yields a Gaussian mixture posterior density consisting of two components, representing the following possible sensor data interpretations:

1. The detection belongs to the target, a regular filtering is executed.
2. The detection is due to a false alarm, the target was not detected.

On the other hand, if the refined GMTI sensor model is considered by inserting (4.30) into (4.31), then due to the $(1 - x)$ structure, each previous mixture component now splits into two components. The resulting four mixture components contain two additional components which can be interpreted as follows:

3. The detection belongs to the target, it is not masked by the Doppler blind zone, removing probability mass out of the blind zone region.
4. The detection is due to a false alarm because the target is masked by the Doppler blind zone.

In other words, the hypothesis that the target is masked (not masked) by the Doppler blind zone induces an inequality constraint on the target state, as the radial velocity has to be smaller (larger) than MDV. As P_d describes a statistical detection probability, the constraint is *soft*.

This example makes clear that due to the increased number of hypotheses established in the filter update step, a tracking filter utilizing the refined GMTI sensor model is able to interpret the sensor output in a more sophisticated manner compared to a standard tracking filter and is capable of handling a sequence of missed detections arising due to Doppler blind zone masking.

4.3 Summary

This Chapter showed how the Bayesian estimation process was modified in order to embed external information such as the context information. The inclusion of this kind of knowledge was done by resorting to constraints affecting the evolution of the target state space. The constraints could be different: soft, hard, equality or inequality. Specifically, the case of hard inequality constraints affecting non-linear

systems has been taken into account for the derivation of the constrained Bayesian formalism and to develop the tracking filters presented in this research work. It has been demonstrated that constraints can be easily inferred in the prediction or in the update steps of the estimation recursion: this leads to the same result from the Bayesian point of view. Finally, some state-of-the-art tracking algorithms have been presented as example of context-based tracking algorithms. The rejection sampling algorithm showed how the constraints impact the prediction step of the estimation process; conversely, the pseudo measurement approach resorted to the modification of the update step. The road-map and the blind zone assisted trackers were also reported as well established state-of-the-art algorithms which deal with the inclusion of context as soft constraint.

CHAPTER V

Innovative Solutions for Maritime Situational Awareness Context-based Target Tracking

The Section presents potential strategies for context-based tracking filters in the area of Maritime Situational Awareness (MSA). As already stated in Chapter 2, MSA is based on the exploitation of data from heterogeneous sources, which concur in providing the *maritime traffic picture* in the observed region. The involved systems include coastal active radars, Navigation Aids, air- and space-based monitoring services, and recently conceived passive sensors. It is clear that one of the major achievements to be sought for future MSA systems is the effective integration of all data sources.

The extraction of the global maritime picture has to cope with the limited performance of each sensor and the complexity of the operational scenario. Target signal fading, anomalous propagation conditions, clutter returns or interferences, transmission channel loss, sensor blockage or malfunctioning, intentional spoofing, etc., make the accurate and reliable extraction of vessel tracks harder. In this perspective, context elements are expected to have an influence on the maritime traffic evolution, since they represent sources of a priori information that can be used in target inference. Geographical information on coastline, ports, maritime highways and corridors, such as information on kinematics and route of each vessel (whose characteristics are summarized in Section 2.2), are elements that can be properly modeled and exploited in the target tracking filtering (i.e., the process of target state vector prediction and measurement update).

The tracking filters hereafter introduced have been conceived and developed with the aim to support the MSA, providing a maritime picture made of multi-sensor tracks

which are build by exploiting some context information of the maritime environment. These techniques rely on the constrained Bayesian filtering presented in Chapter 4. In all the cases, *non-linear* dynamic or measurement models subject to *hard* equality and/or inequality constraints are taken into consideration. Given the non-linearity of the target state estimation problem, the algorithms are based on EKF and PF implementations.

5.1 Navigation Field Assisted Target Tracking

According to the **Navigation Field Assisted EKF** presented by the author in [BU11], the context information plays a fundamental role in the *prediction step* of the target state vector. Under Gaussian assumptions and local linearization - whose parameters vary according to the constraint - the constrained transitional probability density function in Equation 4.6 can be expressed as follows:

$$p(\mathbf{x}_k|\mathbf{x}_{k-1}, C_k) \cong \begin{cases} \mathcal{N}(\mathbf{x}_k; \mathbf{g}_{k-1}(\mathbf{x}_{k-1}); \mathbf{Q^g}_{k-1}) & \text{if } \mathbf{x}_k \in C_k \text{ AND } \mathbf{x}_{k-1} \in D_{k-1}, \\ \mathcal{N}(\mathbf{x}_k; \mathbf{f}_{k-1}(\mathbf{x}_{k-1}); \mathbf{Q^f}_{k-1}) & \text{if } \mathbf{x}_{k-1} \notin D_{k-1}, \\ 0 & \text{otherwise,} \end{cases} \tag{5.1}$$

where C_k is the state vector (equality constraint) that can be reached from the target state $\mathbf{x}_{k-1}$ and D_{k-1} is the ensemble of state vectors that are subject to the influence of the context at time instant t_{k-1}. $\mathbf{f}(.)$ and $\mathbf{g}(.)$ are the transition functions of the state, which allows transiting from $\mathbf{x}_{k-1}$ to C_k and $\mathbf{Q^g}_{k-1}$ and $\mathbf{Q^f}_{k-1}$ are the covariance matrices of the process noises. It is evident that on the basis of the reported pdf, the transitional functions $\mathbf{f}(.)$ and $\mathbf{g}(.)$ to be used by the filter vary and generally their parameters depend on the actual context influence on the state vector $\mathbf{x}_{k-1}$. The influence might be negligible or actual on the basis of the value of some of the components of the state vector at a given time instant. In order to evaluate the expressions in (5.1), context elements generating the constraint are modeled as hereafter reported.

5.1.1 Context Modelling

In the **Navigation Field** model presented in [BU11] context elements are considered as originators of attractive or repulsive forces for targets evolving in their proximity. They are described in a geographic map, whose pixels or cells indicate the *intensity* KC (refer to Equation (5.2)) of their effect on targets. Specifically, for the maritime

environment, ports, coastline, sea highways and corridors, interdicted areas are elements that can be easily represented on the map, providing a better understanding of the scenario (see Figure 5.1).

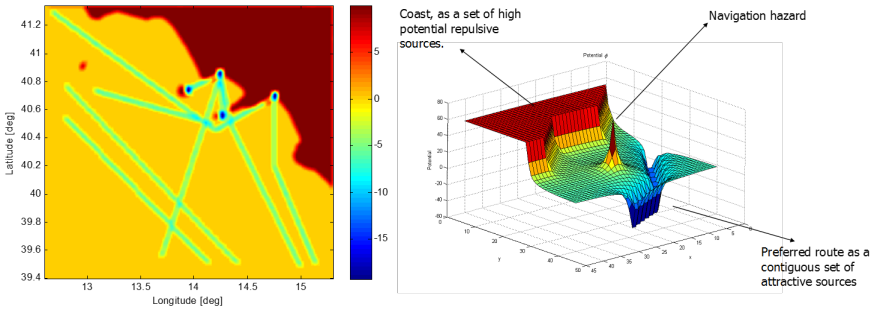

Figure 5.1: Intensity KC map for a reference maritime scenario. Repulsive and attractive sources for transiting vessels are represented by the highest and the lowest values in the map, respectively ([VSB+08]).

If we consider that the context acts like a force on target, we can resort to the Navigation Force Field (NFF) definition in [VSB+08], which describes the resulting effect as superposition of forces.

Let $\vec{F}_{G_i}$ be the force of the i-th context source point acting on a given target. Its strength $|F_i|$ and direction $\angle F_i$ depend on (i) the distance r_i between the target and the i-th element, and (ii) the attractive or repulsive nature of this source. If we choose a force model according to the law of gravity, for the superposition principle the total force exerted on target from N sources is given by:

$$\vec{F}_G = \sum_{i=1}^{N} \vec{F}_{G_i} = \sum_{i=1}^{N} K_i C_i \frac{\vec{r}_i}{{r_i}^3} \quad , \tag{5.2}$$

where K_i is the gravitation coefficient describing the strength of the interaction with the i-th source, and $C_i \pm 1$ denotes the attractive or repulsive nature of the force.

Alternatively, instead of a radial force, the context element can induce a rotational momentum on the target around a pole O:

$$\vec{M}_G = \vec{F}_G \times \vec{l} \quad , \tag{5.3}$$

where $\vec{l}$ is the rotation axis through O.

For a target evolving in a two-dimensional scenario, the total force $\vec{F}_G$ is dynamically evaluated for each discrete time instant t_k as:

$$F_{Gx}(x_k, y_k) = \sum_{i=1}^{N} K_i C_i \frac{x_k - x_i}{{R_{Di}}^3} \tag{5.4}$$

$$F_{Gy}(x_k, y_k) = \sum_{i=1}^{N} K_i C_i \frac{y_k - y_i}{{R_{Di}}^3} \quad , \tag{5.5}$$

where the F_{Gx} and F_{Gy} represent the force components in both X and Y directions, x_k and y_k the coordinates at time t_k and R_{Di} the distance between the target position and the i-th cell. For the sake of simplicity, we assume that the track state is described with a finite set of Motion Models, e.g. $MM = \{S, N, A, R\}$ and the force $\vec{F}_G$ dictates the actuation of the specific MM. In the S (Still) state, the target is steady while in the N (Navigation) state, we assume that it moves along a rectilinear path and is not subject to significant acceleration/deceleration. It can be considered as a pointlike mass mT, not subject to external forces (Constant Velocity model, CV, [BP99]). In the A (Approaching) state, the target approaches a destination: its motion comprises deceleration and quick variation of the heading, which can be described by friction forces. Finally, in the R (Rotating) state the target moves along a circular trajectory with constant speed, in accordance to the Coordinated Turn model, CT [BP99].

The navigation force $\vec{F}_G$ could affect the target by modifying its velocity module and/or its velocity vector orientation. In this case the force is modeled as an additional acceleration which has a direct impact on the target motion (we refer to this as **Model I**). Alternatively, as stated in the equation (5.3), $\vec{F}_G$ is represented by means of rotational momentum $\vec{M}_G$ applied to the target seen as a dipole of length l, with inertial momentum I_T. Under this assumption, the combination of the exerted force, the target speed and the moment of inertia, leads to the angular acceleration $\dot{\omega}$ evaluation, since $\dot{\omega} = M_G/I_T$, (named as **Model II**). For both models, the context information brings non-linearities into the system, independently from the measurement equation applicable to the problem. Thus, each model would require an EKF. It is to be stressed that the effect of the force $\vec{F}_G$ affects only the target state vector and the state covariance matrix predictions; the state vector and the state covariance measurement update equations are not subject to any modification with respect to the well known EKF formulation recalled in Section 3.1.4.1.

5.1.2 Filter Implementation: Model I - Force as Acceleration

Let the state vector at discrete time t_k consist of position, velocity and acceleration components of the target in Cartesian coordinates, i.e. $\mathbf{x}_k^0 = [x_k, y_k, \dot{x}_k, \dot{y}_k, \ddot{x}_k, \ddot{y}_k]$.

For the considered target motion model, the accelerations components $\ddot{x}_k$ and $\ddot{y}_k$ are constant in the time interval $\Delta T = [t_{k-1}, t_k]$ and given by

$$\ddot{x}_k = F_{Gx}(x_k, y_k) \ , \qquad \ddot{y}_k = F_{Gy}(x_k, y_k) \quad . \tag{5.6}$$

Thus, the problem of estimating the target kinematic state is reduced to the evaluation of the following state vector, $\mathbf{x}_k = [x_k, y_k, \dot{x}_k, \dot{y}_k]$.

By resorting to the EKF formulation and taking into account the equation (5.1), the prediction of the target state and covariance are recursively defined as follows:

$$\hat{\mathbf{x}}_{k|k-1} = \mathbf{g}_{k-1}(\hat{\mathbf{x}}_{k-1|k-1}) = \mathbf{G}_{k-1}\hat{\mathbf{x}}_{k-1|k-1} + \mathbf{A}_{k-1} \tag{5.7}$$

$$\mathbf{P}_{k|k-1} = \hat{\mathbf{G}}_{k-1}\mathbf{P}_{k-1|k-1}\hat{\mathbf{G}}'_{k-1} + \mathbf{Q^g}_{k-1} \quad , \tag{5.8}$$

with

$$\mathbf{G}_{k-1} = \begin{bmatrix} 1 & 0 & T & 0 \\ 0 & 1 & 0 & T \\ 0 & 0 & 1 & 0 \\ 0 & 0 & 0 & 1 \end{bmatrix}, \qquad \mathbf{A}_{k-1} = \begin{bmatrix} \frac{T^2}{2}\ddot{x}_{k-1} \\ \frac{T^2}{2}\ddot{y}_{k-1} \\ T\ddot{x}_{k-1} \\ T\ddot{y}_{k-1} \end{bmatrix}, \tag{5.9}$$

where T is the sampling interval and $\mathbf{A}_{k-1}$ is a vector of deterministic inputs that accounts for the observed acceleration (e.g. the constraint), supposed to be constant within the time interval ΔT. The matrix $\mathbf{Q^g}_{k-1}$ in Equation (5.8) represents the covariance of the process noise, while the local linearization $\hat{\mathbf{G}}_{k-1}$ of the non-linear function $\mathbf{g}_{k-1}$ is given by its Jacobian:

$$\begin{aligned} \hat{\mathbf{G}}_{k-1} &= \left[\nabla_{\mathbf{x}_{k-1}} \mathbf{g}^T_{k-1}(\mathbf{x}_{k-1})\right]^T |_{\mathbf{x}_{k-1}=\hat{\mathbf{x}}_{k-1|k-1}} \\ &= \begin{bmatrix} 1 + \frac{T^2}{2}\frac{\partial \ddot{x}}{\partial x} & \frac{T^2}{2}\frac{\partial \ddot{x}}{\partial y} & T & 0 \\ \frac{T^2}{2}\frac{\partial \ddot{y}}{\partial x} & 1 + \frac{T^2}{2}\frac{\partial \ddot{y}}{\partial y} & 0 & T \\ T\frac{\partial \ddot{x}}{\partial x} & T\frac{\partial \ddot{x}}{\partial y} & 1 & 0 \\ T\frac{\partial \ddot{y}}{\partial x} & T\frac{\partial \ddot{y}}{\partial y} & 0 & 1 \end{bmatrix}_{|x=\hat{x}_{k-1|k-1}, y=\hat{y}_{k-1|k-1}} \end{aligned} \quad . \tag{5.10}$$

If the Navigation Field does not impact the target motion (i.e. the acceleration components in Equations (5.6) are zero and the condition $\mathbf{x}_{k-1} \notin D_{k-1}$ holds), the

target state vector and the covariance matrix prediction equations become:

$$\hat{\mathbf{x}}_{k|k-1} = \mathbf{f}_{k-1}(\hat{\mathbf{x}}_{k-1|k-1}) = \mathbf{F}_{k-1}\hat{\mathbf{x}}_{k-1|k-1} \tag{5.11}$$

$$\mathbf{P}_{k|k-1} = \hat{\mathbf{F}}_{k-1}\mathbf{P}_{k-1|k-1}\hat{\mathbf{F}}'_{k-1} + \mathbf{Q}^{\mathbf{f}}{}_{k-1} \quad . \tag{5.12}$$

Specifically we have that $\mathbf{F}_{k-1}$ coincides with $\mathbf{G}_{k-1}$ in accordance to a CV target motion model. The matrix $\hat{\mathbf{F}}_{k-1}$ in Equation (5.12) is computed as usual as:

$$\hat{\mathbf{F}}_{k-1} = \left[\nabla_{\mathbf{x}_{k-1}} \mathbf{f}_{k-1}^T(\mathbf{x}_{k-1})\right]^T |_{\mathbf{x}_{k-1}=\hat{\mathbf{x}}_{k-1|k-1}} \quad . \tag{5.13}$$

The update step of the state estimation process is not influenced by the Navigation Field and follows the EKF formulation presented in Section 3.1.4.1 and hereafter reported:

$$\hat{\mathbf{x}}_{k|k} = \hat{\mathbf{x}}_{k|k-1} + \mathbf{K}_k[\mathbf{z}_k - \mathbf{h}_k(\hat{\mathbf{x}}_{k|k-1})] \quad , \tag{5.14}$$

$$\mathbf{P}_{k|k} = \mathbf{P}_{k|k-1} - \mathbf{K}_k\mathbf{S}_k\mathbf{K}_k^T \quad , \tag{5.15}$$

where

$$\mathbf{S}_k = \hat{\mathbf{H}}_k\mathbf{P}_{k|k-1}\hat{\mathbf{H}}_k^T + \mathbf{R}_k \quad , \tag{5.16}$$

$$\mathbf{K}_k = \mathbf{P}_{k|k-1}\hat{\mathbf{H}}_k^T\mathbf{S}_k^{-1} \quad . \tag{5.17}$$

The matrix $\hat{\mathbf{H}}_k$ results from the linearization of the measurement function $\mathbf{h}_k$ that coincides with the Jacobian of the measurement equation, evaluated at $\hat{\mathbf{x}}_{k|k-1}$:

$$\hat{\mathbf{H}}_k = \left[\nabla_{\mathbf{x}_k} \mathbf{h}_k^T(\mathbf{x}_k)\right]^T |_{\mathbf{x}_k=\hat{\mathbf{x}}_{k|k-1}} \quad . \tag{5.18}$$

We refer to this filter implementation as **NF-CV-CA-EKF** (i.e. Navigation Field - Constant Velocity - Constant Acceleration - EKF).

5.1.3 Filter Implementation: Model II - Force as Angular Acceleration

For this model, the target state vector at discrete time t_k consists of position, velocity and angular velocity, i.e. $\mathbf{x}_k^0 = [x_k, y_k, \dot{x}_k, \dot{y}_k, \omega_k]$.

The force allows the evaluation of the target angular acceleration $\dot{\omega}_k$, from which the target angular velocity ω_k can be extracted:

$$\dot{\omega}_k = f\left\{F_{Gx}(x_k, y_k), F_{Gy}(x_k, y_k), \dot{x}_k, \dot{y}_k\right\} \tag{5.19}$$

$$\omega_k = f\left\{x_k, y_k, \dot{x}_k, \dot{y}_k\right\} = \dot{\omega}_{k-1}T + \dot{\omega}_{k-1} \quad . \tag{5.20}$$

Also in this case, we deal with a reduced dimension target state vector, i.e. $\mathbf{x}_k = [x_k, y_k, \dot{x}_k, \dot{y}_k]$. The prediction of the target state and the covariance matrix are defined as follows:

$$\hat{\mathbf{x}}_{k|k-1} = \mathbf{g}_{k-1}(\hat{\mathbf{x}}_{k-1|k-1}) = \mathbf{G}_{k-1}\hat{\mathbf{x}}_{k-1|k-1} \tag{5.21}$$

$$\mathbf{P}_{k|k-1} = \hat{\mathbf{G}}_{k-1}\mathbf{P}_{k-1|k-1}\hat{\mathbf{G}}_{k-1}^{'} + \mathbf{Q}^{\mathbf{g}}{}_{k-1} \quad . \tag{5.22}$$

It has to be stressed that the state-dependent angular velocity ω_{k-1} derived by the force as in Equation (5.20) is used for the computation of the matrix $\mathbf{G}_{k-1}$. Specifically, on the basis of the CT motion model we have:

$$\mathbf{G}_{k-1} = \begin{bmatrix} 1 & 0 & \frac{\sin(\omega_{k-1}T)}{\omega_{k-1}} & -\frac{1-\cos(\omega_{k-1}T)}{\omega_{k-1}} \\ 0 & 1 & \frac{1-\cos(\omega_{k-1}T)}{\omega_{k-1}} & \frac{\sin(\omega_{k-1}T)}{\omega_{k-1}} \\ 0 & 0 & \cos(\omega_{k-1}T) & -\sin(\omega_{k-1}T) \\ 0 & 0 & \sin(\omega_{k-1}T) & \cos(\omega_{k-1}T) \end{bmatrix}, \tag{5.23}$$

where the sign of the variable ω determines the clockwise and anticlockwise coordinated motion dynamics. Including the definition in the (5.20) in the Equation (5.23), the $\hat{\mathbf{G}}_{k-1}$ is obtained via the Jacobian:

$$\hat{\mathbf{G}}_{k-1} = \left[\nabla_{\mathbf{x}_{k-1}}\mathbf{g}_{k-1}^T(\mathbf{x}_{k-1})\right]^T |_{\mathbf{x}_{k-1}=\hat{\mathbf{x}}_{k-1|k-1}} \quad . \tag{5.24}$$

If the force does not influence the target motion at a given instant of time, the angular velocity ω_{k-1} is not evaluated. Thus, the target prediction is made in accordance to another motion model (i.e. the CV), and the equations (5.21) and (5.22) become:

$$\hat{\mathbf{x}}_{k|k-1} = \mathbf{f}_{k-1}(\hat{\mathbf{x}}_{k-1|k-1}) = \mathbf{F}_{k-1}\hat{\mathbf{x}}_{k-1|k-1} \tag{5.25}$$

$$\mathbf{P}_{k|k-1} = \hat{\mathbf{F}}_{k-1}\mathbf{P}_{k-1|k-1}\hat{\mathbf{F}}_{k-1}^{'} + \mathbf{Q}^{\mathbf{f}}{}_{k-1} \quad , \tag{5.26}$$

where

$$\mathbf{F}_{k-1} = \begin{bmatrix} 1 & 0 & T & 0 \\ 0 & 1 & 0 & T \\ 0 & 0 & 1 & 0 \\ 0 & 0 & 0 & 1 \end{bmatrix}, \qquad \hat{\mathbf{F}}_{k-1} = \left[\nabla_{\mathbf{x}_{k-1}} \mathbf{f}_{k-1}^{T}(\mathbf{x}_{k-1})\right]^{T} |_{\mathbf{x}_{k-1}=\hat{\mathbf{x}}_{k-1|k-1}}. \tag{5.27}$$

Also in this case, the target state update follows the Equations (5.15) to (5.18).

We refer to this filter as **NF-CV-CT-EKF** (i.e. Navigation Filed - Constant Velocity - Coordinated Turn - EKF).

5.2 Sea Lane Assisted Target Tracking

As the **Sea Lane Assisted Tracking** approach is concerned (refer to the Author's work in [BUP+12]), the general assumption is that the context information drives the selection of the target dynamic motion model (DM_k) in the tracking filter at each time step t_k, affecting again the *prediction step* of the target state vector. The constrained transitional density in Equation (4.6) can be expressed as follows:

$$p(\mathbf{x}_k|\mathbf{x}_{k-1}, C_k) \cong \begin{cases} \mathcal{N}(\mathbf{x}_k; \mathbf{f}_{k-1}^{DM}(\mathbf{x}_{k-1}); \mathbf{Q}_{k-1}^{DM}) & \text{if } \mathbf{x}_k \in C_k, \\ 0 & \text{otherwise,} \end{cases} \tag{5.28}$$

where $\mathbf{f}^{DM}(.)$ is the context-driven transition function, which allows transiting from $\mathbf{x}_{k-1}$ to one of the possible states in C_k (inequality constraint) and $\mathbf{Q}_{k-1}^{DM}$ is the covariance matrix of the process noise, which differs depending on the target dynamic motion model. Whereas a Particle filter formulation is required, the constrained transitional density in Equation (5.28) can be written for each $i-th$ particle ($i = 1, ..., N_p$) of the cloud approximating the pdf as follows:

$$p(\mathbf{x}_k|\mathbf{x}_{k-1}^{i}, C_k) \cong \begin{cases} \mathcal{N}(\mathbf{x}_k; \mathbf{f}_{k-1}^{DMi}(\mathbf{x}_{k-1}^{i}); \mathbf{Q}_{k-1}^{DMi}) & \text{if } \mathbf{x}_k \in C_k, \\ 0 & \text{otherwise.} \end{cases} \tag{5.29}$$

The choice of $\mathbf{f}^{DM}$ and $\mathbf{Q}^{DM}$ in Equation (5.28) and for the particles in Equation (5.29) depends on the models adopted to describe the target behavior and the context information. In the following these models are presented as well as the derived target tracking filters.

5.2.1 Target and Context Modelling

The concept of sea lane (including port approaches, shipping lanes, sea highways and traffic separation schemes) has been addressed since it identifies the recommended or most likely route followed by the vessel (see for instance [PHBB14]). The general assumption is that the target is navigating with the aim of reaching a destination or following a predefined path. Therefore, each change of its trajectory (e.g. maneuver) is dictated by the influence of context elements. These considerations allow adopting simple geometrical models describing the target behavior. Specifically, the trajectory is decomposed into linear segments connecting adjacent waypoints. Misaligned segments indicate a maneuver for the target, which is characterized by the time of maneuver, the angular speed and the limiting points. The position of future waypoints and the values of the maneuvering parameters are directly inferred from the context information. We assume that the target proceeds with *constant velocity* along a linear path and then follows a circular trajectory with a *constant angular speed* ω to perform the maneuver. Once completed, the target resumes the linear trajectory. It follows that the trajectory is split in a sequence of Constant Velocity and Coordinated Turn segments. The simplified geometrical model for the target maneuver is reported in the following picture:

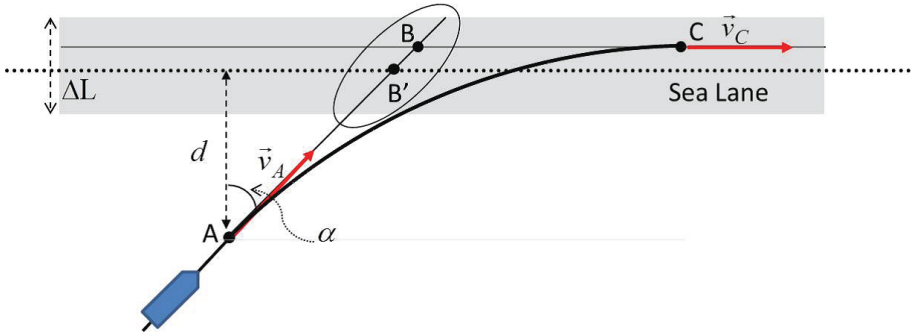

Figure 5.2: Geometrical model for vessel maneuver.

In Figure 5.2, A and C are the start and the end points of the maneuver, respectively. We assume the ship to maintain the same velocity magnitude, i.e. $|v_A| = |v_C|$. The problem is the evaluation of the sea lane entry point C, with $\mathbf{x}_C = [x_C, y_C, \dot{x}_C, \dot{y}_C]$, and the value of ω on the basis of geometric considerations and initial target state vector $\mathbf{x}_A = [x_A, y_A, \dot{x}_A, \dot{y}_A]$. We proceed as follows: (i) point A is chosen with a distance d from the lane axial direction; (ii) point B' is the intersection between the

direction of the ship velocity vector in A and the lane axis; (iii) point B lies in $\overline{AB}'$ direction and has a displacement from B due to the uncertainty of the entry point within the lane. The distance $\overline{AB}$ is given by $\overline{AB} = \overline{AB}' + \xi$, where ξ is a random variable extracted form a truncated Gaussian random process with zero mean value and standard deviation σ_ξ, i.e. $\xi \sim \mathcal{N}(0, \sigma_\xi)$, with

$$\sigma_\xi = \frac{\Delta L}{4cos\alpha}, \qquad \xi \in \left[-\frac{\Delta L}{2cos\alpha}, \frac{\Delta L}{2cos\alpha} \right], \tag{5.30}$$

where ΔL is the lane width. Finally, (iv), point C is given by the intersection of the circle tangent to $\overline{AB}$ in A and the transverse axis passing in B. The value of the angular speed ω is derived from the Coordinated Turn model as follows:

$$\omega = \begin{cases} \frac{\dot{y}_C - \dot{y}_A}{x_C - x_A}, & \text{if } x_A \neq x_C \\ \\ \frac{\dot{x}_A - \dot{x}_C}{y_C - y_A}, & \text{if } y_A \neq y_C \end{cases} . \tag{5.31}$$

5.2.2 Filter Implementation: Context driven Target Model Switching

The context information drives the selection of the target Dynamic Model (DM) in Equation (3.3) for each time instant t_k. It has to be stressed that this selection follows a rule based approach (i.e. target position-sea lane geometry as depicted in Figure 5.2), so the dynamic motion model switching probability is not evaluated.

Let the state vector at the discrete time k consist of position and velocity components of the target in Cartesian coordinates, i.e. $\mathbf{x}_k = [x_k, y_k, \dot{x}_k, \dot{y}_k]$. With respect to the EKF formulation in Section 3.1.4.1 and the transitional pdf in Equation (5.28), the prediction of the target state and the covariance matrix are recursively obtained as:

$$\hat{\mathbf{x}}_{k|k-1} = \mathbf{f}_{k-1}^{DM}(\hat{\mathbf{x}}_{k-1|k-1}) = \mathbf{F}_{k-1}^{DM}\hat{\mathbf{x}}_{k-1|k-1} \tag{5.32}$$

$$\mathbf{P}_{k|k-1} = \hat{\mathbf{F}}_{k-1}^{DM}\mathbf{P}_{k-1|k-1}\hat{\mathbf{F}}'^{DM}_{k-1} + \mathbf{Q}_{k-1}^{DM} \quad . \tag{5.33}$$

Values of $\mathbf{F}_k^{DM}$ and $\mathbf{Q}_k^{DM}$ depend on the selected dynamic model. As the target trajectory is decomposed in linear and curvilinear segments covered at constant velocity, the $\mathbf{F}_k^{DM}$ assumes the form of:

$$\mathbf{F}_{CV} = \begin{bmatrix} 1 & 0 & T & 0 \\ 0 & 1 & 0 & T \\ 0 & 0 & 1 & 0 \\ 0 & 0 & 0 & 1 \end{bmatrix}, \qquad \mathbf{F}_{CT} = \begin{bmatrix} 1 & 0 & \frac{\sin(\omega T)}{\omega} & -\frac{1-\cos(\omega T)}{\omega} \\ 0 & 1 & \frac{1-\cos(\omega T)}{\omega} & \frac{\sin(\omega T)}{\omega} \\ 0 & 0 & \cos(\omega T) & -\sin(\omega T) \\ 0 & 0 & \sin(\omega T) & \cos(\omega T) \end{bmatrix}, \tag{5.34}$$

under the CV and CT assumptions, respectively. T is the sampling interval and ω is the angular velocity for the CT, evaluated as in Equation (5.31). Specifically we have:

$$\begin{cases} \mathbf{F}_k^{DM} = \mathbf{F}_{CT}, \quad \hat{\mathbf{F}}_k^{DM} = \hat{\mathbf{F}}_{CT_k}, \quad \mathbf{Q}_k^{DM} = \mathbf{Q}_k^{CT} & \text{if } (\mathbf{x}_k \in C_k \text{ and } \mathbf{x}_{k-1} \in D_{k-1}) \\ \mathbf{F}_k^{DM} = \mathbf{F}_{CV}, \quad \hat{\mathbf{F}}_k^{DM} = \hat{\mathbf{F}}_{CV_k}, \quad \mathbf{Q}_k^{DM} = \mathbf{Q}_k^{CV} & \text{if } (\mathbf{x}_{k-1} \notin D_{k-1}) \end{cases} \tag{5.35}$$

where D_{k-1} is the ensemble of state vectors that are subject to the influence of the context at time instant $(k-1)$.

The target state update is obtained as follows:

$$\hat{\mathbf{x}}_{k|k} = \hat{\mathbf{x}}_{k|k-1} + \mathbf{K}_k[\mathbf{z}_k - \mathbf{h}_k(\hat{\mathbf{x}}_{k|k-1})] \quad , \tag{5.36}$$

$$\mathbf{P}_{k|k} = \mathbf{P}_{k|k-1} - \mathbf{K}_k\mathbf{S}_k\mathbf{K}_k^T \quad , \tag{5.37}$$

where

$$\mathbf{S}_k = \hat{\mathbf{H}}_k\mathbf{P}_{k|k-1}\hat{\mathbf{H}}_k^T + \mathbf{R}_k \quad , \tag{5.38}$$

$$\mathbf{K}_k = \mathbf{P}_{k|k-1}\hat{\mathbf{H}}_k^T\mathbf{S}_k^{-1} \quad . \tag{5.39}$$

We refer to this filter as **SL-CV-CT-EKF**.

When a *PF technique* is adopted, $\mathbf{F}_k^{DM}$ value differs for each particle of the cloud, as the value of ω depends on the maneuver associated to each particle. Thus, the influence of the context information on the tracking filter is twofold. It drives the switching among different target dynamic models, and it tunes the parameters of the current model (e.g., ω, time for the entire maneuver). We refer to this filter as **SL-CV-CT-PF**.

For practical issues, the value of the constraint C_k can be evaluated in accordance to the procedure depicted in Figure 5.3. C_k can assume two values: 0 when operating with the CV motion model and 1 for the CT case. We assume that in presence of

sensor measurements only the CV model is used. The CV to CT switch takes place when gaps of measurements occur and the target is close to a Knowledge element. Specifically, a proximity criterion is used for the switch. The distances d_j, with $j = 1, .., N_{KB}$, between the vessel and the N_{KB} elements of the KB are evaluated (as in Figure 5.2). If the minimum value of d_j is below the threshold λ, the manoeuvre is initiated with respect to the corresponding KB element. To initialise a new CT mode the angular velocity, ω_k, is evaluated as in Equation (5.31). It will remain constant during the entire time interval T_{AC} (from point A to C in Figure 5.2) required for completing the manoeuvre. The T_{AC} value depends on the geometry and the initial speed of the vessel. The manoeuvring state lasts until its full completion, unless sensor measurements are received.

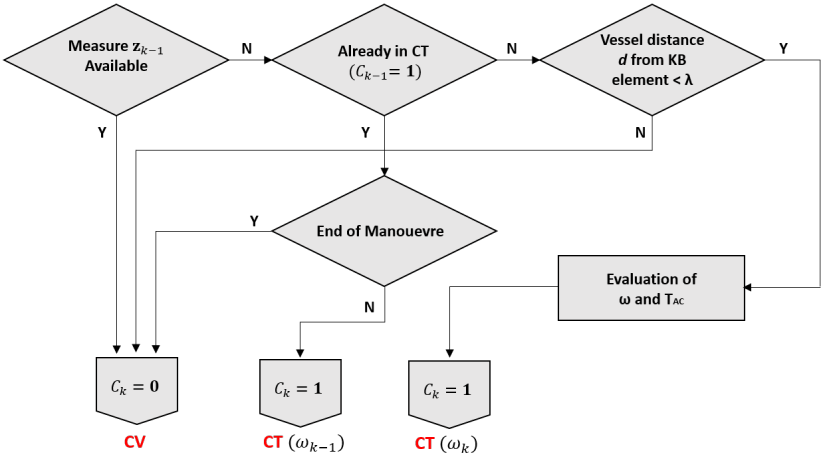

Figure 5.3: Block diagram for target dynamic model switching.

As already said, for the SL-CV-CT-EKF the switching procedure described above is computed for the estimated target state. Conversely, the process is iterated for each particle in SL-CV-CT-PF; hence, they follow manoeuvres that differ both in velocity and start/end points. This phenomenon is depicted in Figure 5.4, where a representative particle cloud splits between particles in "CV mode" and particles in "CT mode". In the background, an exemplary sea lane is also reported representing the context information.

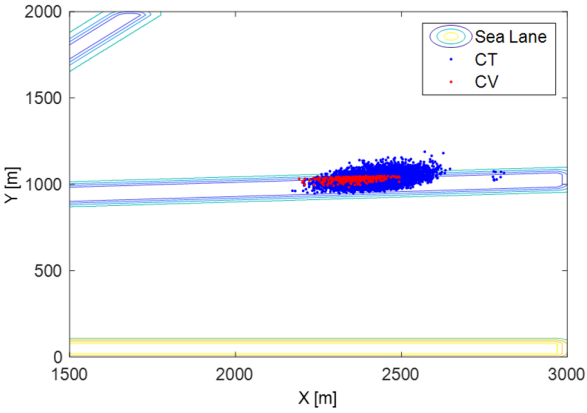

Figure 5.4: Sample particle cloud for PF: particles following different target dynamic models during lack of measurements.

5.3 Knowledge-based Multiple Hypotheses Tracker

With respect to the **Knowledge-based Multiple Hypotheses Tracker (KB-MHT)** approach, we resort to the MHT algorithm described in [Bro12], whose main characteristics are recalled in Section 3.1.5.1. The maritime scenario related context information, i.e. the coastline, the land shape and the clutter conditions, is firstly modeled, properly embedded in specific maps and finally included in the algorithm in the update step of the Bayesian recursion (see [ZDBN12] and [ZBBN14]).

The context information related to the geography can be treated as illustrated in the pseudo measurement approach (Section 4.2.2). The constrained likelihood density function $p(C_k|\mathbf{x}_k)$ in the filter update Equation (4.9) can be approximated as follows:

$$p(C_k|\mathbf{x}_k) = \begin{cases} 1 & \text{if } \mathbf{x}_k \in C_k, \\ 0 & \text{otherwise.} \end{cases} \tag{5.40}$$

Then, the expression in Equation (5.40) is multiplied to the generalized likelihood function $p(Z_k, m_k|\mathbf{x}_k)$ in Equation (3.39), in order to take into account the clutter and false alarm issues in the tracking process.

5.3.1 Context Modelling

Information about specific elements in the maritime environment can be easily embedded in geographic maps that are a priori loaded before the data processing starts and exploited during the different phases of the tracking algorithm (see Section 2.2). As the knowledge-based MHT algorithm is concerned, the basic idea is that each pixel or cell in a geographic map provides the probability (1 or 0) that a vessel can occupy it or not. Specifically such a map encodes the information about coast/terrain and zones interdicted to navigation.

Information about clutter regions are embedded in dedicated clutter maps, which are adaptively generated during the processing phase by estimating the clutter density for each pixel in the area under observation, following the process described in ([MSMM05] and [SD10]). Specifically, the estimation is done by averaging the cell outputs over time and assuming that moving vessels cross the cells in a short time while the clutter remains stationary. This results in the assignment of a probability value within [0,1] for each cell in the map, describing the appearance of the false alarms.

5.3.2 Filter Implementation

The context information related to the geographic map is exploited by the KB-MHT algorithm in the update step of the algorithm, in two different ways: (i) to remodel the transitional pdf in accordance to the context (pseudo-measurement acting on the prediction) and (ii) when new sensor measurements m_k are received as input at time step t_k. In both cases, unrealistic situations such as measurements over land or tracks crossing land are discarded. This allows the reduction of the number of the hypotheses, crucial point for the MHT algorithm, as already mentioned in Section 3.1.5.1. As the information about clutter is concerned, its use affects the track hypotheses update step only.

Let us consider the constrained posterior pdf at t_{k-1} as a Gaussian mixture of n_{k-1} individual track hypotheses:

$$p(\mathbf{x}_{k-1}|\mathcal{Z}^{k-1},\mathcal{C}^{k-1}) = \sum_{i=1}^{n_{k-1}} w_{k-1}^{i}\mathcal{N}(\mathbf{x}_{k-1};\mathbf{x}_{k-1|k-1}^{i},\mathbf{P}_{k-1|k-1}^{i}) \quad , \tag{5.41}$$

where w_{k-1}^{i} is the *i-th* hypothesis weight with $\sum_{i=1}^{n_{k-1}} w_{k-1}^{i} = 1$. The hypotheses in Equation (5.41) are predicted to get the *unconstrained* prior density $p(\mathbf{x}_k|\mathcal{Z}^{k-1},\mathcal{C}^{k-1})$,

assuming the target moving according a linear motion model characterized by white Gaussian noise:

$$p(\mathbf{x}_k|\mathcal{Z}^{k-1},\mathcal{C}^{k-1}) = \sum_{i=1}^{n_{k-1}} w_{k-1}^i \mathcal{N}(\mathbf{x}_k; \mathbf{x}_{k|k-1}^i, \mathbf{P}_{k|k-1}^i) \quad . \tag{5.42}$$

The state estimates $\mathbf{x}_{k|k-1}^i$ and the covariances $\mathbf{P}_{k|k-1}^i$ of each hypothesis are obtained by the Kalman filter prediction Equations:

$$\mathbf{x}_{k|k-1}^i = \mathbf{F}_{k-1}\,\mathbf{x}_{k-1|k-1}^i \quad , \tag{5.43}$$

$$\mathbf{P}_{k|k-1}^i = \mathbf{F}_{k-1}\,\mathbf{P}_{k-1|k-1}^i\,\mathbf{F}_{k-1}^\top + \mathbf{Q}_{k-1} \quad . \tag{5.44}$$

where $\mathbf{F}_{k-1}$ and $\mathbf{Q}_{k-1}$ are the transition matrix of the state and the covariance matrix of the process noise, respectively:

$$\mathbf{F}_{k-1} = \begin{bmatrix} 1 & 0 & T & 0 \\ 0 & 1 & 0 & T \\ 0 & 0 & 1 & 0 \\ 0 & 0 & 0 & 1 \end{bmatrix}, \qquad \mathbf{Q}_{k-1} = \begin{bmatrix} T^3/3 & 0 & T^2/2 & 0 \\ 0 & T^3/3 & 0 & T^2/2 \\ T^2/2 & 0 & T & 0 \\ 0 & T^2/2 & 0 & T \end{bmatrix}. \tag{5.45}$$

Each *i-th* predicted hypothesis is then checked to fulfill or not a geographical constraint (i.e. if the hypothesis prediction lays on the land). To this aim, the prior density in Equation (5.42) is approximated by N random samples, i.e. by a sum of δ - functions, where the *s-th* sample weight is given by $\pi^s = 1/N$:

$$p(\mathbf{x}_k|\mathcal{Z}^{k-1},\mathcal{C}^{k-1}) \approx \sum_{i=1}^{n_{k-1}} w_{k-1}^i \sum_{s=1}^{N} \pi^s \delta(\mathbf{x}_k - \mathbf{x}_{k|k-1}^{is}) \quad . \tag{5.46}$$

For each sample, the correspondent probability value (1 or 0) is extracted from the geographical map: thus, only a subset of the N samples (i.e. the ones that satisfy the condition of laying at sea, with probability 1) will be taken into account in the hypothesis update step. A constrained likelihood function $p(\mathcal{C}_k|\mathbf{x}_k)$, encoding the geo map information, has to be considered for each hypothesis in order to build the constrained posterior pdf $p(\mathbf{x}_k|\mathcal{Z}^k,\mathcal{C}^k)$.

The update step in Equation (4.9) is given by:

$$p(\mathbf{x}_k|\mathcal{Z}^k,\mathcal{C}^k) \propto p(Z_k|\mathbf{x}_k) \sum_{i=1}^{n_{k-1}} w_{k-1}^i \sum_{s=1}^{N} \pi^s p(\mathcal{C}_k|\mathbf{x}_k)\delta(\mathbf{x}_k - \mathbf{x}_{k|k-1}^{is}) \quad . \tag{5.47}$$

Inserting the definition of the constrained likelihood of Equation (5.40) in Equation (5.47) and under Gaussian assumptions we have:

$$\begin{aligned} p(\mathbf{x}_k|\mathcal{Z}^k,\mathcal{C}^k) &\propto p(Z_k|\mathbf{x}_k)\sum_{i=1}^{n_{k-1}} w_{k-1}^i \sum_{\mathbf{x}_{k|k-1}^{is}\in\mathcal{C}_k} \tilde{\pi}^s \delta(\mathbf{x}_k - \mathbf{x}_{k|k-1}^{is}) \\ &\propto p(Z_k|\mathbf{x}_k)\sum_{i=1}^{n_{k-1}} w_{k-1}^i \mathcal{N}(\mathbf{x}_k;\tilde{\mathbf{x}}_{k|k-1}^i,\tilde{\mathbf{P}}_{k|k-1}^i) \quad . \end{aligned} \tag{5.48}$$

where $\tilde{\mathbf{x}}^i$ and $\tilde{\mathbf{P}}^i$ represent the constrained state and the covariance matrix of the *i-th* hypothesis, respectively and $p(Z_k|\mathbf{x}_k)$ is the generalized likelihood function reported in Equation (3.39), which takes into account the clutter density and the false alarm distribution in the FoV of the sensor. Specifically, if we consider m_k sensor measurements received at the time instant t_k and by resorting to the product formula in Equation (3.14), the posterior pdf in Equation (5.48) is again given as a weighted sum of Gaussian:

$$p(\mathbf{x}_k|\mathcal{Z}^k,\mathcal{C}^k) \propto \sum_{i=1}^{n_{k-1}}\sum_{j=0}^{m_k} w_k^{ij}\mathcal{N}(\mathbf{x}_k;\tilde{\mathbf{x}}_{k|k}^{ij},\tilde{\mathbf{P}}_{k|k}^{ij}) \quad , \tag{5.49}$$

where $j=0$ denotes the missing detection case. The weight factor w_k^{ij} is given by:

$$w_k^{ij} = \frac{\hat{w}_k^{ij}}{\sum_{i=1}^{n_{k-1}}\sum_{j=0}^{m_k}\hat{w}_k^{ij}} \quad , \tag{5.50}$$

where

$$\hat{w}_k^{ij} = \begin{cases} 0 & \text{if} \quad j>0 \quad \text{AND} \quad \mathbf{z}_k^j \notin C_k \quad , \\ w_{k-1}^i \frac{P_D}{\rho_F}\mathcal{N}(\mathbf{z}_k^j;\mathbf{H}_k\tilde{\mathbf{x}}_{k|k-1}^i,\mathbf{S}_k^{ij}) & \text{if} \quad j>0 \quad \text{(detection)}, \\ w_{k-1}^i(1-P_D) & \text{if} \quad j=0 \quad \text{(missdetection)}. \end{cases} \tag{5.51}$$

For each recorded measurement $\mathbf{z}_k^j$ at the time instant t_k, the related probability value in the geographic map is extracted on the basis of the geographical coordinates of the measure itself. If the probability value is 0, the measurement is discarded and the hypothesis weight w_k^{ij} set to 0, otherwise the it is taken as possible candidate for new

track generation or it is used to update existent tracks. It has to be stressed that the comparison between the measurement position and the map has to be conducted in the same geographic reference system, this means that some coordinates transformation can be required before starting the processing.

The state vector and the covariance matrix estimates in Equation (5.49) are evaluated via Kalman filtering. Specifically, for $j > 0$ we have:

$$\tilde{\mathbf{x}}^{ij}_{k|k} = \tilde{\mathbf{x}}^{i}_{k|k-1} + \mathbf{K}^{ij}_{k}(\mathbf{z}^{j}_{k} - \mathbf{H}_k\,\tilde{\mathbf{x}}^{i}_{k|k-1}) \quad , \tag{5.52}$$

$$\tilde{\mathbf{P}}^{ij}_{k|k} = \tilde{\mathbf{P}}^{i}_{k|k-1} - \mathbf{K}^{ij}_{k}\,\mathbf{S}^{ij}_{k}\,(\mathbf{K}^{ij}_{k})^{\top} \quad , \tag{5.53}$$

$$\mathbf{S}^{ij}_{k} = \mathbf{H}_k\,\tilde{\mathbf{P}}^{i}_{k|k-1}\,\mathbf{H}^{\top}_{k} + \mathbf{R}^{j}_{k} \quad , \tag{5.54}$$

$$\mathbf{K}^{ij}_{k} = \tilde{\mathbf{P}}^{i}_{k|k-1}\,\mathbf{H}^{\top}_{k}\,(\mathbf{S}^{ij}_{k})^{-1} \quad . \tag{5.55}$$

5.4 Summary

The Chapter presented the description of three innovative solutions for context-based target tracking for the maritime surveillance. The algorithms resort on the constrained Bayesian formalism, which allows the inclusion of constraints in the prediction or the update steps of the recursion. For each technique, the mathematical model to incorporate the available a priori context information into constraints and the tracking filter implementation were described. The Navigation Field assisted target tracking exploited the Navigation Field concept (i.e. force exerted from KB elements on the vessel) to constraint the target state prediction. This led to the formulation of two tracking filters, the NF-CV-CA-EKF and the NF-CV-CT-EKF, depending on the model chosen to describe the navigation force field. The Sea Lane assisted target tracking solution considered the sea lane concepts as main driver for the evolution of the target state. It has been demonstrated how the influence of sea lanes on the filter is twofold. It drives the switching between two different target dynamic models, and it tunes the parameters of the current model. The algorithm could be build by mean of EKF or PF techniques and the derived filters were referred as SL-CV-CT-EKF and SL-CV-CT-PF, respectively. Finally, the Knowledge-based Multiple Hypotheses Tracker (KB-MHT) algorithm allowed incorporating the context information in the update step of the filter. In this case the constrained likelihood function was determined.

CHAPTER VI

Application-Experimentation I: Active Radar Surveillance in Coastal Areas

Active radars are the primary sensors used for real time coastal surveillance purposes. Widely used in VTS systems, as already described in Chapter 2, they allow detecting and tracking different types of vessels (e.g. from rubber boats to cargoes) depending on their specifications and the environmental conditions (e.g. presence of weather and/or sea clutter). However, the target detection and tracking tasks could show deficiencies (e.g. missdetections, false and discontinuous tracks, etc.), mainly due to: (i) radar coverage gaps, (ii) shadowing/masking effects, (iii) dense vessel traffic. In this Chapter, the Navigation Field and the Sea Lane based tracking filters are presented as possible solutions to track vessels monitored by active radars in coastal areas.

6.1 Navigation Field Based Vessel Monitoring

The Navigation Field based tracking filters (NF-CV-CA-EKF and NF-CV-CT-EKF) described in Section 5.1 are hereafter considered. The operative conditions are designed in a such a way the output of a surveillance system (i.e. the maritime traffic picture) results fragmented due, for example, to the presence of gaps of sensors coverage. In such conditions, the tracking filters, which exploit the context information embedded in the navigation field, are expected to bring improvements in the tracking task, in a way that allows faithful reconstruction of vessel trajectories in specific cases, e.g. when scarceness of sensor measurements is recorded.

6.1.1 Test Scenarios and Simulation Rationale

In order to build a realistic scenario for the application, several historical AIS recordings have been analyzed. These data are referred to AIS equipped vessels, such as cargoes and passenger ships, providing information about their positions, speed over ground, rate of turn, etc. This allows investigating the behavior of real targets in the maritime environment and deriving standard motion parameters for the addressed class of ships. The analysis of ship trajectories and dynamics reveals typical vessel behaviors characterized by:

- uniform quasi-rectilinear motion with no significant acceleration, interleaved with curvilinear segments, aimed at slowly re-orienteering ship's heading;
- curvilinear motion with significant acceleration/deceleration within mooring areas.

On the basis of the above analysis, synthetic targets have been generated and injected in a representative scenario for which external information is available from public sources or easily inferred. This "unsensed" information, which is collected before the measurement and estimation process and eventually updated, is expected to influence the evolution of the maritime traffic. Specifically, ports, coastline, sea highways and corridors, interdicted areas, are taken into consideration and embedded in a geographic map, which represents a reference for sensor data processing and interpretation, hence for the implementation of the tracking algorithms. Figure 6.1 shows the geographic area in which the targets evolve (left hand side), and the correspondent geographic map containing the context information (right hand side). Figure 6.2 reports the synthetic target tracks (e.g. ground truth) evolving in the same area.

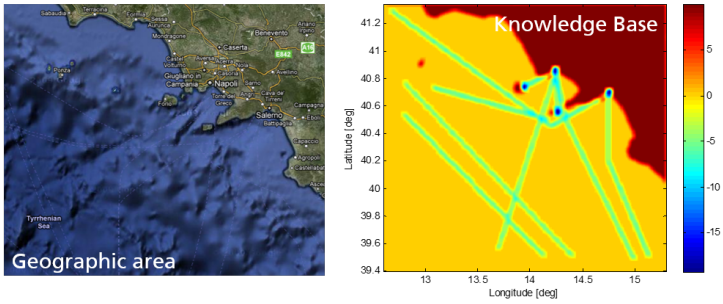

Figure 6.1: Scenario under test: Area of Interest (left hand side) and Geographic Map embedding the context information (right hand side).

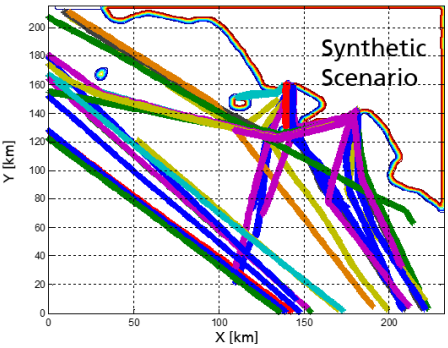

Figure 6.2: Scenario under test: synthetic target tracks over an interval of few hours.

Specifically, the map color scale in Figure 6.1 indicates the "intensity" KC of the effect caused by each KB geographic element on a transiting ship, as reported in the Equation (5.2). In particular, the sea as a whole is considered a neutral element in the map, with 0 intensity, since it does not have effect on the target motion. Therefore, it shall not affect the tracking algorithm, which exploits the Knowledge Base information. Conversely, elements such as land areas and sea lanes are represented in the map by means of positive and negative intensity values, respectively. This spatial environment where the vessels evolve introduces navigational constraints similar to the trafficability concept proposed and applied to the $\alpha - \beta$ filter in [GCS09]. We assume that ports, interdicted areas, etc. exert an attractive or repulsive "force" on the vessel during its motion. This effect is quantified in Section 5.1. In contrast to the trafficabilty concept in [GCS09], the forces considered here include the description of the long range influence of environmental elements on the vessels.

In order to test the NF-filters, two data sets have been generated. The first one contains the targets that have to be monitored. In particular, true vessel state vectors are used as ground truth, while the correspondent shore-based radar sensor measurements are simulated on the basis of typical VTS (Vessel Traffic Service) radar accuracy ([oMAtNI07b]). Gaps of sensor measurements are randomly inserted in the observation during the target path evolution. Specifically, gaps of L minutes ($L = 30, 60min$) are considered for each 2-hour navigation segment. The targets evolution duration is 4 hours on average. The measurement vector is given by $\mathbf{z}(t_k) = \mathbf{z} \in \mathbb{R}^2$, $\mathbf{z}(t_k) = \big[\rho(t_k), \theta(t_k)\big]$, where $\rho(t_k)$ and $\theta(t_k)$ are the range and azimuth measurements at the time instant t_k. The elevation measurement is here neglected. The standard

deviations of the measurement errors are given by $\sigma_\rho = 5m$ and $\sigma_\theta = 0.1°$ in range and azimuth, respectively. The second data set, i.e. the "training set", is used to infer routine trajectories (e.g. the a priori information as in Figure 6.1). An example of simulated measurements is reported in Figure 6.3.

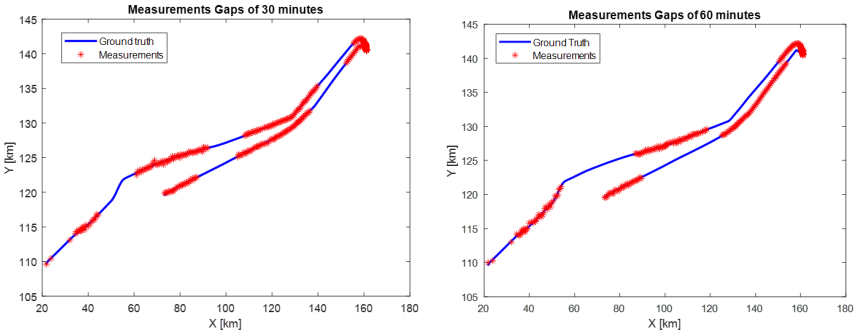

Figure 6.3: Example of simulated vessel trajectories with gap of measurements.

The collected measurements are then transformed into Cartesian coordinates, thus representing the input for tracking filters. The target state vector becomes $\mathbf{x}(t_k) = \mathbf{x} \in \mathbb{R}^4$, $\mathbf{x}(t_k) = \left[x(t_k), y(t_k), \dot{x}(t_k), \dot{y}(t_k)\right]$, where $x(t_k)$, $y(t_k)$ and $\dot{x}(t_k)$, $\dot{y}(t_k)$ are the position and the velocity components of the vessel at the time instant t_k.

It has to be stressed that the current investigation is focused on the filtering performance only, avoiding any association problem. Thus, well separated targets are considered under the hypotheses of a probability of detection $P_D = 1$ and no false detections. The NF-filters are compared with the non KB counterpart, i.e. the Constant Velocity Kalman filter (CV-KF) and the performance assessment is given in terms of vessel track continuity and track accuracy. In order to evaluate the track continuity over the observation time the following criterion is taken into account: a track is lost if the state estimation error exceeds the value of $3\sigma_m$, where σ_m is the RMS measurement error. As the track accuracy is concerned, it will be given as the time percentage over the entire observation of a track in which the context based-filter outperforms its counterpart in terms of RMS error. It is worth to note also that the NF-filters are used when sensor measurements are not available (e.g. during the gaps) and that the analysis addresses the navigation (N) and rotation (R) states only (see Section 5.1).

6.1.2 Simulation Results

Figure 6.4 reports as example the filtering performance for non-intermittent signals received along a single target path, taken as reference.

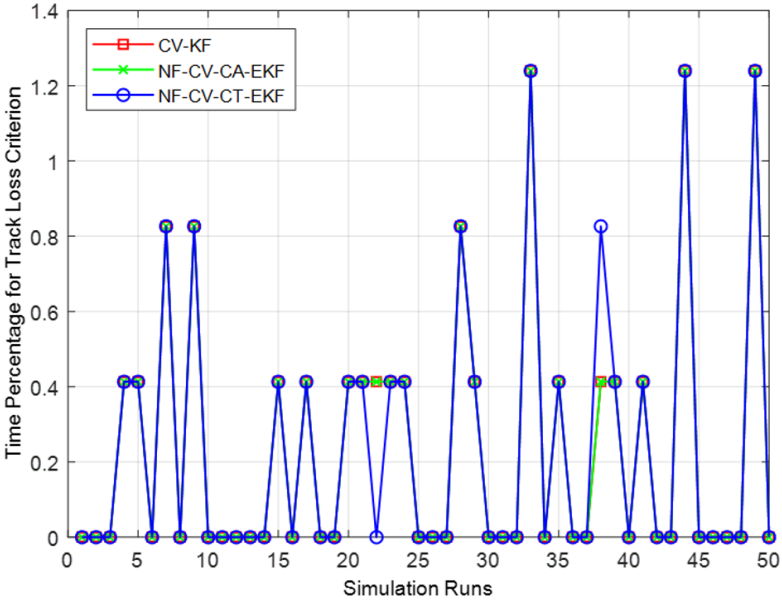

Figure 6.4: Track evolution over a single reference ship target of the considered tracking filters with full measurements coverage.

Three filters (CV-KF, NF-CV-CA-EKF and NF-CV-CT-EKF) are hereafter compared. Specifically, a set of 50 Monte Carlo runs has been carried out with random measurement errors, while the Continuous White Noise Acceleration model (CWNA) was used to describe the target dynamics. The covariance matrix of the process noise was given by:

$$\mathbf{Q} = \begin{bmatrix} \frac{T^3}{3} & 0 & \frac{T^2}{2} & 0 \\ 0 & \frac{T^3}{3} & 0 & \frac{T^2}{2} \\ \frac{T^2}{2} & 0 & T & 0 \\ 0 & \frac{T^2}{2} & 0 & T \end{bmatrix} \tilde{q} \tag{6.1}$$

where T is the sampling interval and $\tilde{q} = {\sigma_v}^2 T$ is the power spectral density of the process noise, with physical dimension $[length]^2/[time]^3$. A process noise with standard $\sigma_v = 0.2m/s^2$ was adopted for the simulation. The performance has been recorded in terms of percentage of occurrences of the track-loss condition (evaluated over the entire track duration) to provide a measurement of the track continuity. It is evident that the introduction of the knowledge does not affect the filters performance in case of measurements availability.

Figure 6.5 shows the results obtained by tracking the vessel with the proposed filters when gaps of $L = 30min$ and $L = 60min$ are randomly selected along the navigation path. It is evident that the NF-CV-CT-EKF outperforms the other filters in most cases. However, the recorded improvement for the track under test is not very significant for small temporal gaps. In case of larger coverage gaps ($L = 60min$), the track continuity definitely increases even though NF-CV-CT-EKF parameters need to be further optimized.

These results suggested to perform the analysis on the complex traffic scenario composed by the 30 ship targets in Figure 6.2 taking into account the NF-CV-CT-EKF formulation only. The results are reported in Figure 6.6. Here the track loss indicator is depicted for coverage gaps of $L = 30min$ and $L = 60min$, respectively. The track loss indicator shows the improvement introduced by the NF-CV-CT-EKF with respect to the CV-KF that does not exploit the context information. The average reduction of track loss condition is around $10\% - 20\%$.

A global improvement might be achieved by adapting the KB filter configuration. In the presented analysis, the filter has been tuned globally for the entire maritime scenario: it does not consider local parameters, such as ship characteristics, sea conditions, navigation rules, etc. These features might have - on average - a non negligible effect on the prediction of the target path, which should be taken into account in the building up of the Knowledge Base. On the other hand, the reported results also suggest that the exploitation of the KB might have a superior impact on later processing stages, e.g. track association, which are not bound to the specific EKF assumptions.

In the following, three case studies, which are representative of complex vessel trajectories with maneuvers, are reported as reference for the application. The considered target trajectories are quite complex, as the vessels are surrounded by several context elements (e.g. ports, coastline and preferred routes), and they follow highly non-linear paths. As usual, random gaps of measurements with duration $L = 30, 60min$ are inserted each 2 hours of navigation. For these case studies, some NF-based filter parameters have been optimized in order to minimize the estimation error along the observation gap. Specifically, the parameters subject to tuning process are: (i) the geographical area around the target for KB evaluation, (ii) the geographical area for preferred route evaluation, (iii) the moment of inertia contributing to the force evaluation and (iv) the process noise gain. The description of these parameters is reported in Section 5.1. Finally, the estimation error between the NF-based filter and the classical CV filter is compared. The measure of performance are evaluated by resorting to 500 Monte Carlo runs per target.

The scenario for the first case study (i.e. target entering the port through the sea lane) is reported in the Figure 6.7, the one for the second test case (i.e. target leaving the port through the sea lane) is depicted in Figure 6.8, while Figure 6.9 is related to the third case study (i.e. long journey and maneuvering target). Each picture in the Figures shows the possible outputs of the considered tracking filters (NF-CV-CT-EKF and CV-KF) and the collected sensor measurements (black crosses).

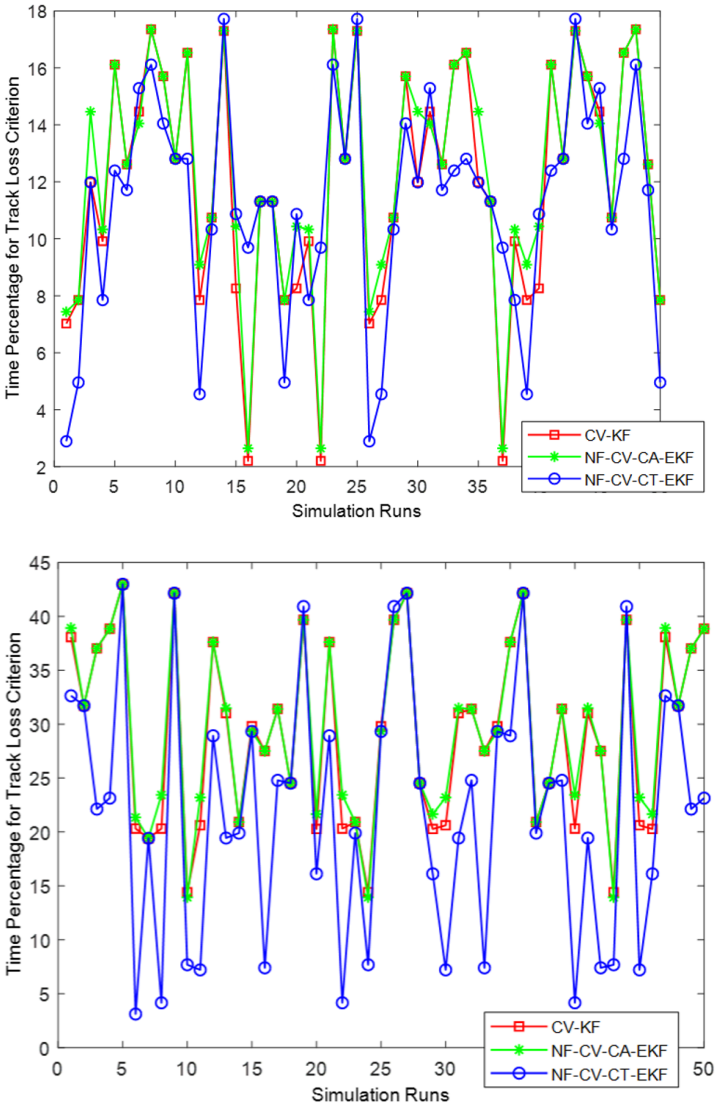

Figure 6.5: Simulated performance over a single ship target for the considered tracking filters with intermittent measurements: Occurrence of track loss condition, with coverage gaps of L=30min (top) and L=60min (bottom).

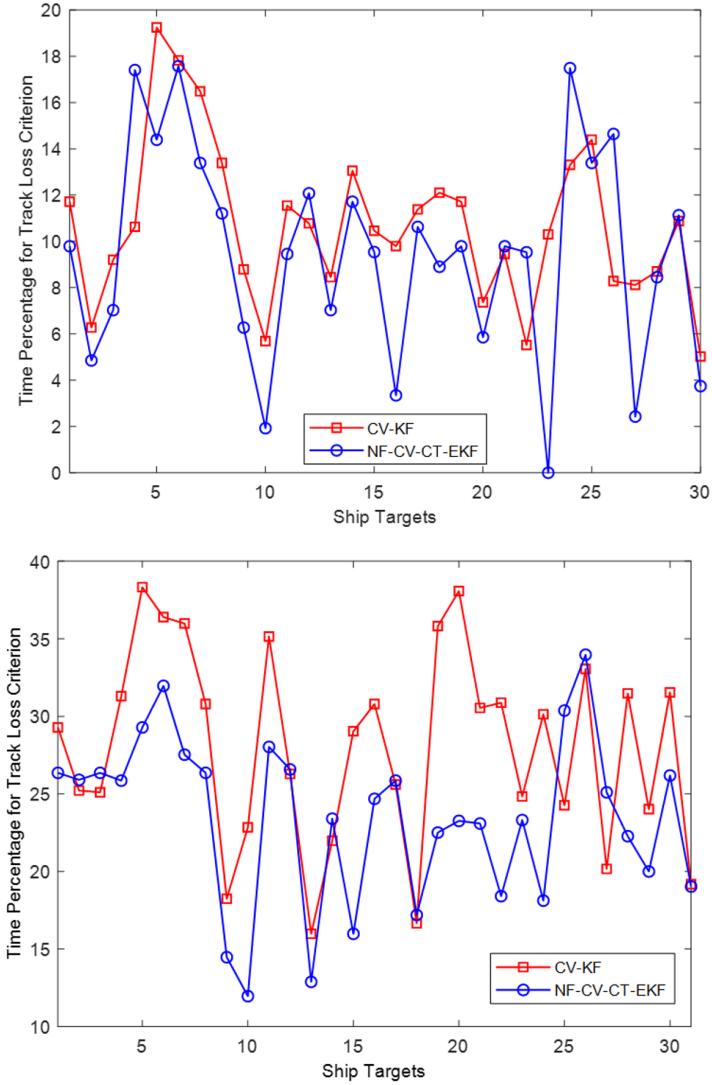

Figure 6.6: Simulated performance over 30 ship targets for the considered tracking filters with intermittent measurements: Occurrence of track loss condition, with coverage gaps of L=30min (top) and L=60min (bottom).

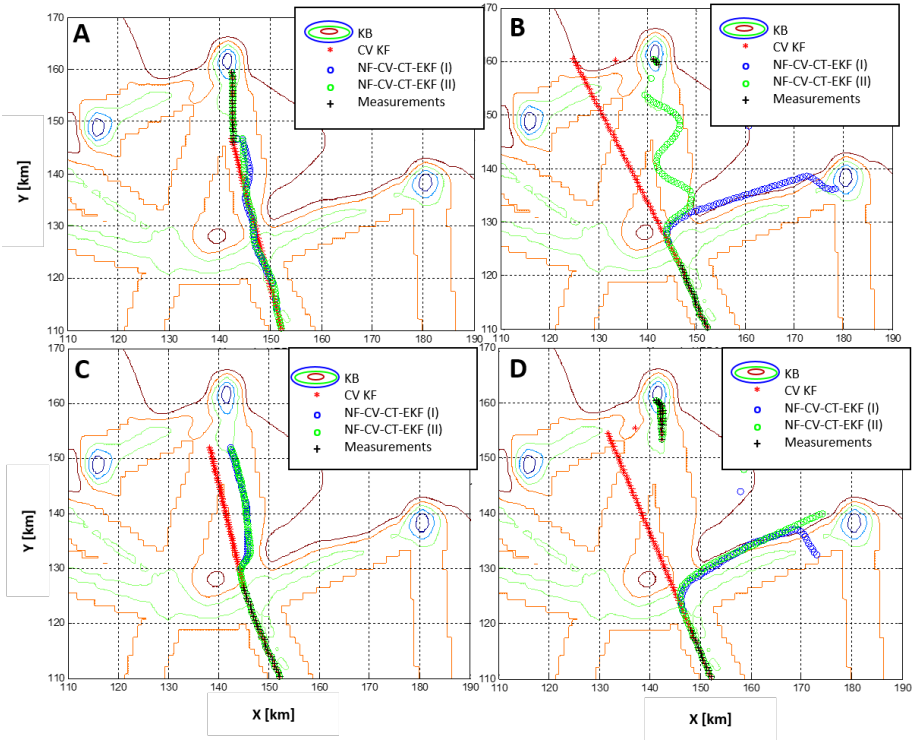

Figure 6.7: Case Study I: target entering the port through the sea lane.

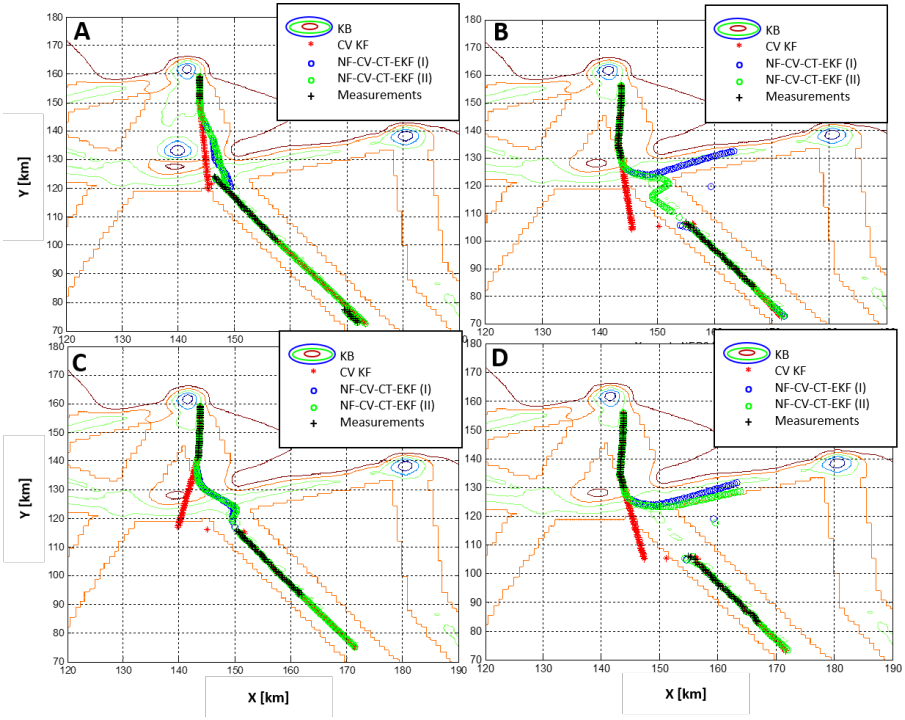

Figure 6.8: Case Study II: target leaving the port through the sea lane.

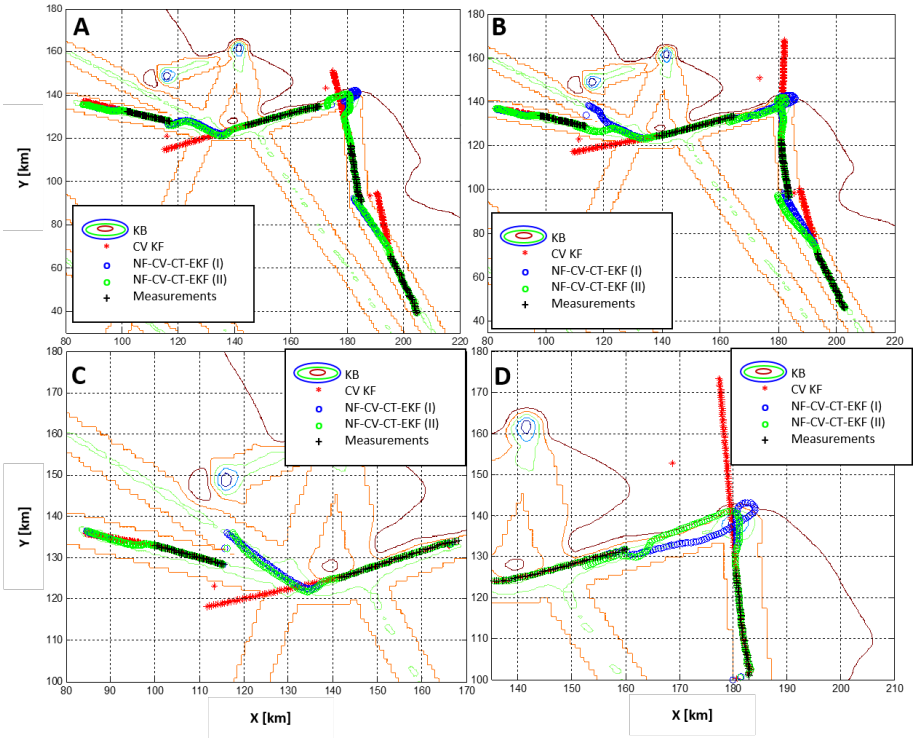

Figure 6.9: Case Study III: long journey and maneuvering target.

The Table 6.1 reports the results of the analysis related to the position estimation error evaluated over the entire track life for the three targets addressed in the case studies. Specifically, the μ_{ET} expresses the percentage of time in which the estimation error provided by the NF-CV-CT-EKF is lower than the CV-KF error, while the N_L value indicates the percentage of time in which the track positioning errors remain within the sea lane (i.e. within its width). Moreover, the Table 6.2 reports the average of the Root Mean Square Error (RMSE) in position evaluated over the three reference targets.

Table 6.1: Position estimation errors over the entire track life.

	Target 1	**Target 2**	**Target 3**
μ_{ET} (Gap 60 min)	52%	48%	50%
N_L (CV-KF, Gap 60 min)	48%	68%	59%
N_L (NF-CV-CT-EKF, Gap 60 min)	55%	74%	65%

Table 6.2: Average position RMSE over three reference targets.

RMSE (Gap 60 min)	**CV-KF** $\approx 3.6km$	**NF-CV-CT-EKF** $\approx 3.1km$
Along Track direction	$3.4km$	$3km$
Across Track direction	$1.4km$	$0.9km$

These results show how the NF-based filter reduces the estimation error in the 50% of the entire tracks duration (see μ_{ET} parameter), on average. But if we observe the time spent by the estimated track within the lane (N_L), it sums to 60-70% for the NF-based filter. This is confirmed by the average track error of the filter in Table 6.2, which is around $1km$ in the across-track (i.e. across-lane) direction for the position estimates for the NF-CV-CT-EKF. However, this is only an average error over the observation gap. It is natural to expect an increasing error during the measurement gap. The worst condition is experienced when sensor data restart after a gap and the estimated position might be very far from the new incoming measurement.

Table 6.3 reports the results of the analysis related to the position estimation error evaluated at track reinitialization step for the three targets. In this case, the μ_{NM} represents the percentage of time in which the estimation error provided by the NF-CV-CT-EKF is lower than the CV-KF error evaluated after a measurement gap.

Table 6.3: Position estimation errors evaluated at the track reinitialization step.

	Target 1	**Target 2**	**Target 3**
μ_{NM} (Gap 60 min)	74%	65%	67%

Table 6.4 reports the average of the RMSE in position evaluated over the three reference targets. It is possible to notice that at the time instant of the track reinitialization, the RMSE provided by the NF-based filter is still acceptable for the application, as it is exactly the transverse lane dimension ($2.5km$ circa).

Table 6.4: Average position RMSE over three reference targets evaluated at the track reinitialization step.

RMSE (Gap 60 min)	**CV-KF** $\approx 9.3km$	**NF-CV-CT-EKF** $\approx 7.2km$
Along Track direction	$8.4km$	$6.8km$
Across Track direction	$4km$	$2.5km$

6.2 Sea Lane Based Vessel Monitoring

In this Section the sea-lane based tracking filters (SL-CV-CT-EKF and SL-CV-CT-PF) described in Section 5.2 are used to track vessels monitored by active radars in coastal areas. The observation conditions might result problematic: shadowing effects, presence of strong sea clutter and failure in data transmissions can affect the sensor detection capability and consequently the vessel tracking task. This leads to a fragmented vessel traffic picture that is undesirable in the coastal surveillance applications.

6.2.1 Test Scenarios and Simulation Rationale

In order to analyze the use of the context information for the two non-linear Bayesian algorithms we resort to Monte Carlo simulations over complex test scenarios. The presented analysis has two objectives. The first one (Objective A) is to assess the improvement coming from the use of the sea-lane information. Specifically, we want to demonstrate how the filters follow more reliably the evolution of the track if the knowledge information is used when the measurements fail. The second objective (Objective B) aims at comparing the predisposition of the tracking filters to easily incorporate the context information, i.e. which of the considered knowledge based filters maintains the track more faithfully in presence of measurement gaps. Given

these considerations, the Objective A requires the comparison of each filter (SL-CV-CT-EKF and SL-CV-CT-PF) with its standard counterpart (EKF or PF); the Objective B resorts on the their direct comparison.

Two test scenarios have been considered for the performance assessment. In both cases, a vessel proceeding with a constant speed of $v = 16knots$ is monitored in an area of $[3 \times 2]km$ by an active coastal radar. The vessel is totally observed for a maximum period of $T_{obs} = 420s$ and the collected information is processed each $T = 2s$ (i.e., update rate for the tracking filter). The probability of detection is assumed $P_D = 1$, but drops to zero when gaps of measurement are simulated in the observation time T_{obs}. Figure 6.10 shows the vessel path (i.e. the ground truth) for the Scenario I. A passenger ship begins its voyage approximately $2km$ far from the littoral, then approaches the coast, enters the closest sea lane and proceeds along the lane direction, which is approximately parallel to the coastline. The turning maneuver starts roughly $450m$ before the lane. Different possibilities are indicated for the radar position. The final one will be chosen in the following for the assessment of the Objectives A and B. In Figure 6.11 the Scenario II is reported. In order to approach the port, the passenger ship performs a double maneuver, which comprises two changes in direction to follow the depicted sea lanes.

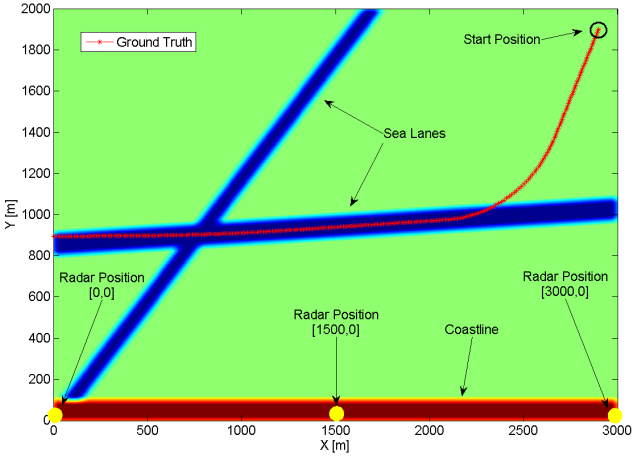

Figure 6.10: Simulated Scenario I: single maneuver target tracking in proximity of the coast accordingly to one sea lane.

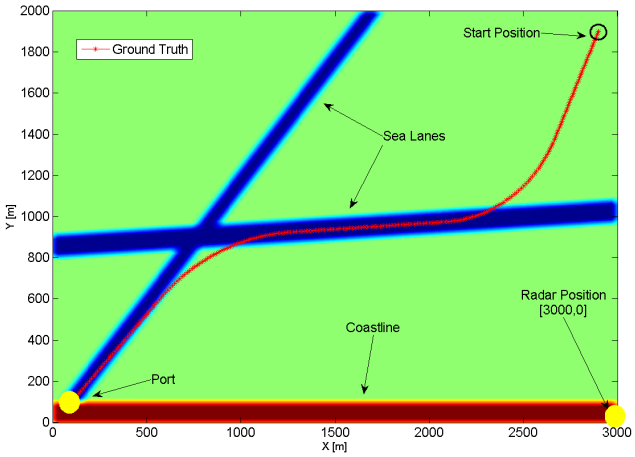

Figure 6.11: Simulation Scenario II: double maneuver target tracking for approaching the port berthing area, accordingly to two sea lanes.

The analysis for the Objectives A and B is performed over both scenarios. Specifically, the single maneuver scenario is also taken as reference to determine the radar location along the coast and to tune the filters parameters. The identified setting is then applied to the more complex observation conditions of Scenario II. A number of $N_{RUN} = 50$ Monte Carlo trials have been run per each analysis. Random measurements with zero-mean Gaussian errors are generated in accordance to the observation conditions described above and the sensor model. Specifically, the measurement vector is given by $\mathbf{z}(t_k) = \mathbf{z} \in \mathbb{R}^2$, $\mathbf{z}(t_k) = \left[\rho(t_k), \theta(t_k)\right]$, where $\rho(t_k)$ and $\theta(t_k)$ are the range and azimuth measurements at the time instant t_k. For the sake of simplicity, the radar measurements in the elevation direction are neglected. The standard deviations of the measurement error are $\sigma_\rho = 10m$ and $\sigma_\theta = 1^\circ$ in range and azimuth, respectively. These values are specified in [oMAtNI07b] as basic performance achieved in Vessel Traffic Services. Gap of measurements have been inserted during the observation period to simulate the lack of information. Specifically, only one gap of measurements ($\Delta_{GAP} = 60s$) is generated in the fixed interval of $T_I = [80, 140]s$ for the Scenario I. Conversely, many gaps of $\Delta_{GAP} = 72s$ are simulated randomly for Scenario II. Then the measurements are injected in the sea lane based filters (SL-CV-CT-EKF and SL-CV-CT-PF) and in their non-knowledge based counterparts (EKF

and PF), thus the measurements transformation from the polar coordinates system to the the Cartesian space is required. The target state vector becomes $\mathbf{x}(t_k) = \mathbf{x} \in \mathbb{R}^4$, $\mathbf{x}(t_k) = \left[x(t_k), y(t_k), \dot{x}(t_k), \dot{y}(t_k)\right]$, where $x(t_k)$, $y(t_k)$ and $\dot{x}(t_k)$, $\dot{y}(t_k)$ are the position and the velocity components of the vessel at the time instant t_k. Under the hypothesis of a constant velocity of the vessel during the observation period T_{obs}, the Continuous White Noise Acceleration model (CWNA) is used in the simulations to describe the target dynamics. As derived in [BSLK01], the resulting process noise covariance matrix for the EKF formulation in Section 3.1.4 is given by

$$\mathbf{Q} = \begin{bmatrix} \frac{T^3}{3} & 0 & \frac{T^2}{2} & 0 \\ 0 & \frac{T^3}{3} & 0 & \frac{T^2}{2} \\ \frac{T^2}{2} & 0 & T & 0 \\ 0 & \frac{T^2}{2} & 0 & T \end{bmatrix} \tilde{q} \tag{6.2}$$

where $\tilde{q}$ is the power spectral density of the process noise, with physical dimension $[length]^2/[time]^3$. Also the choice of $\tilde{q}$, hereafter defined as $\tilde{q} = \sigma^2 T$, will be considered in the tuning process reported in the following.

The performance assessment is given in terms of the Kullback-Leibler Divergence (KLD), whose estimator $\hat{D}_{KL}(p, q)$ is used to compare two continuous densities p and q. The comparison between the EKF and PF distribution follows the process described in Section 3.2.2. Moreover, for the filters tuning phase, in which the most important parameters for the tracking task are identified, we resort also to the Root Mean Square Error (RMSE) formulation, as defined in Section 3.2.1.

6.2.2 Simulation Results over Scenario I

Before proceeding with the filter parameters definition, a proper radar position that guarantees adequate performance in vessel monitoring has to be defined along the coastline. The aim is to identify non-linearity conditions dictated by the observation model and reduce the effect.

The vessel in Figure 6.10 is observed by a radar displaced in three different locations. It has to be stressed that no gap of measurements have been simulated during the observation time (i.e. $P_D = 1$ in T_{OBS}) for this analysis. The collected measurements are given as input to the standard EKF and PF (Section 3.1.4). The tracker outputs are then compared with the vessel ground truth, represented by a reference probability distribution based on PF ($\mathrm{PF_{Ref}}$) and generated with a high number of particles ($\mathrm{N_{pRef}} = 10^5$). Also the posterior densities of the two non-linear filters have been

sampled with the same number of particles, specifically ($\mathrm{N_{pEKF}} = \mathrm{N_{pRef}}$) for the EKF and ($\mathrm{N_{pPF}} = \mathrm{N_{pRef}}$) for the PF formulation. The results, given in terms of $\hat{D}_{KL}(p,q)$ mean value, are reported in Figure 6.12.

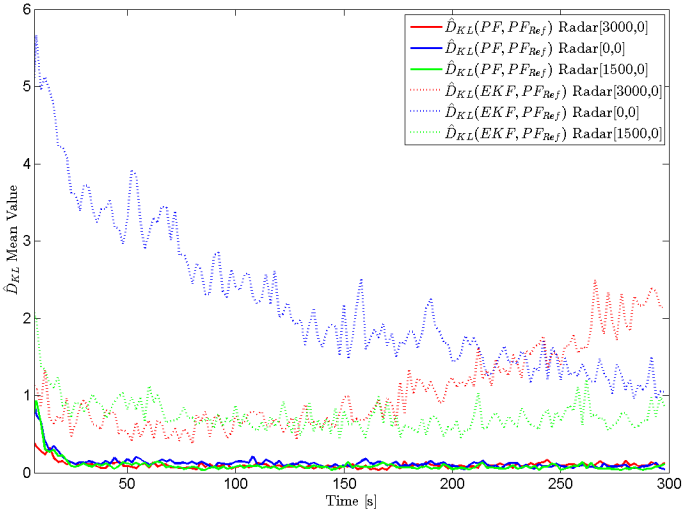

Figure 6.12: $\hat{D}_{KL}$ mean value for Scenario I with all measurements. $\hat{D}_{KL}(\mathrm{PF}, \mathrm{PF_{Ref}})$ and $\hat{D}_{KL}(\mathrm{EKF}, \mathrm{PF_{Ref}})$ are evaluated over 50 Monte Carlo runs with radar position in $[3000, 0]m$, $[1500, 0]m$ or $[0, 0]m$. Filters are tuned for linear acceleration with $\sigma_v = 1m/s^2$. Temporal filter update $T = 2s$; total duration $T_{obs} = 300s$.

As the non-linearity gets severe, the non-Gaussianity of the posterior PDF of the state becomes more pronounced. In such cases, we expect the performance of the EKF schemes to degrade significantly. As described in [DFG01] the particle-based description of the PDF better approximates the true distribution (KLD $\simeq 0$) as the non-linear transformation is applied to the Gaussian measurement vector. Figure 6.12 shows that the performance of the two classes of filters diverge more significantly for the radar located in $[0, 0]m$ (i.e. blue plots), where the non-linearity effect is higher due to the angle among the target trajectory and the sensor range, and the larger target distance from the radar. For the forthcoming analysis we select the sensor in $[3000, 0]m$, which allows a fair comparison being an intermediate situation in terms of non-linearity. In addition, this latter viewing condition leads to RMS errors, which

are still acceptable (Figure 6.13).

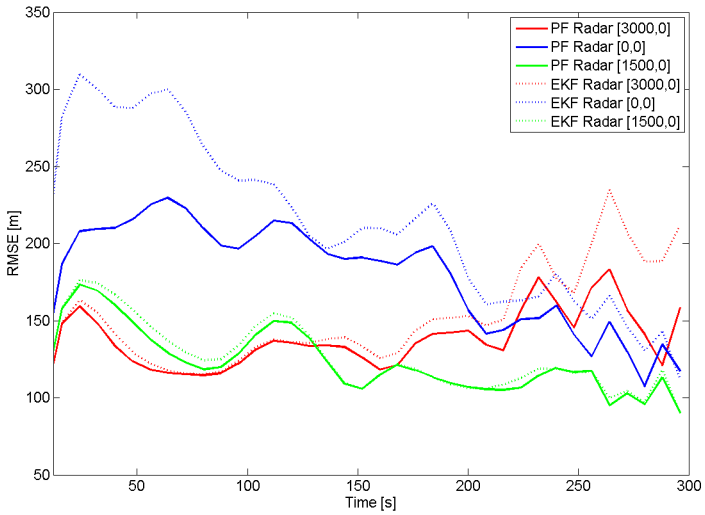

Figure 6.13: RMSE mean value for Scenario I with all measurements. RMSE of PF and EKF are evaluated over 50 Monte Carlo runs with radar position in $[3000, 0]m$, $[1500, 0]m$ or $[0, 0]m$. Filters are tuned for linear acceleration with $\sigma_v = 1m/s^2$. Temporal filter update $T = 2s$; total duration $T_{obs} = 300s$.

Filter Tuning Phase

Next step is devoted to the choice of the number of particles to be used in the PF formulation. Figure 6.14 shows the $\hat{D}_{KL}$ in terms of mean value and variance for a PF with particles cloud of different dimension. As expected, the KLD estimate converges as the number of particles increase. It is evident that the convergence is reached also for $\mathrm{N_p} = 3000$, this means that no drastic improvement is envisaged when a larger cloud is used. Thus, the value of 3000 particles is chosen for the analysis.

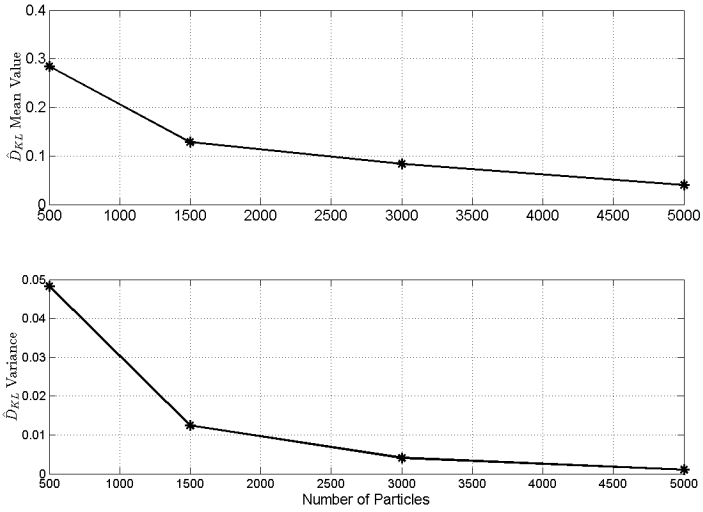

Figure 6.14: $\hat{D}_{KL}$ mean value (Top) and variance (Bottom) for a PF over Scenario I. Steady filter behavior as a function of particles number is reported. All measurements are considered for radar in position $[3000, 0]m$. PF is tuned for linear acceleration with $\sigma_v = 1m/s^2$. Temporal filter update $T = 2s$; total duration $T_{obs} = 300s$; number of Monte Carlo runs = 50.

The last step is related to the tuning of the standard deviation value of the process noise (σ_v) for the tracking task. This parameter contributes to the covariance matrix prediction in the EKF, and the particle cloud prediction for PF (Section 3.1.4). Figure 6.15 shows that a process noise with standard deviation $\sigma_v = 0.3m/s^2$ allows the EKF to better approximates the PF_{Ref}. For PF, a small performance degradation is observed during the initial phase, which is anyhow negligible for most of the observation time. This setup is used for the further analyses.

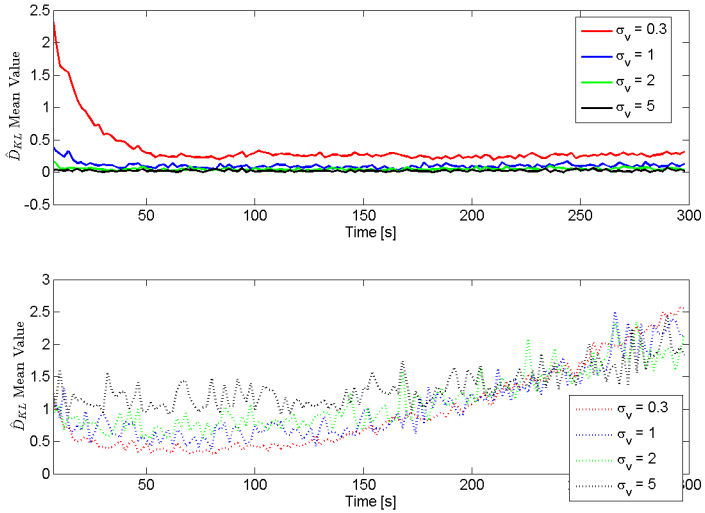

Figure 6.15: $\hat{D}_{KL}$ mean value for Scenario I with all measurements. $\hat{D}_{KL}(\mathrm{PF}, \mathrm{PF}_{\mathrm{Ref}})$ (Top) and $\hat{D}_{KL}(\mathrm{EKF}, \mathrm{PF}_{\mathrm{Ref}})$ (Bottom) are evaluated over 50 Monte Carlo runs with radar position in $[3000, 0]m$ and different *rms* velocity errors σ_v of $0.3m/s^2$, $1m/s^2$, $2m/s^2$ and $5m/s^2$. Temporal filter update $T = 2s$; total duration $T_{obs} = 300s$.

Objective A - Knowledge Based Improvement

The assessment is given in terms of $\hat{D}_{KL}$. The SL-CV-CT-EKF and SL-CV-CT-PF are compared with the standard EKF and PF to assess the improvement coming from the exploitation of the sea lanes. The reference distribution $\mathrm{PF}_{\mathrm{Ref}}$, with $\mathrm{N}_{\mathrm{P}_{\mathrm{Ref}}} = 10^5$, which represents the ground truth, is generated without exploiting the context information since it runs over the continuous set of measurements (i.e., estimation with no measurement gaps as it is the ideal situation we tend to). The posterior *pdf* of the EKF is generated with $\mathrm{N}_{\mathrm{PEKF}} = \mathrm{N}_{\mathrm{pRef}}$. The PF filter is run with $\mathrm{N}_{\mathrm{PPF}} = 3000$.

Figure 6.16 shows the results of the comparison for the Scenario I. In the time interval ($T_I = [80, 140]s$) in which the measurement gap occurs and in which the target maneuvers, the KB filters outperform EKF and PF. The performance is based on the assumption of perfect knowledge of the maneuver by the filters (i.e. ω value, start-end points, T_{AC} in Figure 5.2).

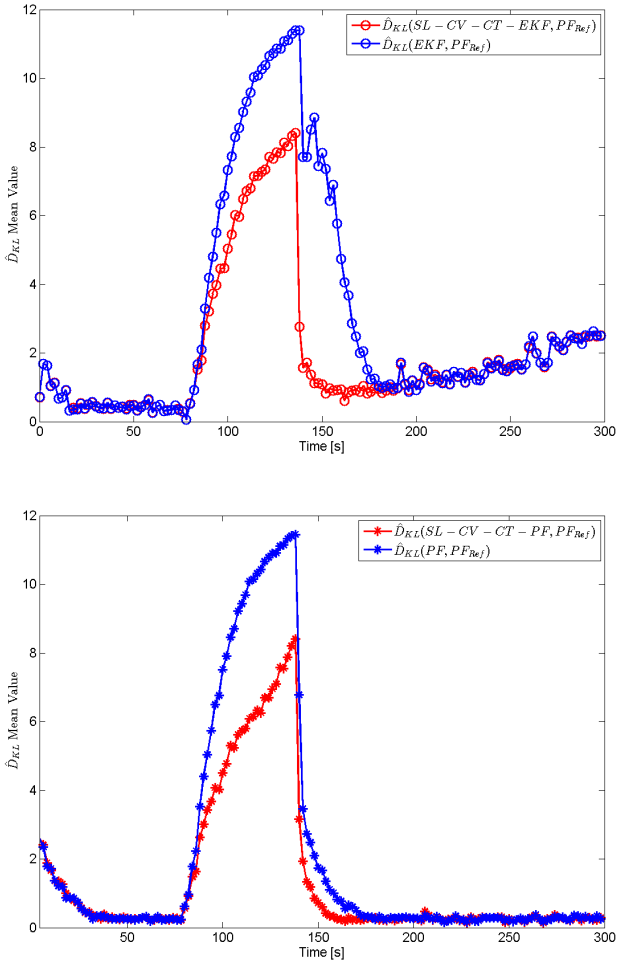

Figure 6.16: $\hat{D}_{KL}$ mean value for Scenario I, evaluated with Δ_{GAP}=60s in $T_I = [80, 140]s$, T=2s and T_{OBS}=300s. Radar position in $[3000, 0]m$ and $\sigma_v = 0.3m/s^2$. Top: EKF case. Bottom: PF case

Objective B - PFvsEKF

The comparison between the SL-CV-CT-EKF and the SL-CV-CT-PF is here reported for Scenario I. For computing the KLD estimator, a new reference distribution based on the context exploitation (i.e. $\mathrm{SL}-\mathrm{CV}-\mathrm{CT}-\mathrm{PF}_{\mathrm{Ref}}$) is generated with $\mathrm{N}_{\mathrm{pRef}} = 10^5$ over an intermittent set of measurements, randomly simulated during the observation period. The distribution for the SL-CV-CT-EKF is generated with $\mathrm{N}_{\mathrm{pEKF}} = \mathrm{N}_{\mathrm{pRef}}$ while the SL-CV-CT-PF filter is run with $\mathrm{N}_{\mathrm{PPF}} = 3000$ particles.

Figure 6.17 shows the $\hat{D}_{KL}$ mean value and variance obtained with respect to the reference distribution $\mathrm{SL}-\mathrm{CV}-\mathrm{CT}-\mathrm{PF}_{\mathrm{Ref}}$. In other words, the measurements gap (fixed in this case) is considered for all filters, so that the approximation loss for SL-CV-CT-EKF and SL-CV-CT-PF can be observed. It is evident that the PF based technique yields a much better capability in approximating the asymptotically true *posterior pdf* with respect to the EKF counterpart.

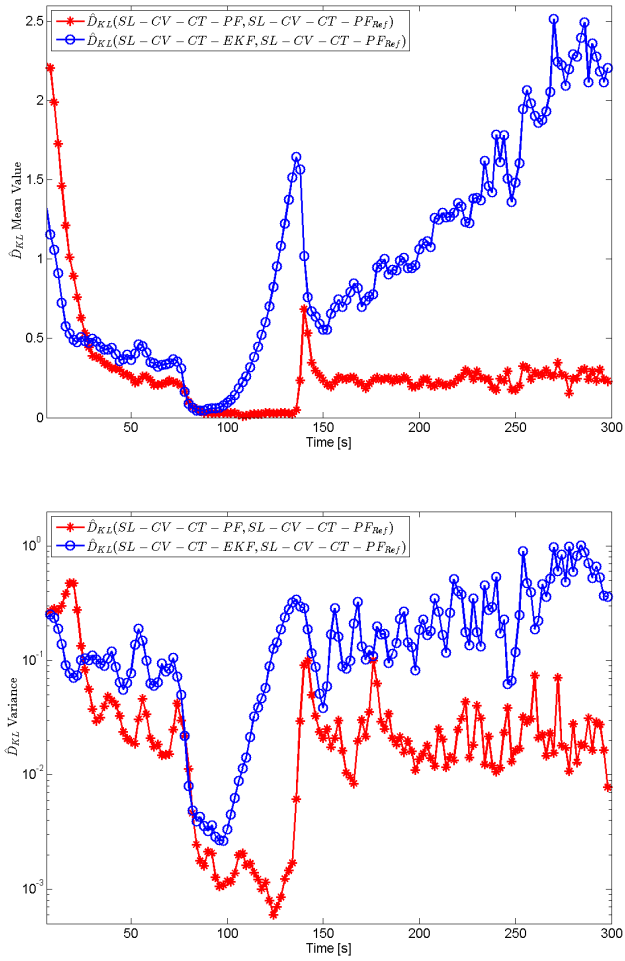

Figure 6.17: Comparison between the SL-CV-CT-EKF and SL-CV-CT-PF for Scenario I in terms of $\hat{D}_{KL}$ mean value (Top) and variance (Bottom), evaluated with Δ_{GAP}=60s in $T_I = [80, 140]s$, T=2s and T_{OBS}=300s. Radar position in $[3000, 0]m$ and $\sigma_v = 0.3m/s^2$.

6.2.3 Simulation Results over Scenario II

The filters setup - identified in the previous analysis - has been applied to the second test scenario, which offers a double ship manoeuvre study case. We considered two or three measurement gaps, each of 72 seconds, randomly simulated over the entire observation period of 420 seconds. Additional losses are inserted by mismatching the used manoeuvre model with respect to the true trajectory. Adopted manoeuvres fall in the ranges defined in Table 6.5 for large ships. All parameters definitions are extracted from [RT01]. Specifically, the tactical diameter is taken as 4 times the ship length and the speed on turn is taken as 1.2 the circle diameter. Finally, all parameters are defined for vessel navigating with a speed of 16 knots.

Table 6.5: Typical vessel manouvring parameters.

IALA Type	**Description**	**Sample Length [m]**	**Tactical Diameter [m]**	**Advance [m]**	**Speed on Turn [deg/s]**
5	Fishing or patrol vessel	30	120	144	6
6	Passenger ship	100	400	480	2
7	Cargo ship	200	800	960	1

Objective A - Knowledge Based Improvement

Figure 6.18 reports the results for Scenario II. The performance improvement due to the use of the context (i.e., the two sea lanes and the port location) is still very high. The robustness of the knowledge based filters to the model mismatch is promising, especially for the SL-CV-CT-PF case, which allows to better handle the non-linearity conditions experienced at the end of the observation period (i.e. vessel approaches the port).

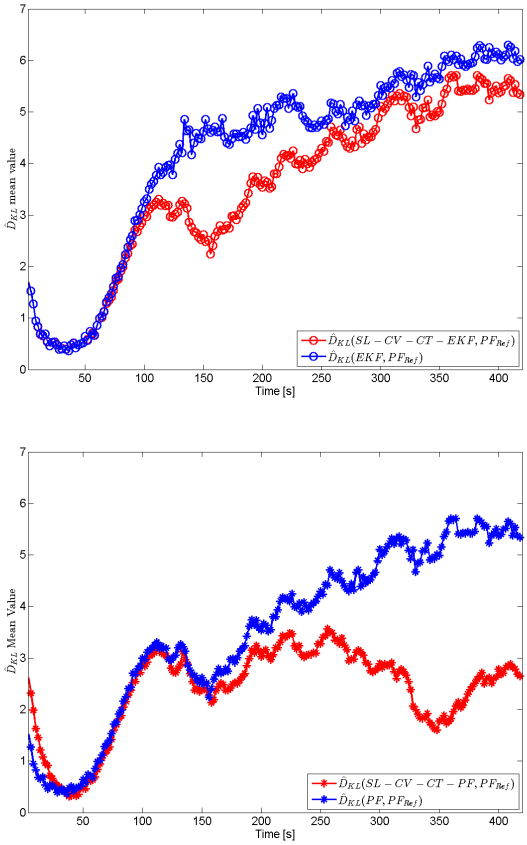

Figure 6.18: $\hat{D}_{KL}$ mean value for Scenario II, evaluated with random measurement gaps of Δ_{GAP}=72s, T=2s and T_{OBS}=420s. Radar position in $[3000, 0]m$ and $\sigma_v = 0.3m/s^2$. Top: EKF case. Bottom: PF case

Objective B - PFvsEKF

Figure 6.19 reports the comparison between the SL-CV-CT-EKF and SL-CV-CT-PF for Scenario II in terms of KLD mean value and variance. Also for this Scenario, the knowledge-based PF technique outperforms the EKF counterpart.

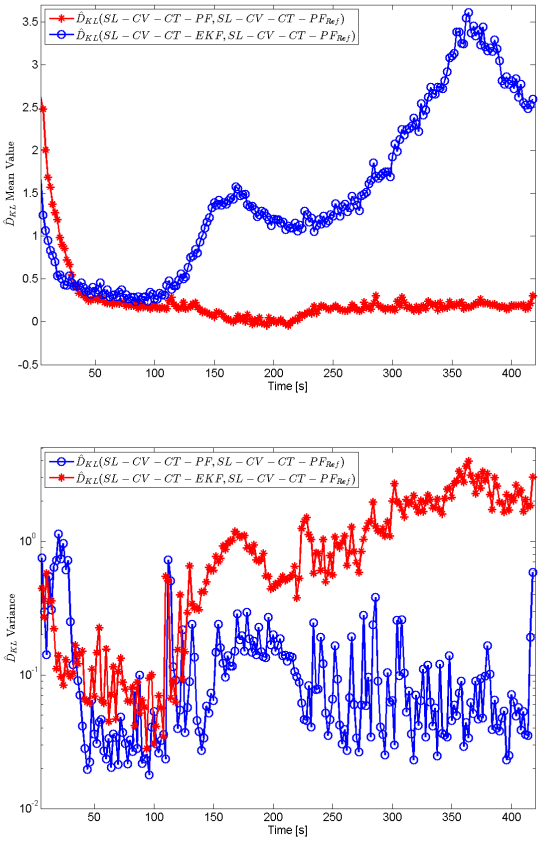

Figure 6.19: Comparison between the SL-CV-CT-EKF and SL-CV-CT-PF for Scenario II in terms of $\hat{D}_{KL}$ mean value (Top) and variance (Bottom), evaluated with random measurement gaps of Δ_{GAP}=72s, T=2s and T_{OBS}=420s. Radar position in $[3000, 0]m$ and $\sigma_v = 0.3m/s^2$.

6.3 Summary

In this Chapter the innovative Navigation Field (NF) and the Sea Lane (SL) based tracking filters were used to track vessels monitored by active radars in coastal areas. Results over synthetic data in a real scenarios demonstrate that the KB filters are promising techniques for achieving increased track continuity in the absence of continuous measurements, i.e., tracking information sources that are intermittent due to sensor coverage gaps, loss of communication, non-cooperative targets, etc.

For the NF-based filters, tracking performance were given in terms of track continuity and track accuracy. With respect to the track continuity definition (i.e. a track is lost if the error on the state estimate exceeds 3 times the RMS measurement error), it has been demonstrated that the KB-filters reduced the track-loss condition of 10% to 20% on average with respect to the standard KF. This value increased when larger gaps of measurements were registered. As track accuracy is concerned, the time percentage over the entire observation of a track in which a NF-filter outperforms its non KB counterpart in terms of RMS position error was evaluated. The results showed how the NF-based filters reduce the estimation error in the 50% (on average) of the entire tracks duration.

For the SL-based filters, the performance on tracks accuracy were provided through the evaluation of the Kullback-Leibler Divergence in terms of mean value and variance. The performance analysis over two simulated scenarios yielded a significant improvement coming from the exploitation of the a priori information about the sea lane. For both scenarios the SL-filters outperformed their non-KB counterparts. In addition, the PF scheme demonstrated increased robustness with respect to the EKF as highly non-linear tracking conditions were experienced.

CHAPTER VII

Application-Experimentation II: Collaborative Vessel Traffic Monitoring In High Seas and Coastal Areas

The use of collaborative vessel traffic monitoring systems like AIS (terrestrial and/or satellite based) or LRIT is well established for maritime surveillance and safety at sea purposes. Today, over half a million vessels use AIS to transmit their position and other useful information, which are collected by a network of AIS receivers on other vessels, deployed in land stations or in satellites. The combination of data from satellite and land-based receivers has enabled the creation of a worldwide network that can collect, share and interpret the information broadcast by each ship, to provide users with a real-time picture of global shipping traffic.

However, such collaborative systems could suffer from unexpected interruptions of signal transmission due to systems' malfunctioning other wanted turning off. AIS signals are indeed expected to be continuous in time within the transmission range. Any unrealistic changes within this range may indicate suspicious activities. The AIS transmitter could have been switched off or it could have been manipulated to send incorrect information about the vessel. Specifically, static information like vessel's name, type, dimensions, IMO number, relative position of the AIS unit, the destination, the ETA and also draught can be manipulated and/or not correctly updated by the vessel's officer. Finally, the lack of AIS receivers especially in high seas navigation condition does not consent a continuous vessel monitoring. These aspects could represent a problem for the vessel tracking task, which has to deal with discontinuous information and/or incorrect data. In such conditions, the exploitation

of maritime context information, i.e. the knowledge of navigational routes, represents the key to support the vessel monitoring, since it allows keeping the target tracking during the information gaps.

In this Chapter, an operative solution based on vessel route prediction concept is presented to track vessels in high seas and coastal areas.

7.1 Vessel Route Prediction

The basic idea of route prediction is to obtain the estimates of the vessel position during a long observation interval under the influence of intrinsic parameters (e.g. vessel motion characteristics) and external information (e.g. perturbing factors due to the environment). This can be used to support the compilation of the traffic picture and to detect anomalous behaviors of the vessels. This concept has been embedded in the Route Propagation Module (RPM), developed by the author for the EU-FP7 funded project NEREIDS (New Service Capabilities for Integrated and Advanced Maritime Surveillance, [fIS]), and hereafter presented. The module addresses the problem of tracking maneuvering vessels for long time intervals, in which no new information (reports) on the vessels' state is received. This means that the module can support the tracking task either in remote coastal areas characterized by a poor sensor coverage, or in high seas, where vessels are monitored by specific satellite based technology sensors (see Section 2.1). For track maintenance purposes, the RPM algorithms exploit a priori information such as the knowledge of maritime traffic patterns, sea lanes, and the bathymetry of the monitored area of interest. The capabilities of this context-aided technique are assessed for realistic scenarios that include typical vessel maneuvers. The results on real data show that the use of the a priori information yields improvements in the accuracy of the predicted vessel position.

The RPM main objective is to identify the most likely locations where vessels might be in the future within a given scenario. This could be required for two main reasons: (i) the information about the vessels (e.g. current track estimates) is not available anymore (i.e. track drop, sensor coverage/data transmission problems, etc...), but it is necessary to get the vessels' state estimate after a given time period, and (ii) even when the information is available, there is the need to compare the actual vessel behavior with the results of the RPM estimation process for monitoring purposes (e.g., anomaly detection).

Specifically, the vessels' position predictions are provided at time instants $(t_k + \Delta T)$ much larger than 1 hour, after having received the vessels' state at time t_k. This puts the RPM algorithms somehow in between Level 1 and Level 2 of the Joint Directors

of Laboratories' (JDL) model for data fusion, [HM04]. From one side the RPM performs the prediction step of JDL Level 1 tracking algorithms, but the time interval is definitely larger with respect to the ones adopted in JDL level 1. Since no further information contributes to the track estimates update during ΔT, the uncertainty of the estimation process largely increases with respect to the conventional JDL Level 1 techniques. On the other hand, the RPM might be seen as predicting the "intent" of a tracked target, which falls into category 2 of the JDL model. Sample solutions for "extended track prediction" are based on deterministic motion models, preferred routes and non-linear filtering techniques ([PVB13], [RAG04] and [BSLK01]). The algorithm developed for the RPM belongs to the latter class ([BUP+12]) whereas it relies on a priori knowledge information, such as coastlines, bathymetry, preferred routes, ship characteristics, planned journey, etc., in order to reduce the uncertainty in the estimation process.

7.1.1 Route Prediction Module Architecture

The RPM block diagram is depicted in Figure 7.1, where the inputs/output and the main building blocks are clearly identified. Their high-level description is provided in the following subsections, with a reference to the techniques (e.g., Knowledge-based Particle Filter) that have been selected for the implementation of the RPM functionalities.

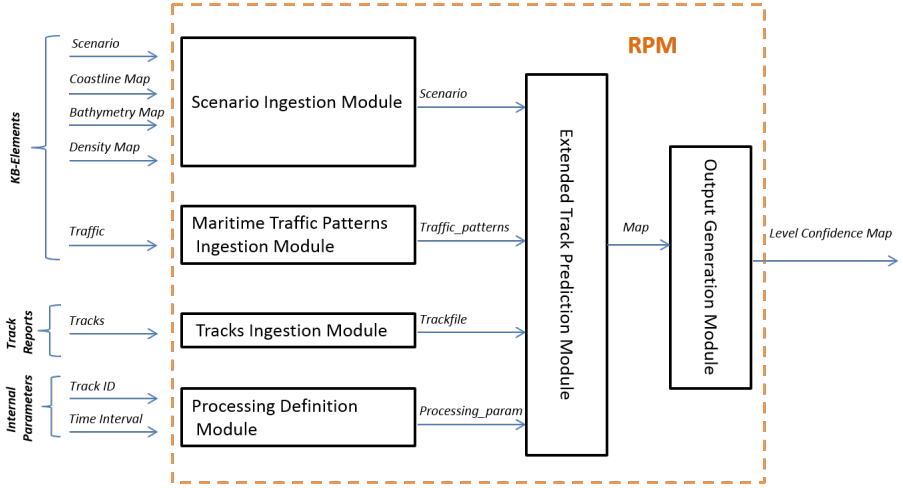

Figure 7.1: RPM logical block diagram.

7.1.1.1 Inputs

The RPM main input data consist of **Knowledge Base (KB) elements** and **Track Reports**. The first type of input (i.e. context based) is in the form of raster/vector layers or structures containing relevant information about the Area of Interest (AoI). Specifically, the characteristics of the scenario, the shape of the coast, the bathymetry, the vessel traffic density and the maritime traffic patterns are fundamental for the main task of the RPM, which is the execution of extended track prediction in case of lack of sensor measurements. An example of the context information exploited by the RPM is illustrated in Figure 7.2. Specifically, the large amount of information contained in the traffic patterns plays a key role in the prediction process. Generally they are complex structures derived through a methodology based on a set of classes progressively shaped by vessel objects behaviors [VBBV12]. For the specific case of the RPM, only a subset of characteristics is taken into account per each maritime pattern. It includes the pattern direction, the average Course over Ground (COG) and the average Speed over Ground (SOG) of the vessels contributing to the pattern, and the identification number of the ships (MMSI) that follow that pattern. For a detailed description of these fields, refer to the Section 2.1. This leads to a simplified maritime traffic pattern network, a graph whose nodes (waypoints) and edges (sea lanes described by linear objects) have specific properties.

As the track reports are concerned, they contain the measurements provided by the sensors usually involved in the maritime surveillance, such as the Terrestrial and/or Satellite Automatic Identification System (T-AIS or S-AIS), Long Range Identification and Tracking (LRIT) and Vessel Monitoring System (VMS), (Section 2.1). They can also be provided in terms of augmented state vectors describing a track (e.g. as result of a conventional tracker for coastal radars, as Vessel Traffic Service - VTS - output). For the application under consideration, T-AIS and S-AIS data are taken into account.

Finally, additional parameters related to the data processing feed the module as input as well.

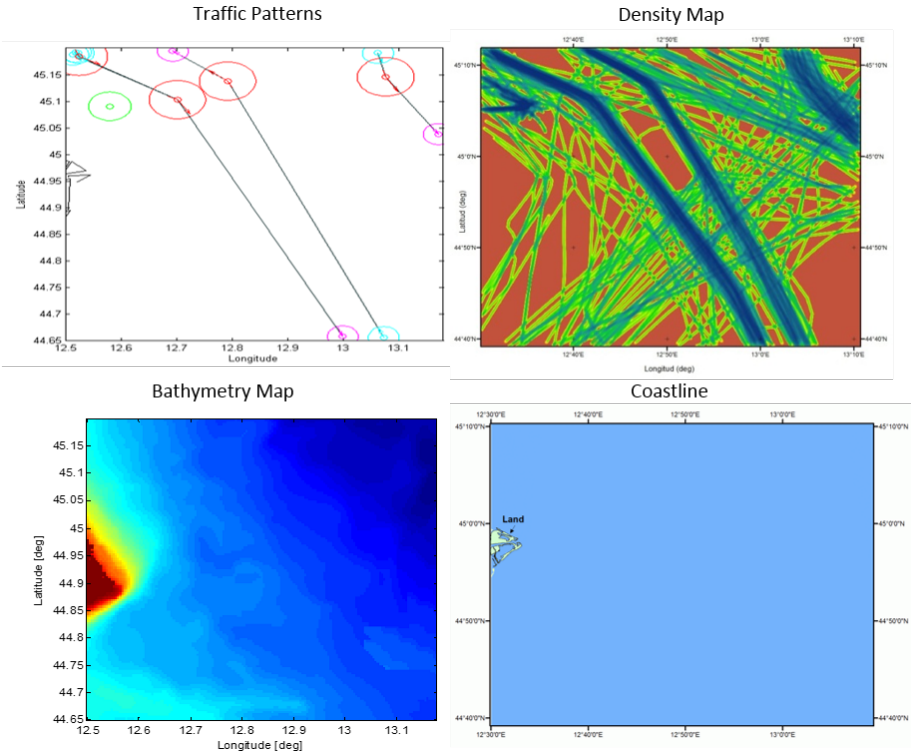

Figure 7.2: RPM inputs - Knowledge Base elements.

7.1.1.2 Outputs

Output data consists of georeferenced maps containing the confidence level (probability) for a vessel being at position (x, y) at time t_k. The maps take the shape of raster images, where each pixel identifies the vessel location probability. Figure 7.3 reports an example of the module's output and shows the evolution of the confidence level map during the time interval ΔT in which no sensor measurements have been recorded. Specifically, the cyan points show the exact vessel positions (i.e. the ground truth) along the navigational route while the yellow dot represents the position of the last recorded measurement for that vessel. The magenta points are the position estimates evaluated at different prediction time intervals ΔT, which are associated with the correspondent ground truth positions.

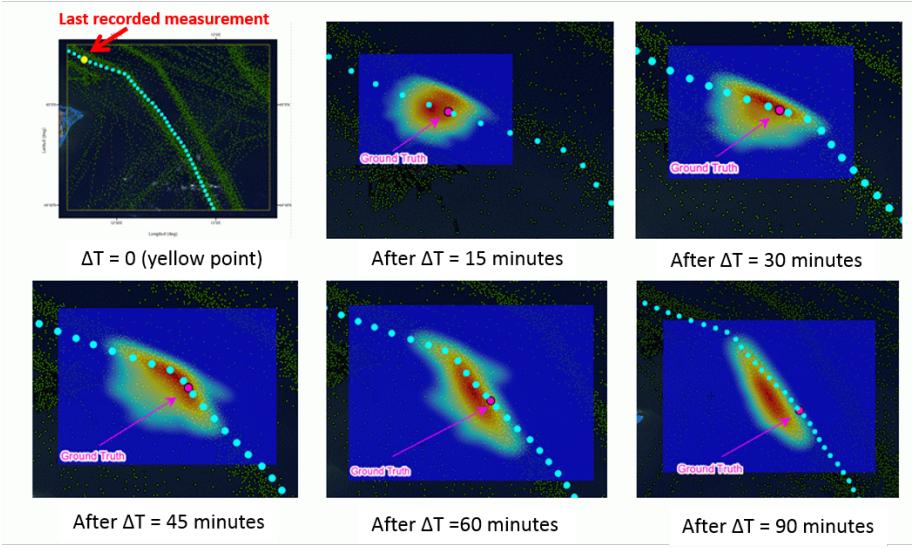

Figure 7.3: RPM output - Evolution in time of the confidence level map.

7.1.1.3 Main Blocks

The block diagram in Figure 7.1 shows the main components of the RPM. Specifically, three blocks are devoted to the input ingestion. The **Scenario Ingestion Module** manages the a priori geographic information on the AoI, coastline, bathymetry, and the additional information of the traffic density. The **Maritime Traffic Patterns Ingestion Module** is in charge of the maritime traffic patterns extrapolation, whereas the **Track Ingestion Module** deals with the state vectors (i.e. target track) of the vessel for which the user is interested in performing the extended prediction. These modules interpret the input data and rearrange them in specific structures for further processing. The **Processing Definition Module** is used for the definition of processing parameters (e.g. the identification number of the fused track for which the RPM output should be provided and the processing duration). The **Extended Track Prediction Module** represents the core module of the RPM. It implements the forward prediction of the maritime traffic picture through a sequential non-linear filtering based on a Particle Filter. It is to be stressed that the extended tracker module exploits the a priori knowledge listed before. This context information allows improving the estimation accuracy in target positioning. The module outputs are the

Confidence Level Maps described above. Finally, the **Output Generation Module** rearranges the content of the "Map" for the final delivery.

7.1.2 Route Prediction Module Algorithms

This subsection describes the algorithms implemented in the extended track prediction module, which perform the functions of (i) track initialization, (ii) knowledge base track propagation, (iii) track update and, (iv) confidence level map generation.

7.1.2.1 Constrained particle filter for extended track prediction

As already mentioned, the RPM addresses the problem of tracking maneuvering vessels for long time intervals, in which no new information on the vessels' state is received. For this reason, it attempts to calculate the target position estimate (i.e. target state *probability density function, pdf*) also in lack of updated target information with the help of a priori information. Moreover, given the maritime application field, the problem of estimating the vessel position and velocity on the basis of sensor measurements is highly non-linear. Therefore, a **constrained bayesian filter** formulation based on particle filtering is used, which introduces the expression for the *posterior pdf* in the presence of hard constraints (Section 4.1). Specifically, the SL-CV-CT-PF described in Section 5.2 is taken into account for this application. The constraints are dictated by the context information and they drive the selection of the target dynamic model for the target state prediction from two consecutive instants of time. The use of different Dynamic Models (DM) in the filter derives from the model adopted to simulate vessel trajectories when approaching specific knowledge base elements, such as the sea lanes. It has to be stressed that this algorithm allows the estimation of the *posterior pdf* of the target state resorting on a PF technique. This means that this *pdf* is represented by a weighted sum of particles.

7.1.2.2 Kernel density estimator for target existence probability density map

In order to determine the main output of the RPM (i.e. confidence level map on target positioning), a continuous density has to be estimated on the basis of the particle distribution. This is implemented in the confidence level map generation function of the RPM extended track prediction module. There are two basic approaches for doing this: (i) the parametric approach, which consists of equipping the unknown density with a finite set of parameters, and (ii) the non-parametric approach, which does not restrict the possible form of the density function by assuming the PDF to belong to a pre-specified family of density functions ([Hae91]).

In this case, the second type, which is mostly applied when no precise information about the form and the class of the true density is available, is utilized. Specifically, a **Kernel Density Estimator (KDE)** is considered for the confidence level map generation. The KDE can be expressed as follows:

$$\hat{f}_h(\mathbf{x}) = \frac{1}{n}\sum_{i=1}^{n} K_h(\mathbf{x} - X_i) = \frac{1}{nh}\sum_{i=1}^{n} K\left(\frac{\mathbf{x} - X_i}{h}\right) \tag{7.1}$$

where K is the kernel function, h is the bandwidth that regulates the degree of smoothness for kernel smoothers, n is the total number of the samples drawn for the distribution (i.e. the number of the particles in our case) and X is the *i-th* sample. Different kernel functions can be chosen for the implementation of the Equation 7.1. The following Gaussian Kernel is used:

$$K(\mathbf{u}) = \frac{1}{\sqrt{2\pi}} exp\left(-\frac{1}{2}\mathbf{u}^2\right) \tag{7.2}$$

Figure 7.4 summarizes the main functions implemented in the extended track prediction module:

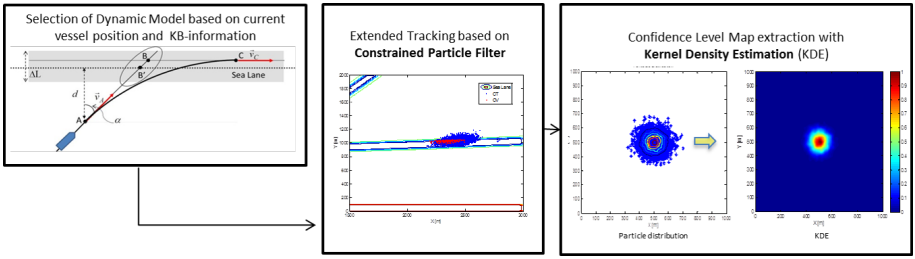

Figure 7.4: Extended track prediction module functionalities.

7.1.3 Test Scenarios and Simulation Rationale

The Route Propagation Module was tested over real data collected during two live campaigns conducted in the Gulf of Gabes (Tunisia) and Lampedusa (Italy) in June 2013 and in the Norwegian Sea in May 2014. Figure 7.5 (top) shows the two areas of interest for the operative scenarios, with the context information (coast shape and maritime traffic patterns) exploited by the route propagation algorithm.

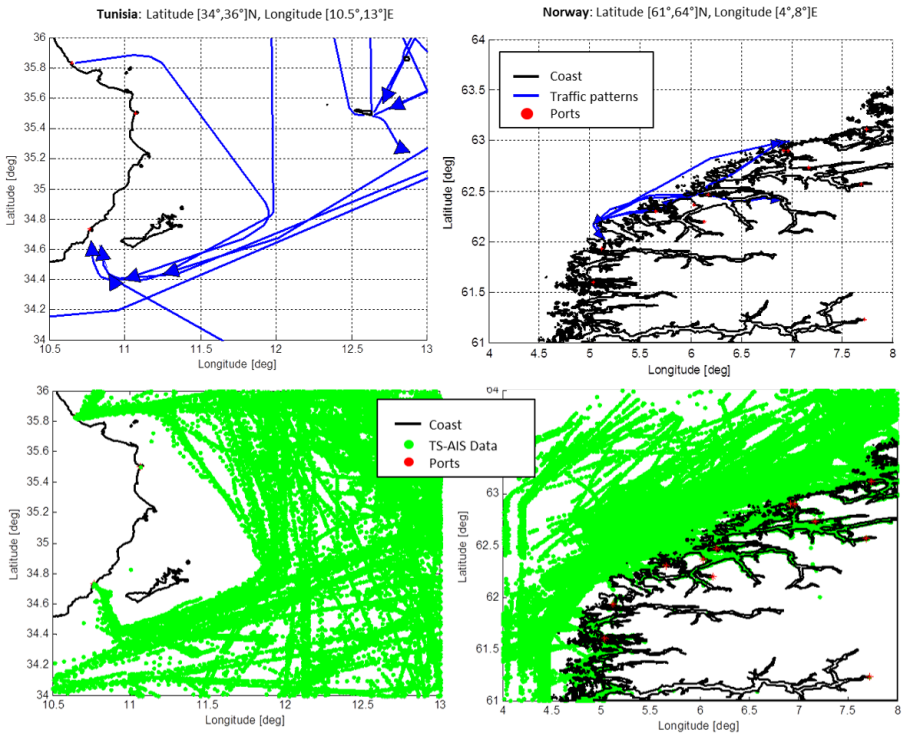

Figure 7.5: Areas of interest (Top) and real data from AIS (Bottom) for the live campaigns in Tunisia/Italy - Gulf of Gabes (Left) and Norway (Right).

Real data from T-AIS and S-AIS were acquired for over a month, bringing into the NEREIDS general toolbox approximately 1500 different vessel tracks to deal with. They are also reported in Figure 7.5 (bottom). The data analysis showed an intermittent AIS transmission (lack of sensor measurements) for a significant time intervals (greater than 1.5 hour) for a large number of vessels (about 200). The reason for the measurement gaps has to be investigated and clarified (e.g. no coverage due to the shoreline) but it is out of the scope of the results presented for this application. The vessels characterized by discontinuous measurements are the object of the analysis and they represent the input in terms of track reports for the RPM. The confidence level maps provided as output are then analyzed in the light of users needs and requirements.

A typical example of the use of the RPM could be described by this storyboard:

- The operator follows a given vessel on the screen (VTS function);
- @ $T0$ the vessel track disappears from the current picture even if its position should be still in the coverage of the sensors (e.g. T-AIS, S-AIS);
- @ $T1$ the operator runs the RPM for that track. The RPM outputs the confidence areas at $T3 = T0 + \Delta T$;
- @ $T2 < T3$ the operator evaluates the risk associated to the vessel (e.g. suspicious, hazardous materials, estimated position close to sensitive area, etc.) and takes a decision on how to proceed.

There are many possibilities related to the operator's decision. She/he could, for example, (i) wait until new data come and then check the vessel behavior, (ii) check the ship position through other available sensors or maritime patrol aircraft, or (iii) intercept the vessel with a boat. Other decisions are indeed possible. In the following section, results related to the above mentioned operative cases are reported as example.

7.1.4 Results on Real Data Sets

For each test case, the "intermittent" vessel trajectory due to the lack of sensor measurements is provided as input to the RPM (i.e. red plots on left hand side of the Figures representing the ground truth), together with the maritime traffic patterns (i.e. blue lines). The results are given in terms of one or more areas (Confidence Level Maps) in which the vessel is expected after ΔT minutes of navigation after $T0$ (right hand side of the following Figures). In those maps, scarlet colors represent pixels with high probability of finding a vessel (and also high density of particles) whereas blue ones a low probability (low density of particles). For these test cases, it is important to point out that the RPM tracking algorithm exploits information about the coastline, some features contained in the traffic patterns (vessel Maritime Mobile Service Identity - MMSI, path direction) and the information provided by the AIS message (vessel MMSI, destination port), if available and correct.

7.1.4.1 Example I: Operator waits for new data and checks the vessel behavior.

The operative scenario and the results for this example are shown in Figure 7.6.

A vessel is navigating in the Norwegian waters along the cost from North to South with declared direction Kvinesdal. The AIS reports are lost for a long time interval,

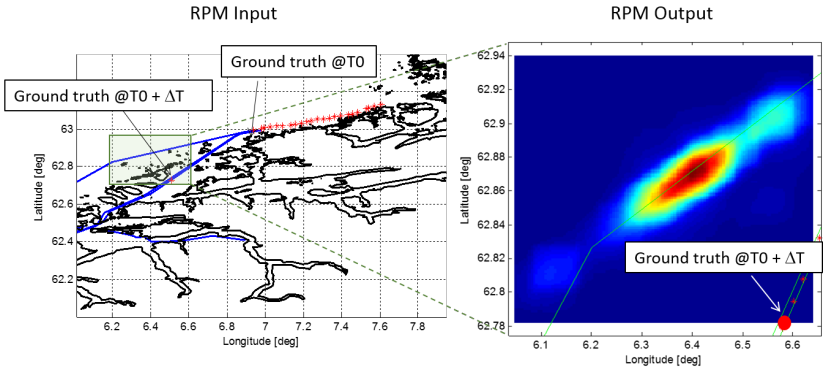

Figure 7.6: Input (Left) / Output (Right) data for real test Scenario I.

appearing again after $\Delta T = 120$ minutes of navigation. The extended target position prediction, which starts at T0, is made by resorting to the SL-CV-CT-PF algorithm and exploiting two kinds of a priori knowledge: (i) the information about the destination port (e.g. city of Kvinesdal in Norway) provided by the AIS message and (ii) the vessel MMSI contained in one of the traffic patterns (i.e. the upper blue line in Figure 7.6, left).

The output (e.g. the confidence level map on the right) is also provided at $T0 + \Delta T$. Unfortunately, the area with high probability to find the vessel after the extended prediction does not contain the target position after the long time interval (red dot in Figure 7.6, right). This is due to the fact that the prediction is made in accordance to the specific pattern containing the vessel MMSI; however, in the actual situation the ship takes the alternative route to reach its final destination. This deviation form the expected traffic pattern (e.g. anomalous behavior), suggests the operator to wait for new data: as soon as updated information about the vessel is received from AIS, an alarm could be generated and the vessel contacted for clarifications.

7.1.4.2 Example II: Check ship position through satellite image data.

The operative scenario and the results for the second test case in Norwegian waters is shown in Figure 7.7. A vessel is navigating in the Norwegian waters from South to North with declared direction Hirtshals, in Denmark. Also in this case, no AIS updates are received for about 2 hours of navigation. Unfortunately, the a priori knowledge about the port destination extracted from the AIS message cannot be exploited by the tracking filter since it is wrong (i.e. it has been observed that the

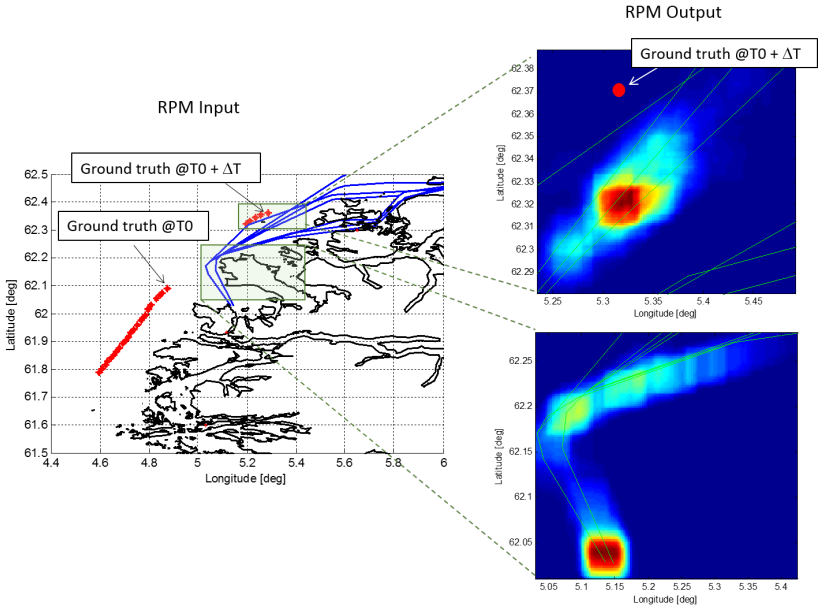

Figure 7.7: Input (Left) / Output (Right) data for real test Scenario II.

indicated port is on the opposite direction with respect to the vessel path). Moreover none of the traffic patterns contains the MMSI of the ship. This means that the extended prediction algorithm is performed following all the available sea lanes fitting with the vessel route.

Thus, two possibilities for the vessel position estimation at $T0 + \Delta T$, with $\Delta T = 120$ minutes, are provided. The results are encoded into two maps of areas of $[15 \times 15]km$ each; one of them, shown on top right of the Figure 7.7, contains the real vessel position, which is provided by the AIS after ΔT. The ship is only $5km$ far from the particle cloud center. Given these observation conditions, the vessel position could be also checked trough the use of alternative data sources, especially if the data provided by the AIS are not received. Specifically, SAR images covering the area containing the predicted target position @ ΔT (i.e. including the particles cloud) can be acquired. These images, if taken in high resolution, could support the operator in vessel detection and identification.

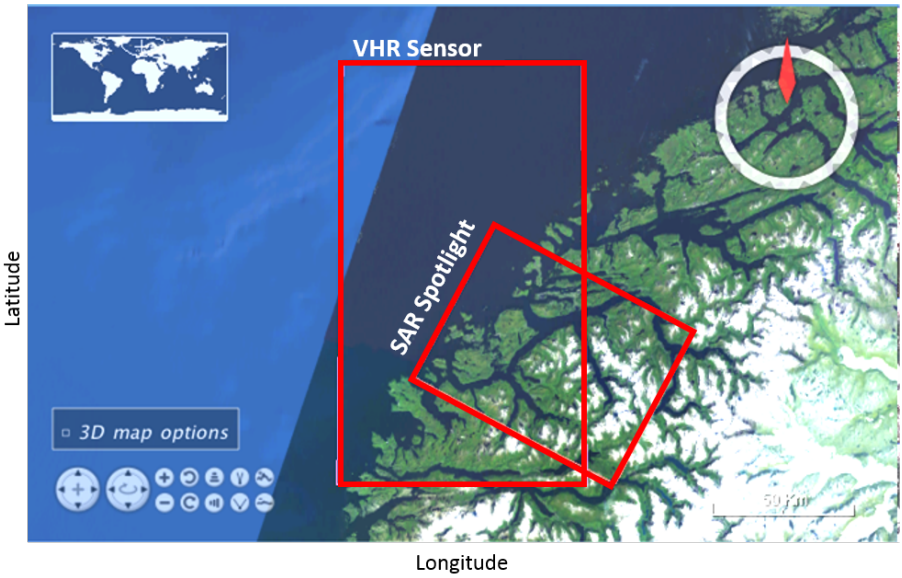

Figure 7.8: Example of SAR footprints for SAR image acquisition for real test Scenario II.

In Figure 7.8 an example of possible footprints of SAR images is provided. Specifically, a footprint of a SAR spotlight image (e.g. from Cosmo-SkyMed or TerraSAR-X) with $[10 \times 10]km$ swath and resolution $< 1m$ and another from a VHR Sensor (e.g. SPOT) with swath depth $< 60km$ and resolution $< 2.5m$ are depicted in the Figure. Both are useful for vessel identification and classification.

7.1.4.3 Example III: Intercept the Vessel.

This last test case is performed in the Tunisian waters. The RPM tracking algorithm can exploit only the information about the coast shape for the extended prediction, since other a priori information sources are not available. The recorded AIS message reports the wrong information about the port destination (i.e. Porto Nogaro in Italy) and the traffic patterns built for the area do not contain the MMSI of the vessel under observation. The RPM Input/Output are shown in Figure 7.9. The output area of $[20 \times 20]km$ provided by the tool at $T0 + \Delta T$, with $\Delta T = 170$ minutes, not only contains the vessel, but the distance between the real vessel position (ground truth) and the particle cloud center is just few meters. In this case, given the precision

provided by the the confidence level map, the RPM output can support interception forces in detecting the vessel with the on-board sensors by narrowing the search area.

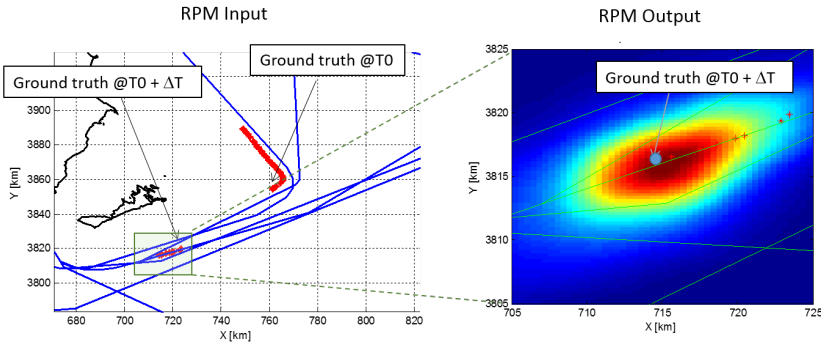

Figure 7.9: Input (Left) / Output (Right) data for real test Scenario III.

7.2 Summary

The Chapter presented a tool, the Route Propagation Module (RPM), based on the vessel route prediction concept to support the maritime surveillance in coastal areas and high waters. The tool resorts on the non-linear Bayesian tracking filter technique for the target state estimation (i.e. the constrained SL-CV-CT-PF algorithm in Section 5.2) and exploits the context information for the target state prediction over long time intervals (ΔT) and in absence of sensor measurements. Information about coastline, bathymetry, vessel traffic density and maritime traffic patterns is ingested and used by the "extended tracker".

Specifically, the RPM has been tested in complex real scenarios characterized by intermittent data as input. The AIS data (terrestrial and from satellite) have been collected over two areas of interest (Tunisia and Norway) within two acquisition campaigns. The results, given in terms of areas (maps) in which the vessel has a high probability to be located after ΔT, show the added value brought by the use of the RPM. The provided Confidence Level Maps could indeed support the operators and/or the users in different tasks such as the decision making and the detection of anomalous vessel behaviors.

CHAPTER VIII

Application-Experimentation III: Passive Radar Surveillance in Coastal Areas

In the last years, the use of passive radar systems for surveillance applications is representing a key research and development path for private companies, research laboratories and governmental institutions throughout the world (see Section 2.1.6). In this Chapter, the use of passive radar technologies to monitor the vessel traffic situation in coastal areas is presented. Specifically, two scenarios are addressed. The first one at the Baltic Sea is characterized by dense vessel traffic conditions and an heavy clutter environment due to the presence of wind parks. Also the choice of proper transmitting stations among the many possibilities in the area represents a challenge for the system setup. Given the bistatic nature of a passive radar system, its performance is indeed influenced by the selected transmitters-receiver geometry. This scenario will be adopted to assess the performance of the Knowledge-based MHT (KB-MHT) algorithm presented in Section 5.3. It will be demonstrated how the exploitation of context elements such as the probability of detection maps, the adaptive clutter maps and the geographical maps encoding information about coast and terrain bring an improvement in the tracking algorithm in terms of track continuity and false track rate reduction.

The second scenario is set in the remote regions of the Canadian Arctic. On the contrary it presents a low vessel traffic density and adverse climate and navigation conditions due to the presence of ice and scarceness and/or total absence of monitoring sensors. Given this latter point, it will pointed out how the use of an innovative system based on the passive radar technology could support the already existent solutions for traffic monitoring in such remote areas, which usually resort on satellite based data

only (e.g. S-AIS). Moreover, the a priori knowledge of transmitting base stations in the area, the context information about the digital elevation model of the terrain and the bathymetry map allows the definition or the refinement of the bistatic geometries of the passive radar surveillance system. It will be demonstrated how optimized transmitter-receiver configurations lead to improved vessel tracking performances.

8.1 Vessel Monitoring in the Baltic Sea

The availability of a large number of GSM transmitting stations along the Baltic Sea coast and some their specific features (e.g. a proper orientation of transmitting antennas), suggest the exploitation of a GSM based Passive Coherent Location (PCL) system to monitor the vessels traffic in the area. Such a system could complement the existing ones based on active radar sensors technology and cooperative identification radio systems like AIS, which suffer from some deficiencies, as reported in Section 2.1. Also passive radar systems based on GSM technology present some problematic to take into account for monitoring purposes. Even though the discrimination in the azimuth direction is good due to the relatively high frequencies broadcast by GSM Base Transceiver Stations (BTSs), the range resolution is poor due to the low signal bandwidth, [Nic14]. Also the transmitting signal power is relatively low. These lead to deficiencies in the target detection task. It has been demonstrated, [Bro12], that the fusion of information from multiple bistatic geometries (i.e. TX-RX pairs) allows a better target localization and coverage. This represents the major tasks of the tracking algorithm, which is fundamental for this application. Specifically, the KB-MHT is taken into account for the vessel monitoring. In particular the improvement that can be gained by exploiting different kinds of a priori information is discussed and tested over real data acquired in the Baltic Sea trough the experimental system GAMMA-2 developed by Fraunhofer FKIE, [Zem16], whose main characteristics are reported in the next Section for the sake of completeness.

8.1.1 Experimental System Set Up

8.1.1.1 GAMMA-2 System Receiver and Data Processing

The guideline for the system concept of GAMMA-2 was to realize a software defined radar as much as possible, [ZBBN14]. This leads to the design of a Uniform Linear Array (ULA) with 16 elements and 16 digital receivers. The ULA guarantees maximum spatial target discrimination as well as deep and narrow nulling of interference for a given number of channels, hence minimizing the clutter in the transmitter direction, [ZNW09]. The output of this array can be used for all tasks: reference signal acquisition, surveillance signal extraction and BTS monitoring.

For this application the receiving system GAMMA-2 shown in Figure 8.1(b) has been used. Each element of the ULA is composed of columns of 3 Vivaldi antennas in the frequency range of [1.5 GHz-2.15 GHz], which are summed in the analogue domain. Each column has a 3 dB elevation beamwidth of 27° and a gain of 10 dB (at 1.8 GHz), which results in an array gain of 22 dB. For the reception of GSM1800 signals, the distance between the elements is set to 8 cm, which corresponds to a spacing of the half wavelength for a frequency of 1874 MHz. As a compromise between processing speed and flexibility, the hardware of the digital receiver has been designed to extract in parallel up to eight GSM frequency channels (demodulated I&Q) of 200 kHz width within the system receiving bandwidth of 30 MHz. Each frequency channel is subsequently digitally down converted and stored for further signal processing steps. This special realization of the hardware limits the number of transmitters that can be used in parallel.

A standard signal processing is then considered, where the reference signal is extracted by conventional beamforming ([Wir13]). The Field of View (FoV) for the surveillance signal ($[-60°, 60°]$) is sampled by a set of fixed beams in azimuth. For each beam with a given angle of arrival (AoA) a digital adaptive beamforming and clutter cancellation are performed to obtain the corresponding surveillance signal ([ZNW09]). The clutter cancellation method is based on the projection of the received signal onto the subspace orthogonal to the clutter subspace ([CCL06]). Then the signal power is accumulated by coherent integration. The Coherent Integration Time (CIT) is selected as the longest time interval in which the evolving target remains in the resolution cell. According to [Nic14] and the application scenario a CIT of 1.8 s is obtained, which produces a very fine Doppler resolution ($\Delta_{Doppler}$= 0.56 Hz) corresponding to a radial velocity less than 0.05 m/s. The long CIT is suited for the detection of maritime targets. The Doppler is therefore an excellent criterion to distinguish closely located vessels in areas with high target density. Finally, the range-Doppler-bin for which the signal strength exceeds a predefined threshold is declared as detection and it is forwarded to the tracker. In contrast, the range resolution Δ_{rg} of this system is poor due to the low effective signal bandwidth of 81 kHz, which leads to Δ_{rg} = 1.9 km for the monostatic case, [Wir13]. However, the achievable accuracy in range σ_{rg} (i.e. the standard deviation of the peak of the complex ambiguity function) can be significantly improved depending on the estimation method used [Weh95]. For system performance evaluation, perfect operative conditions, i.e. high SNR, perfect system calibration, multipath free reception, etc. are assumed.

8.1.1.2 Parameter Accuracies

To characterize the measurement accuracies for target tracking a simple bin processing strategy is assumed. Of course, a detailed analysis of the achievable accuracies must include all effects, starting with the implemented estimation and calibration algorithms, the environmental effects like multipath and the target SNR, but it is out of the scope of this work.

Let us considering a simple grid search over the range domain. The grid cell dimension, Δ_{cell}, is selected according to the sampling frequency of the Analogue to Digital Converter (ADC) and is smaller than the resolution limit Δ_{rg}. Thus, the range accuracy for high SNR values is determined by:

$$\sigma_{rg}^2 = \frac{\Delta_{rg}^2}{12} \tag{8.1}$$

This is valid under the following assumptions: (i) the unknown target position is uniformly distributed within the cell, and (ii) no fine estimation technique is implemented (e.g. interpolation or range monopulse). In this experiment the signals are sampled at a frequency equal to 240 kHz. Thus, the monostatic range accuracy is about 360 m. This is less than the range resolution but still not satisfying for moving targets position estimation. It has to be stressed that, when operating in Cartesian coordinates, the achieved position estimation accuracy depends not only on the measurement errors, but also on the bistatic geometry. Thus, the position estimate can also be worse than 360 m.

For the azimuth angle estimation a simple search of the maximum response over the 16 look directions (beams) within the FoV is considered. Thus, the angular cell Δ_{az} defines the angular accuracy. In the case of a uniformly distributed target over the angular cell and considering an angle bin of $\Delta_{az} = 7.5^\circ$, the angular accuracy is about $\sigma_{az} = 2.15^\circ$. Such an angular accuracy can only be attained if targets are well separated without any clutter influence. In reality clutter cancellation and especially direct signal cancellation is imperfect and this will influence this parameter. To deal with this, a distribution of the angle error over two adjacent beams is assumed. Thus, the angular accuracy becomes $\sigma_{az} \sim 5^\circ$.

Following the same argumentation as above, the Doppler accuracy $\sigma_{Doppler}$ for an integration time CIT = 1.8 s results into 0.56 Hz. This high accuracy compensates the low accuracy in range and allows target discrimination and tracking as will be seen in the following.

8.1.2 Test Scenario and Simulation Rationale

The trial scenario considers the maritime traffic in the Fehmarn Belt, between Germany and Denmark. The system receiver GAMMA-2 is mounted on a tower of 56 m height, as shown in Figure 8.1 and it is located at the Eastern cape of the Fehmarn island (Figure 8.2), pointing at 0° with respect to the North direction. The area covered by the receiver is represented by the orange sector in the Figure, which is characterized by a Field of View of 120° in the azimuth direction and an illumination range of 40 km. Three GSM Base Transmitter Stations (BTS), indicated by black triangles, are considered in the scenario. Each BTS typically covers a sector of 120° in azimuth, as represented by the small red sectors in the Figure 8.2, one for each BTS.

Figure 8.1: Receiver system GAMMA-2. (a) GAMMA-2 mounted on the tower; (b) GSM PCL antenna and GAMMA-2 receiver

The characteristics of the BTSs are summarized in Table 8.1. Also others illuminators are available in the area, but they are discarded due to their operative carrier frequency that results beyond the receiver bandwidth of 30MHz. In such conditions, they cannot be simultaneously used, as stated in [Zem16].

Figure 8.2 shows typical vessel paths, which indicate the trajectories of a cargo ship (black line) and a ferry (white line), respectively. Finally the blue area indicates the geographic location of wind park, which represents the main clutter source for the application.

The collected system measurements represent the major input for the KB-MHT algorithm described in Section 5.3, which is used in the application to track the vessel

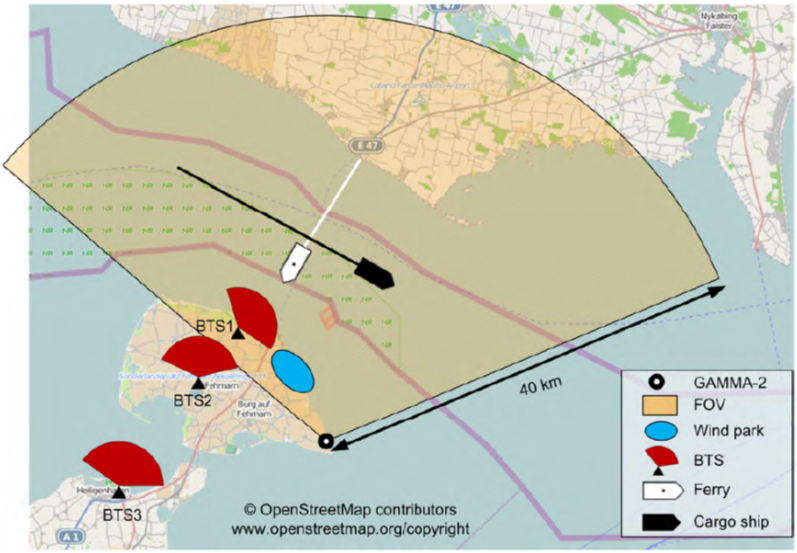

Figure 8.2: Operative scenario in the Fehmarn Belt, [Zem16].

Table 8.1: GSM-BTS parameters in the Fehmarn Belt.

BTS ID	Lat [deg]	Lon [deg]	Frequency [kHz]	Pointing [deg]	Height [m]
BTS1	54.495183	11.198764	1860.8	60	59.2
BTS2	54.454546	11.137672	1860.2	0	40
BTS3	54.372576	10.986496	1848.8	30	40

in the Belt. As already stated in the Chapter introduction, the main objective of this simulation is to demonstrate how the use of context elements (i.e. probability of detection maps, adaptive clutter maps and geographical maps) in the MHT algorithm brings an improvement in terms of track continuity and false track rate reduction. Before proceeding with the general case for the simulation, the theoretical performance bounds that can be achieved for the above described scenario are evaluated, as reported in following Section.

8.1.2.1 Theoretical Performance Bounds

The theoretical analysis is conducted trough the evaluation of the CrÃ¡mer Rao Lower Bound (CRLB), which provides a lower bound to the position estimation performance, as reported in [TB07]. The more the vessel position estimation accurate is, higher is the algorithm capability in maintaining the vessel track (i.e. improved track continuity). Given the dependency of the system detection capability from the different bistatic geometries, the CRLB is evaluated for each TX-RX pair in the scenario. Specifically, the CRLB of the *i-th* TX-RX pair is calculated by the inverse of the Fisher Information Matrix (FIM) for a single time scan as follows, [Bec00]:

$$\mathbf{FIM}^i(\mathbf{x}_k) = \frac{\partial \mathbf{h}^i(\mathbf{x}_k)^T}{\partial \mathbf{x}_k} \mathbf{R}^{-1} \frac{\partial \mathbf{h}^i(\mathbf{x}_k)}{\partial \mathbf{x}_k} \quad , \tag{8.2}$$

where $\mathbf{h}^i$ is the *i-th* non-linear function of the target state vector $\mathbf{x}_k$ and $\mathbf{R}$ is the measurement covariance matrix $\mathbf{R} = diag(\sigma^2_{rg}, \sigma^2_{Doppler}, \sigma^2_{az})$. The result of fusion of the N bistatic geometries is simply obtained from the sum of the correspondent FIMs:

$$\mathbf{FIM}(\mathbf{x}_k) = \sum_{i=1}^{N} \mathbf{FIM}^i(\mathbf{x}_k) \quad . \tag{8.3}$$

The additivity is a property of the information matrix and does not depend on the fusion scheme (i.e. centralized, decentralized [HM04], etc.), which is chosen for tracking. In particular, this reflects the theoretical consideration that adding measurements of an additional TX-RX pair will result in an increase of the information and consequently in a decrease of the estimation uncertainty (described by the CRLB). This can be further extended to multiple time scans by incorporating the target propagation model, [TMN98]. In particular, when considering multiple time scans, the impact of the target velocity estimate (which is based on Doppler measurements) on the position estimate can be analyzed.

For passive radar applications, a performance prediction tool based on the CRLB calculation has been developed in [Bro12]. This tool is here applied for the Fehmarn Belt scenario. As first step, the *i-th* coverage map for the probability of detection P_D^i is generated for each bistatic geometry. The process to obtain these maps will be illustrated in the following (see Section 8.2.1.3). The Figure 8.3 shows the sum of the three probability of detection maps ${P_D}^i$ for the addressed scenario. The Figure also reports the real AIS data collected for a vessel crossing the bay.

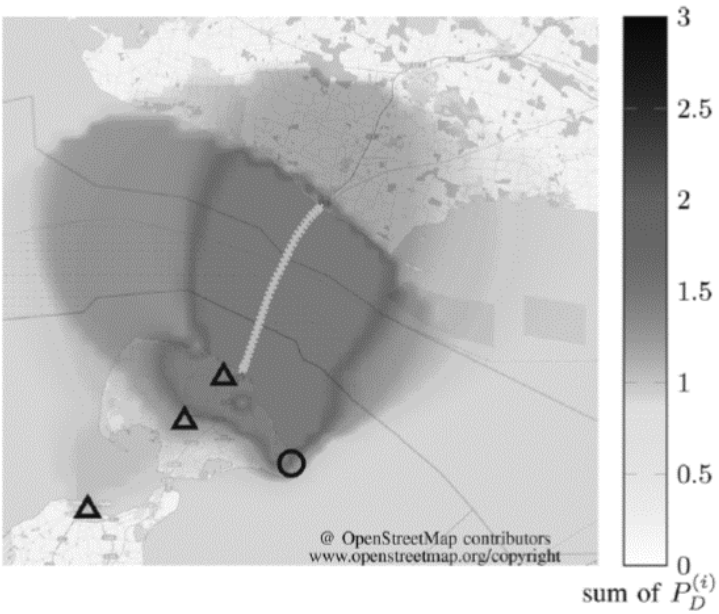

Figure 8.3: Coverage area for the Fehmarn Belt scenario, [ZBBN14].

It has to be stressed that the maximal value of the colourmap in the Figure is therefore equal to the number of the available transmitters. The objective of this representation is to highlight the regions of high and low coverage in terms of detection by multiple transmitters, contrary to the cumulative probability of detection P_D^C. This is not a characterization of the P_D of the fused tracks, but gives the expected number of observations from different bistatic pairs. This has a significant influence on estimation performance, as discussed in the following.

The probability of detection ${P_D}^i$ of a single TX-RX pair is an input parameter for the calculation of the CRLB. By use of the information reduction factor as introduced by [ZWBS05] this results in a scaling of FIM according to:

$$\mathbf{FIM}(\mathbf{x}_k) = \sum_{i=1}^{N} {P_D}^i \mathbf{FIM}^i(\mathbf{x}_k) \quad . \tag{8.4}$$

In Figure 8.4 the CRLB for the expected position errors is reported. The three transmitters (black triangles) are nearly placed on a line. The receiver position is indicated by the black circle. In the bottom left side of each figure, the direction of the velocity vector used in the CRLB evaluation is indicated. It is possible to notice that for a single time scan large position errors are recorded, especially in the region between the Fehmarn island and Rodby in Denmark (Figure 8.4(a)). These errors can be reduced by considering three time scans, as shown in Figure 8.4(b). Finally, Figure 8.4(c) shows the results obtained when an alternative velocity vector with respect to the Doppler measurements (e.g. perpendicular to the measurement) is considered for the evaluation of the CRLB.

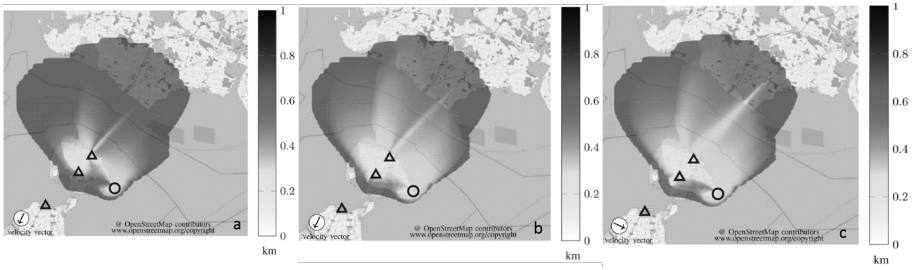

Figure 8.4: CRLB Position Estimates: (a) Single Time Scan; (b) Three Time Scans; (c) Three Time Scans Alternative Velocity Vector, [ZBBN14].

8.1.3 Results on Real Data Set

Once evaluated the theoretical boundaries for the performance, the experimental monitoring system is tested over real data, i.e. passive radar measurements from vessels navigating in the Fehmarn Belt (Section 8.1.2). In order to test and validate the results, the reference ground truth is built up by exploiting the AIS data acquired in real time from the vessels. Specifically, the information about vessels positions and velocities, provided by the AIS respectively in the WGS84 domain and knots, is properly transformed into the range-Doppler-azimuth domain in order to be further compared with the measurements provided by the GMS PCL system. As a first step, the association between the vessel ground truth and the incoming measurements is made via the Global Nearest Neighbor (GNN) approach [BP99]. Then, the associated measurements are processed by the UKF to obtain estimates of the target position and velocity as well as the covariances [DNK12]. An example of the results for a ferry approaching the Fehmarn island from Rodby in Denmark is reported in Figure 8.5.

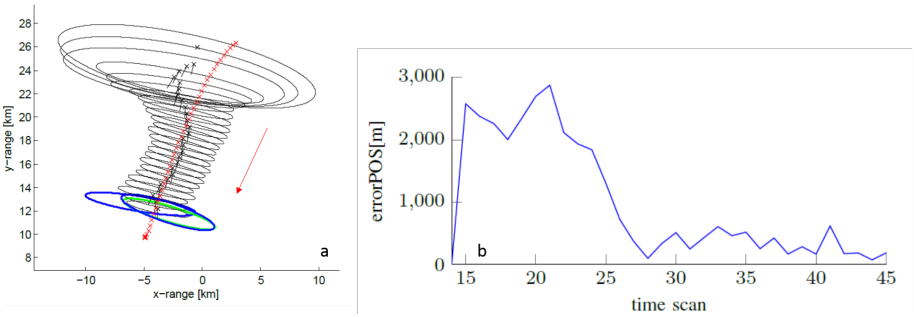

Figure 8.5: Position estimation results: (a) Covariances; (b) Position error.

Specifically, Figure 8.5(a) shows the sequence of the estimation results. The AIS data of the observed vessel (i.e. the reference ground truth) are depicted as red crosses. The resulting GSM track (provided for several time scans) is represented by black crosses, which represent the mean values of the estimated positions, and by appended black lines, which describe the mean velocities. The black ellipses show the corresponding track position uncertainty (described by the track covariance). Finally, the blue and green ellipses illustrate the position uncertainty given by the plots (after transformation into Cartesian domain) of one time instant for each of the bistatic configurations that provide detection. The uncertainty ellipses are plotted according to the 3-sigma volume (3-times the standard deviation). Figure 8.5(b) reports the position RMSE over the track time. The fusion of the three available BTSs delivers indeed a more accurate position estimation than with only one BTS, but it is not satisfying. This performance can be referred to the inconvenient choice of the BTSs, which are almost on the same line with respect to the trajectory of the ferry (see Figure 8.2). Thus, the corresponding position ellipses coincide. No significant accuracy improvement can be expected from the fusion of the BTSs during the first half of the scenario. Only the fusion over time (according to the adopted motion model) improves the performance. In the second half of the scenario, the target is moving in an area of better estimation performance, which is confirmed by the tracking result (Figure 8.5(b)).

It has to be stressed that the presented data evaluation is made on the basis of a simplified association strategy based on the AIS data. The tracking results for the full KB-MHT (without AIS support) are discussed in the following Section.

8.1.3.1 Tracking Results

The quality of the adopted target tracking algorithm is generally limited by the number of false alarms, which can lead to the generation of unwanted false tracks in the observation regions. As the addressed application is concerned, numerous false alarms due to clutter residues in the BTS direction for each bistatic TX-RX pair are registered. Moreover, the presence of other clutter sources in the area (i.e. wind parks) contributes to this phenomenon. The presence of such false detections is in part related to the adopted conventional signal processing technique and the hardware imperfections both characterizing the experimental GAMMA-2 monitoring system. A detailed description of their generation and how to handle this problem from the signal processing point of view is provided in [Zem16] and it is out of the scope of this work. The objective here is to demonstrate how the use of a specific target tracking algorithm (i.e. KB-MHT) could handle the false tracks generation problem.

As the Fehmarn Belt scenario is concerned (see Figure 8.2), the wind park at the coast of the Fehmarn island represents the principal source of false alarms. This clutter contribution has been properly modeled following the procedure recalled in Section 5.3.1 and embedded in the target tracking algorithm. Thus, an adaptive clutter map has been generated for each BTS in the area on the basis of all collected measurements in the region ([MSMM05] and [SD10]). This is done under the assumption that the clutter is stationary and the targets, which move, are average out. The clutter map identifies the regions of high false alarm level. This means that for each BTS and for each range-Doppler cell a probability value describing the appearance of a false alarm is assigned. The generated clutter map for one BTS is reported in Figure 8.6.

It has to be stressed that the targets associated to the AIS data have been removed from the adaptive statistic. The contribution of the wind park becomes apparent in the first two range cells. This context information is exploited by the tracker in the plot to track association by the factor ρ_F (i.e. the spatial false alarm intensity), by influencing the hypothesis weights $\hat{w}_k^{ij}$, as stated in the Equation (5.51) in Section 5.3.2. In addition, a threshold on the false alarm probability has been introduced to avoid track initiation in a region of high false alarm level. However, an existing track can be maintained in a clutter region.

In addition to the clutter map, the geographic information of the coastline can be inserted in order to discard detections on the land. A geographic map of admissible areas as the one shown in Figure 8.7 is taken into account in the KB-MHT algorithm.

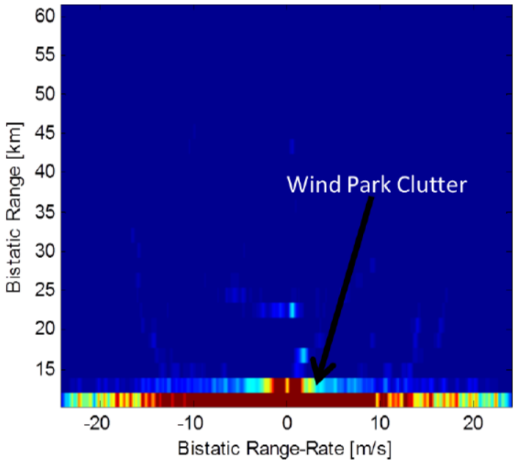

Figure 8.6: Clutter map for the BTS1-RX bistatic configuration.

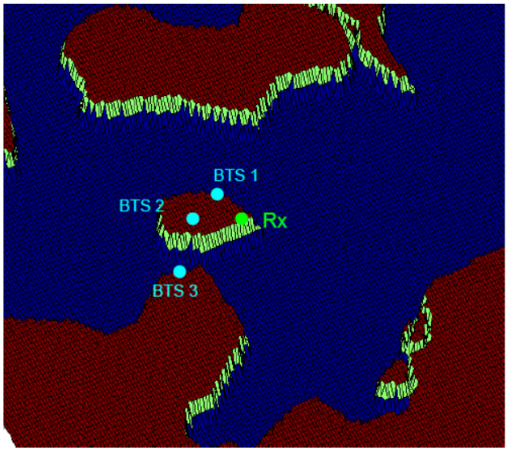

Figure 8.7: Geographical map for the Baltic Sea.

The basic idea is that each pixel or cell in the map provides the probability (1 or 0) that vessels can occupy it or not. The exploitation of this information makes the target state estimation more accurate with respect to the target position components, because the effect of a low sensor angular accuracy is mitigated. It is well known that tracking algorithms are prone to strange behaviors (fluctuations, divergence, etc.) in case of low accuracy measurements. For this application, the geographic map is preloaded before the processing starts. The tracker listens to this context information in two different steps of the processing: (i) when new sensor measurements are received as input for the algorithm and (ii) when already existing tracks are predicted. In both cases the unrealistic cases (e.g. measurements over land, or tracks crossing land) are discarded in order to reduce the number of the hypotheses.

Using both forms of context knowledge (clutter and land maps) an impressively clean situation picture can be achieved only on the basis of GSM measurements. Figure 8.8 and Figure 8.9 report the tracking results for the Fehmarn Belt scenario (with three BTSs) with and without exploiting the clutter and the geographical maps, respectively.

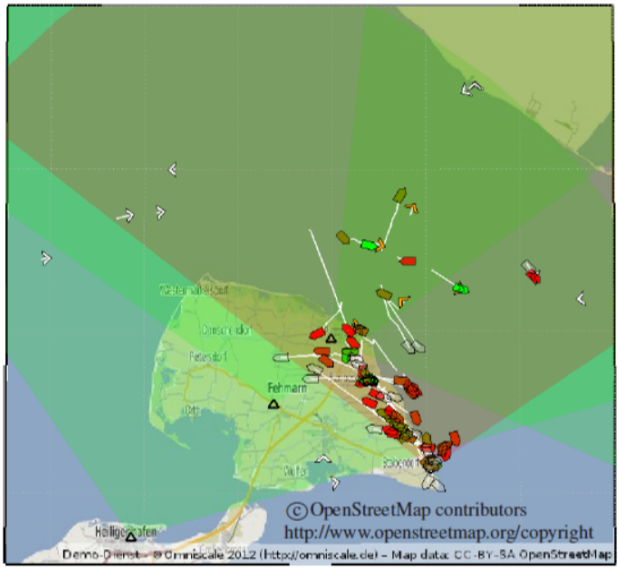

Figure 8.8: Tracking results for MHT (without context information).

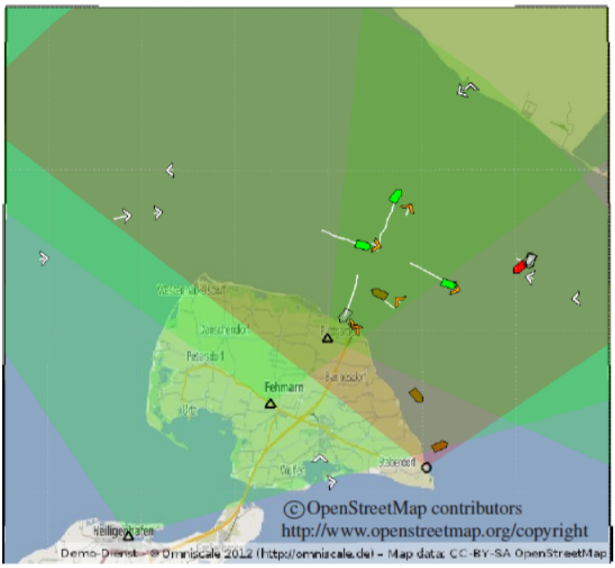

Figure 8.9: Tracking results for KB-MHT (with context information).

The visualization symbols of the tracking results are listed in Table 8.2.

Table 8.2: Visualization scheme for tracking results.

Tracks	Small Ship Symbols	Green: high-probability track Red: low-probability track Grey: identify an inactive track
Ground Truth (from AIS)	Triangles	Orange: AIS target detected by the GSM system White: no associated measurement
Look Direction	Shaded Area	Red: receiver Green: transmitter

The tracking results are also reported in Figure 8.10. The GSM tracks (i.e. blue plots) and the AIS data available for the addressed scenario (i.e. red plots) are both shown. In the Figure 8.10(a) the passive radar measurements have been processed

trough the MHT algorithm. In this case the detections that lie on the land and the clutter contributions have not been filtered out before and during the tracking phase. This leads to an high number of false tracks (i.e. false track rate of 57% in this case). If the information about the context is taken into account in the processing, the use of the KB-MHT algorithm leads to the results in Figure 8.10(b). In this case the number of false tracks is significantly reduced (i.e. false track rate of 4%).

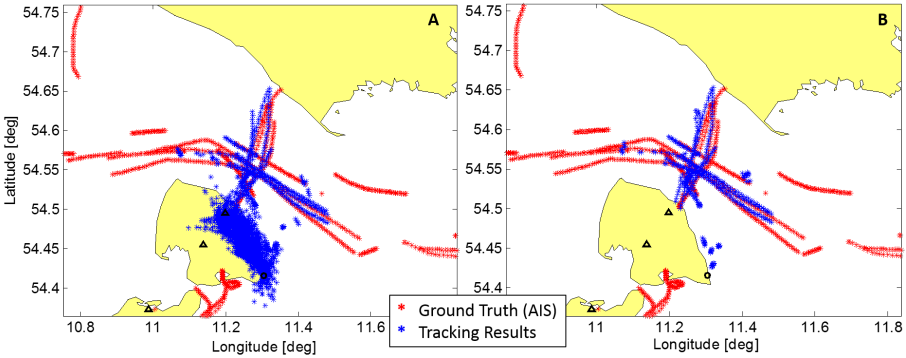

Figure 8.10: Tracking results for the Fehmarn Belt scenario.

8.2 Vessel Monitoring in the Canadian Arctic

The possibility to track vessel in remote icy waters (e.g. North West Passage, NWP, in the Canadian Arctic) by means of passive radar technologies is presented in this Section.

The combination of technological, economical, and climatic factors nowadays leads to a growth in maritime traffic in the Arctic. The observed reduction in ice coverage, thickness, and duration - combined with improved ship building - facilitates Arctic shipping for longer periods of the year and at higher latitudes. This enhances the investment in - and operation of - resource extraction vessels, transarctic shipping, vessels for resupply of the local communities, cruise ship and adventurer tourism in these waters. On the other hand, the remoteness, the harsh weather and ice conditions, and the lack of emergency response facilities lead to serious risks for the ships operating in the Arctic, as well as for communities and the environment. It is therefore important to monitor continually the vessel traffic in the Arctic in order to provide government agencies and mariners with the degree of Maritime Domain Awareness (MDA) that they need to conduct safe operations and voyages and to manage risks such as maritime accidents or spills or transiting of illegitimate vessels. On the basis of recommendations from civil and military parts, which both recognize the insufficient Arctic surveillance for vessel tracking capability, different system concepts for improving the MDA have been presented in the past years, (e.g. [Fea08, Art15]). They investigated the exploitation of heterogeneous and complementary surveillance sensors, whose outputs (e.g. passive underwater sonar and electromagnetic detections, active and passive radio-frequency detections, and active and passive optical and infrared detections) were stored and eventually fused to present effectively and efficiently the integrated surveillance data. At present, the backbone for MDA in the Arctic is the Satellite-based Automatic Identification System (S-AIS). Operating in the VHF range, the AIS transponders on board ships are a very effective cooperative data source for monitoring coastal and territorial waters from shore-based base stations. Through the installation of ad hoc AIS receivers on board a network of Low Earth Orbit satellites, the satellite based AIS (S-AIS) has extended the coverage of the system over the global seas, and it is now a powerful, standardized and proven technology for vessel traffic monitoring. It turns out, however, that S-AIS alone is not sufficient to provide continuous and comprehensive MDA. Reasons are (i) temporal gaps due to limited satellite coverage and low reporting frequency, (ii) AIS transponders are not mandatory for small vessels and, (iii) the existence of false AIS reports due to technical failure or even spoofing (see Section 2.1).

It is therefore necessary to research additional sensors and techniques that are able to complement the data provided by the S-AIS. Considering the remoteness and vastness of the area, space borne sensors such as Synthetic Aperture Radars (SAR) and optical imagery can be considered for the scope, even if they are also subject to observation gaps due to limited satellite coverage. For locations of high interest (e.g. choke points or entry/exit points of NWP routes) or for specific operations (e.g. search and rescue), local sensors such as active and passive radar systems (ground-based, air- or shipborne) can be considered to supplement the space-based sensor data. However, the use of local sensors introduces challenges in terms of installation, operations and maintenance costs due to the remoteness of the considered Arctic areas (e.g., no access point to the power grid).

In the recent years, passive means for vessel detection and tracking have gained attention due to their reduced electromagnetic pollution and interference to pre-existing radio-frequency systems, the reduced installation and maintenance costs, and finally for not being subject to safety authorities' authorization. Given these considerations, in this Section a vessel tracking application based on passive radar technologies and illuminators of opportunity (i.e., GSM base stations and VHF radio stations) is therefore presented, with the aim to show an enhanced MDA capability and to implement a covert surveillance for non-cooperative vessels, minimizing the impact on the environment (e.g. electromagnetic pollution) and the costs for future implementation. Moreover, the collected information is connected with some maritime context information, whose exploitation will be described in detail in the following. The use of passive radar technologies combined with a priori information here suggested represents a new research path to be addressed with respect to the system concepts in [Fea08] and [Art15].

8.2.1 Passive Radar Measurements and Tracks Simulator

The vessel tracking application resorts on a passive radar measurements and tracks simulator, which has been developed in the framework of the Canadian-German research project PASSAGES (Protection and Advanced Surveillance System for the Arctic: Green, Efficient, Secure [PASSftAG]), operating in the complex real scenario of the NWP in the Canadian Arctic. The description of the passive radar technology and its measuring and working principle are well documented in the literature ([Che07], [GB17]) and reported partially in Section 2.1. Its detailed explanation is beyond the scope of this Section, where only some notions related to the simulators' main functions are recalled for the sake of simplicity. Figure 8.11 depicts the Passive Radar Data Simulator Block Diagram with a clear reference to the order for the execu-

tion of the main functions in the simulation process. The blocks' main functionalities and the Input/Output structures are described in the following subsections.

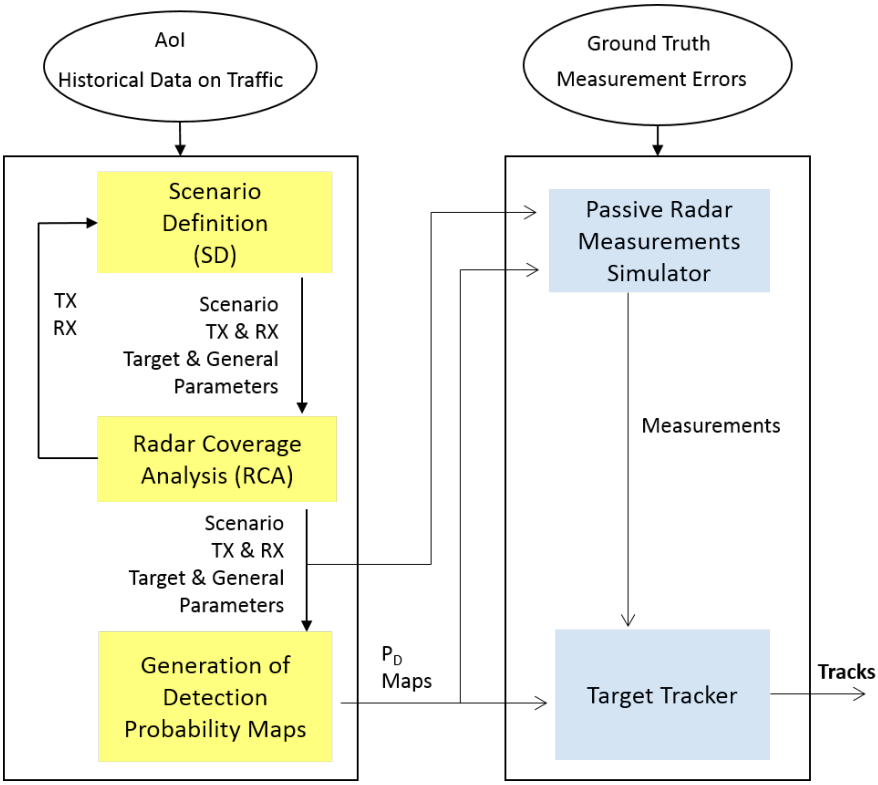

Figure 8.11: Passive radar data simulator block diagram.

Finally, it has to be stressed that for the application, the a priori knowledge of the context information is used as follows:

- Bathymetry maps and the information about the coastline is exploited for the definition of the vessel ground truth;
- The Digital Terrain Elevation Data (DTED) are taken into account to perform the passive radar Line of Sight (LoS) analysis. This is used to evaluate the positions of the simulated transmitting base-stations and the passive radar re-

ceiver and consequently to determine the Probability of Detection Maps for each TX-RX pair;

- Clutter and land maps represent an input for the target tracking algorithm to remove false and/or inaccurate passive radar measurements.

8.2.1.1 Scenario Definition Module

The module aims at defining (i) the operative scenario for the vessel traffic monitoring, (ii) the passive radar sensors (i.e. transmitting and receiving units) and (iii) the general processing parameters for the overall simulation.

The scenario and the reference vessel traffic picture are defined on the basis of the geographical boundaries of the Area of Interest (AoI) and the historical data on traffic (e.g. real data from Satellite-AIS). If the latter input is available, it provides information on kinematic data (e.g. position, Course over Ground and Speed over Ground) and type (e.g. cargo, tanker, fishing and passenger) of vessels navigating in the AoI. Such features are fundamental for the transmitter-receiver (TX-RX) configuration design phase. The defined fields are stored in a dedicated output structure "Scenario".

Subsequently, already existent illuminators in the scenario are identified. In particular, real GSM base stations and/or VHF radio stations are taken into consideration in this application. If such transmitters are available, their major characteristics and operative parameters (e.g. position, height, orientation, operative frequency, transmitting power, etc.) are stored and saved in the "TX" output structure. Otherwise, new transmitting stations have to be simulated and fully characterized. In the same way, passive receiving stations ("RX" structure) have to be deployed in the AoI.

Finally, the target motion related parameters together with general ones (e.g. radar cross section, probability of false alarm, etc) are defined for further use in the other simulator blocks (i.e. generation of probability of detection maps, sensor measurements and tracks generator).

8.2.1.2 Radar Coverage Analysis

The module evaluates the coverage of the transmitting and receiving stations identified in the Scenario module. Specifically, the purpose of a Radar Coverage Analysis (RCA) is to collect precise information about the area the sensors can reach, i.e. which parts of the Earth's surface and the space above it can be observed when the sensors are deployed at a certain location. This is important to know because in a natural environment with mountains, valleys, lakes and the open sea some areas can be hidden.

The locations of the TX-RX units have to be chosen in order to fulfill the coverage requirements. However, the location found may not be acceptable due to reasons like not getting the necessary infrastructure there. This means that the analysis has to be iteratively performed in order to identify and evaluate the suitability of the chosen sensors locations.

The RCA analysis uses a spherical Earth model, whose radius is the average of the two radii of the WGS84 ellipsoid, high-resolution Digital Terrain Elevation Data (DTED) offering terrain data with various resolutions in height and in a Longitude-Latitude (Lon-Lat) grid, and basic parameters of the sensors under consideration, such as instrumented range and the geometry of scan sectors. The RCA can be applied both for monostatic and bistatic (multistatic) radar configurations. For the latter, the covered area results from transmitter-receiver (TX-RX) pair specific coverage areas by intersection. The algorithm for calculating the radar coverage consists of the following steps:

- Calculate for a given azimuth direction the terrain height profile from the radar position to a point at the border of the map;
- Calculate the visible terrain points;
- Calculate the visible points at a target dependent height above the selected profile, e.g. sea level;
- If desired consider an elevation sector or other restrictions to the elevation of the radar field of view.

These steps are repeated until all required azimuth directions are covered. As already mentioned, the RCA tool is used to optimize the TX-RX geometry for a given AoI and employed in the generation of radar measurements for a specific simulated scenario.

8.2.1.3 Detection Probability Maps Generator

The module evaluates the target's probability of detection (PD) for each transmitter-receiver pair in the AoI. To this aim, the Bistatic Signal to Noise Ratio (SNR) has to be evaluated per each pixel of the AoI grid [Che07]:

$$SNR = \frac{P_R}{P_N} = \frac{P_T G_T \sigma_0 \lambda^2 G_R}{(4\pi)^3 {R_T}^2 {R_R}^2 L_T L_R L_s} G_{int} \frac{1}{kT_0 FB}, \tag{8.5}$$

In the Equation 8.5, P_R and P_T are the power of the received and transmitted signals, respectively. G_R and G_T are the gain coefficients for the transmitting and receiving

antennas; σ_0 the bistatic radar cross section (RCS) of the target and λ the wavelength. R_T is the range of the target relative to the transmitter while R_R represents the range of the target relative to the receiver. L_T are the losses that appear during wave propagation in the area of the transmitter-target; in the same way L_R are the losses that appear during the wave propagation in the area of the target-receiver and L_s represents the system losses. The term $P_N = kT_0FB$ represents the receiver noise power: k is the Boltzmann's constant, T_0 is a reference temperature of $290K$, F is the receiver noise figure and B is the receiver bandwidth. Finally, G_{int} is the gain factor related to the coherent processing time interval T_{cpi} adopted in the signal processing [Nic14]. All the parameters in Equation 8.5 can be directly taken from the data structures defined in the Scenario module (which also represent the inputs for the detection probability maps generator module) or can be evaluated from them (e.g. $G_{int} = T_{cpi}N_{pulses}$). Then, the definition of the Probability of False Alarm (P_{FA}), i.e. the probability of exceeding the detection threshold when no signal is present, the choice of the target distribution model and the SNR in Equation 8.5 allow the evaluation of the Probability of Detection (P_D), [Sko08]. This is calculated for each TX-RX pair and represents the major output of the module.

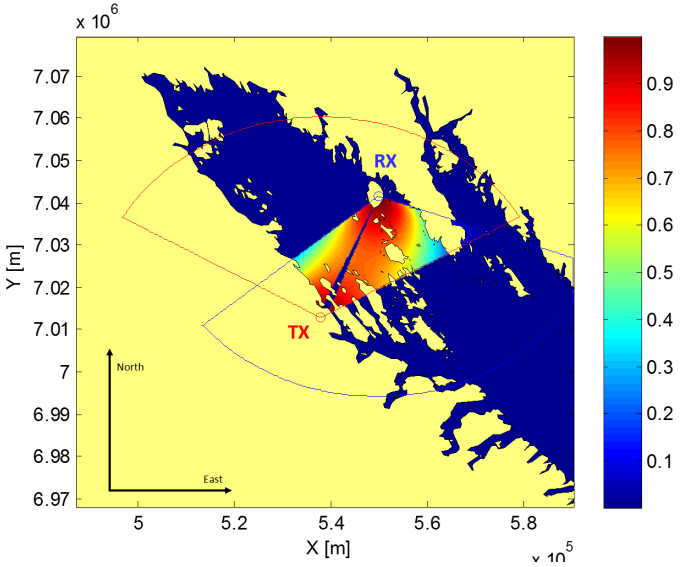

Figure 8.12: Example of a detection probability map for a TX-RX pair in the AoI.

Figure 8.12 shows an example of the target detection probability map for typical vessel ($RCS = 100m^2$) and a transmitter-receiver pair in the AoI, obtained through the above described steps. Specifically, the TX and RX positions are indicated together with the TX and RX antennas' sectors. The sectors' shapes are dictated by the antenna Field of Views (FoV), which determine the sectors' aperture and the Distance of Views (DoV), which establish the maximum detection range. It is evident that the P_D assumes significant values in the intersection of the sectors, except in the area close to the direct path that connects the TX and RX antennas, where there is no possibility to detect the target. Specifically, the echoes from particular angles of arrival and cells in range in this region are not Doppler-shifted with respect to the direct signal due to the observation geometry between transmitter, target and receiver. The absence of the Doppler component makes the detection impossible.

The availability of different TX-RX pairs in the monitored area allows improving the target detection capability. If the measurements of N bistatic geometries are gathered simultaneously, the cumulative probability of detection ${P_D}^C$ can be written as:

$$ {P_D}^C = 1 - \prod_{i=1}^{N} (1 - {P_D}^i), \tag{8.6} $$

where ${P_D}^i$ represents the probability of the i-th TX-RX pair [Nic14]. An example of the cumulative ${P_D}^C$ is shown in Figure 8.13.

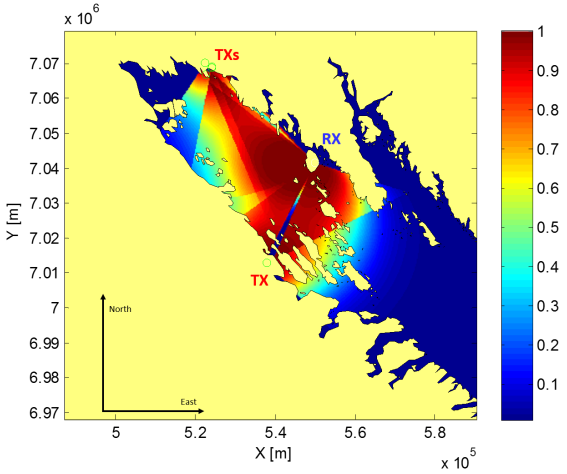

Figure 8.13: Example of a cumulative detection probability map for the AoI.

8.2.1.4 Measurements Simulator Module

The module simulates the passive radar measurements for each bistatic geometry in the AoI. In order to derive a measurement vector $\mathbf{z}_k$ for a given time t_k, the bistatic geometry in Figure 8.14 is taken as reference:

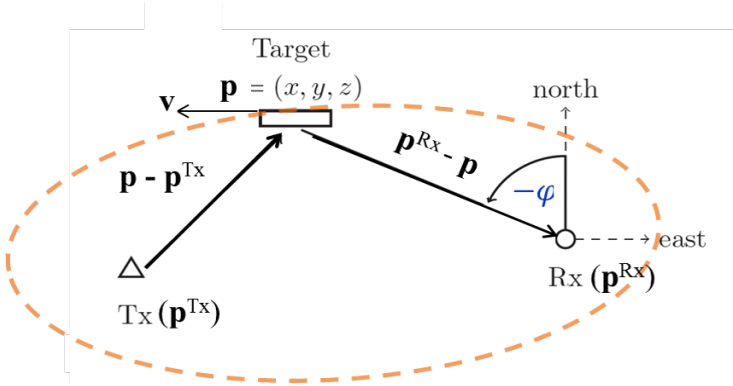

Figure 8.14: Bistatic Geometry and Notations.

Specifically, the target state is described in 3D Cartesian coordinates assuming a constant velocity dynamic model. The target state vector is given by:

$$\mathbf{x}_k = (\mathbf{p}_k, \mathbf{v}_k)^T = (x_k, y_k, z_k, \dot{x}_k, \dot{y}_k, \dot{z}_k)^T, \tag{8.7}$$

which includes the position $\mathbf{p}_k$ and the velocity $\mathbf{v}_k$ components at time t_k. In the same way, the positions and the velocities of the transmitter and receiver are respectively given by

$$\mathbf{x}_k^{Tx} = (\mathbf{p}_k^{Tx}, \mathbf{v}_k^{Tx})^T = (x_k^{Tx}, y_k^{Tx}, z_k^{Tx}, \dot{x}_k^{Tx}, \dot{y}_k^{Tx}, \dot{z}_k^{Tx})^T, \tag{8.8}$$

and

$$\mathbf{x}_k^{Rx} = (\mathbf{p}_k^{Rx}, \mathbf{v}_k^{Rx})^T = (x_k^{Rx}, y_k^{Rx}, z_k^{Rx}, \dot{x}_k^{Rx}, \dot{y}_k^{Rx}, \dot{z}_k^{Rx})^T. \tag{8.9}$$

Assuming the target to be moving at height zero with constant velocity ($\mathbf{v}_k = \mathbf{v}$), the measurements equation can be computed as in 3.2:

$$\mathbf{z}_k = \mathbf{h}_k(\mathbf{x}_k) + \mathbf{w}_k = (r_k, \varphi_k, \dot{r}_k)^T + \mathbf{w}_k, \tag{8.10}$$

where $\mathbf{h}_k$ is the non-linear measurement function and $\mathbf{w}_k$ is a zero mean white Gaussian sequence with diagonal covariance $\mathbf{R}_k$. r_k is the bistatic range, φ_k is the azimuth angle and $\dot{r}_k$ the bistatic range rate, which is proportional to the Doppler shift:

$$r_k = \left\|\mathbf{p}_k - \mathbf{p}_k^{Tx}\right\| + \left\|\mathbf{p}_k - \mathbf{p}_k^{Rx}\right\|, \tag{8.11}$$

$$\varphi_k = atan2(x_k - x_k^{Rx}, y_k - y_k^{Rx}) \in (-\phi, \phi], \tag{8.12}$$

$$\dot{r}_k = -f_d\lambda = \left(\frac{\mathbf{p}_k - \mathbf{p}_k^{Tx}}{\left\|\mathbf{p}_k - \mathbf{p}_k^{Tx}\right\|} + \frac{\mathbf{p}_k - \mathbf{p}_k^{Rx}}{\left\|\mathbf{p}_k - \mathbf{p}_k^{Rx}\right\|}\right)^T \cdot \mathbf{v}. \tag{8.13}$$

$\|\cdot\|$ denotes the Euclidean Norm, f_d the bistatic Doppler frequency and λ the wavelength. Moreover we assume a stationary transmitting and receiving platforms, thus their velocity components are equal to zero.

The module takes as input the reference ground truth generated by interpolating real Satellite AIS tracks of the vessels navigating in the AoI, which suffer from gaps of information due to the satellite constellation's revisit time (see Section 2.1). The estimation of the target positions between consecutive data bursts is realized by a simple and linear interpolation algorithm (e.g. in time and space over the entire observation period), which keeps the vessel speed constant between the consecutive

original messages. The vessels' positions, originally provided in the WGS84 reference system by the S-AIS, are converted in the Cartesian space and chronologically ordered. The interpolation algorithm uses a parameter that defines the maximum allowed spatial distance (d_{max}) between two S-AIS data. If two consecutive S-AIS messages for the same vessel have a distance (d_{AIS}) that exceeds this threshold, the interpolation is executed. The number of the interpolated points n_{interp} in the gap is given by:

$$n_{interp} = \left\lfloor \frac{d_{AIS}}{d_{max}} \right\rfloor \tag{8.14}$$

Subsequently, the WGS84 coordinates in terms of latitude and longitude of the new points are evaluated. This basic algorithm performs well in open waters but not in narrow passages or close to the coastline where the interpolation may lead to tracks that cross over landmasses. In order to avoid this unrealistic behavior, the algorithm exploits bathymetry maps and coastline information in the AoI to force the interpolated tracks to follow corridor points in the route where no intersections with the land are foreseen and where the water is sufficiently deep for the vessel to pass. The Figure 8.15 shows an example of S-AIS real data with information gaps for a given vessel (A), the result of the simple linear interpolation algorithm (B), and the improvement in the interpolation process when driven by external a priori information such as bathymetry and coastline (C).

Finally, the positions of the derived ground truth are converted again in the Cartesian space, taking the coordinates of the receiving station as the origin of the XYZ plane. Then, the passive radar measurements (i.e. measurement vectors) are expressed in the Doppler-Bistatic Range domain through the Equations 8.11, 8.12 and 8.13. For an exhaustive simulation, the measurement vectors have to be generated in according to proper measurement errors. For the application a Gaussian distribution with given accuracies in range (σ_r), azimuth (σ_φ) and range rate ($\sigma_{\dot{r}}$) is taken into account. In addition, only the measurements with Probability of Detection larger than 0 (e.g. evaluated truth the exploitation of the P_D maps) are provided as the main output of the module. Finally, false target detections are generated for each TX-RX pair, i.e. false alarms are uniformly distributed in the AoI in accordance with the false alarm probability parameters and the P_D map. An example of the overall measurement simulation process will be provided in the following sections.

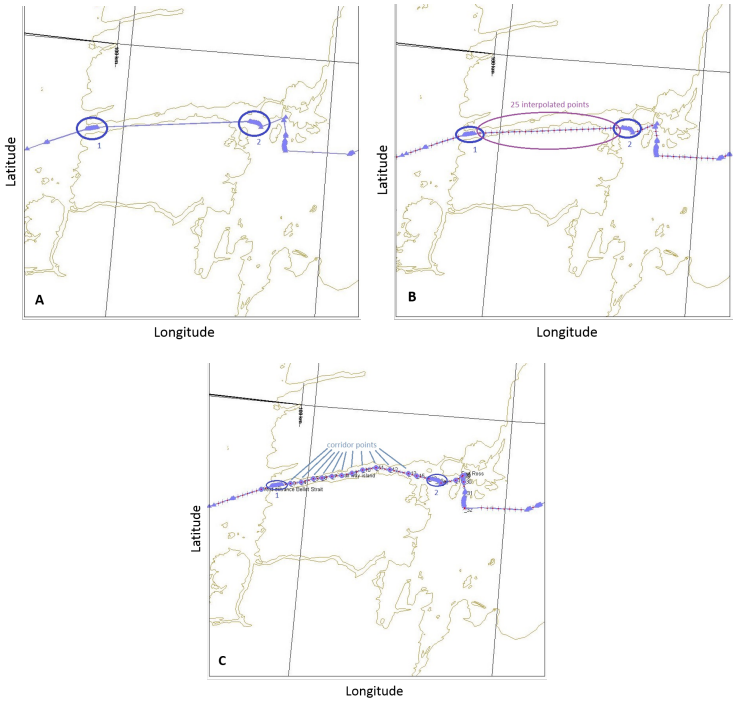

Figure 8.15: Example of ground truth generation as Input for passive radar measurement simulator Module: A) S-AIS real data with information gaps for a given vessel, B) result of the linear interpolation algorithm, C) result of the linear interpolation algorithm supported by a priori knowledge of corridor points.

8.2.1.5 Target Tracker Module

The module aims at generating the passive radar tracks. Target tracking is the estimation of the state of one or multiple (generally an unknown number) of evolving objects (targets) based on a time series of measurements coming from one or several sources (sensors). The goals of target tracking are (i) to establish a one-to-one correspondence between the estimated objects (tracks) and the true targets in the scene, and (ii) to generate estimates of the kinematic state of the targets (potentially augmented by further attributes), including measures of the accuracy and reliability of the estimates. Generally, target tracking comprises the tasks of data alignment, association, filtering, and track management [HM04], which are repeated at each iteration

or update of the estimated tracks. Data alignment supports indeed the association step by pre-processing (e.g., interpolating or extrapolating) the collected sensor data, if required by the selected processing scheme. Then, input data (e.g. measurements) are assigned to the existing tracks or used to initiate new tracks through a given plot-to-track association strategy. This step is particularly challenging in the case of dense target scenarios and a high false alarm rate, i.e. high rate of input measurements that do not originated from true targets (e.g. due to measurement noise, clutter or interferences). For each successful data association, the state estimate of that track is updated in the filtering step, using the actual measurement. Finally, track management consists of several functions to establish a clear and unique track picture, like track extraction (initialization), track split, track merging, track numbering and track-to-track fusion. There exists a vast body of literature on the topic of target tracking ([BP99, BSLK01, Koc14]), which is today addressed in the framework of sensor data and information fusion [HM04].

In this application, we refer to the approach reported in Section 4.1, where the sequential processing scheme of track prediction and measurement update within the context based Bayesian estimation theory is presented, and Section 5.3, where the algorithm to handle the inclusion of specific context based element in the Multiple Hypotheses Tracker (MHT) is described. Specifically, the information about the coastline and the P_D maps represent the a priori knowledge for this example. The measurement-target association task is handled by resorting to the MHT technique based on Unscented Kalman Filter (UKF, [JU04]) formulation, since the measurement equation is non-linear for this passive radar based application. The association problem between measurements and transmitters, which appears when multiple TX-RX pairs contribute to the target tracking, is well known in a GSM/VHF PCL based system ([ZBBN14]) and it is not hereafter addressed.

8.2.2 Test Scenario and Simulation Rationale

The geography of the NWP presents a limited set of options for a transiting vessel, which varies according to the ice and weather conditions and the season of the year. Figure 8.16 (A) shows the major traffic routes in the Arctic, identified trough the analysis of historical data on maritime traffic (e.g. data collected in the years 2011-2013). Specifically, we focus on the high traffic route to the Hudson Bay and Frobisher Bay (black circle in Figure 8.16 (A)) as the reference corridor for the demonstrating the improved MDA for this application (see Figure 8.16 (B)).

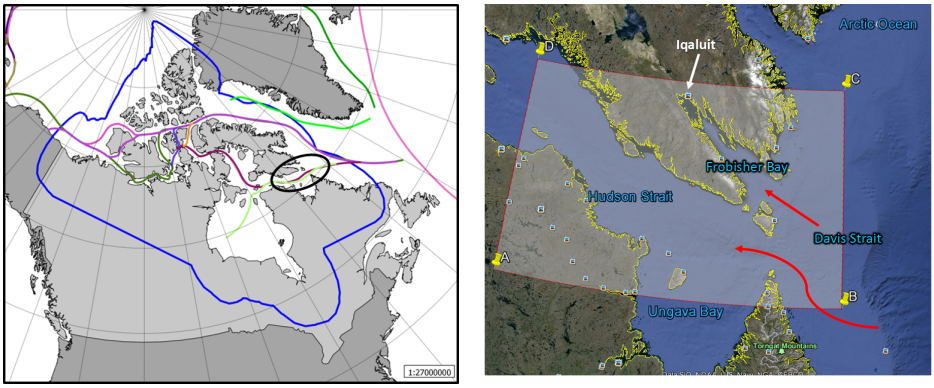

Figure 8.16: Test scenario: A) The Arctic Ocean with routes, B) AoI for the application.

The identified area, which is approximately $300km \times 300km$, is interesting to monitor for several reasons. First of all, Frobisher Bay is the only waterway leading to Nunavut's capital Iqaluit, which is the the largest city in the NWP area (over 6000 inhabitants). The Bay is a $230km$ long inlet that varies in width between $40km$ and $20km$, with a tidal difference between $7m$ and $11m$. The islands situated at the narrow inner end of the inlet, the presence of ice and the absence of port and any sort of beach security, make the navigation in the area extremely challenging and time consuming. For example, unloading supplies on the beach in Iqaluit takes at least 30 - 40 days and most ships suspend their voyage whenever the traditional navigation routes in Frobisher Bay are impassable because alternative and safer routes are not available or simply unknown. Moreover, Hudson Strait and Davis Strait are popular fishing grounds, but they are not monitored on a regular basis and it happens that many fishing vessels there do not use their AIS to report the position because they are competing for the best fishing grounds with each other.

The only regular source of information on transiting, fishing or stationary vessels are satellite S-AIS reports. Possibly, information derived from S-SAR images can additionally contribute to the maritime picture. Cost-benefit considerations and the fact that Iqaluit is close-by, suggest the possibility to exploit already existing sensors and information sources in the area for vessel monitoring purposes. One option is to use existing transmitters of radio frequencies to apply the efficient and covert passive radar methodology. Specifically, the advantages resulting from the use of an optimized network of passive sensors that exploit GSM base stations and VHF radio stations as illuminators of opportunity is addressed in this scenario.

The setup of this vessel traffic monitoring service is tackled through different steps. First of all the Area of Interest (AoI) and the reference traffic picture are defined on the basis of historical data. Figure 8.17 shows the maritime traffic obtained from available S-AIS data covering a time period of 8 days in August 2013.

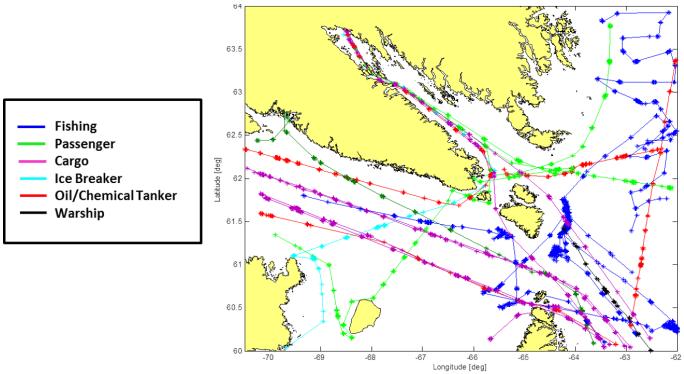

Figure 8.17: Example of S-AIS dataset for August 2013.

This analysis leads to the identification of different types of vessels crossing the selected area, such as fishing and passenger vessels, cargo ships and tankers (occasionally transporting hazardous materials), which have similar or different routes according to their specific destinations. The vessel kinematics (e.g. position, course over ground and speed over ground) and the vessel type (e.g. cargo, tanker, fishing, passenger, etc.) are relevant for the design of transmitters-receiver configurations. Specifically, this requires an iterative analysis. The first step foresees the identification of available transmitters in the AoI (e.g. already existent GSM base stations and/or VHF radio stations) and the deployment of the passive receiving station, together with the specification of their major characteristics and operative parameters (e.g. position, height, orientation, operative frequency, transmitting power, etc.). This is made also in accordance to the RCA analysis previously described. Then the evaluation of the vessel P_D is carried out for each TX-RX pair. To this aim the bistatic SNR is calculated for the entire AoI under the assumption of a stationary target, whose RCS is constant throughout a single radar scan (e.g. Swerling I Model) and for a given P_{FA}. If the achieved performance is not satisfactory, new transmitters are introduced and the configuration is iteratively optimized. Then, passive radar measurements are simulated for the reference traffic picture and PR tracks are generated by resorting to the MHT algorithm.

In order to test over real data the capability of a passive radar based monitoring system exploiting the KB-MHT algorithm in Section 5.3 three sub areas in the entire AoI have been identified. They are reported in Figure 8.18, together with the S-AIS data registered in two consecutive days in August 2013 for three different vessels (passenger ship, cargo and tanker). As expected, the S-AIS data present gaps over the entire observation period. The passive radar measurements and the derived tracks are expected to fill completely or partially these gaps ensuring a continuous vessel monitoring.

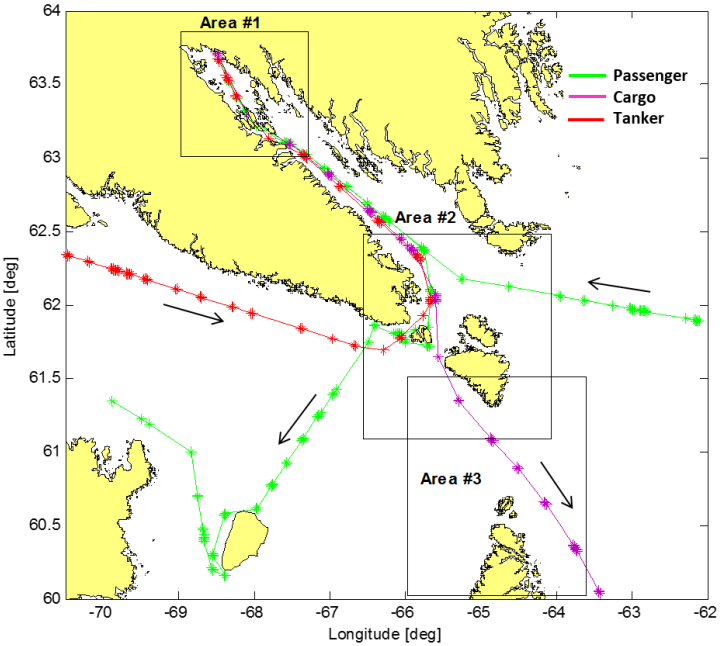

Figure 8.18: Sub Areas.

In the first sub area, which covers part of the Frobisher Bay with an extension of $100km \times 100km$, only four real GSM transmitting base stations exist, almost co-located in Iqaluit. Other illuminators are simulated in order to cover the Bay with adequate probability of detection (P_D) values, together with the receiver base station. Figure 8.19 shows an example of the adopted bistatic geometries: the transmitting

(real and simulated) and receiving stations are reported together with the global coverage created in the area. Specifically, for each sensor, the Field of View (FoV) and the orientation (heading angle defined clockwise with respect to the North direction) are reported. For the simulated TX and RX two illumination sectors have been considered.

Name	Type	Type	FoV	Heading
Iqaluit Crystal	GSM TX	Real	120°	100°
Iqaluit Airport	GSM TX	Real	120°	150°
Iqaluit Astro	GSM TX	Real	120°	100°
Iqaluit Center	GSM TX	Real	120°	130°
TX1	GSM TX	Sim	120°	0°
TX1	GSM TX	Sim	120°	80°
RX1	GSM RX	Sim	120°	170°
RX1	GSM RX	Sim	120°	260°

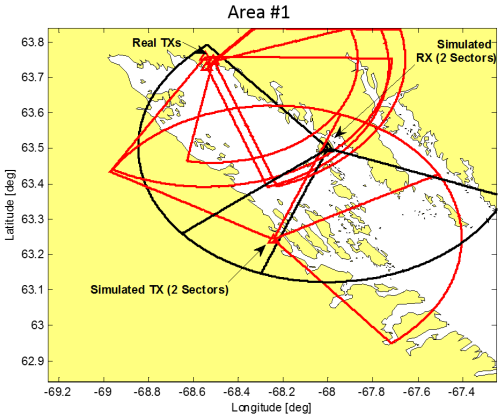

Figure 8.19: Position of the GSM transmitting and receiving stations in the Sub-Area#1.

The choice of the simulated TX and RX positions has been supported by the radar coverage analysis. The exploitation of the Digital Terrain Elevation Data allows to determine the proper sensors' locations in order to maximize their coverage. Figure 8.20 shows an example of this process: TX and RX positions (Latitude, Longitude and Height) have been refined in accordance to the DTEM. The colors in the picture (e.g. red and yellow) represent the sensor coverage evaluated for different terrain heights, red color for $0m$ and yellow for $50m$ AMSL, respectively.

	Transmitter (Tentative Loc)	Transmitter (After RCA)
Latitude	63.2423°	63.252°
Longitude	-68.2442°	-68.220889°
H (AMSL)	136.3 m	281.7 m
H (antenna)	10 m	10 m
H (sum)	146.3 m	291.7 m

	Receiver (Tentative Loc)	Receiver (After RCA)
Latitude	63.5°	63.506°
Longitude	-68°	-68.019778°
H (AMSL)	91 m	173.4 m
H (antenna)	10 m	10 m
H (sum)	101 m	183.4 m

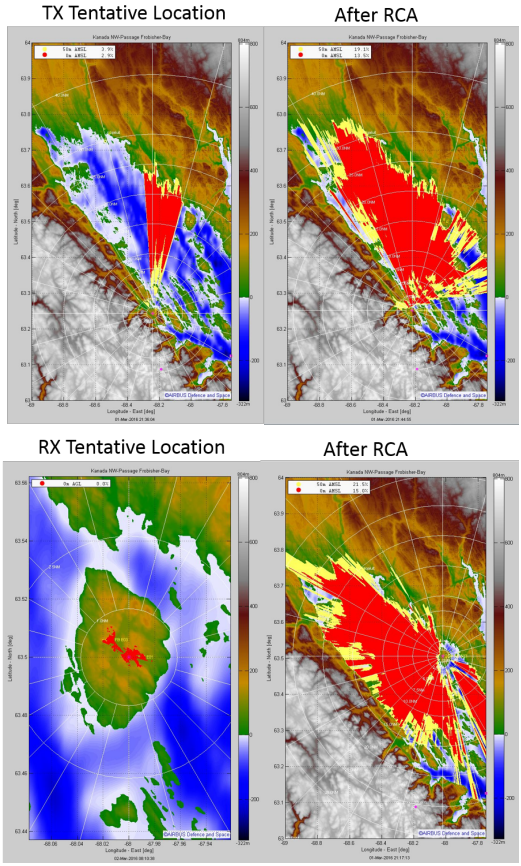

Figure 8.20: Refinement of the TX and RX positions in accordance to the RCA.

For each TX-RX configuration, the correspondent P_D map is generated. An example of one P_D map and the cumulative is P_D is depicted in Figure 8.21 and Figure 8.22, respectively. They are evaluated on the basis of the parameters reported in the Table 8.3 for the GSM case.

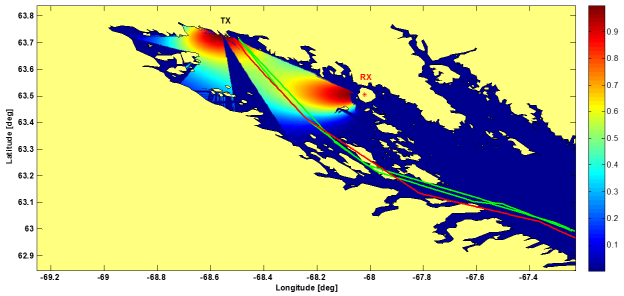

Figure 8.21: P_D map for one TX-RX configuration in the Sub-Area #1.

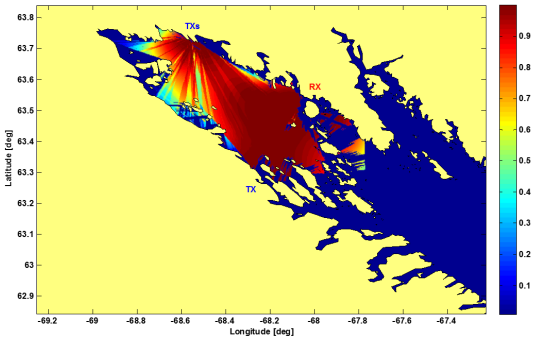

Figure 8.22: Cumulative P_D map for the sensor configuration adopted in the Sub-Area#1.

Then, passive radar measurements and tracks are then simulated. The S-AIS tracks of the vessels are subject to the procedure described in the previous Section to generate the ground truth in WGS84 Coordinates. Then, the simulated radar measurements are provided in terms of bistatic range, Doppler and azimuth angle, taking into account the probabilities of detection and the measurement errors. Specifically, for this application we took $\sigma_r = 300m$, $\sigma_\varphi = 2^\circ$ and $\sigma_{\dot{r}} = \lambda\sigma_d = \lambda 2Hz$ as reference values for the simulation, where σ_d represents the accuracy in Doppler. In addition, only the measurements with Probability of Detection larger than 0 are provided as result of the simulation. Figure 8.23(A) shows the detection region for a given TX-RX bistatic geometry, with two vessels crossing the area. The passive radar measurements gener-

Table 8.3: Parameters for P_D generation and passive radar measurements and tracks simulations.

TX Parameters	**Value**	**RX Parameters**	**Value**
Frequency	$1900MHz$	Frequency	$1875MHz$
Beamwidth	$4.15MHz$	Beamwidth	$81.3kHz$
Field of View	$120°$	Field of View	$120°$
Distance of View	$40km$	Distance of View	$40km$
Antenna Gain	$10dB$	Antenna Gain	$10dB$
Transmitting Power	$10W$	Noise Figure	$10W$
		Losses	$5dB$
		CPI	$1.8s$
		Pulses	500
Target Parameters	**Value**	**Other Parameters**	**Value**
RCS	$100m^2$	P_{FA}	10^{-3}
Height	$20m$	Azimuth Resolution	$3.2°$
MDV	$4m/s$		

ated by considering measurement errors and in accordance to the detection probability map are reported in Figure 8.23(B).

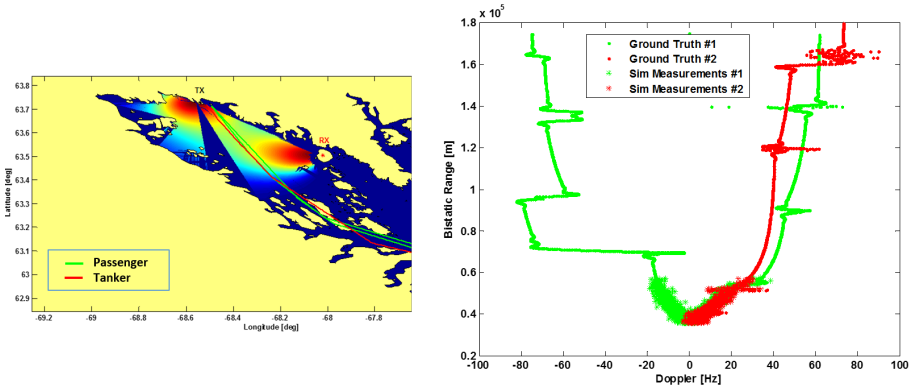

Figure 8.23: (A): P_D map for one TX-RX configuration in the Sub-Area#1, (B) Simulated passive radar measurements

These measurements and the false target detections generated for each TX-RX pair (i.e. false alarms uniformly distributed in the AoI in accordance with the false alarm probability parameters in Table 8.3 and the P_D map) represent the main input for the tracking algorithm. The output is depicted in Figure 8.24.

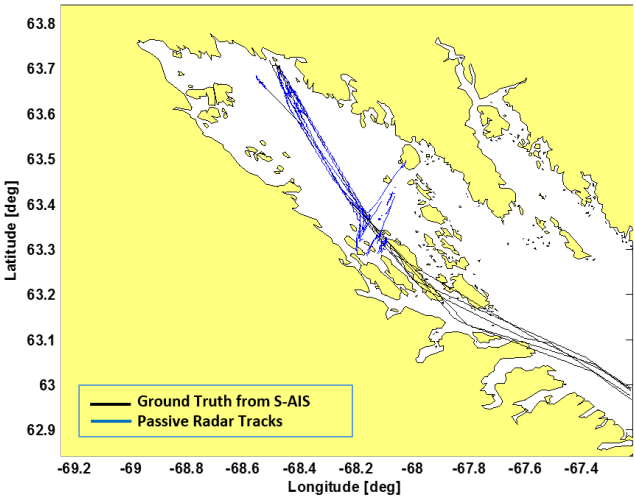

Figure 8.24: Ground truth and simulated passive radar tracks in the Sub-Area#1

The black plots represent the ground truth, while the blue ones are the simulated passive radar tracks. They have been evaluated by fusing the contribution of all the TX-RX bistatic geometries in the AoI and by resorting to the cumulative probability of detection depicted in Figure 8.22. In particular five targets are navigating in the AoI in the considered time window: for the selected processing parameters the tracker provides 52 track segments as output. They are post-processed to get continuous tracks, as depicted in Figure 8.25, where the results are shown for a passenger ship and a tanker. Specifically, due to the probability of detections, the passenger ship final track is made of 12 segments, (e.g. track continuity of 45.6%), while the tanker track results continuous (only 1 segment, track continuity of 99.9%). The track continuity is evaluated over the time intervals in which the $P_D > 0$, for both the target separately.

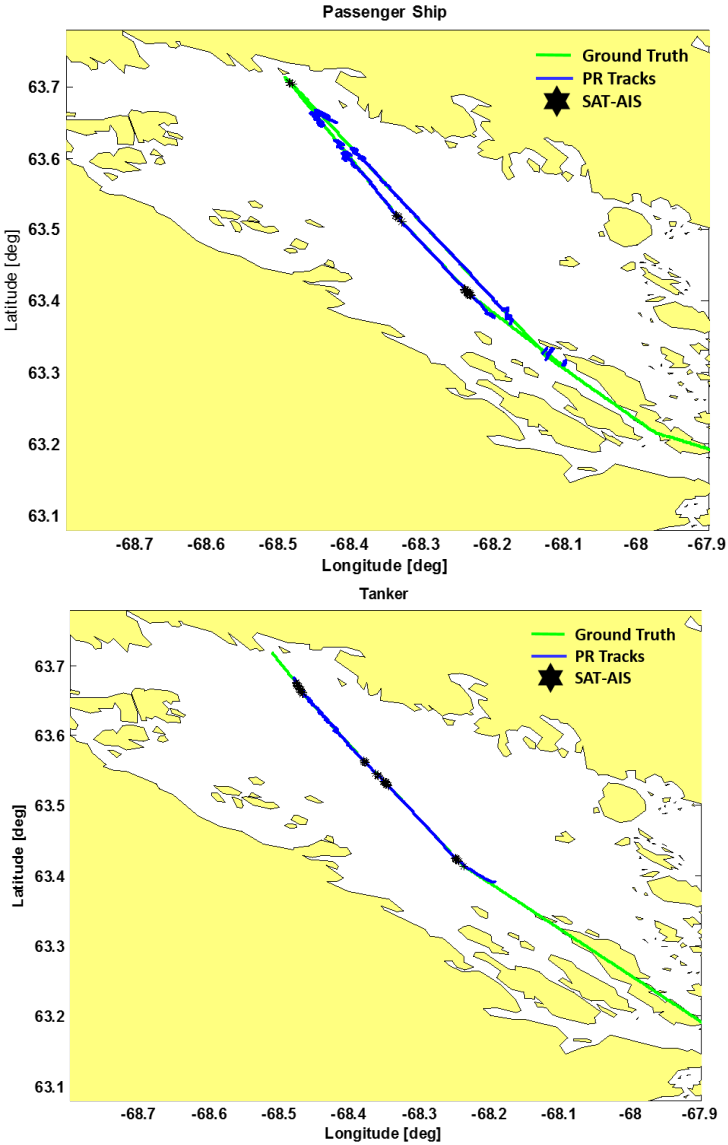

Figure 8.25: Ground truth and simulated passive radar tracks for passenger ship and tanker in the Sub-Area#1

If we compare this results with the S-AIS tracks for the same vessels (i.e. the black stars in Figure 8.25), it its evident to see how the exploitation of passive radar data brings a significant improvement for the vessel monitoring task, filling the gap between S-AIS detections, as depicted in Figure 8.26 for passenger ship (left) and for the tanker (right).

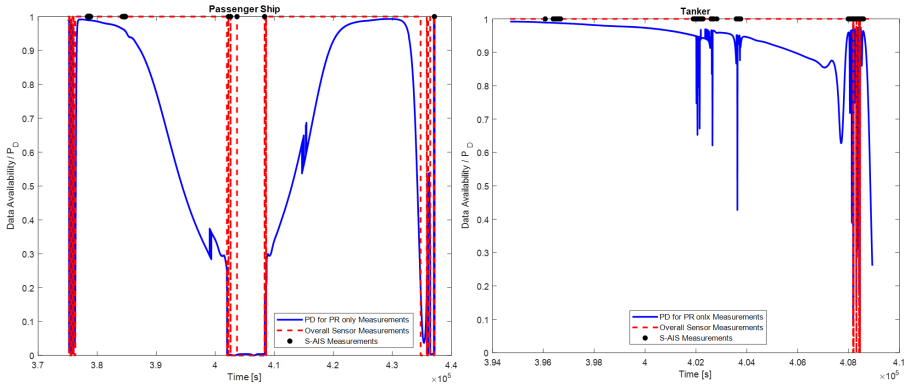

Figure 8.26: Sensor data availability for passenger ship (left) and for tanker (right) in Sub-Area#1.

As the other two Sub-Areas#2 and #3 in Figure 8.18 are concerned, the overall data simulation and processing took place by resorting to real GSM BTS and simulated VHF transmitting stations, whose coverage in range is greater than the GSM case with a FoV of 360°. The position of the BTSs and the tracking results are reported in Figure 8.27 and Figure 8.28 for both Sub-Areas.

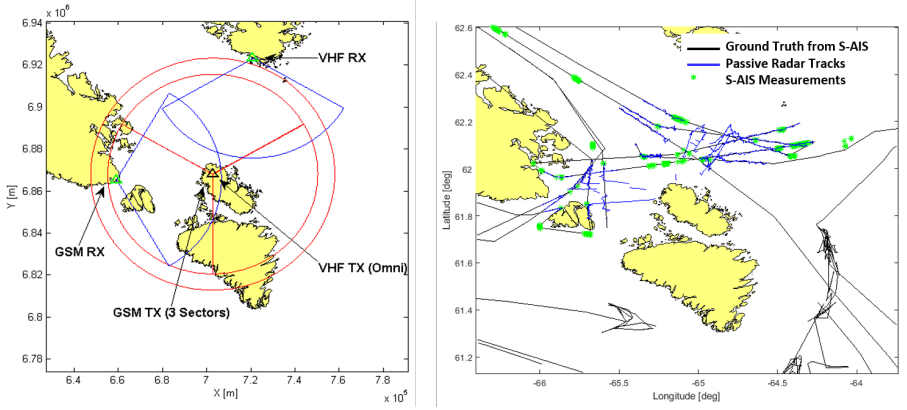

Figure 8.27: Positions and illuminating sectors of BTSs (left); Ground truth and simulated passive radar tracks in the Sub-Area#2 (right).

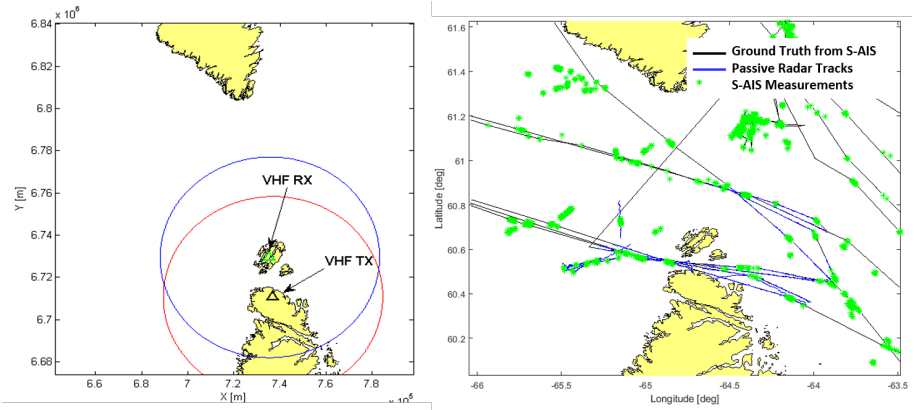

Figure 8.28: Positions and illuminating sectors of BTSs (left); Ground truth and simulated passive radar tracks in the Sub-Area#3 (right).

For both cases, the fusion of S-AIS data with the simulated passive radar tracks brought to a continuous vessel monitoring. Figure 8.29 shows the sensor data availability for the passenger ship and the tanker along their journey through the selected Sub-Areas, as depicted in Figure 8.18.

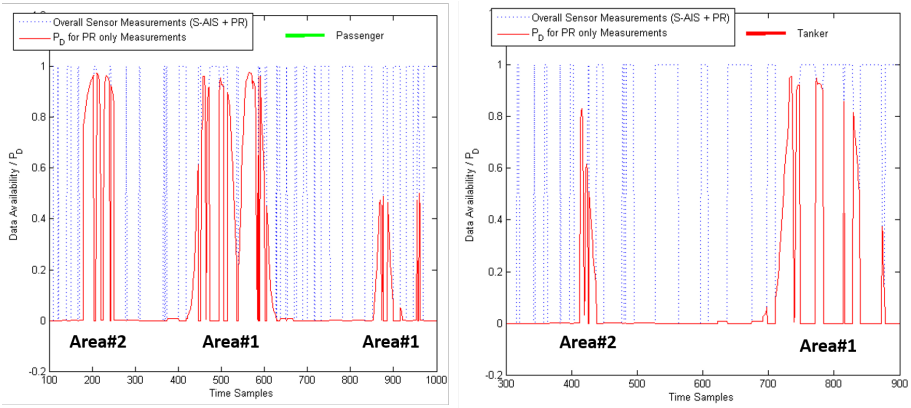

Figure 8.29: Sensor data availability for passenger ship (left) and for tanker (right) through all Sub-Areas.

8.3 Summary

In this Chapter the use of passive radar technologies supporting already established coastal surveillance systems was presented. Specifically, a GSM-PCL based system has been tested to monitor vessels in two scenarios: in the Baltic Sea, characterized by dense traffic conditions and dense clutter environment, and in the remote region of the Canadian Arctic, which suffers from the lack of common surveillance systems and infrastructure.

In both cases, it was demonstrated how the exploitation of the context information (i.e. target detection probabilities, clutter distributions and DTED models) encoded in georeferenced maps brought added value to the overall system. For the Baltic Sea scenario case, an improvement in the vessel tracking task was envisaged. Specifically, the adopted KB-MHT algorithm allowed achieving better performance in terms of track continuity and false track rate reduction. As the Canadian Arctic scenario is concerned, the terrain and bathymetry models were used to support the choice of the TX-RX configuration, which is demonstrated to be extremely important for the system performance given its bistatic nature, while resorting to the P_D maps allowed improving the tracks continuity.

CHAPTER IX

Conclusions

The objective of the presented research work is to demonstrate that background knowledge can be effectively exploited to improve the situational awareness in different operative applications in the maritime environment. Specifically, the tracking and data fusion processing scheme, which forms the basis for compiling the traffic picture, has been considered as "recipient" of the innovative features. Diverse features have been taken into consideration during the work, since the maritime environment is rich of a priori knowledge (sea lanes, coastlines, bathymetry, etc.) and common practices that might be promisingly used to better infer the presence and dynamic behaviour of moving targets.

Having identified the knowledge base, state-of-the-art tracking algorithms have been successfully modified in order to constrain or modify the evolution of the target state based on the available knowledge. Constrained Bayesian theory has been widely used in this work as framework for the mathematical derivation of the knowledge-based filtering techniques.

Since both the availability of knowledge and the available sensor measurements largely depend on the specific application, it has been decided to address a wider range of solutions that cope with the different operative applications. The addressed solutions are presented in this work with focus on (i) active radar surveillance in coastal areas, (ii) collaborative vessel traffic monitoring in high seas and coastal areas, and (iii) passive radar surveillance in coastal areas.

An extensive use of live data has been made, which have been collected during test campaigns performed within European and international research consortia. These

data provided a reliable basis for simulating complexer scenarios, which have been then processed by the innovative algorithms. The building of test scenarios and characteristics of knowledge elements derived from extensive discussions with operators and stakeholders for the addressed applications.

The research results demonstrate improvements in track continuity and track accuracy for the addressed test scenarios. A significant effort has been provided in the customization of the techniques to the specific use cases and in the tailoring of the algorithms' parameters. The analysis of environment characteristics, sensor measurements, dependencies of track evolution from each contributing parameters as well as the real influence of the addressed knowledge features, has built up a significant expertise on this topic, which combines theoretical aspects and the "practical data analysis" experience. The achieved results have been addressed as promising by the stakeholders themselves.

Summarizing the results, the work confirms and assesses the potential benefits of constrained filtering for maritime surveillance as well as highlights the dependency of the optimal formulation of the knowledge-based technique on the scenario. It is realistic to say that the optimum solution does not exist, i.e., a tool that generally outperforms the non-constrained techniques for all the addressed cases. The data analysis experience is the key enabler for mapping the theoretical formulation into the operative solution.

Based on the achieve results, it is author's opinion that the herein described techniques has laid down a wide mathematical framework for future research activities, and has paved the way with several examples on how to turn this into application-specific solutions. Future research work will move on from this basis by addressing higher level of inference and assessing the impact that knowledge might have on these. Specifically, it is worth mentioning the following processing steps, which have not been covered by this work:

- measurement-to-measurement, measurement-to-track and track-to-track association;
- target classification and identification;
- inference on intention and level of risk.

List of Figures

Chapter 1

1.1 Example use case addressed in this PhD work. 4

1.2 The sinking cruise ship Costa Concordia on January 13th, 2012. . . . 7

1.3 Result of the collision between the Lady Aziza and Gokbel merchant vessels on December 28th, 2015. 8

1.4 Collision of US military ships due to AIS spoofing. 9

Chapter 2

2.1 VTS operative center. 14

2.2 VTS radar tower in Hamburg (Germany). 18

2.3 Automatic Identification System (AIS). 22

2.4 exactEarth infrastructure for the operation of satellite-based AIS for vessel monitoring. 25

2.5 Real time satellite global coverage. 26

2.6 exactEarth-RT (Real Time) global vessel detection and tracking. . . . 26

2.7 LRIT system components. 27

2.8 Copernicus Maritime Surveillance (CMS) Service Tasks. 29

2.9 SAR Images from TerraSAR-X (a) and Radarsat-2 (b). 30

2.10 Fraunhofer FKIE experimental passive radar system based on GSM signals. 32

2.11 European Commission Blue Hub - Transform data into knowledge. . . 33

Chapter 3

3.1 Components of the general estimation problem. 40

3.2 Evolution of exemplary MHT hypothesis tree. 53

Chapter 4

4.1 Left: Exemplary road network consisting of three road sections. Right: Local roads generated for a target which moves from left to right and approaches the junction. 66

4.2 Scheme of one iteration of the roadmap assisted tracking filter. 68

Chapter 5

5.1 Intensity KC map for a reference maritime scenario. 77

5.2 Geometrical model for vessel maneuver. 83

5.3 Block diagram for target dynamic model switching. 86

5.4 Sample particle cloud for PF. 87

Chapter 6

6.1 Scenario under test: area of interest and geographic map embedding the context information. 94

6.2 Scenario under test: synthetic target tracks over an interval of few hours. 95

6.3 Example of simulated vessel trajectories with gap of measurements. . . 96

6.4 Track evolution over a single reference ship target of the considered tracking filters with full measurements coverage. 97

6.5 Simulated performance over a single ship target for the considered tracking filters with intermittent measurements. 100

6.6 Simulated performance over 30 ship targets for the considered tracking filters with intermittent measurements. 101

6.7 Case Study I: target entering the port through the sea lane. 102

6.8 Case Study II: target leaving the port through the sea lane. 103

6.9 Case Study III: long journey and maneuvering target. 104

6.10 Simulated Scenario I: single maneuver target tracking in proximity of the coast accordingly to one sea lane. 107

6.11 Simulation Scenario II: double maneuver target tracking for approaching the port berthing area, accordingly to two sea lanes. 108

6.12 $\hat{D}_{KL}$ mean value for Scenario I with all measurements. 110

6.13 RMSE mean value for Scenario I with all measurements. 111

6.14 $\hat{D}_{KL}$ mean value and variance for a PF over Scenario I. 112

6.15 $\hat{D}_{KL}$ mean value for Scenario I with all measurements. 113

6.16 $\hat{D}_{KL}$ mean value for Scenario I, evaluated with Δ_{GAP}. 114

6.17 Comparison between the SL-CV-CT-EKF and SL-CV-CT-PF for Scenario I in terms of $\hat{D}_{KL}$ mean value and variance, evaluated with Δ_{GAP}. 116

6.18 $\hat{D}_{KL}$ mean value for Scenario II, evaluated with random measurement gaps of Δ_{GAP}=72s, T=2s and T_{OBS}=420s. 118

6.19 Comparison between the SL-CV-CT-EKF and SL-CV-CT-PF for Scenario II in terms of $\hat{D}_{KL}$ mean value and variance, evaluated with random measurement gaps. 119

Chapter 7

7.1 RPM logical block diagram. 123

7.2 RPM inputs - Knowledge Base elements. 125

7.3 RPM output - Evolution in time of the confidence level map. 126

7.4 Extended track prediction module functionalities. 128

7.5 Areas of interest and real data from AIS for the live campaigns in Tunisia/Italy - Gulf of Gabes and Norway. 129

7.6 Input/Output data for real test Scenario I. 131

7.7 Input/Output data for real test Scenario II. 132

7.8 Example of SAR footprints for SAR image acquisition for real test Scenario II. 133

7.9 Input/Output data for real test Scenario III. 134

Chapter 8

8.1 Receiver system GAMMA-2. (a) GAMMA-2 mounted on the tower; (b) GSM PCL antenna and GAMMA-2 receiver 139

8.2 Operative scenario in the Fehmarn Belt, [Zem16]. 140

8.3 Coverage area for the Fehmarn Belt scenario, [ZBBN14]. 142

8.4 CRLB Position Estimates: (a) Single Time Scan; (b) Three Time Scans; (c) Three Time Scans Alternative Velocity Vector, [ZBBN14]. . 143

8.5 Position estimation results: (a) Covariances; (b) Position error. 144

8.6 Clutter map for the BTS1-RX bistatic configuration. 146

8.7 Geographical map for the Baltic Sea. 146

8.8 Tracking results for MHT (without context information). 147

8.9 Tracking results for KB-MHT (with context information). 148

8.10 Tracking results for the Fehmarn Belt scenario. 149

8.11 Passive radar data simulator block diagram. 152

8.12 Example of a detection probability map for a TX-RX pair in the AoI. 155

8.13 Example of a cumulative detection probability map for the AoI. 157

8.14 Bistatic Geometry and Notations. 157

8.15 Example of ground truth generation as Input for passive radar measurement simulator Module: A) S-AIS real data with information gaps for a given vessel, B) result of the linear interpolation algorithm, C) result of the linear interpolation algorithm supported by a priori knowledge of corridor points. 160

8.16 Test scenario: A) The Arctic Ocean with routes, B) AoI for the application. 162

8.17 Example of S-AIS dataset for August 2013. 163

8.18 Sub Areas. 164

8.19 Position of the GSM transmitting and receiving stations in the Sub-Area#1. 165

8.20 Refinement of the TX and RX positions in accordance to the RCA. . . 166

8.21 P_D map for one TX-RX configuration in the Sub-Area #1. 167

8.22 Cumulative P_D map for the sensor configuration adopted in the Sub-Area#1. 167

8.23 (A): P_D map for one TX-RX configuration in the Sub-Area#1, (B) Simulated passive radar measurements 168

8.24 Ground truth and simulated passive radar tracks in the Sub-Area#1 . 169

8.25 Ground truth and simulated passive radar tracks for passenger ship and tanker in the Sub-Area#1 170

8.26 Sensor data availability for passenger ship (left) and for tanker (right) in Sub-Area#1. 171

8.27 Positions and illuminating sectors of BTSs (left); Ground truth and simulated passive radar tracks in the Sub-Area#2 (right). 172

8.28 Positions and illuminating sectors of BTSs (left); Ground truth and simulated passive radar tracks in the Sub-Area#3 (right). 172

8.29 Sensor data availability for passenger ship (left) and for tanker (right) through all Sub-Areas. 173

List of Tables

Chapter 2

2.1 Relationship between VTS functions and VTS objectives. 15
2.2 Target reflection characteristics. 19
2.3 Radar tracking performance parameters. 21
2.4 AIS message frequency transmission. 23
2.5 AIS message types. 24
2.6 A priori information for maritime domain (part I). 35
2.7 A priori information for maritime domain (part II). 36

Chapter 6

6.1 Position estimation errors over the entire track life. 105
6.2 Average position RMSE over three reference targets. 105
6.3 Position estimation errors evaluated at the track reinitialization step. . 106
6.4 Average position RMSE over three reference targets evaluated at the track reinitialization step. 106
6.5 Typical vessel manouvring parameters. 117

Chapter 8

8.1 GSM-BTS parameters in the Fehmarn Belt. 140

8.2 Visualization scheme for tracking results. 148

8.3 Parameters for P_D generation and passive radar measurements and tracks simulations. 168

Acronyms

ADC	**A**nalogue to **D**igital **C**onverter
AIS	**A**utomatic **I**dentification **S**ystem
AoA	**A**ngle of **A**rrival
AoI	**A**rea of **I**nterest
AR	**A**ctive **R**adar
ASL	**A**bove **S**ea **L**evel
AToN	**A**id **T**o **N**avigation
BTS	**B**ase **T**ransceiver **S**tation
CIT	**C**oherent **I**ntegration **T**ime
COP	**C**ommon **O**perational **P**icture
CPA	**C**losest **P**oint of **A**pproach
CT	**C**oordinated **T**urn
CV	**C**onstant **V**elocity
CWNA	**C**ontinuous **W**hite **N**oise **A**cceleration
DoA	**D**ifference of **A**rrival
DTED	**D**igital **T**errain **E**levation **D**ata
EKF	**E**xtended **K**alman **F**ilter
ETA	**E**stimated **T**ime of **A**rrival
ETD	**E**stimated **T**ime of **D**eparture
FoV	**F**ield of **V**iew
GAMMA	**G**ruppen-**A**ntenne für **M**ilitärische **M**obilfunk **A**ufklärung
GNSS	**G**lobal **N**avigation **S**atellite **S**ystem
GSM	**G**lobal **S**ystem for **M**obile Communications
IALA	**I**nternational **A**ssociation of Marine Aids to Navigation and **L**ighthouse **A**uthorities
IMO	**I**nternational **M**aritime **O**rganization
JDL	**J**oint **D**irectors of **L**aboratories

KB	**K**nowledge **B**ase
KF	**K**alman **F**ilter
KLD	**K**ullback **L**eibler **D**ivergence
LRIT	**L**ong **R**ange **I**dentification and **T**racking
MAP	**M**aximum a **P**osteriori
MDA	**M**aritime **D**omain **A**wareness
MDV	**M**inimum **D**etectable **V**elocity
MHE	**M**oving **H**orizon **E**stimation
MHT	**M**ultiple **H**ypotheses **T**racker
MMSE	**M**inimum **M**ean **S**quare **E**rror
MMSI	**M**aritime **M**obile **S**ervice **I**dentity
MSA	**M**aritime **S**ituational **A**wareness
NF	**N**avigation **F**ield
NFF	**N**avigation **F**orce **F**ield
NWP	**N**orth **W**est **P**assage
P_D	**P**robability of **D**etection
P_{FA}	**P**robability of **F**alse **A**larm
PCL	**P**assive **C**oherent **L**ocation
pdf	**p**robability **d**ensity **f**unction
PF	**P**article **F**ilter
PR	**P**assive **R**adar
RCA	**R**arad **C**overage **A**nalysis
RCS	**R**arad **C**ross **S**ection
RMP	**R**ecognized **M**aritime **P**icture
RMSE	**R**oot **M**ean **S**quare **E**rror
RPM	**R**oute **P**ropagation **M**odule
S-AIS	**S**atellite **A**utomatic **I**dentification **S**ystem
SIR	**S**ampling **I**mportance **R**esampling
SL	**S**ea **L**ane
SMC	**S**equential **M**onte **C**arlo
SNR	**S**ignal to **N**oise **R**atio
STAP	**S**pace **T**ime **A**daptive **P**rocessing
TCPA	**T**ime to **C**losest **P**oint of **A**pproach
TDoA	**T**ime **D**ifference of **A**rrival
UKF	**U**nscented **K**alman **F**ilter
ULA	**U**niform **L**inear **A**rray
UT	**U**nscented **T**rasformation
VHF	**V**ery **H**igh **F**requency
VTS	**V**essel **T**raffic **S**ervices

Own Publications

Conferences

1. Vespe, M.; Sciotti, M.; Burro, F.; **Battistello, G.**; Sorge, S., *"Maritime Multi-Sensor Data Association Based on Geographic and Navigational Knowledge"*, in Proceedings of IEEE Radar Conference (RADAR), 2008, pp.1-6, Rome (IT), 26-30 May 2008.

2. Vespe, M.; **Battistello, G.**; Sciotti, M., *"Decision Support Real-Time Tools in Maritime Traffic Surveillance Systems"*, in Proceedings of RTO-MP-SET-125 Symposium on Sensors and Technology for Defence Against Terrorism, 2008, Mannheim (DE), 22-25 April 2008.

3. Vespe, M.; Sciotti, M.; **Battistello, G.**, *"Multi-Sensor Autonomous Tracking for Maritime Surveillance"*, in Proceedings of International Conference on Radar, 2008, pp.525-530, Adelaide (Australia), 2-5 Sept. 2008.

4. Vespe, M.; Sciotti, M.; Burro, F.; **Battistello, G.**; Sorge, S., *"Decision Support Platforms for Satellite-Extended Vessel Traffic Services"*, in Proceedings of International Conference on Radar, 2008, pp.670-675, Adelaide (Australia), 2-5 Sept. 2008.

5. **Battistello, G.**; Koch, W., *"Knowledge-aided Multi-Sensor Data Processing for Maritime Surveillance"*, in Proceedings of Informatik 2010, Service Science - neue Perspektiven für die Informatik. Vol.2 : Beiträge zur 40. Jahrestagung der Gesellschaft für Informatik e.V., 2010, pp.796-799, Leipzig (DE), 27 Sept. - 01. Oct. 2010.

6. **Battistello, G.**; Ulmke, M.; Koch, W., *"Knowledge-aided Multi-Sensor Data Processing for Maritime Surveillance"*, in Proceedings SPIE 8047, Ground/Air Multisensor Interoperability, Integration, and Networking for Persistent ISR II, 80470N, 2011, Orlando, Florida (US), 25 April 2011.

7. **Battistello, G.**; Ulmke, M., *"Exploitation of a priori Information for Tracking Maritime Intermittent Data Sources"*, in Proceedings of the 14th International Conference on Information Fusion (FUSION), 2011, pp.1-8, Chicago, Illinois (US), 5-8 July 2011.

8. Papi, F.; Podt, M.; Boers, Y.; **Battistello, G.**; Ulmke, M., *"Bayes Optimal Knowledge Exploitation for Target Tracking with Hard Constraints"*, in Proceedings of 9th IET Data Fusion and Target Tracking Conference (DFTT 2012): Algorithms and Applications, pp.1-6, London (UK), 16-17 May 2012.

9. **Battistello, G.**; Ulmke, M.; Papi, F.; Podt, M.; Boers, Y., *"Assessment of Vessel Route Information Use in Bayesian Nonlinear Filtering"*, in Proceedings of 15th International Conference on Information Fusion (FUSION), 2012, pp.447-454, Singapore, 9-12 July 2012.

10. Papi, F.; Podt, M.; Boers, Y.; **Battistello, G.**; Ulmke, M., *"On Constraints Exploitation for Particle Filtering Based Target Tracking"*, in Proceedings of 15th International Conference on Information Fusion (FUSION), 2012, pp.455-462, Singapore, 9-12 July 2012.

11. Zemmari, R.; Daun, M.; **Battistello, G.**; Nickel, U., *"Target Estimation Improvement of GSM Passive Coherent Location System"*, in Proceedings of IET International Conference on Radar Systems (Radar 2012), pp.1-6, Glasgow (UK), 22-25 Oct. 2012.

12. Gonzalez, J.; **Battistello, G.**; Schmiegelt, P.; Biermann, J., *"Semi-automatic Extraction of Ship Lanes and Movement Corridors from AIS Data"*, in Proceedings of IEEE International Geoscience and Remote Sensing Symposium (IGARSS), 2014, pp.1847-1850, Quebec (Canada), 13-18 July 2014.

13. **Battistello, G.**; Gonzalez, J.; Ulmke M., *"Vessel Route Prediction for Maritime Surveillance"*, in Proceedings of 9th Security Research Conference (Future Security), 2014, pp. 348-355, Berlin (DE), 16-18 Sept. 2014.

14. **Battistello, G.**; Ulmke M.; Mohrdieck, C., *"Enhanced Maritime Traffic Picture for the Canadian Arctic"*, in Proceedings of 10th Security Research Conference (Future Security), 2014, pp. 41-48, Berlin (DE), 15-17 Sept. 2015.

15. **Battistello, G.**; Ulmke M.; Gonzalez, J.; Mohrdieck, C., *"Multi-sensor Data Fusion for Improved Maritime Traffic Monitoring in the Canadian Arctic"*, in 9th Symposium of the International Society of Digital Earth (ISDE), 2015, Halifax, Nova Scotia (Canada), 5-9 Oct 2015.

16. Gonzalez, J.; Madhogaria, S.; **Battistello, G.**; Ulmke M., *"Assignment of Probabilities to Ship Detections from Satellite SAR Imagery Based on Ice Cover and Satellite AIS Density Maps"*, in Proceedings of 36th European Association

of Remote Sensing Laboratories (EARSeL) Symposium, 2016, Bonn (DE), 24-26 June 2016.

17. **Battistello, G.**; Gonzalez, J.; Ulmke, M.; Koch, W.; Mohrdieck, C., *"Multi-sensor Maritime Monitoring for the Canadian Arctic: Case Studies"*, in Proceedings of 19th International Conference on Information Fusion (FUSION), 2016, Heidelberg (DE), 5-8 July 2016.

Journals

1. Zemmari, R.; Broetje, M.; **Battistello, G.**; Nickel, U., *"GSM Passive Coherent Location System: Performance Prediction and Measurement Evaluation"*, in IET Radar, Sonar and Navigation, vol.8, no.2, pp.94-105, February 2014, [DOI: 10.1049/iet-rsn.2013.0206].

Book Chapters

1. **Battistello, G.**; Mertens, M.; Ulmke, M.; Koch, W., *"Context Exploitation for Target Tracking"*, Chapter in the Book: "Context-Enhanced Information Fusion - Boosting Real World Performance with Domain Knowledge", L. Snidaro, J. Garcia, J. Llinas and E. Blasch Editors, Springer, 2016.

Bibliography

[Age15] European Maritime Safety Agency. *Vessel Tracking Globally - Understanding LRIT*. EMSA, 2015.

[Age18] European Maritime Safety Agency. *Copernicus Maritime Surveillance Service - Info Sheet*. European Maritime Safety Agency, 2018.

[AGOR02] M. S. Arulampalam, N. Gordon, M. Orton, and B. Ristic. A Variable Structure Multiple Model Particle Filter for GMTI Tracking. In *Proc. 5th International Conference on Information Fusion*, Annapolis, 2002.

[Art15] B. A. Mc Arthur. A System Concept for Persistent, Unmanned, Local-Area Arctic Surveillance. *SPIE Proceedings Unmanned/Unattended Sensors and Sensor Networks XI; and Advanced Free-Space Optical Communication Techniques and Applications,*, 9647, 2015.

[AS03] C. Agate and K. J. Sullivan. Road-Constraint Target Tracking and Identification Using a Particle Filter. In *Proc. Signal and Data Processing of Small Targets, vol. 5204, SPIE*, 2003.

[BBP09] B. Bell, J. Burke, and G. Pillonetto. An inequality constrained nonlinear kalman-bucy smoother by interior point likelihood maximization. *Automatica*, 45(1):25 – 33, 2009.

[Bec00] K. Becker. *Target Motion Analysis aus Winkelmessungen: Parametrische Studie in drei Dimensionen*. FKIE Bericht 12, FGAN, Wachtberg-Werthoven, 2000.

[Bla04] S. Blackman. Multiple Hypothesis Tracking for Multiple Target Tracking. *IEEE Aerospace and Electronic Systems Magazine*, 19:5 – 18, 2004.

[BP99] S. Blackman and R. Popoli. *Design and Analysis of Modern Tracking Systems*. Artech House, Norwood, MA, 1999.

[Bri04] J. Briggs. *Target Detection by Marine Radars*. IEE Publishing, Stevenage, UK, 2004.

[Bro12] M. Broetje. *Multistatic Multihypothesis Tracking Techniques for Underwater and Air Surveillance Applications*. Siegen: GCA-Verlag Waabs, 2012.

[BSL95] Y. Bar-Shalom and X.-R. Li. *Multitarget-Multisensor Tracking: Principles and Techniques*. YBS Publishing, Storrs, CT, 1995.

[BSLK01] Y. Bar-Shalom, X.-R. Li, and T. Kirubarajan. *Estimation with Applications to Tracking and Navigation: Theory, Algorithms and Software*. John Wiley & Sons, 2001.

[BU11] G. Battistello and M. Ulmke. Exploitation of a priori Information for Tracking Maritime Intermittent Data Sources. In *Proc. 14th International Conference on Information Fusion*, Chigago, 2011.

[BUP+12] G. Battistello, M. Ulmke, F. Papi, M. Podt, and Y. Boers. Assessment of Vessel Route Information Use in Bayesian non-linear Filtering. In *Proc. 15th International Conference on Information Fusion*, Singapore, 2012.

[CCL06] F. Colone, R. Cardinali, and P. Lombardo. Cancellation of Clutter and Multipath in Passive Radar Using a Sequential Approach. In *Proc. of IEEE Radar Conference*, Verona, NY, USA, 2006.

[CGPB11] R. Chou, M. Geist, M. Podt, and Y. Boers. Performance Evaluation for Particle Filters. In *Proc. 14th International Conference on Information Fusion*, Chicago, USA, 2011.

[Che07] M. Cherniakov. *Bistatic Radar. Principle and Practice*. John Wiley and Sons Ltd., 2007.

[Cop] *https://www.copernicus.eu/en*.

[CWGS10] K. Chetty, K. Woodbridge, H. Guo, and G.E. Smith. Passive Bistatic WiMAX Radar for Marine Surveillance. In *Proc. IEEE International Radar Conference*, 2010.

[DFG01] A. Doucet, N. De Freitas, and N.J. Gordon. *Sequential Monte Carlo Methods in Practice*. Springer, 2001.

[DNK12] M. Daun, U. Nickel, and W. Koch. Tracking in Multistatic Passive Radar Systems Using DAB/DVB-T Illumination. *Signal Processing*, 92(6):1365–1386, 2012.

[DW88] H. F. Durrant-Whyte. *Integration, Coordination and Control of Multi-Sensor Robot Systems*. Springer, Boston, MA, 1988.

[ea14] A. Alessandrini et al. Data Driven Contextual Knowledge from and for Maritime Situational Awareness. In *Proceedings of the 1st International Workshop on Context-Awareness in Geographic Information Services*, 2014.

[exa15a] exactEarth. *Satellite AIS*. exactEarth, 2015.

[exa15b] exactEarth. *www.exactearth.com/products*. exactEarth, 2015.

[Fea08] J. L. Forand and et al. Surveillance of Canada's high Arctic. In *Proc. of Oceans 2008*, Quebec City, QC, 2008.

[fIS] NEREIDS: New Service Capabilities for Integrated and Advanced Maritime Surveillance. *http://maritimesurveillance.security-copernicus.eu/fp7-supporting-projects/nereids*.

[FRH86] J. Fussell, D. Rundquist, and J.A. Harrington. On defining Remote Sensing. *Photogrammetric Engineering and Remote Sensing*, 52(9):1507–1511, 1986.

[GB05] H.D. Griffiths and C.J. Baker. Passive Coherent Location Radar Systems. Part 1: Performance Prediction. *IEE Proceedings Radar, Sonar and Navigation*, 152(3):153–159, 2005.

[GB17] H.D. Griffiths and C.J. Baker. *An Introduction to Passive Radar*. Artech House, 2017.

[GBB+02] H.D. Griffiths, C.J. Baker, J. Baubert, N. Kitchen, and M. Treagust. Bistatic radar using satellite-borne illuminators. In *Proc. IEEE International Conference on Radar*, 2002.

[GCS09] J. George, J.L. Crassidis, and T. Singh. Threat Assessment Using Context-Based Tracking in a Maritime Environment. In *Proc. 12th Int. Conference on Information Fusion*, Seattle, WA, USA, 2009.

[GH07] N. Gupta and R. Hauser. Kalman filtering with equality and inequality state constraints. *Source: http:// arxiv.org/ pdf/ 0709.2791.pdf* , page URL last checked December 2014, 2007.

[GR08] F. Gini and M. Rangaswamy. *Knowledge Based Radar Detection, Tracking and Classification*. Wiley-Interscience, 2008.

[Gue03] J. R. Guerci. *Space-Time Adaptive Processing for Radar*. Artech House, Boston, London, 2003.

[GWB08] H. Guo, K. Woodbridge, and C.J. Barker. Evaluation of wifi beacon transmissions for wireless based passive radar. *Proc. IEEE Radar Conference*, pages 1–6, 2008.

[Hae91] W. K. Haerdle. *Smoothing Techniques - With Implementation in S.* Springer - Verlag, 1991.

[HKGN06] G. Hendeby, R. Karlsson, F. Gustafsson, and N.Gordon. Performance Issues in Non-Gaussian Filtering Problems. In *Proc. of IEEE Nonlinear Statistical Signal Workshop*, 2006.

[HL97] D.L. Hall and J. Llinas. An introduction to multisensor data fusion. *Proceedings of the IEEE*, 85:6–23, 1997.

[HM04] D.L. Hall and S. McMullen. *Mathematical Techniques in Multisensor Data Fusion.* Artech House, 2004.

[HMR05] P.E. Howland, D. Maksimiuk, and G. Reitsma. Fm radio based bistatic radar. *Proc. IEE Radar Sonar Navigation*, 152(3):107–115, 2005.

[How99] P.E. Howland. Target tracking using television-based bistatic radar. *Proc. IEE Radar Sonar Navigation*, 146(3):166–174, 1999.

[(IM97] International Maritime Organisation (IMO). *Resolution A.857(20), Guidelines for Vessel Traffic Service.* IMO, 1997.

[(IM08] International Maritime Organisation (IMO). *Resolution MSC.263(84), Revised performance standards and functional requirements for the LRIT of ships.* IMO, 2008.

[IR14] ITU-R. *Recommendation ITU-R M.1371-5: Technical characteristics for an automatic identification system using time division multiple access in the VHF maritime mobile frequency band.* ITU-R, 2014.

[JU97] S. J. Julier and J. K. Uhlmann. A New Extension of the Kalman Filter to Nonlinear Systems. In *Proc. 11th International Symposium Aerospace/Defense Sensing, Simulation and Controls (AeroSense)*, 1997.

[JU04] S. J. Julier and J. K. Uhlmann. Unscented Filtering and Nonlinear Estimation. *Proceedings of the IEEE*, 92(3):401 – 422, 2004.

[Kal60] R.E. Kalman. A New Approach to Linear Filtering and Prediction Problems. *Journal of Basic Engineering*, 82(35):35–45, 1960.

[KB61] R.E. Kalman and R.S. Bucy. New Results in Linear Filtering and Prediction Theory. *Journal of Basic Engineering*, 83(1):95–108, 1961.

[KB07] S. Ko and R. Bitmead. State Estimation for Linear System with State Equality Constraints. *Automatica*, 43(8):1363–1368, 2007.

[KBSPK00] T. Kirubarajan, Y. Bar-Shalom, K. Pattipati, and I. Kadar. Ground Target Tracking with Variable Structure IMM Estimator. *IEEE Transactions on Aerospace and Electronic Systems*, 36(1):26 – 46, 2000.

[KK01] W. Koch and R. Klemm. Ground Target Tracking with STAP Radar. *IEE Proceedings - Radar, Sonar and Navigation*, 148(3):173 – 185, 2001.

[KKU06] W. Koch, J. Koller, and M. Ulmke. Ground Target Tracking and Road Map Extraction. *ISPRS Journal of Photogrammetry & Remote Sensing, Elsevier*, 61:197 – 208, 2006.

[Kle06] R. Klemm. *Principles of Space-Time Adaptive Processing*. 3rd Edition, IET Radar, Sonar and Navigation, Series 21, 2006.

[Koc06a] W. Koch. Advanced Target Tracking Techniques. *Advanced Radar Signal and Data Processing*, Educational Notes RTO-EN-SET-086, Paper 2, France, 2006.

[Koc06b] W. Koch. Tracking and Data Fusion Applications. *Advanced Radar Signal and Data Processing*, Educational Notes RTO-EN-SET-086, Paper 9, France, 2006.

[Koc07] W. Koch. On Exploiting 'Negative' Sensor Evidence for Target Tracking and Sensor Data Fusion. In *Proc. 10th International Conference on Information Fusion*, Quebec, Canada, 2007.

[Koc10] W. Koch. On Bayesian Tracking and Data Fusion: a Tutorial Introduction with Examples. *IEEE Aerospace and Electronic System Magazine*, 25(7):29 – 52, 2010.

[Koc14] W. Koch. *Tracking and Sensor Data Fusion - Methodological Framework and Selected Applications*. Springer Verlag Berlin Heidelberg, 2014.

[Lap14] S. Lapinski. *LRIT and AIS: An analysis of October 2010 data*. DRDC Atlantic TM 2012-234; Defence Research and Development Canada-Atlantic, 2014.

[Lof90a] O. Loffeld. *Estimationstheorie, Bd.1, Grundlagen und stochastische Konzepte*. R. Oldenbourg Verlag GmbH, Muenchen, 1990.

[Lof90b] O. Loffeld. *Estimationstheorie, Bd.2, Anwendungen, Kalman-Filter*. R. Oldenbourg Verlag GmbH, Muenchen, 1990.

[LSE16] J. Llinas L. Snidaro, J. Garcia and E. Blasch Editors. *Context-Enhanced Information Fusion - Boosting Real World Performance with Domain Knowledge*. Springer, 2016.

[MKK14] M. Mertens, T. Kirubarajan, and W. Koch. Exploiting Doppler Blind Zone Information for Ground Moving Target Tracking with Bistatic Airborne Radar. *IEEE Transactions on Aerospace and Electronic Systems*, 50(1):130 – 148, 2014.

[MSMM05] D. Musicki, S. Suvorova, M. Morelande, and B. Moran. Clutter Map and Target Tracking. In *Proc. 8th International Conference on Information Fusion*, Philadelphia, 2005.

[NAT08] NATO. *Multinational Experimentation 5 MSA, final report*. 2008.

[Nic14] U. R. O. Nickel. System Considerations for Passive Radar with GSM Illuminators. In *Proc. of IEEE International Symposium on Phased Array Systems and Technology (ARRAY)*, 2014.

[Off07] National Maritime Domain Awarness Coordination Office. *National Concept of Operations for Maritime Domain Awareness*. 2007.

[oMAtNI07a] International Association of Marine Aids to Navigation and Lighthouse Authorities (IALA). *Establishment of VTS Radar Services 1056*. Saint Germain en Laye, France, 1st Edition, 2007.

[oMAtNI07b] International Association of Marine Aids to Navigation and Lighthouse Authorities (IALA). *Recommendation V-128 on Operational and Technical Performance Requirements for VTS Equipment*. Saint Germain en Laye, France, 3rd Edition, 2007.

[oMAtNI09] International Association of Marine Aids to Navigation and Lighthouse Authorities (IALA). *Recommendation V-119 on Implementation of Vessel Traffic Services*. Saint Germain en Laye, France, 2nd Edition, 2009.

[oMAtNI12] International Association of Marine Aids to Navigation and Lighthouse Authorities (IALA). *IALA Guideline 1089 on Provision of Vessel Traffic Services*. Saint Germain en Laye, France, Edition 1, 2012.

[oMAtNI16] International Association of Marine Aids to Navigation and Lighthouse Authorities (IALA). *VTS Manual*. Saint Germain en Laye, France, Edition 6, 2016.

[ORB] ORBCOMM. *ORBCOMM Website, http://www.orbcomm.com/services-ais.htm*.

[Org80] International Maritime Organization. *International Convention for the Safety of Life at Sea (SOLAS), 1974 - Chapter V - Safety of Navigation.* International Maritime Organization, 1980.

[OSG09] U. Orguner, T.B. Schon, and F. Gustafsson. Improved target tracking with road network information. *Aerospace conference, 2009 IEEE*, pages 1–11, March 2009.

[oSTTAB08] B. o. S. Teixeira, L. A. B. Torres, L. A. Aguirre, and D. S. Bernstein. Unscented Filtering for Interval-Constrained Nonlinear Systems,. In *Proceedings of 47th IEEE Conference on Decision and Control*, Cancun, Mexico, 2008.

[PASSftAG] PASSAGES: Protection and Secure Advanced Surveillance System for the Arctic: Green, Efficient. *http://passages.ie.dal.ca/.*

[PHBB14] G. Pallotta, S. Horn, P. Braca, and K. Bryan. Context-enhanced Vessel Prediction Based on Ornstein-Uhlenbeck Processes Using Historical AIS Traffic Patterns: Real-world Experimental Results. In *Proceedings of the 17th International Conference on Information Fusion*, 2014.

[PPB+12] F. Papi, M. Podt, Y. Boers, G. Battistello, and M. Ulmke. On Constraints Exploitation for Particle Filtering Based Target Tracking. In *Proceedings of the 15th International Conference on Information Fusion*, 2012.

[PVB13] G. Pallotta, M. Vespe, and K. Bryan. Vessel Pattern Knowledge Discovery from AIS Data: a Framework for Anomaly Detection and Route Prediction. *Entropy*, 6(15), 2013.

[RAG04] B. Ristic, S. Arulampalam, and N. Gordon. *Beyond the Kalman Filter: Particle Filters for Tracking Applications.* Artech House, 2004.

[RD00] R.L. Rothrock and O.E. Drummond. Performance metrics for multiple-target tracking. *Proc. SPIE 4048, Signal and Data Processing os Small Targets 2000*, 2000.

[RRL01] C. Rao, J. Rawlings, and J. Lee. Constrained Linear State Estimation - a Moving Horizon Approach. *Automatica*, 37(10):1619 – 1628, 2001.

[RRM03] C. Rao, J. Rawlings, and D. Mayne. Constrained State Estimation for Nonlinear Discrete-Time Systems: Stability and Moving Horizon Approximations. *IEEE Transactions on Automatic Control*, 48(2):246 – 258, 2003.

[RT01] K.J. Rawson and E.C. Tupper. *Basic Ship Theory.* Butterworth-Heineman, Elsevier, 2001.

[SC02] D. Simon and T. L. Chia. Kalman Filtering with State Equality Constraints. *IEEE Transactions on Aerospace and Electronic Systems*, 38(1):128 – 136, 2002.

[SC05] R. Saini and M. Cherniakov. DTV signal ambiguity function analysis for radar application. *Proc. IEE Radar Sonar Navigation*, 152(3):133–142, 2005.

[SD10] I. Schlangen and M. Daun. Different Tools for Clutter Mapping. In *Proc. of INFORMATIK 2010-Jahrestagung der Gesellschaft fuer Informatik e.V. (GI) 5th German Workshop Sensor Data Fusion (SDF 2010)*, Leipzig, 2010.

[Sim10] D. Simon. Kalman Filtering with State Constraints: a Survey of Linear and Nonlinear Algorithms. *IET Control Theory and Applications*, 4(8):1303 – 1318, 2010.

[Sko08] M. Skolnik. *Radar Handbook*. Third edition, McGraw-Hill, 2008.

[Sor85] H. W. Sorenson. *Kalman filtering: Theory and Application*. IEEE Press, 1985.

[SS10] D. Simon and D. L. Simon. Constrained Kalman Filtering via Density Function Truncation for Turbofan Engine Health Estimation. *Int. Journal of System Science*, 41(2):159–171, 2010.

[Str08] D. Streller. Road Map Assisted Ground Target Tracking. In *Proc. 11th International Conference on Information Fusion*, Cologne, 2008.

[Tan96] H. Tanizaki. *Nonlinear Filters: Estimation and Applications*. Second Edition, Springer-Verlag, 1996.

[TB07] H. L. V Trees and K. L. Bell. *Bayesian Bounds for Parameter Estimation and Nonlinear Filtering/Tracking*. Wiley-Interscience, New York, 2007.

[TMN98] P. Tichavsky, C. Muravchik, and A. Nehorai. Posterior Cramer-Rao Bounds for Discrete-Time Nonlinear Filtering. *IEEE Transaction on Signal Processing*, 46(5):1386, 1998.

[TSL+05] D.K.P. Tan, H. Sun, Y. Lu, M. Lesturgie, and H.L. Chan. Passive radar using Global System for Mobile communication signal: theory, implementation and measurements. *Proc. IEE Radar Sonar Navigation*, 152(3):116–123, 2005.

[UK06] M. Ulmke and W. Koch. Road-Map Assisted Ground Moving Target Tracking. *IEEE Transactions on Aerospace and Electronic Systems*, 42(4):1264 – 1274, 2006.

[VBBV12] M. Vespe, K. Bryan, P. Braca, and I. Visentini. Unsupervised Learning of Maritime Traffic Patterns for Anomaly Detection. In *Proceedings of 9th IET Data Fusion and Target Tracking Conference*, London, 2012.

[vK02] G. van Keuk. MHT extraction and track maintenance of a target formation. *IEEE Transaction on Aerospace and Electronic Systems*, 288(38):525–531, 2002.

[VSB+08] M. Vespe, M. Sciotti, F. Burro, G. Battistello, and S. Sorge. Maritime Multi-Sensor Data Association Based on Geographic and Navigational Knowledge. In *Proceedings of IEEE Radar Conference,2008*, Rome, 2008.

[WCC02] L. Wang, Y. Chiang, and F. Chang. Filtering Method for Nonlinear System with Constraints. *IEE Proc. on Control Theory Application*, 149(6):525–531, 2002.

[WDW92] W. Wen and H. Durrant-Whyte. Model-based multi-sensor data fusion. In *IEEE Int. Conf. on Robotics Automation*, 1992.

[Weh95] D.R. Wehner. *High-Resolution Radar*. Artech House, 1995.

[Why87] F.E. Whyte. Data Fusion Lexicon. In *Joint Directors of Laboratories, Technical Panel for C3, Data Fusion Sub-Panel*, Naval Ocean Systems Center, San Diego, 1987.

[Wir13] W.D. Wirth. *Radar Techniques Using Array Antennas*. Second Edition, IET, 2013.

[WKV09] Q. Wang, S.R. Kulkarni, and S. Verdu. Divergence Estimation for Multidimensional Densities via k-Nearest-Neighbor Distances. *IEEE Trans. on Information Theory*, 55(5):2392–2405, 2009.

[WLH09] Q. Wang, Y. Lu, and C. Hou. An experimental WiMAX based passive radar study. In *Microwave Conference 2009*, 2009.

[YB08] C. Yang and E. Blasch. Kalman Filtering with Nonlinear State Constraints. *IEEE Transactions on Aerospace and Electronic Systems*, 45(1):70 – 84, 2008.

[ZBBN14] R. Zemmari, M. Broetje, G. Battistello, and U. Nickel. GSM Passive Coherent Location System: Performance Prediction and Measurement Evaluation. *IET Radar, Sonar and Navigation*, 8(2):94 – 105, 2014.

[ZDBN12] R. Zemmari, M. Daun, G. Battistello, and U. Nickel. Target Estimation Improvement of GSM Passive Coherent Location System. In *IET International Conference on Radar Systems*, Glasgow (UK), 2012.

[Zem16] R. Zemmari. *GSM Passive Coherent Location Signal Processing: Impact on System Performance*. Siegen: GCA-Verlag Waabs, 2016.

[ZKL08] M. Zhang, S. Knedlik, and O. Loffeld. An Adaptive Road-Constrained IMM Estimator for Ground Target Tracking in GSM Networks. In *11th International Conference on Information Fusion*, Cologne, 2008.

[ZNW09] R. Zemmari, U. Nickel, and W. D. Wirth. GSM Passive Radar for Medium Range Surveillance. In *European Radar Conference, EURAD*, Rome (IT), 2009.

[ZWBS05] X. Zhang, P. Willett, and Y. Bar-Shalom. Dynamic Cramer-Rao Bound for Target Tracking in Clutter. *IEEE Transaction on Electronic Systems*, 41(4):1154 – 1167, 2005.